Stabilization of peptides by site-specific incorporation of fluorinated amino acids:

Model studies and the development of fluorinated, peptide-based HIV-1 fusion inhibitors

Inaugural-Dissertation

to obtain the academic degree

Doctor rerum naturalium (Dr. rer. nat.)

submitted to the Department of Biology, Chemistry and Pharmacy

of Freie Universität Berlin

by

SUSANNE HUHMANN, M.Sc.

from Goslar, Germany

July 2018

Declaration

The research presented in this doctoral thesis was performed under supervision of Prof. Dr. Beate Koksch from December 2013 until July 2018 at the Institute of Chemistry and Biochemistry in the Department of Biology, Chemistry and Pharmacy of Freie Universität Berlin.

I hereby confirm that I have prepared this dissertation entitled "Stabilization of peptides by site-specific incorporation of fluorinated amino acids: Model studies and the development of fluorinated, peptide-based HIV-1 fusion inhibitors" autonomously and without impermissible help. All external sources and resources have been specified and properly cited or acknowledged. This thesis has not been submitted, accepted, rated as insufficient or rejected in any other doctorate degree procedure.

Berlin, July 2018   Susanne Huhmann

Publications, Oral and Poster Presentations

Publications*

(8) **S. Huhmann**, A. A. Berger, B. Koksch, Fluorinated protease substrates show position-dependent turnover. *In Frontiers of Organofluorine Chemistry*, I. Ojima, Eds., World Scientific, London, **2018**, in revision.

(7) **S. Huhmann**, B. Koksch, Fine-tuning the proteolytic stability of peptides with fluorinated amino acids. *Eur. J. Org. Chem.* **2018**, DOI: 10.1002/ejoc.201800803.

(6) **S. Huhmann**, A.-K. Stegemann, K. Folmert, D. Klemczak, J. Moschner, M. Kube, B. Koksch, Position-dependent impact of hexafluoroleucine and trifluoroisoleucine on protease digestion. *Beilstein J. Org. Chem.* **2017**, *13*, 2869-2882.

(5) J. R. Robalo, **S. Huhmann**, B. Koksch, A. Vila Verde, The Multiple Origins of the Hydrophobicity of Fluorinated Apolar Amino Acids. *Chem* **2017**, *3*, 881-897.

(4) S. Vukelić, J. Moschner, **S. Huhmann**, R. Fernandes, A. A. Berger, B. Koksch, Synthesis of Side Chain Fluorinated Amino Acids and their Effects on the Properties of Peptides and Proteins. *In Modern Synthesis Processes and Reactivity of Fluorinated Compounds: Progress in Fluorine Science*, H. Groult, F. Leroux, A. Tressaud, Eds., 1st Edition, Elsevier: London, 2016, pp 427-464.

(3) **S. Huhmann**, E. K. Nyakatura, H. Erdbrink, U. I. M. Gerling, C. Czekelius, B. Koksch, Effects of single substitutions with hexafluoroleucine and trifluorovaline on the hydrophobic core formation of a heterodimeric coiled coil. *J. Fluorine Chem.* **2015**, 175, 32-35.

(2) J. Mortier, E. K. Nyakatura, O. Reimann, **S. Huhmann**, J. O. Daldrop, C. Baldauf, G. Wolber, M. S. Miettinen, B. Koksch, Coiled-Coils in Phage Display Screening: Insight into Exceptional Selectivity Provided by Molecular Dynamics. *Journal of Chemical Information and Modeling* **2015**, *55*, 495-500.

(1) H. Erdbrink, E. K. Nyakatura, **S. Huhmann**, U. I. M. Gerling, D. Lentz, B. Koksch, C. Czekelius, Synthesis of enantiomerically pure (2*S*,3*S*)-5,5,5-trifluoroisoleucine and (2*R*,3*S*)-5,5,5-trifluoro-allo-isoleucine. *Beilstein J. Org. Chem.* **2013**, *9*, 2009-2014.

Oral Presentations at Conferences and Workshops

(7) „Fluorine changes the proteolytic stability of peptides"; 58th Kollegseminar of the research training group 1582 "Fluorine as key element", Berlin/Germany, 02/10/**2017**.

(6) „Impact of fluorinated amino acids on the proteolytic stability of peptides"; 17. Deutscher Fluortag, Schmitten/Germany, 09/20/**2016**.

* Publications **(3)** and **(6)** emerged from this doctoral thesis.

(5) „Towards fluorinated HIV-1 fusion inhibitors"; 7th PhD workshop of the research training group 1582 "Fluorine as key element", Strausberg/Germany, 04/20/**2016**.

(4) „Impact of fluorinated amino acids on the proteolytic stability of model peptides"; 6th PhD workshop of the research training group 1582 "Fluorine as key element", Schwielowsee/Germany, 10/16/**2015**.

(3) „Effects of Single Substitutions with Hexafluoroleucine and Trifluorovaline on the Hydrophobic Core Formation of a Heterodimeric Coiled Coil"; 5th PhD workshop of the research training group 1582 "Fluorine as key element", Wandlitz/Germany, 11/20/**2014**.

(2) „Effects of Single Substitutions with Hexafluoroleucine and Trifluorovaline on the Hydrophobic Core Formation of a Heterodimeric Coiled Coil"; 16. Deutscher Fluortag, Schmitten/Germany, 09/23/**2014**.

(1) „Effects of Single Substitutions with Hexafluoroleucine and Trifluorovaline on the Hydrophobic Core Formation of a Heterodimeric Coiled Coil"; 39th Kollegseminar of the research training group 1582 "Fluorine as key element", Berlin/Germany, 07/03/**2014**.

Posters

(9) „Impact of fluorinated amino acids on the proteolytic stability of peptides"; GDCh-Wissenschaftsforum Chemie, Berlin/Germany, 09/10 - 09/14/**2017**.

(8) „Fluorine changes the proteolytic stability of peptides"; 25th American Peptide Symposium and 9th International Peptide Symposium, Whistler B.C./Canada, 06/17 - 06/22/**2017**. (**Travel Award Winner**)

(7) „Impact of fluorinated amino acids on the proteolytic stability of peptides"; 13th German Peptide Symposium, Erlangen/Germany, 03/20 - 03/23/**2017**.

(6) „Towards fluorinated peptidic HIV-1 fusion inhibitors"; 34th European Peptide Symposium and 8th International Peptide Symposium, Leipzig/Germany, 09/04 - 09/09/**2016**.

(5) „Impact of fluorinated amino acids on the proteolytic stability of peptides"; Bremen Fluorine Days (5th International Symposium on Organofluorine Compounds in Biomedical, Materials and Agriculture Sciences), Bremen/Germany, 07/03 - 07/07/**2016**.

(4) „Effects of Single Substitutions with Hexafluoroleucine and Trifluorovaline on the Hydrophobic Core Formation of a Heterodimeric Coiled Coil"; 5. Berliner Chemie Symposim, Berlin/Germany, 04/12/**2016**. (**Poster Price Winner**)

(3) „Effects of Single Substitutions with Hexafluoroleucine and Trifluorovaline on the Hydrophobic Core Formation of a Heterodimeric Coiled Coil"; 21st International Symposium on Fluorine Chemistry, Como/Italy, 08/23 - 08/28/**2015**.

(2)	„Impact of trifluoroisoleucine on the proteolytic stability of model peptides“; 29. Tag der Chemie, Berlin/Germany, 06/18/**2015**.

(1)	„Hydrophobicity and Helix-propensity of Fluorinated Isoleucine Variants”; 17th European Symposium on Fluorine Chemistry, Paris/France, 07/21 - 07/25/**2013**.

Acknowledgements

Above all, I would like to thank Prof. Dr. Beate Koksch for the confidence she has shown in me, and her support and guidance throughout my studies. She gave me encouragement and freedom to pursue my research interests. I am deeply grateful for her continuing promotion to present the results of my work at several national and international academic conferences. Besides benefiting for my research, I could thereby develop myself further. Many thanks!

I also wish to thank Prof. Dr. Nediljko Budisa for being the second supervisor of this dissertation.

Additionally, I am very grateful for the excellent research environment, and the pleasant and motivating working atmosphere in the Koksch group. Everyday lab work, discussions, lunch and coffee breaks as well as the many cake times would not have been so inspiring, enjoyable and relaxing without all the current and former group members. All have broadened my scientific horizon and promoted this thesis tremendously.

Especially, I would like to extend my sincere thanks to Dr. Elisabeth Nyakatura and Dr. Ulla Gerling-Driessen for the kind welcoming in the group and introduction to several methods and techniques; to Dr. Allison Berger for proofreading English manuscripts and this doctoral thesis; to Dr. Johann Moschner for his kind advice and willingness to discuss questions regarding organic synthesis or joint projects. I also thank him, Dipl.-Chem. Valentina Stulberg and Dipl.-Chem. Katharina Hellmund for carefully proofreading this thesis.

My deepest gratitude goes to M. Sc. Kristin Folmert for introducing me to the wonders of HPLCs, her understanding and endearing character, and for being the best labmate one could wish for. Without her support it would not have been possible to achieve some of the results. Thank you for our great friendship and always being there.

I would like to thank my students Anne, Damian, Jakob, Michelle, and Ayşe for their experimental support and contribution to my research in the course of internships or master and bachelor theses.

I am also greatly indebted to Prof. Dr. Czekelius, Dr. Holger Erdbrink and Dr. Johann Moschner for providing the fluorinated amino acids. Moreover, I thank Dr. Bernhard Loll, Claudia Alings and Nicole Holton from the Wahl group for their advice and assistance in crystallization experiments and ITC measurements. Thanks are due to all the staff members of the Core Facility BioSupraMol and Material Management for their friendly service and provision of the necessary infrastructure.

I wish to acknowledge the Deutsche Forschungsgemeinschaft in the context of the Research Training Group 1582 "Fluorine as Key Element" for financial support.

"You can't connect the dots looking forward. You can only connect them looking backwards. So you have to trust that they will somehow connect in your future."

STEVE JOBS

Kurzzusammenfassung

Die Modifikation von Peptiden und Proteinen mit Seitenketten-fluorierten Aminosäuren ist eine weit verbreitete Strategie um biophysikalische und pharmazeutische Eigenschaften dieser anzupassen. Systematische Untersuchungen können dabei wertvolle Einsichten in das Verhalten dieser nicht-kanonischen Aminosäuren in natürlichen Proteinumgebungen liefern. Dazu werden in dieser Doktorarbeit zwei bewährte Modellsysteme genutzt, um den Einfluss einfacher Substitutionen mit sterisch anspruchsvollen und hoch-fluorierten Aminosäuren auf die *coiled-coil* Struktur und Stabilität sowie auf die Stabilität gegenüber Proteasen zu beurteilen.

Zunächst zeigte der Einbau von Hexafluoroleucin und zwei Trifluorovalin-Diastereoisomeren an zwei verschiedenen Positionen im hydrophoben Kern eines parallelen, heterodimeren *coiled-coil* Modellsystems, dass diese Aminosäuren problemlos in stabilen, dimeren α-helikalen Bündeln akzeptiert werden. Die einfache Substitution von Leucin mit Hexafluoroleucin führt zu einem deutlichen Anstieg der thermischen Stabilität, bedingt durch die größere Hydrophobie und effiziente Packung.

Zweitens verbessern fluorierte Leucin- und Isoleucin-Derivate in einigen Fällen die Resistenz eines Modellpeptides gegenüber verschiedenen Proteasen. Der Einfluss von Fluor kann jedoch nicht verallgemeinert werden, da ebenfalls Destabilisierungen für bestimmte Sequenzen beobachtet wurden. Dies könnte durch spezifische Wechselwirkungen zwischen den fluorierten Resten und den entsprechenden Enzymbindungstaschen erklärt werden. Bemerkenswert ist, dass Trifluoroisoleucin die Peptide gegen die Proteolyse durch alle getesteten Enzyme deutlich schützen kann, wenn es *N*-terminal zur Spaltstelle positioniert wird.

Schließlich wurden Studien zur Entwicklung stabiler, fluorierter, peptid-basierter HIV-1 Fusionsinhibitoren durchgeführt. Die Hüllproteinuntereinheit gp41 spielt eine Schlüsselrolle in der Infektion der Wirtszelle durch die Ausbildung eines Sechs-Helix-Bündels, welches aus drei *N*-terminalen (NHR) und drei *C*-terminalen *Heptad Repeat* (CHR) Sequenzen besteht. Mit der Erzeugung von synthetischen, fluorierten CHR-Analoga kann die Bündelbildung und damit der Zelleintritt verhindert werden. Das zuvor konzipierte, aus CHR-abgeleitete Peptid C31 dient hier als Startpunkt für rationale Substitutionen mit Difluoroethylglycin, Trifluoroisoleucin oder Hexafluoroleucin an einer Position, die wichtig für die helikale Bündelbildung ist. In der Tat bilden die daraus resultierenden fluorierten C31 Peptide helikale Bündel mit einem NHR-Peptid aus, allerdings zeigten die entstandenen Komplexe eine verringerte thermische Stabilität. Obwohl die Bindung entropisch nicht begünstigt ist, ermöglicht die hohe negative Enthalpie einen spontanen Bindungsprozess. Zwei der fluorierten Analoga weisen sogar eine höhere Bindungsaffinität zur NHR-Region im Vergleich zum nativen, nicht fluorierten System auf. Zudem wurde ein hetero-tetrameres Gerüst synthetisiert, welches eine trimere Oligomerisierung

des NHR-Segmentes ermöglicht und für eine genauere Analyse der kinetischen Parameter der Helixbildung mittels Oberflächenplasmonenresonanzspektroskopie genutzt werden soll.

Die Ergebnisse dieser Arbeit tragen so zu einer rationalen Anwendung fluorierter Aminosäuren bei der Entwicklung stabiler, peptid-basierter Wirkstoffkandidaten bei.

Abstract

The modification of peptides and proteins using side-chain fluorinated amino acids is a widely used strategy to modulate their biophysical and pharmaceutical properties. Systematic investigations can provide valuable insights into the behavior of these non-canonical amino acids in natural protein environments. To this end, the research conducted in this doctoral thesis made use of two well established model systems to evaluate the impact on coiled-coil structure and stability, and proteolytic stability of single substitutions with sterically demanding and highly fluorinated amino acids.

First, the incorporation of hexafluoroleucine and two trifluorovaline stereoisomers at two different positions of the hydrophobic core of a parallel heterodimeric coiled-coil model system showed that these amino acids are readily accommodated into stable dimeric α-helical bundles. Remarkably, the single substitution of leucine with hexafluoroleucine leads to a significant increase in thermal stability due to its greater hydrophobicity and efficient packing.

Second, fluorinated leucine and isoleucine derivatives in some cases improve the resistance of a model peptide towards different proteases; however, fluorine's impact cannot be generalized as destabilization was also observed for certain sequences. This might be explained by specific interactions between the fluorinated residues and the respective enzyme binding sites. Noteworthy is that trifluoroisoleucine is able to significantly protect peptides from proteolysis by all tested enzymes when positioned *N*-terminal to the cleavage site.

Finally, studies were carried out towards developing stable, fluorinated peptide-based HIV-1 fusion inhibitors. Envelope protein subunit gp41 plays a key role in host cell infection due to the formation of a six-helical bundle consisting of three *N*-terminal (NHR) and three *C*-terminal heptad repeat (CHR) sequences. By generating synthetic, judiciously fluorinated CHR-analogues bundle formation and, therefore, cell entry may be inhibited. The previously designed CHR-derived peptide C31 serves as starting point for single substitutions with difluoroethylglycine, trifluoroisoleucine or hexafluoroleucine at a position crucial for helix bundle formation. The resulting fluorinated C31 peptides indeed undergo helix-bundle formation with an NHR-peptide, but the resulting complexes exhibit decreased thermal stabilities. Although binding is entropically disfavored, the large negative enthalpy enables a spontaneous binding process. Two of the fluorinated analogues exhibit even higher binding affinities to the NHR-region compared to the native, non-fluorinated parent. Moreover, a hetero-tetrameric scaffold was synthesized that enables a trimeric oligomerization of the NHR-derived segment and will be applied in surface plasmon resonance experiments for a more detailed analysis of the kinetic parameters underlying helical assembly.

The results of this thesis will contribute to the rational application of fluorinated amino acids to the development of stable, peptide-based drug candidates.

Contents

Symbols and Abbreviations

6-HB	six-helix bundle
Å	Angstrom (1 Å = 10^{-10} m or 0.1 nm)
aa	amino acid
ACN	acetonitrile
AIDS	acquired immunodeficiency syndrome
Boc	*tert*-butyloxycarbonyl
calcd.	calculated
C-arom.	aromatic carbon
CAT	chloramphenicol acetyltransferase
CCR5	C-C chemokine receptor type 5
CD	circular dichroism
CD4	CD4 receptor
CHR	*C*-terminal heptad repeat
COSY	correlation spectroscopy
CXCR4	C-X-C chemokine receptor type 4
d	doublet
Da	Dalton
DBU	1,8-diazabicyclo[5.4.0]undec-7-en
DCM	dichloromethane
DIC	diisopropylcarbodiimide
DIPEA	*N,N*-diisopropylethylamine
DMAC	*N,N*-dimethylacetamide
DMF	dimethylformamide
DMSO	dimethyl sulfoxide
DNA	deoxyribonucleic acid
DPP IV	dipeptidyl peptidase IV
dRI	differential Refractive index
DSC	*N,N′*-disuccinimidyl carbonate
E. coli	*Escherichia coli*
EDT	1,2-ethanedithiol
eq.	equivalents
ESI	electron spray ionization
ESI-ToF	electron spray ionization - time of flight
Et_2O	diethyl ether
FI	fusion inhibitor
FDA	U. S. Food and Drug Administration

Fmoc	9-*N*-fluorenylmethyloxycarbonyl
GLP	glucagon-like-peptide
GndHCl	guanindine hydrochloride
gp120	glycoprotein 120
gp160	glycoprotein 160
gp41	glycoprotein 41
HAART	highly active antiretroviral therapy
H-aliphat.	aliphatic hydrogen
H-arom.	aromatic hydrogen
HATU	1-[bis(dimethylamino)methylene]-1*H*-1,2,3-triazolo[4,5-b]pyridinium 3-oxide hexafluorophosphate
HCTU	*O*-(1*H*-6-Chlorobenzotriazole-1-yl)-1,1,3,3-tetramethyluronium hexafluorophosphate
HFIP	1,1,1,3,3,3-hexafluoro-2-propanol
HIV	human immunodeficiency virus
HMQC	heteronuclear multiple quantum coherence
HOAt	1-hydroxy-7-azabenzotriazole
HOBt	1-hydroxy-benzotriazole
HPLC	high performance liquid chromatography
INI	integrase inhibitors
ITC	isothermal titration calorimetry
J	NMR coupling constant
KIH	knobs-into-holes
LBD	lipid-binding domain
LC/MS	liquid chromatography/mass spectrometry
m	multiplet
m/z	*mass per charge*
MALS	multi-angle static light scattering
MD	molecular dynamics
MeOH	methanol
MPER	membrane proximal external region
MS	mass spectrometry
MW	microwave
M_W	molecular weight
MWCO	molecular weight cut-off
NCL	native chemical ligation
NHR	*N*-terminal heptad repeat

NHS	*N*-hydroxysuccinimide
NMP	*N*-methyl-2-pyrrolidone
NMR	nuclear magnetic resonance
NNRTI	non-nucleoside reverse transcriptase inhibitor
N-PAGE	native polyacrylamide gel electrophoresis
NRTI	nucleoside reverse transcriptase inhibitor
NtRTI	nucleotide reverse transcriptase inhibitor
obs.	observed
PBD	pocket binding domain
PDB	protein data bank
PEG	polyethylene glycol
PET	positron emission tomography
PI	protease inhibitor
PIE	pocket-specific inhibitors of entry
Pip	piperidine
pK_a	logarithmic acid dissociation constant
PyBop	(benzotriazol-1-yloxy)tripyrrolidinophosphonium hexafluorophosphate
RNA	ribonucleic acid
RP	reversed phase
RP-HPLC	reversed phase high performance liquid chromatography
rpm	rounds per minute
rt	room temperature
s	singlet
SEC	size exclusion chromatography
SIV	simian immunodeficiency virus
SLS	static light scattering
SPPS	solid phase peptide synthesis
SPR	surface plasmon resonance
t	triplet
TA	thioanisole
TBTU	*O*-(Benzotriazol-1-yl)-*N*,*N*,*N'*,*N'*-tetramethyluronium tetrafluoroborat
ᵗBu	*tert*-Butyl
TCEP	tris-(2-carboxyethyl)phosphine
TFA	trifluoroacetic acid
TFE	2,2,2-trifluoroethanol
TIS	triisopropylsilane
T_M	melting temperature

ToF	time-of-flight
Tris	2-amino-2-(hydroxymethyl)propane-1,3-diol
tRNA	transfer ribonucleic acid
UV	ultra violet
vdW	van der Waals
δ	chemical shift
λ	wavelength

Abbreviations of the 20 canonical amino acids are consistent with the one- and three-letter code recommended by the IUPAC-IUB Joint Commission on Biochemical Nomenclature (JCBN) [*Eur. J. Biochem.* **1984**, *138*, 9–37].

Abbreviations of non-coded amino acids relevant to the present thesis are given below. If not stated otherwise, the abbreviations correspond to the L-amino acids.

2-Aha	(2*S*)-2-aminoheptanoic acid
(3*R*)-4^3-F$_3$Val	(2*S*,3*R*)-4,4,4-trifluorovaline
	(2*S*,3*R*)-2-amino-4,4,4-trifluoro-3-methylbutanoic acid
(3*S*)-4^3-F$_3$Val	(2*S*,3*S*)-4,4,4-trifluorovaline
	(2*S*,3*S*)-2-amino-4,4,4-trifluoro-3-methylbutanoic acid
4'^{3}-F$_3$Ile	4',4',4'-trifluoroisoleucine
	(2*S*,3*S*)-2-amino-3-(trifluoromethyl)pentanoic acid
5^3-F$_3$Ile	5,5,5-trifluoroisoleucine;
	(2*S*,3*S*)-2-amino-5,5,5-trifluoro-3-methylpentanoic acid
5^3,5'^{3}-F$_6$Leu	5,5,5,5',5',5'-hexafluoroleucine
	(2*S*)-2-amino-5,5,5-trifluoro-4-(trifluoromethyl)pentanoic acid
Abu	(2*S*)-2-aminobutanoic acid
Abz	*o*-aminobenzoic acid
DfeGly	difluoroethylglycine;
	(*S*)-2-amino-4,4-difluorobutanoic acid
DfpGly	difluoropropylgylcine
	(*S*)-2-amino-4,4-difluoropentanoic acid
MfeGly	monofluoroethylglycine;
	(*S*)-2-amino-4-fluorobutanoic acid
Nle	norleucine
TfeGly	trifluoroethylglycine
	(*S*)-2-amino-4,4,4-trifluorobutanoic acid

1.   Introduction

Peptides and proteins have various biological functions determined by the physical and chemical properties of their amino acid building blocks. Through folding they are precisely arranged in a three-dimensional structure.[1-2] α-Helices constitute the most abundant structural folding motif, and are thus found to underlie several important intracellular protein-protein interactions mediating a number of critical housekeeping events, such as transcriptional control, cellular differentiation, and replication, as well as numerous pathogenic processes.[2-5] For example, helical bundle formation of surface exposed proteins is a key step in several infection processes and enables the entry of viruses like the human immunodeficiency virus (HIV) into host cells. Therefore, selective disruption of helix-helix interactions emerged as an excellent strategy for drug discovery.

In the case of HIV infection, its envelope glycoprotein gp41 constitutes as promising drug target, as a critical step in the mechanism of cell entry involves a helix-helix interaction between the *N*- and *C*-terminal heptad repeats (NHR and CHR) of gp41 that form a coiled-coil six-helix bundle (6-HB). During the formation of this structure, a pre-hairpin intermediate with a relatively long lifetime is formed that can be deactivated by the binding of synthetic peptides derived from CHR or NHR to inhibit the formation of the fusion active conformation, and thus, HIV infection by interaction with their counterparts in gp41.

HIV is a retrovirus that exists in two prevalent subtypes (HIV-1, HIV-2) and causes the devastating acquired immunodeficiency syndrome (AIDS). Although a 48% decline in AIDS-related deaths was observed between 2005 and 2016 (from 1.9 million to 1.0 million) that can primarily be attributed to a global scale-up of antiretroviral therapy,[6-8] the prevention and treatment of HIV still remain challenging. In 2016 there were 1.8 million new infections worldwide, adding up to a total of 36.7 million people living with HIV.[8]

With the current standard of care of at least three antiretroviral drugs, the so-called highly active antiretroviral therapy (HAART), the HIV-1 infection is treated and the time until the outbreak of AIDS is extended. Currently administered antiretroviral drugs can be divided into the following groups of drug substances: nucleoside or nucleotide reverse transcriptase inhibitors (NRTIs or NtRTIs), non-nucleoside reverse transcriptase inhibitors (NNRTIs), protease inhibitors (PIs), fusion inhibitors (FIs) and integrase inhibitors (INIs). Reverse transcriptase inhibitors and protease inhibitors are most common, and only two fusion inhibitors are approved for clinical use - among these one peptidic antiviral drug.[9] T20 was approved in 2003 as the first and currently only peptidic fusion inhibitor for clinical use.

The widespread interest in peptides and proteins as highly potent pharmaceuticals relies on their inherent biocompatibility as well as their largely unmatched bioactivity, high specificity and low toxicity.[10-12] However, the application of peptides as drugs is limited by low bioavailability

in vivo, which results from rapid degradation by proteases, slow passive transport in blood, and generally low membrane penetration.[13-14] This motivates attempts towards the *de novo* design of peptides and proteins with superior properties such as chemical and metabolic resistance as well as thermodynamic stability. It holds also true for T20 that requires frequent high dose administration and furthermore some HIV strains are resistant against it.[9] Hence, the development of novel peptide-based HIV fusion inhibitors with improved stability and antiviral potency is necessary.

Strategies to improve the properties, especially the proteolytic stability against proteases of the blood plasma or digestive system, of peptide-based drugs include PEGylation, stapling/crosslinking or cyclization of peptide sequences.[15-17] The latter was used for the design of a new potent HIV-1 entry inhibitor VIR-576 that is currently in clinical trials.[18] VIR-576 exhibits a ring structure established by the formation of a disulfide bond and is able to effectively block HIV-1 entry into the host cell by binding to the end of the gp41 fusion peptide, thereby inhibiting the anchoring of the virus to the host cell.

Another strategy to improve pharmacological properties of the peptides relies on the incorporation of non-native amino acids such as D-amino acids, *N*-methylated amino acids, α,α-dialkylated residues or β- and γ-amino acids.[12] Such residues might not be recognized by the proteases; thus, no cleavage of the adjacent peptide bond occurs. In these cases, however, the residues need to be placed judiciously to maintain the active conformation of a peptide. Therefore, the introduction of amino acids that carry heteroatoms in their side chain, which are absent from the pool of canonical amino acids has gained much attention. Among these, fluorine has emerged as a promising candidate.

Due to its unique properties, namely its small size, extremely low polarizability, and the strongest inductive effect among all chemical elements,[19] fluorine has become a key element for modulating the properties of pharmaceuticals and biologically active compounds, exemplified by 25% of all pharmaceuticals on the market containing fluorine.[20] In this respect, the incorporation of side-chain fluorinated amino acids has been established as an efficient strategy to alter distinct functionalities of peptides and proteins, such as hydrophobicity, acidity/basicity, and conformation and thus can result in advanced pharmacological properties of peptide-based drugs.[21] In addition, fluorine addition can have significant effects on protein-protein as well as ligand-receptor interactions.

Nevertheless, general consequences of the hydrogen replacement by fluorine on the structure and activity of peptides and proteins are still not completely understood and cannot be generalized.[14] Even the incorporation of just one fluorinated amino acid can have a huge impact on protein structure,[22] whereas extensively fluorinated amino acids closely preserve and even strengthen the structure.[23-24] This makes it difficult to predict the influence of fluorine incorporation on protein stability and other pharmacological properties.

To fully utilize the power of this unique element one needs to understand the structural consequences of incorporating non-canonical side chains into a protein in a more detailed manner. To this end, systematic studies of the consequences of fluorination on the interactions of peptides with natural protein environments or proteases provide a valuable knowledge base, that can ideally be transferred and applied for substitution studies in biologically relevant interaction domains, such as gp41 of HIV.

The ultimate goal is the rational design of proteins using fluorinated amino acids as novel building blocks to develop stable peptide therapeutics with improved oral bioavailability, longer plasma half-lives, and perhaps even greater selectivity and affinity to their targets than their hydrocarbon counterparts.

2. Fluorine - a unique element for tuning properties of peptides and proteins

Besides its application as an analytical probe, e.g. in ^{19}F-NMR spectroscopy or positron emission tomography (PET), fluorine substituents are widely used for the decoration of organic molecules. Especially in medicinal chemistry fluorine introduction is a well-known strategy, but also in crop and material science, fluorine has gained much attention in recent years.[25] Fluorine's unique properties and the effect of the resulting carbon-fluorine bond[26] often impart in features that cannot be achieved by any other known functional group. Molecular properties such as conformation, pK_a values of neighboring functional groups or hydrophobicity can be dramatically changed upon fluorine introduction and thereby biological half-lives, bioavailability and -activity or interactions with proteins, membranes or receptors can be considerably improved.[20, 25, 27] Thus, it is not surprising that nowadays around 25% of the marketed drugs contain at least one fluorine atom, and they are employed for a wide variety of applications such as depression, cancer, and infectious disease therapies.[28-30]

In this regard fluorine has been proven promising also in the context of peptide and protein engineering. Incorporation of fluorinated amino acids can change biophysical, chemical, biological as well as pharmacological properties of peptides and proteins.[21] Especially the influence on structure, activity, folding, and stability towards thermal and chemical denaturation is described in several studies and reviewed extensively by the Koksch group and others.[21, 31-33] Within the scope of this doctoral thesis, only aspects regarding the impact of aliphatic, side-chain fluorinated amino acids will be discussed in the following.

2.1 Properties of fluorine and its relevance for medicinal chemistry and peptide engineering

Fluorine is a small atom with a van der Waals radius of 1.47 Å that is between that of oxygen (1.52 Å) and hydrogen (1.20 Å).[34] Therefore fluorine is often used as an oxygen- or hydrogen-mimic in organic chemistry. Especially the substitution of one hydrogen atom with a fluorine atom causes only minimal steric perturbation and is considered as shape-conservative or bioisosteric.[23-25, 35]

However, the steric bulk of fluorocarbon groups seems to disproportionately increase with the extent of fluorine substitution[14] and is controversy discussed in literature. One reason for this might be that the data is always dependent on the applied experimental method, and that its subsequent interpretation is often solely based on steric size, disregarding electronic contributions, rotation and shape of the considered residues. Thus, the values given in literature for the steric demand of a trifluoromethyl group vary from as large as a methyl group[36] up to the

size of a *sec*-butyl or phenyl group.[37] Other studies suggest that the trifluoromethyl group in a protein can rather be compared with larger alkyl groups - like an *iso*propyl group - than with a methyl residue,[38] or estimate that the van der Waals volume is close to that of an ethyl group.[39] Nevertheless, in addition to its volume, also the shape and flexibility of a substituent have to be taken into account, since steric interactions depend on these features.

Furthermore, fluorine is the most electronegative element ($\chi = 4$ in the Pauling scale), and it has the smallest value of polarizability per molecule volume. This results in a short, strong, and very low polarized C-F bond.[40] It is suggested that the increase in bonding strength in comparison to a C-H bond may enhance the metabolic stability and thus the bioavailability of a fluorinated compound.[41] Moreover, the C-F-bond causes a reduced overall molecular polarizability throughout the carbon framework of a fluorinated compound.[14, 42]

Because fluorine exerts a strong inductive effect, it influences the acidity or basicity of nearby functional groups. The pK_a values might be changed significantly by several log units, depending on the degree and position of the fluorine substitution. The acidity of COOH, C-OH and C-H is increased, whereas the basicity of amines is reduced.[43] Moreover, this change may have a strong influence on the pharmacokinetic properties of a molecule and its binding affinity to receptors since hydrogen bonds and electrostatic interactions play an important role in these properties.[20] It is suggested, that the reduced basicity of amines upon fluorination results in a better membrane permeability and, therefore, in an improved bioavailability.[44]

Since hydrogen bonds are essential for the formation on higher-ordered peptide and protein structures and they thus provide a significant contribution to the biological function of these macromolecules, the value of fluorocarbon-modified amino acids for peptide design and engineering might be connected to the ability of fluorine to contribute to the formation of hydrogen bonds.[14] This aspect is controversy discussed in literature.[40, 45] Through screening of the Cambridge Crystallographic Structural Database and *ab initio* calculations, it was shown that organic fluorine is only a very weak hydrogen bond acceptor.[46] Most of the hydrogen bonds are formed between a carbon-bound fluorine and a polarized carbon-bound hydrogen, whereas interactions with other functional groups such as amine or hydroxy groups are less common.[47] However, these interactions are referred to as weak dipolar interactions rather than hydrogen bonds. This may be explained by the high electronegativity and low polarizability of fluorine, whereby it does not like to donate its lone electron pairs. In contrast to hydrogen bonding, the participation of fluorine in electrostatic/polar interactions is widely accepted and may contribute to the enhanced binding affinity of organo-fluorine compounds for the enzyme's active site.[25] For instance, it was demonstrated for a set of fluorine-substituted thrombin inhibitors that C-F···C=O interactions can play a significant role in protein-ligand interactions and can lead to improved binding affinities.[48]

Despite the highly dipolar character of the C-F bond, fluorination of an organic compound generally results in an increased lipophilicity or hydrophobicity.[42] This may be because fluorine lowers the overall polarizability of a molecule and is itself a weak hydrogen bond acceptor. Furthermore, fluoroalkyl groups possess larger van der Waal volumes than their non-fluorinated analogues. This is described as polar hydrophobicity.[42] Thus, it can be a useful tool to improve the membrane permeability or receptor-ligand interactions.[49] However, it must be taken into account that fluorination does not always increase the hydrophobicity. While for fluorinated aromatic and olefinic compounds the hydrophobicity is increased in comparison to their hydrogen analogues, partial aliphatic fluorine substitution might actually reduce rather than increase hydrophobicity. An example for this is the terminal mono-, di- or trifluorination of an alkane due to the strong electron withdrawing capabilities of the fluorine.[19] Moreover, a critical number of fluorine atoms per alkyl chain is required to achieve the so-called hyper-hydrophobicity.[50] One reason for the extreme hydrophobicity of highly fluorinated aliphatic hydrocarbons is the low polarizability of fluorine. Due to that dispersive interactions with water and other hydrocarbons are disfavored. Therefore, perfluorinated compounds tend to segregate from both aqueous and hydrophobic environments to form a third, fluorous phase. This is referred to as the fluorous effect.[51]

There a today many marketed drugs containing one or more fluorine atoms, possessing increased pharmaceutical effectiveness due to this substitution, and thus underpinning the role of fluorine as a key element in drug design. Around one-third of the top-performing drugs that are currently on the market contain fluorine atoms in their structure,[28] and some examples of the small molecule top-selling, blockbuster drugs that contain this unique element are depicted in Figure 2.1.[30, 52-53]
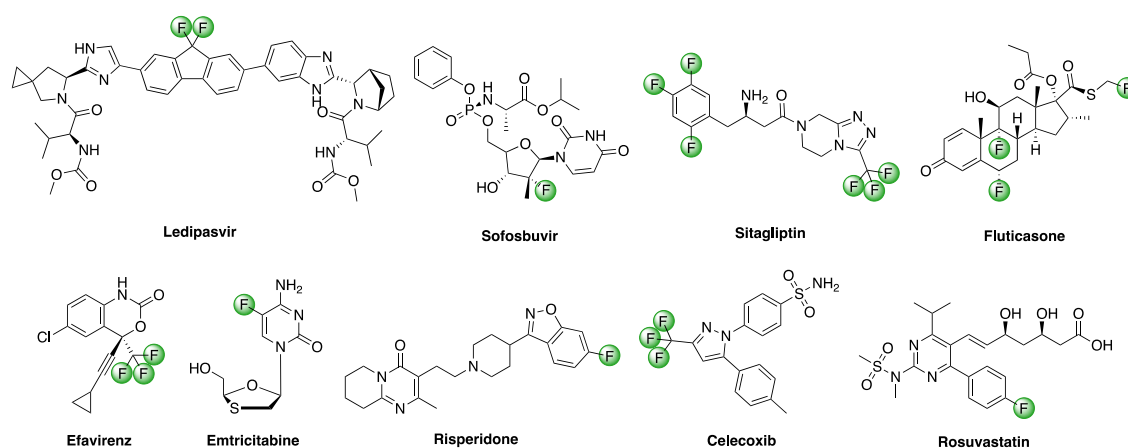
Figure 2.1: Fluorine containing drugs. Ledipasvir and Sofosbuvir are used in combination for treatment of hepatitis C. Sitagliptin is an oral antihyperglycemic for treatment of diabetes mellitus type 2. It inhibits the dipeptidyl peptidase IV (DPP-IV). Fluticasone is a synthetic glucocorticoid and an anti-inflammatory, anti-allergic, and immunosuppressive agent that find use, inter alia, in the treatment of asthma or chronic obstructive pulmonary disease. Efavirenz and Emtricitabine are antiretroviral medications used to treat and prevent HIV/AIDS. Efavirenz is a non-nucleoside reverse transcriptase inhibitor and Emtricitabine a nucleoside reverse transcriptase inhibitor. Risperidone is an antipsychotic drug and mainly used to treat schizophrenia or bipolar disorder. Celecoxib is an anti-inflammatory drug and used to treat the pain and inflammation of e.g. rheumatoid arthritis. Rosuvastatin is used to treat high cholesterol and related conditions, and to prevent cardiovascular disease.

To sum up, the described unique properties of fluorine made this element an attractive tool for medicinal chemists in the rational design of molecules with a beneficial reactivity and biological activity. Thus, with the introduction of fluorine atoms different physicochemical and pharmacokinetic properties of small, organic molecules can be altered:

(i) Metabolic stability

Oxidative metabolism by liver enzymes usually limits the bioavailability of compounds. Replacement of an oxidizable C-H group by a C-F group increases the metabolic stability, and thus bioavailability of a molecule by blocking metabolically labile sites.[20, 25]

(ii) Acidity/Basicity

If a fluorine substituent is introduced in proximity to a basic group, its basicity is reduced, which may result in an increased membrane permeability and improved bioavailability of a molecule.[20, 25]

(iii) Binding affinity

Fluorine substituents can modify the binding affinity of a drug candidate by alteration of pK_a values of adjacent groups or due to a direct interaction of fluorine.[20, 25]

(iv) Molecular conformation

Due to steric variations imposed upon fluorine substitution and fluorine's electronegativity, the preferred molecular conformation of a molecule can be altered.[20, 25] Electrostatic repulsive or attractive interactions of fluorine or a CF$_3$ group with other functional groups in a molecule lead to significant conformational changes.[28]

(v) Lipophilicity

For pass through the cell membrane the lipophilicity of a drug molecule needs to be as such that it can pass into the lipid core without becoming trapped in it. Using fluorine substituents the lipophilicity can be fine-tuned.[25]

Not only in medicinal chemistry but also for peptide engineering introduction of fluorine atoms or fluoroalkyl groups has emerged as a well-established strategy. Several groups took advantage of the described unique properties of fluorine to design peptides and proteins with superior properties over fully native sequences. Therefore, they introduced fluorinated amino acids into various peptide and protein sequences to investigate their influence on structure, activity, folding, and stability towards thermal and chemical denaturation.[21, 31-33] Such non-natural building blocks are of great interest for the development of highly potent pharmaceuticals and bio-inspired materials.[11, 54] Aspects regarding the influence of fluorine on the stability of peptides will be discussed in the next sections.

2.2 Fluorine's influence on stabilization and folding of coiled-coil structures

A full review on the impact of fluorinated amino acids on peptide and protein properties was published in 2012 by the Koksch group.[21] With regard to the fluorinated amino acids used in this thesis, the following section briefly summarizes the applications of fluorinated analogues of aliphatic amino acids such as leucine, isoleucine or valine with focus on coiled-coil structures.

2.2.1 The coiled-coil folding motif and its use as model structure

Isolated α-helices are only marginally stable in solution; thus they are stabilized in proteins by being packed together through hydrophobic side chains. These interactions are maximized within a helical interface, when the helices are being wound around each other in a superhelix, a so-called coiled-coil arrangement.[55] The coiled-coil structure was first postulated in the early 1950s by Crick and Pauling & Corey individually through investigation on α-keratin,[56-59] and is found to be one of the most abundant folding motifs in nature.[5] Approximately 3-5% of all amino acid residues in naturally occurring proteins form coiled-coil structures, as suggested by an analyses of various primary sequences.[60] Typically, α-helical coiled coils consist of two to five amphipathic right-handed α-helices wrapped around one another to form a left-handed supercoil,[61] but also seven-helix coiled-coil arrangements are reported.[62] The individual α-helical strands can thereby align in a parallel or antiparallel orientation to each other and the helices composing the supercoil can be identical (homotypic) or distinct (heterotypic).[4, 63-64] The simplest form is a dimeric α-helical coiled coil as depicted in Figure 2.2 A and B. Whereas regular α-helices possess 3.6 amino acids residues per turn, the distortion imposed upon each helix within

a left-handed coiled coil reduces this value to around 3.5 and allow the position of the side chains to repeat after two turns.[4, 61] This (pseudo-)repetitive sequence of seven amino acids, referred to as heptad repeat, is characteristic for coiled coils and usually denoted (a-b-c-d-e-f-g)$_n$ in one helix, and (a'-b'-c'-d'-e'-f'-g')$_n$ in the other.[65] These seven residues are usually depicted in a so-called helical wheel diagram, which gives the arrangement of the residues along the helical axis (Figure 2.2 D). The number of the heptads n can vary from two in designed coiled coils[66] to 200 in natural fibrous proteins.[67]
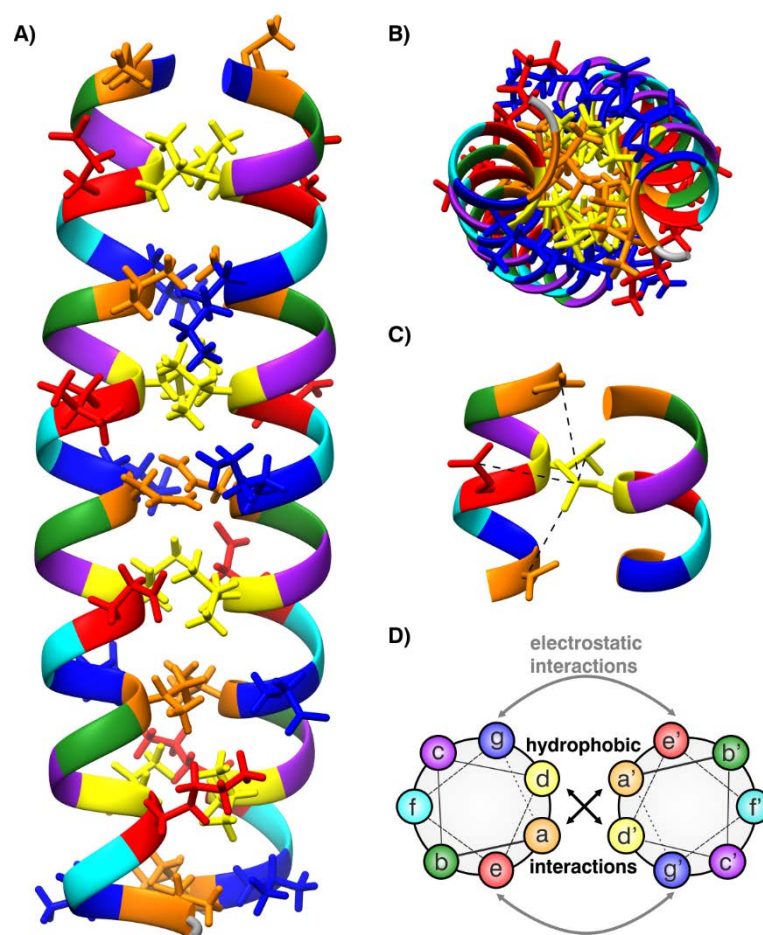
Figure 2.2: Structure of a classical coiled-coil dimer (PDB code: 2ZTA). **A)** Side view perpendicular to the superhelical axis, and **B)** top view along the superhelical axis. The backbone is represented by ribbons, side chains that make up the knobs-into-holes (KIH) interactions as sticks, and the heptad positions a-g colored separately. In this way, the hydrophobic core can be easily followed in orange and yellow. **C)** A single KIH interaction between a 'knob' from one helix (shown in yellow on the right helix) and a 'hole' formed by four residues on the other (left helix). **D)** Helical wheel diagram of a parallel coiled coil showing the different recognition motifs. Yellow and orange residues represent hydrophobic interactions, coulomb interactions occur between oppositely charged residues (marked in red and blue). (Adapted with permission from Testa *et. al.*[68] Copyright © 2008, Oxford University Press)

Positions **a** and **d** are typically occupied by hydrophobic residues, positions **e** and **g** by charged residues and positions **b**, **c** and **f** by polar or charged residues. Hydrophobic side chains such as Leu, Ile, Val, or Met at the **a**- and **d**-positions are located on one side of the helix. Thus, in aqueous solution, the α-helices of the coiled coil associate *via* hydrophobic and van der Waals interactions

to bury their hydrophobic surface area and form the so-called hydrophobic core.[61, 64] This provides the thermodynamic driving force for oligomerization. The side chains facilitate a tight knobs-into-holes (KIH) packing, first noted by Crick in 1953.[59] In this arrangement one residue (knob) fits into a space generated by four residues of the opposing helix (hole) (Figure 2.2 C). This hydrophobic core packing provides the thermodynamic driving force for the formation of α-helical coiled coils and is the dominant determinant for coiled-coil stability.[64] Charged residues such as Glu or Lys preferably populate the positions **e** and **g** of the heptad repeat, which flank the hydrophobic core. These residues can form interhelical electrostatic interactions that can be attractive or repulsive. Thereby they further contribute to the coiled-coil stability, folding specificity (parallel or antiparallel), pairing (homo- or heterotypic) and oligomerization (dimer, trimer, etc.).[69-78] If complementary charges in **e** and **g** positions are placed accordingly, the hetero- and orientation specificity in dimeric coiled-coils can be controlled (Figure 2.3).
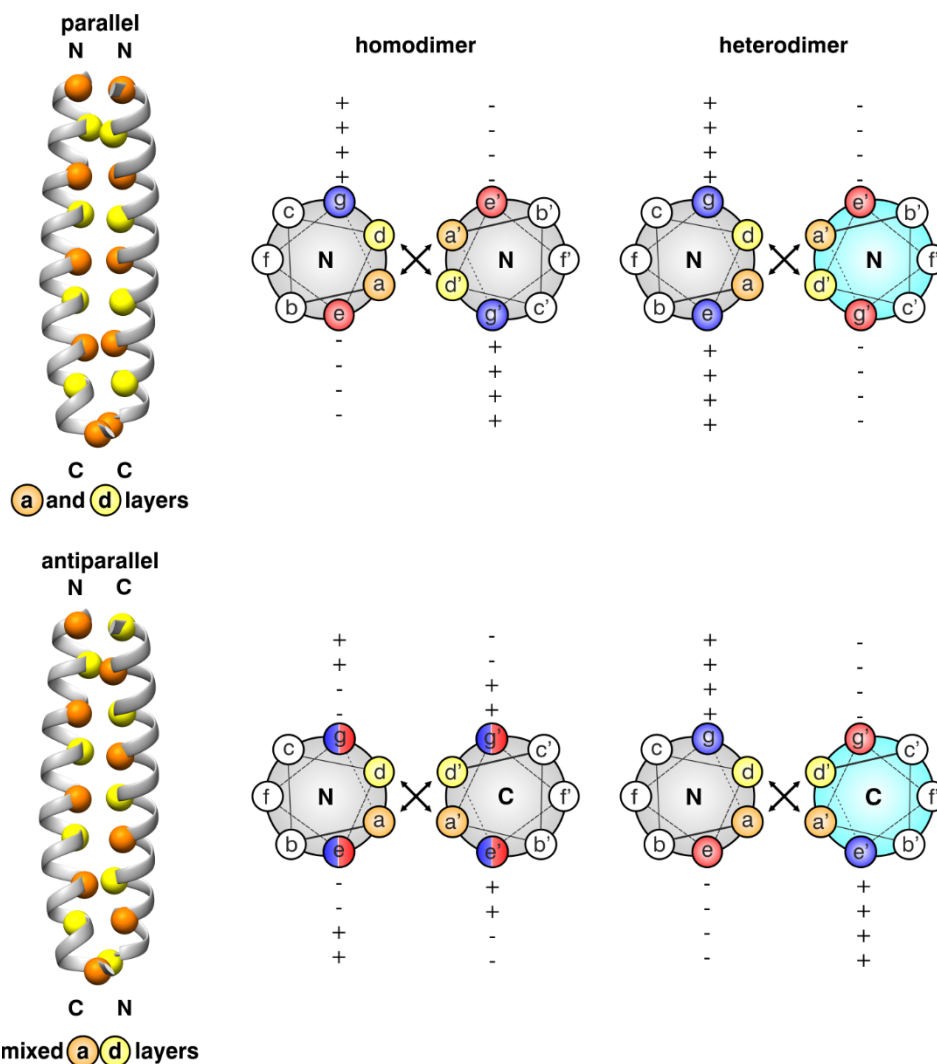
Figure 2.3: Orientation and homo/hetero specificity of coiled-coil assemblies specified by charge. N and C refer to the *N*- and *C*-termini of a peptide chain, respectively. Charge complementarity (matching oppositely charged side chains) of the e and g positions can generate different possibilities: parallel homodimer, parallel heterodimer, antiparallel homodimer, and antiparallel heterodimer. (Adapted from Yu,[64] Copyright © 2002, with permission from Elsevier)

The remaining heptad repeat positions **b**, **c** and **f** are solvent exposed and located at the opposite side of the hydrophobic core residues, so they are usually occupied by hydrophilic or charged residues. These residues mainly contribute to the solubility of the peptides, but are also able to stabilize a certain conformation of the α-helical coiled coil through the formation of salt-bridges.[79] These intramolecular ionic interactions occur between charged residues in the **c**- and **g**- or **b**- and **e**- positions.[77]

At the hydrophobic core of dimeric parallel coiled coil, is not only the type of residue important (hydrophobic, polar or charged), but also its placement in either **a**- or **d**-position. It was shown that β-branched hydrophobic residues like Ile and Val provide significantly greater stability to the coiled coil than the similarly sized γ-branched amino acid Leu, when placed in position **a**, whereas Leu appeared to provide more stability at position **d**.[80-82] These positional preferences arise from structural differences in the **a**- and **d**- positions. Two fundamentally different packing geometries occur in a dimeric parallel helix arrangement (Figure 2.4).[78] The side chains in an **a**-position show a structural geometry in which the Cα−Cβ bond vector of the amino acid side chain extends parallel to the Cα−Cα helix vector, so that the side chain points out of the hydrophobic core (*parallel packing*). In contrast, in position **d**, the Cα−Cβ side-chain vector extends perpendicular to the Cα−Cα helix vector and thus, directing the side chain into the core and directly towards the neighboring helix (*perpendicular packing*). As a consequence, hydrophobic β-branched amino acids are the most stabilizing amino acids in parallel packing arrangements, because they project the aliphatic hydrocarbon from the β-carbon atom directly into the helical interface, whereas perpendicular packing precludes β-branched residues from occupying these sites and γ-branched amino acids are favored.[83-84] In trimeric coiled coils also a third way of packing can occur. The Cα−Cβ bond vector of the amino acid side chain forms an acute angle (~ 50°) with the Cα−Cα helix vector (*acute packing*). This is why in this type of packing arrangement branched and unbranched residues are nearly equally represented and distributed evenly between the **a**- and **d**-positions.[85]
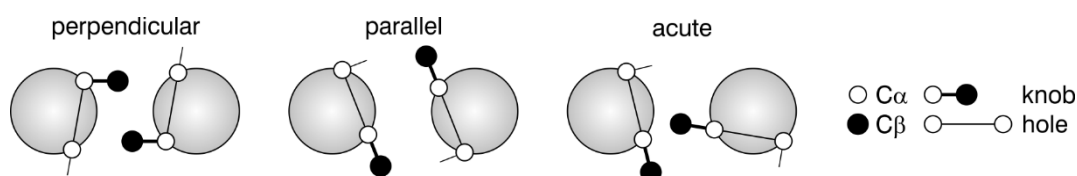
Figure 2.4: Schematic drawing of three types of knobs-into-holes packing geometries. The relative positions of the Cα–Cβ and Cα–Cα vectors for perpendicular, parallel, and acute knobs-into-holes packing are depicted. (From Harbury *et al.*,[86] Copyright © 1993. Adapted with permission from the American Association for the Advancement of Science)

Since in naturally occurring α-helical coiled-coil structures 80% of the **a**- and **d**-positions are occupied by hydrophobic amino acid residues, the hydrophobic packing appears to be crucial for the stability of the coiled coils.[69, 80] Through the incorporation of unnatural, strongly hydrophobic

amino acids in the **a**- and/or **d**- position, the stability may be increased even further.[87-88] However, the hydrophobic packing does not only influence coiled-coil stability but can also alter the structural specificity. For instance, Harbury *et al.* showed that the coiled-coil structure of GCN4 leucine zipper mutants can be either two-, three- or four-stranded depending on the positioning of Ile and Leu residues in **a** or **d** positions.[85-86] Another example was described by Monera *et al.*, who could switch a synthetic coiled coil from two-stranded to four-stranded upon the relative positions of Ala residues in the hydrophobic core.[89] Polar amino acid residues fill the other 20% of the hydrophobic interaction domain[69, 80] and contribute more to the structural specificity (orientation, heterospecificity and oligomerization) and less to the stability.[83-84, 90-91]

The coiled-coil structure has emerged as one of the most diverse proteins folds in nature and is involved in a wide variety of biological functions like membrane fusion, signal transduction, and solute transport.[92] These structures enable processes such as muscle contraction, transcription and metabolisms, and are part of membrane channels and molecular chaperones, which demonstrates the significance of such domains.[4-5, 64, 67] Examples are the transcription factor GCN4[93] or viral fusions proteins like the gp120/gp41protein complex of HIV-1[94], which is responsible for the entry of the virus into the host cell.

Due to the described structural simplicity and diverse biological functions, the coiled-coil folding motif evolved as excellent target in protein engineering, and with use of a small number of quantifiable principles a large structural and functional diversity can be achieved that are not possible with other *de novo* approaches.[4-5, 63-64, 92, 95] For example engineered coiled coils can be used for biosensor based applications and affinity chromatography,[96] as drug delivery system[64, 97] or as a model system to evaluate the impact of natural and non-natural amino acids in peptide structures, e.g. of fluorination on hydrophobic protein-protein interactions.[21] In that manner, the VPE/VPK-system was designed in the Koksch group to study the influence of fluorinated amino acids in different hydrophobic microenvironments.[79]

2.2.2 Globular substitution

Side-chain fluorinated analogues of aliphatic amino acids such as Ile, Leu and Val (Figure 2.5) are the most commonly used building blocks for peptide and protein modifications.[21, 31-33]
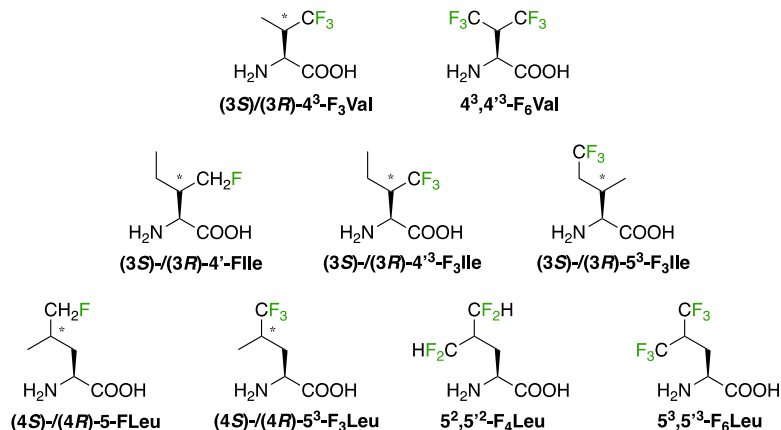

Figure 2.5: Side-chain fluorinated analogues of the aliphatic amino acids Val, Ile and Leu. The (2S)-form is depicted.

As described in Section 2.2.1, coiled-coil peptides constitute ideal and simple model systems for studying the impact of fluorination on protein-protein interactions. Since the coiled-coil formation is mainly driven by the hydrophobic effect, the substitution of residues at the **a**- and **d**-positions within the hydrophobic core by more hydrophobic fluorinated analogues might create highly stable coiled-coil peptides. Many reports indeed demonstrate the stabilization of such structures towards thermal and chemical denaturation when fluorine is globally introduced into the hydrophobic core.

   In the early 2000s Tang *et al.* incorporated 5,5,5-trifluoroleucine (5^3-F$_3$Leu) for Leu at all **d**-positions of a leucine-zipper peptide as equimolar mixture of the (2S,4S)- and (2S,4R)-diastereomers using *in vivo* techniques.[36] By modification of the leucyl-tRNA synthetase activity also the incorporation of 5,5,5,5',5',5'-hexafluoroleucine (5^3,$5'^3$-F$_6$Leu) was successful.[88] A maximum amount of 92% 5^3-F$_3$Leu substitution and 74% of 5^3,$5'^3$-F$_6$Leu substitution could be achieved.[36, 88] Analysis by circular dichroism (CD) and ultracentrifugation revealed no significant structural difference between the wild-type, non-fluorinated peptide and the 5^3-F$_3$Leu or 5^3,$5'^3$-F$_6$Leu containing version. Thermal and chemical unfolding studies showed that the fluorinated peptides are highly resistant to denaturation, with each 5^3-F$_3$Leu residue accounting for 0.4 kcal mol^{-1},[36] and each 5^3,$5'^3$-F$_6$Leu for 0.6 kcal mol^{-1} of stabilization.[88] An increase of 13°C in the melting temperature T_M was observed when three fluorine atoms were introduced into the Leu side chain, as well as 2.5-fold increased amount of urea was needed for denaturation.[36] Adding three more fluorine atoms, enhanced the T_M further by 9°C and the peptide remained far from complete unfolding even in 8 M urea solution, which is explained by the increased hydrophobic character of the additional trifluoromethyl group and suggested a

correlation between stability and fluorine content.[88] In another study Tang *et al.* introduced the same mixture of 5^3-F$_3$Leu at all four **d**-position Leu residues of a dimeric *C*-terminal coiled-coil subdomain of the leucine-zipper peptide GCN4-p1, a naturally occurring transcription factor (Figure 2.6).[87] The authors also generated a fluorinated analogue of the full-length bZip transcriptional activation factor. Fluorine introduction retains the dimeric α-helical structure of the native peptides, and the fluorinated peptides furthermore exhibited remarkably enhanced thermal stabilities, higher resistances towards denaturation, with no loss in DNA-binding affinity observed. Molecular dynamics (MD) simulations determined that the coiled-coil binding energy is 55% more favorable upon fluorination and indicated that there might be a difference between the different isomers of 5^3-F$_3$Leu.
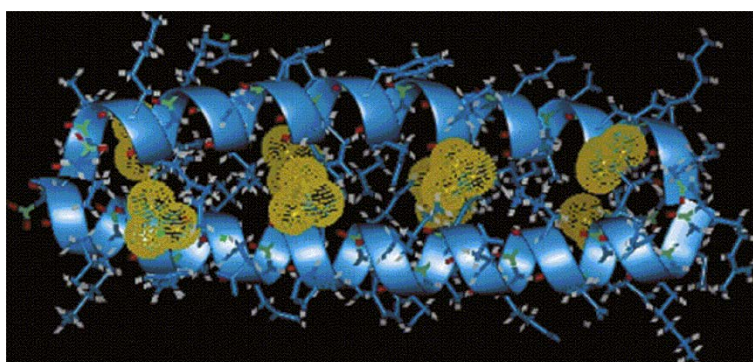
Figure 2.6: Structure of the GCN4-p1 dimer substituted with 5^3-F$_3$Leu at the four **d**-positions. The van der Waals radii of the fluorine atoms are depicted as yellow spheres. (Reprinted with permission from [87], Copyright © 2001 American Chemical Society.)

Kumar *et al.* synthesized a highly fluorinated analogue of the GCN4-p1 coiled-coil domain by incorporation of fluorinated amino acids in **a**- as well as in **d**-positions using solid phase synthesis.[98] Four Leu (**d**-positions) and three Val residues (**a**-positions) were replaced by 5^3-F$_3$Leu and 4,4,4-trifluorovaline (4^3-F$_3$Val) respectively. The amino acids were mixtures of (2*S*,4*S*)- and (2*S*,4*R*)-5^3-F$_3$Leu or (2*S*,3*S*)- and (2*S*,3*R*)-4^3-F$_3$Val. The single conserved Asn residue in **a**-position was retained to specify oligomerization and orientation.[71, 86, 99-100] As concluded by CD spectra, the fluorinated as well as the native peptide are α-helical, while the fluorinated analogue possesses a higher level of helicity.[98] In addition, both peptides form dimers as determined by sedimentation equilibrium experiments, suggesting that both 5^3-F$_3$Leu and 4^3-F$_3$Val residues are incorporated in the hydrophobic core with only minimal structural distortions. The fluorinated peptide is highly stable towards thermal denaturation, exhibiting a T$_M$ that is 15°C higher than that of the parent peptide with a hydrocarbon core. Interestingly, in comparison to the earlier studied analogue described by Tirrell and co-workers, in which only all **d**-positions were substituted with 5^3-F$_3$Leu, the thermal stabilization is almost equal.[87] The fully fluorinated variant was also slightly more stable towards denaturation by chaotropic reagents, and the free energy of unfolding was increased by approximately 1.0 kcal mol^{-1}.[98] The authors

concluded that the observed stabilization upon fluorine introduction can be explained by the segregation of the hydrophobic trifluoromethyl groups from aqueous solvent.

Since in the described studies diastereomeric mixtures of 5^3-F$_3$Leu were used, in a more recent report the enantiomerically pure (2*S*,4*S*)-and (2*S*,4*R*)-5^3-F$_3$Leu residues were incorporated separately into the **d**-positions of the coiled coil to investigate the effects of stereochemistry on coiled-coil peptide biosynthesis and stability.[101] Fluorination did not affect the secondary structure of the parent peptide, and no difference between the stereoisomers was detected. The peptides containing either (2*S*,4*S*)- and (2*S*,4*R*)-5^3-F$_3$Leu both stabilize the dimer to a similar extent, possessing a 10°C higher T$_M$ than that of the native, non-fluorinated analogue. In addition, a 1:1 mixture of the (2*S*,4*S*)- and (2*S*,4*R*)-5^3-F$_3$Leu substituted variants was investigated that exhibited an additional 3°C increase in T$_M$, which is identical to the earlier investigated dimer containing the diastereomeric mixture of 5^3-F$_3$Leu.[36] This result suggests that the fluorinated peptides form heterodimers rather than homodimers upon mixing. However, in this studies non-purified products and mixtures were used and the level of fluorinated amino acid incorporation was in the range of 90% only.[101]

The Tirrell group studied the influence of the Ile or Val replacement by either 5,5,5-trifluoroisoleucine (5^3-F$_3$Ile) or (2*S*,3*R*)-4^3-F$_3$Val, respectively, at the **a**-positions of coiled-coil peptides derived from GCN4 (Figure 2.7).[102] These peptides have been expressed in *E. coli* with extents of residue-specific incorporation of 90 and 88 %, respectively. Both CD and equilibrium sedimentation studies showed that the secondary and higher-order protein structure is maintained upon fluorine introduction. While the substitution of Ile for 5^3-F$_3$Ile yielded in an increase of 27°C in T$_M$, (2*S*,3*R*)-4^3-F$_3$Val accounted for an only 4°C higher T$_M$ compared to the Val containing peptide. A similar trend was observed for the stability towards chemical denaturation, where the free energy of unfolding was 2.1 kcal mol^{-1} higher for substitution of Ile for 5^3-F$_3$Ile, and only 0.3 kcal mol^{-1} higher when Val is replaced by (2*S*,3*R*)-4^3-F$_3$Val. Fluorination left the DNA-binding affinities and specificities unchanged compared to those of the respective non-fluorinated sequence, which is in agreement with the above described studies by Tang *et al.* on fluorinated variants of GCN4-p1.[87] It is suggested that the great difference in the enhancement in stability caused by 5^3-F$_3$Ile or (2*S*,3*R*)-4^3-F$_3$Val might arise from both entropic and packing effects. The steric bulk of the γ-CF$_3$ group presumably leads to steric clashes with the helix backbone, resulting in loss of side-chain entropy of Val, and thus a less pronounced stabilizing effect.[102]
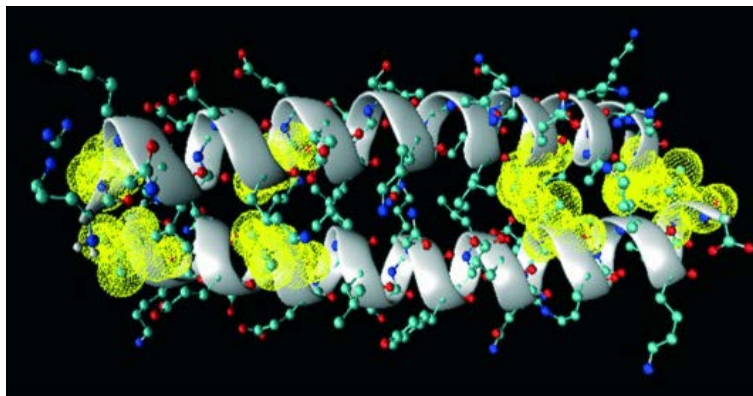
Figure 2.7: Schematic structure of the coiled-coil region of the zipper peptides based on the X-ray crystal structure of GCN4. The four **a**-positions are highlighted in yellow, and were mutated to either Ile or Val, and subsequently substituted by the fluorinated analogues 5^3-F$_3$Ile and $(2S,3R)$-4^3-F$_3$Val. The conserved Asn residue in the **a**-position of the third heptad repeat was retained in the design of all the peptides because of its crucial role in determining oligomerization state, orientation specificity, and the overall geometry of the coiled-coil assembly. (Taken from Son, Tanrikulu and Tirrell[102] with permission, Copyright © 2006, John Wiley and Sons)

Kumar and co-workers also designed a peptide H that forms a parallel homodimeric coiled-coil assembly, containing Leu at seven out of eight **a**- and **d**-positions. Subsequently, these Leu residues were replaced by $5^3,5^{'3}$-F$_6$Leu to gain a peptide that is referred to as F.[103-104] The peptides used contain an *N*-terminal Cys residue to enable dimer formation *via* a disulfide bond. A disulfide bound heterodimer of one $5^3,5^{'3}$-F$_6$Leu core peptide and one Leu core peptide HF was prepared and its preference for sorting into homodimers was examined by a disulfide-exchange assay. Within 30 min an apparent equilibrium was established with only 3% of the initial heterodimer remained in solution while the remaining peptides exclusively form HH and FF disulfide bridged homodimers (Figure 2.8). All three disulfide bonded dimers HH, FF and HF form α-helical structures, and the FF is remarkably more stable towards thermal and chemical denaturation than either the heterodimer HF or the hydrocarbon homodimer HH, which show comparable values. This stability of the FF assembly was suggested to be partly responsible for the observed preference for the formation of homodimers. Sedimentation equilibrium analysis revealed that the HH assembly is present as a monomer (one disulfide bonded species with two helices), whereas in the FF assembly two disulfide bound peptide dimers align into a putative four-helix bundle.[103] The interactions of fluorinated side chains with hydrocarbon side chains seem to be disfavored and contribute less to stability, which may be explained with the fluorous effect.
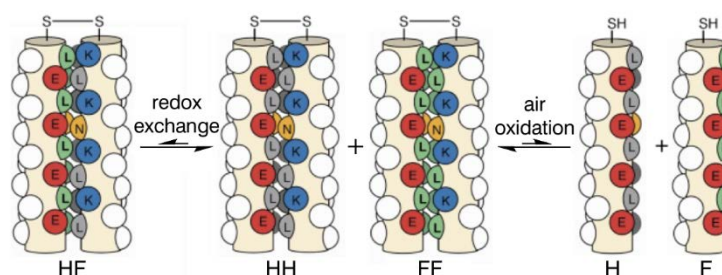
Figure 2.8: Self-sorting behavior of hydrocarbon- and fluorocarbon-core coiled-coil peptides. Covalently bound heterodimer HF undergoes disulfide exchange *via* monomeric peptides to yield covalently bound homodimers HH and FF in > 90% yield. Air oxidation of the individual thiol monomers H and F produces the same mixture. (Adapted from Yoder and Kumar,[105] with permission of the Royal Society of Chemistry, Copyright © 2002)

The Marsh lab developed a tetrameric, antiparallel coiled-coil model system α_4H with Leu in all **a**- and **d**-positions to systematically investigate the effects of Leu to $5^3,5'^3$-F_6Leu substitutions on the stability and structure of this system.[106-107] The hydrophobic core of this arrangement comprises six layers with four Leu residues, and either two, four or all six layers were packed with $5^3,5'^3$-F_6Leu, giving the peptides α_4F_2, α_4F_4 and α_4F_6 (Figure 2.9). It was shown that upon fluorine introduction the peptides retain their helical tetrameric structure as intended. NMR spectroscopic studies suggested that with an increasing degree of fluorination the peptides exhibit a more structured backbone. Furthermore, the free energy of unfolding increased by 0.3 kcal mol^{-1} per residue on introducing $5^3,5'^3$-F_6Leu at the central two layers. Interestingly, a smaller and almost linear increase by additional 0.12 kcal mol^{-1} for each $5^3,5'^3$-F_6Leu residue is observed when packing the further layers. Thus, α_4F_6 was observed to be ∼ 25% more stable than the non-fluorinated α_4H. Hence, it was suggested that the stabilization may be attributed to the highly hydrophobic nature of $5^3,5'^3$-F_6Leu rather than to specific fluorine-fluorine interactions between these residues within the hydrophobic core.

α_4F_2 α_4F_4 α_4F_6

Figure 2.9: Modeled structures of α_4F_2, α_4F_4 and α_4F_6 peptides showing the packing of $5^3,5'^3$-F_6Leu residues in the hydrophobic cores. The fluorinated side chains are highlighted in green. (Reprinted with permission from Lee *et al.*.[106] Copyright © 2006, American Chemical Society.)

More recent studies on the same system examined the effects of $5^3,5'^3$-F$_6$Leu introduction at different positions wit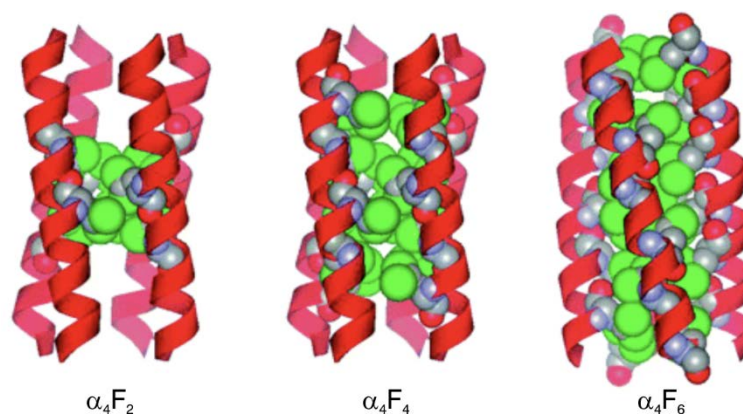hin the hydrophobic core.[108] It was reported that the stabilizing effect of $5^3,5'^3$-F$_6$Leu depends strongly on the positions at which this amino acid is incorporated, and the positioning $5^3,5'^3$-F$_6$Leu at all **a**-positions or all the **d**-positions of the hydrophobic core, thereby creating an alternating packing arrangement of Leu and $5^3,5'^3$-F$_6$Leu, was found to result in very stably folded proteins that exhibit even higher per-residue stabilization than proteins which hydrophobic cores are packed entirely with $5^3,5'^3$-F$_6$Leu. Thus, it was concluded that the fluorous effect does not appear to be primarily responsible for the self-segregating properties observed and rather efficient packing of the fluorous amino acid within the hydrophobic core seems to be a crucial factor for enhancing protein stability.

This suggestion was underpinned by high-resolution X-ray structures for different *de novo* designed α_4 peptides.[23-24] Analyzing the obtained data revealed that fluorinated amino acids are especially effective at stabilizing proteins because, although larger, they closely preserve the shape of the natural side chains they replace while increasing the buried hydrophobic surface area. Thus, this kind of residue is accommodated within a peptide or protein with only minimal structural perturbations. In addition, no evidence was found for the fluorous effect, meaning fluorinated residues form favorable contacts with each other, which is a commonly supported opinion of why fluorinated residues stabilize peptide structures. This means that the same principles that underpin the stability of natural proteins (efficient packing of side chains and conventional hydrophobic effects) seem to be responsible for the enhanced stability of fluorinated proteins.[24]

Pendley *et al.* performed MD simulations on highly fluorinated parallel coiled-coil heterodimer that contained $5^3,5'^3$-F$_6$Leu at all **d**-positions and showed that fluorination of Leu increases the stability of the helical interactions, thereby enhancing coiled-coil formation.[109]

To sum up, fluorination of the side chain of aliphatic canonical amino acids can significantly increase the stability of coiled-coil peptides and proteins towards thermal and chemical denaturation, while usually exerting only marginal structural disturbance. The extent of stabilization hereby depends on the identity of the fluorinated amino acid, the substitution position, as well as the degree of fluorination.

However, destabilizations are also observed for global substitutions with fluorinated amino acids. Panchenko *et al.* globally replaced all Leu residues in the enzyme chloramphenicol acetyltransferase (CAT) with 5^3-F$_3$Leu and found that this substitution results in a loss of thermal and chemical stability, although the enzyme activity is retained, and the secondary structure content greatly improved.[110] A reduced thermodynamic stability for this system was also described by others,[111] but it should be noted that CAT is a more complex globular protein.

Side-chain fluorinated aromatic amino acids resulted in either an increased or a decreased stability depending on the substitution position, and degree of fluorination. Whereas

pentafluorophenylalanine is usually destabilizing,[112] the highly but not fully fluorinated analogue tetrafluorophenylalanine was found to exert a large stabilizing effect.[113] Such fluorinated Phe residues are of special interest, because they differ significantly in their electrostatic potential from the hydrocarbon analogue, resulting in altered electrostatic interactions or stacking modes. That might be used to fine-tune protein folding and stability. Taking advantage of these types of interactions protein structures are usually found to be stabilized (*vide infra*, see Section 2.3).

2.2.3 Single substitutions

The above described studies focus on the effects of multiple or global substitutions of amino acids by their highly fluorinated analogues, and in the applied coiled-coil systems the fluorinated amino acids usually interact with each other.

In contrast, the Koksch group designed dimeric coiled-coil models, in which single substitutions are carried out in only one strand, thus the fluorinated side chain exclusively interacts with non-fluorinated side chain so that the influence of fluorination can be investigated in a native polypeptide environment.[79, 114-115] For this purpose, fluorinated analogues of 2-aminobutanoic acid (Abu) were applied (Figure 2.10).
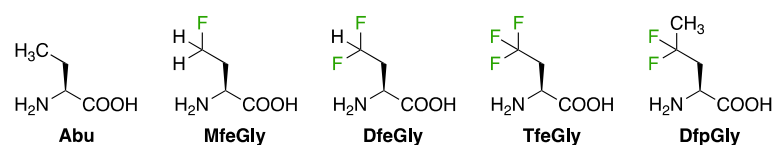
Figure 2.10: Non-canonical amino acids used for single substitutions within the hydrophobic core of a coiled-coil dimer: Abu and its analogues MfeGly, DfeGly, and TfeGly as well as DfpGly. The (2*S*)-configuration is depicted.

In a first study, (2*S*)-difluoroethylglycine (DfeGly) and (2*S*)-trifluoroethylglycine (TfeGly) were incorporated individually at either position 9 within the hydrophobic core or position 8 within the charged surface of a 41 amino acid peptide sequence, that was synthesized *via* thioester-mediated chemical ligation.[114] The developed peptide consists of five full heptad repeats and is able to act autocatalytically in templating its own synthesis by accelerating the thioester-promoted amide-bond formation. It folds into an antiparallel coiled-coil homodimer,[116] and this antiparallel orientation ensures that the fluorinated building blocks exclusively interact with native amino acid residues in defined positions at the opposing helix, which are Glu29 in the charged surface and Leu30, Leu33, combined with Leu37 for the hydrophobic core. The different synthesized peptides were investigated for their coiled-coil peptide formation and stability.[114] The T_M values were lowered by 5.0-19.5°C upon introduction of DfeGly or TfeGly with the most pronounced impact when the Leu residue in position 9 is replaced. Furthermore, it was observed that both fluorinated amino acids result in a strong retardation of the self-replication rate relative to the control sequence. However, it could be shown that the screens used in this study were sensitive enough to detect even the difference of one single fluorine atom within the coiled-coil assembly.

In a second study, this library was extended by (2*S*)-4,4-difluoropropylglycine (DfpGly) and the non-fluorinated analogue Abu for comparison.[115] This allows for a systematic study of fluorine's impact in regard to side-chain length and degree of fluorine substitution. As observed before, all substitutions of Leu9 in the hydrophobic core strongly destabilize the coiled coil towards thermal denaturation compared to the native sequence, lowering the T_M significantly by 14.9-22.3°C. Interestingly, stepwise introduction of fluorine atoms of the Abu side chain slightly increases the T_M, where the effect for the DfeGly analogue is only small with a 0.4°C enhanced T_M compared the Abu analogue, while the peptide bearing one more fluorine atom possesses a 5°C increased thermal stability. A further enlargement due to the incorporation of DfpGly however led to a dramatic decreased stability, suggesting that the polarization of hydrogen atoms in the neighboring alkyl groups upon fluorine introduction drastically disturbs an efficient packing within the hydrophobic core. The replacement of Lys8 in contrast showed a lower impact on the thermal stability, reducing the T_M by only maximal 5.6°C. This was explained by the loss of the stabilizing Lys8-Glu29 salt bridge. In this case all fluorinated peptides show comparable thermal stabilities that are even slightly decreased compared to the Abu containing variant.
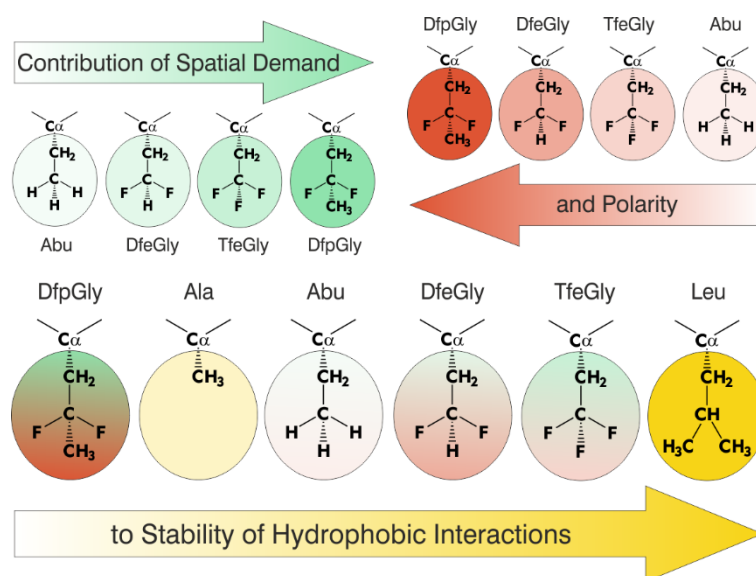
Figure 2.11: Influence of polarity and spatial demand of different fluoroalkyl groups on stability of hydrophobic domains of a coiled-coil peptide. (Adapted with permission from reference [115]. Copyright © 2006, John Wiley and Sons)

In a more recent study, a rationally designed parallel heterodimeric coiled-coil peptide system, referred to as VPE/VPK, was used to evaluate the impact of fluorinated amino acid substitutions within different hydrophobic protein microenvironments.[79] Therefore, different peptide variants were synthesized that contain amino acids with variable fluorine content in either position **a**16 or **d**19 of the VPK strain within the hydrophobic core. Here, also DfeGly, TfeGly, and DfpGly were used, and the non-fluorinated Abu residue was included for comparison. Later the introduction of (2*S*)-4-monofluoroethylglycine (MfeGly) was reported as well.[117] This allowed for the

determination of the influence of a gradual increase on the fluorine content, and thus size and hydrophobicity of the side chain, on the coiled-coil stability.

Structural analysis by CD spectroscopy, FRET, and analytical ultracentrifugation of equimolar mixtures of VPE with the different VPK analogues indicated that all form stable α-helical structures, while maintaining the dimeric oligomerization state and suggest that the substitution of Leu19 or Val16 by Abu and its fluorinated analogues only causes minor structural perturbations.[79, 117] However, in both substitution positions Abu and its fluorinated analogues considerably decreased the thermodynamic stability of the coiled-coil when compared to the analogue containing only the canonical amino acids. This effect of the fluorine substitution was shown to be position dependent, and the substitution at position **a**16 seemed to be less tolerated than substitution at position **d**19. While at the central **a**16 position the stability of the coiled-coil dimer increases with the size of the side chain (DfpGly > TfeGly > DfeGly > MfeGly), such a correlation could not be detected when these residues were incorporated at the central **d**19 position. The result for DfpGly is somewhat contrary to the result for the antiparallel coiled-coil system described before, where this residue was found to disturb folding the strongest when positioned an **a**-position.[114-115] The findings obtained for the VPE/VPK system were related to the different packing characteristics and relative orientation of the side chains in **a**- and **d**-positions within the parallel coiled coil.[79, 117] Figure 2.12 illustrates these different packings at the two substitution positions exemplarily for TfeGly. In position **d**19 the highly polarized β-methylene group of the studied fluorinated amino acids points towards the interacting hydrophobic groups in the opposing VPE strand. In position **a**16 the bulk of the side chains is exposed and the β-methylene groups are turned away from the hydrophobic core. Therefore, the fluorine-induced polarity has a stronger destabilizing effect at **d**-positions, while at **a**-positions the side-chain volume is the crucial factor for coiled-coil stability.
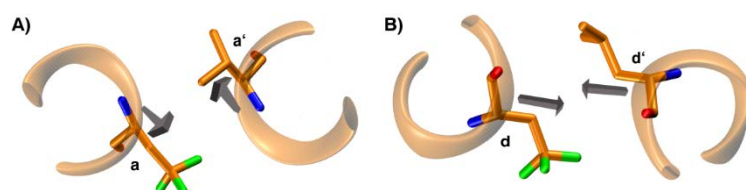
Figure 2.12: Depiction of the different packing and orientation of TfeGly against the direct interaction partners at **A)** position **a**16 and **B)** position **d**19 according to MD simulations. The Cβ atoms of the interacting side chains are closer in **d**- than in **a**-position. The gray arrows display the Cα–Cβ vectors. (Adapted with permission from Salwiczek *et al*.,[79] Copyright © 2009 Wiley-VCH Verlag GmbH & Co. KGaA, Weinheim)

To conclude, single amino acid substitutions with different small, fluorinated Abu analogues within the hydrophobic core usually lead to a destabilization of coiled-coil dimers. The effect of the fluorine-induced polarity and degree of fluorination on the stability is hereby strongly dependent on the characteristics of the microenvironment at the certain substitution position.

Phage display studies recently showed that with the selection of preferred interaction partners of the fluoroalkyl-substituted amino acids evolved microenvironment can be created, which gave rise to increased thermal stabilities of coiled-coil systems.[118-119] Thus, the destabilizing effect of fluorine introduction can be compensated if correct packing of the fluorinated residue is provided.

2.3   The impact of CH···π interactions on protein stability

Non-covalent interactions influence biomolecular interactions are important for essentially all cellular processes and are also responsible for the folding and stabilization of peptide and protein structures.[120-122] Despite interactions such as hydrogen bonds and salt bridges that are widely recognized and well-studied non-covalent interactions present in proteins, weak non-covalent interactions gradually gaining importance in recent years.[123] Among them are CH···π interactions that are ubiquitous in chemistry and biology[124] and found in different molecular systems including organic crystals, proteins and nucleic acids.[125] In proteins, many CH···π interactions involving side-chain π-systems are local, and either direct neighbors along the sequence or close neighbors in α-helices or β-turns have the tendency to form this kind of interactions,[121] but they can be found in almost any type of structural motif.[122] Most CH···π interactions hereby occur between amino acid residue side chains that are separated by nine or less residues in the sequence. They are energetically favorable and can contribute to the overall stability of proteins as well as of small molecules.[121-122] They are also known to play an important role in protein-ligand interactions,[126] carbohydrate-peptide recognition,[122, 127] and can even build up in whole networks.[122, 125] A substantial number of CH···π interactions is furthermore found in catalytic and ligand binding sites suggesting their possible role in maintaining active site geometry.[122, 125]

CH···π interactions are stable in both polar and non-polar solvents. The overall stabilization energy of about 0.5-1 kcal mol^{-1} per interaction is enough to make it a potentially important contributor to the overall protein stability, which is not more than a few kcal mol^{-1} itself.[121] More recent reports state that in typical CH···π hydrogen bonds involving aliphatic and aromatic CH-groups as the hydrogen donor and a C_6 aromatic ring as the CH-acceptor, the stabilization energy of a one unit CH···π hydrogen bond is ∼ 1.5–2.5 kcal mol^{-1}.[122, 127-128] The energy comes, essentially, from the dispersion force[124, 128] and the exact value depends on the nature of the participating molecular fragments, the CH donor and the π-acceptor groups.[122, 127-128] The stronger the proton donating ability of the CH group, the larger the stabilizing effect, meaning

that interactions involving aromatic CHs are usually stronger than the aliphatic ones.[127] Thus, the CH···π interactions are commonly classified as weak H-bonds.[121]

Screenings of the Protein Data Bank (PDB) revealed that CH···π interactions are most prominent formed between aromatic CH donor groups and aromatic π-acceptors and between aliphatic CH donor groups and aromatic π-acceptors.[121, 125] Among the studied cases, three quarters of the Trp-rings, half of the Phe and Tyr-rings and a quarter of the Hi-rings were found to serve as acceptors in CH···π interactions. Aromatic CH groups, but also the aliphatic side chains of amino acid residues Lys, Arg, Met and Pro preferably act as donors. This CH···π interactions are predominately found in the interior of the protein, however the more hydrophilic the participating groups are, the interactions were also found to be located closer to the surface.[121-122, 125]

As many CH···π interactions are observed between aromatic CH donor groups and aromatic π-acceptors,[129] aromatic-aromatic interactions in proteins were investigated in the recent years and in this regard also the impact of fluorination was investigated.[113, 130] Zheng *et al.* incorporated tetrafluorinated Phe residues into the villin headpiece subdomain HP35, a 35-residue α-helical protein, which features three interacting Phe residues in the hydrophobic core (Figure 2.13).[113] The HP35 domain enables solely edge-to-face interactions: H-4 of F6 packs against the phenyl ring of F17 and the H-6 of F10 packs against the π-cloud of F6. The used fluorinated Phe substituents exhibit an enhanced hydrophobicity in comparison to the native Phe and the remaining hydrogen has an increased partial positive charge.[113] The authors showed the HP35 variants bearing the tetrafluorinated Phe analogues exhibit increased thermal and thermodynamic stability, which was attributed to strengthened CH···π interactions. In contrast, the incorporation of the pentafluorophenylalanine weakens the protein stability, which is attributed to a potentially elimination of CH···π interactions.
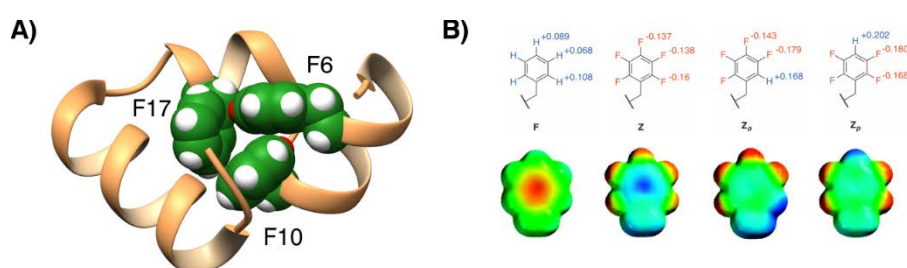
Figure 2.13: A) Structure of HP35 (PDB code: 1YRF) highlighting the interacting Phe residues (F6, F10, and F17) in the hydrophobic core in green. The hydrogen atoms engaging in CH···π interactions are highlighted in red. **B)** Structures and space-filling models of the Phe side chain and its fluorinated analogues showing the partial charges and electrostatic potentials. Negative electrostatic potentials are indicated in red, positive in blue. (Adapted with permission from Zheng *et al.*,[113] Copyright © 2009, American Chemical Society)

In 2012, Pace *et al.* used the model protein system α_2D, a 35 residue polypeptide originally designed by DeGrado and co-workers[131] to assess the energetic scale of CH$\cdots\pi$ contacts.[120] This peptide forms a dimeric four-helix bundle containing two stacked Phe-Phe pairs in the hydrophobic core (Figure 2.14).[131] The core was mutated in a way so that it comprises a phenyl and cyclohexyl pair. In this conformation, they are forced into a stacking conformation to favor CH$\cdots\pi$ interactions.[120] In addition, also a pentafluorophenylalanine moiety (Z) was incorporated. It was found that the CH$\cdots\pi$ contact between cyclohexylalanine (Cha) and phenylalanine (F) contributes -0.7 kcal mol^{-1} to the protein stability. In contrast, in the here described case the incorporation of pentafluorophenylalanine results in a much smaller change probably due to the absence of these favorable CH$\cdots\pi$ contacts.
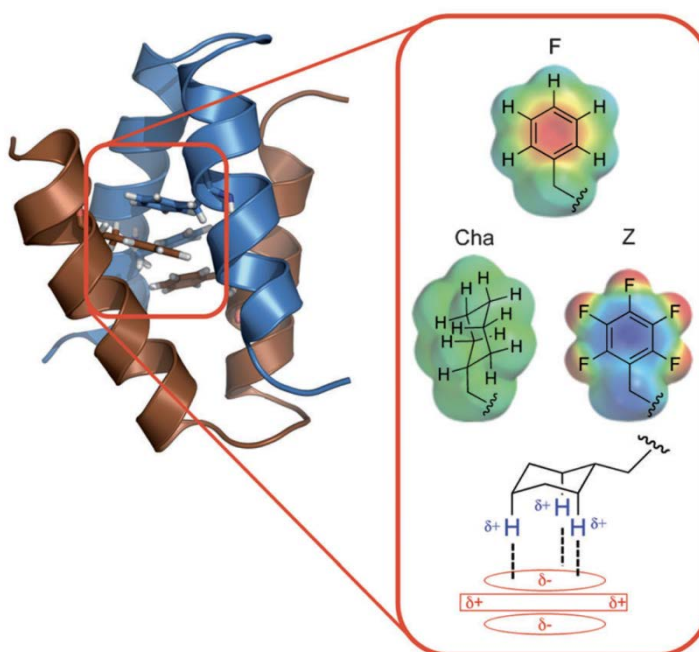
Figure 2.14: Dimeric structure of the α_2D peptide with the Phe residues as sticks (**left**). Electrostatic potential maps for F, Cha, and Z residues that highlight the distinct differences in electronics despite their similar size with electron-rich and electron-poor regions depicted in red or blue, respectively (**right**). The F-Cha stacking pair in the core of α_2D is illustrated was well, with the electron-rich π-cloud of F interacting with the partially positive hydrogen atoms of Cha. (Reproduced with permission from reference [120], Copyright © 2012, John Wiley and Sons)

Another recognition motif that plays a significant role in protein folding and protein-protein interactions is based on the stacking behavior of aromatic rings, often referred to as π-π interactions or quadrupole interactions. In this context, the tendency of aromatic and perfluoroaromatic molecules to associate with each other is focus of several reports.[130, 132-133]

Aromatic compounds such as benzene exhibit a negative potential at the π-face and a positive potential around the periphery.[133] This electron distribution is referred to as quadruple. On the contrary, perfluoroaromatic molecules possess a reversed quadruple with a negative potential on

the periphery and a positive potential on the aromatic ring. This might be attributed to the electron withdrawing effect of the fluorine atoms, which results in an electrostatic interaction between aromatic and perfluoroaromatic compounds that differ from the ones when only non-fluorinated aromatics are interacting with each other. The so obtained different preferred stacking modes (edge-face, offset-stacked or face-face) can be used to induce strong non-covalent and selective protein-protein interactions and to stabilize protein structures.[130, 132-133] These π-π stackings are not of crucial importance for the understandings of this dissertation and thus will not be discussed further.

The CH⋯π interactions between aliphatic CH-donors and aromatic π-acceptors are the most prominent class of this kind of interactions in protein structures.[121, 125] Besides Lys, Arg, Met and Pro side chains, common donors are both methyl groups of Leu and Val, but also other aliphatic amino acid residues like Ile and Ala are frequently found to engage in CH⋯π interactions. As stated before, interactions generally occur between direct neighbors, but within α-helices interactions with a distance of i and $i + 4$ are almost as often observed.[121, 125] However, the significance of aliphatic fluorinated amino acids as donors in such interactions within protein systems has been hardly explored so far. It is known, that the incorporation of fluorine results in a significant polarization of adjacent CH-bonds,[79] and the hydrophobicity of fluorinated aliphatic amino acids should be increased in comparison to their hydrocarbon analogues.[50, 134-136] In line with the studies on fluorinated aromatic amino acids by Gao and coworkers,[113, 120, 130, 132-133] the fluorination of aliphatic amino acids might also strengthen CH⋯π interactions and thus, protein stability might be increased. Hence, the influence of such interactions are probed within the scope of this doctoral thesis (see Section 5.4).
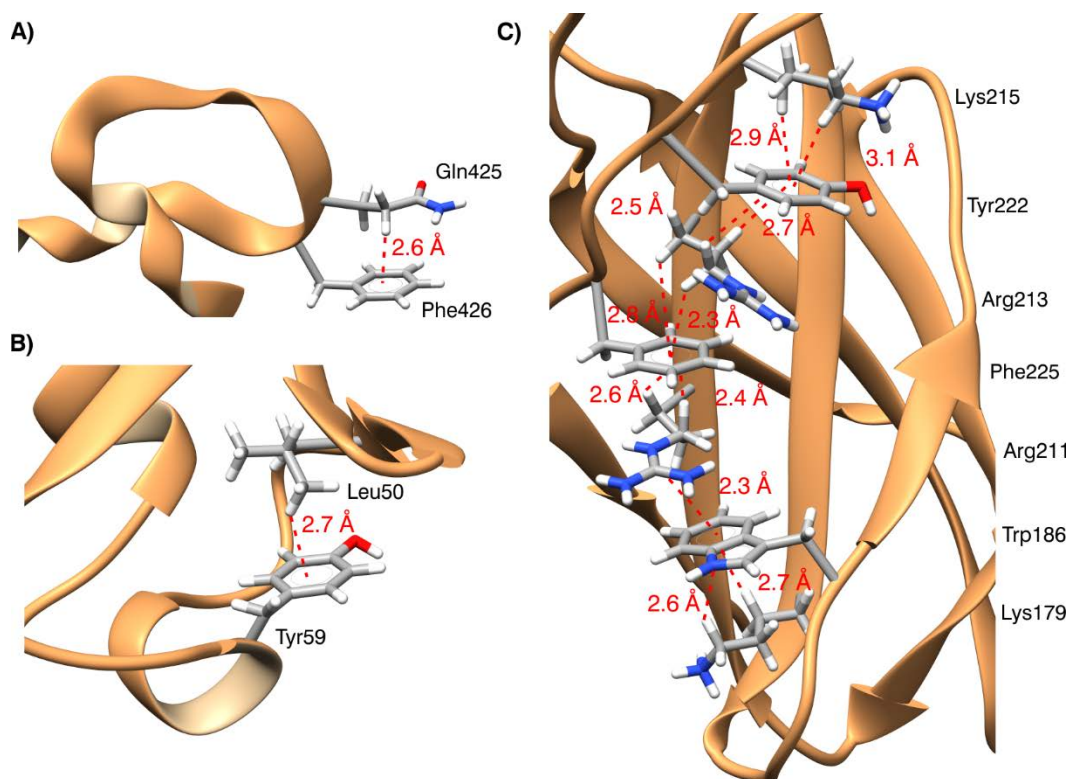
Figure 2.15: Examples of CH···π interaction with aliphatic CH-donors and aromatic π-acceptors. **A)** Interaction between Gln425 and Phe426 at the dimerization interface of the human cellular coagulation factor XIII (PDB code: 1F13).[137] **B)** CH···π hydrogen bond between methyl group of Leu50 and aromatic ring of Tyr59 in ubiquitin (PDB code: 1UBQ).[138] **C)** Multiple CH···π interactions found in the human growth hormone (PDB code: 3HHR). Lys179, Arg211, Arg213 and Lys215 are sandwiched by aromatic residues Trp186, Phe225, and Tyr222, and vice versa.[139]

2.4 Influence of fluorine on the proteolytic stability of peptides and proteins

Peptides show generally excellent specificity and high affinity for recognizing and binding to their targets and are therefore desirable lead compounds in drug development. However, their application as drugs is limited due to several factors such as poor membrane permeability and a short half-life attributable in part to low stability in plasma, and sensitivity to proteases; resulting in low bioactivity and poor oral bioavailability.[12, 15-17, 140] Strategies to overcome these limitations, especially to prolong the half-life and enhance resistance towards proteases, include cyclization, stapling of peptide sequences, blockage of *C*- or *N*-terminal ends *via N*-acylation or *C*-amidation, PEGylation, but also the introduction of noncanonical amino acids such as D-amino acids, α- or *N*-methylated amino acids or β-amino acids.[15-17] Here, also fluorinated amino acids have found widespread application for improving the resistance of peptides towards proteolytic degradation. For instance, sterically constrained α-trifluoromethyl substituted amino acids that carry a CF$_3$ group instead of the Cα-proton of proteinogenic amino acids were investigated for their potential of peptide stability modification. Due to the incorporation of such amino acids, strong conformational restrictions are exerted on a peptide sequence and neighboring substituents

experience considerable polarization effects. Both factors usually resulted in an increased proteolytic stability of the substituted peptides, but advantageous interactions of the fluoroalkyl group with the particular enzyme's binding site observed in other cases, yielded in a more rapid digestion of the fluorinated substrate by the protease.[141-143]

A more frequently used class of fluorinated amino acids investigated in this purpose are canonical, aliphatic amino acids bearing the fluorine substituent in the side chain. Their impact on proteolytic stability was investigated for biologically active peptides and model systems, and the results are summarized in the next paragraphs.*

Biologically active peptides

5,5,5,5',5',5'-hexafluoroleucine ($5^3,5'^3$-F_6Leu) was used to improve the potency and proteolytic stability of potential therapeutic peptides.[144-146] Meng *et al.* reported the replacement of two or five different residues at the nonpolar face of the antimicrobial peptides buforin II (BII)[147] and magainin 2 amide (M2)[148] (Figure 2.16 A and B) by $5^3,5'^3$-F_6Leu, and analyzed the resulting fluorinated peptides for their resistance towards proteolytic cleavage by trypsin, and their antimicrobial and hemolytic activity.[144] Almost all of the fluorinated peptides displayed an 1.4- to 2.3-fold increased proteolytic stability towards trypsin compared to the non-fluorinated parent peptides. Only one fluorinated buforin variant was degraded at a slightly faster rate than the parent peptide, whereas the highly fluorinated magainin 2 peptide containing five $5^3,5'^3$-F_6Leu residues was extremely resistant. Over 78% of the whole-length peptide still remained in solution after 3 h. In contrast, the non-fluorinated magainin 2 is completely digested within 40 min. It is suggested that this observation can be attributed to the steric bulk of $5^3,5'^3$-F_6Leu, leading to a occlusion of the fluorinated substrates from the enzyme's active site.[144] Furthermore, some fluorinated peptide showed a different cleavage pattern compared to the non-fluorinated one, and fluorine introduction retained or even increased the antimicrobial activity.
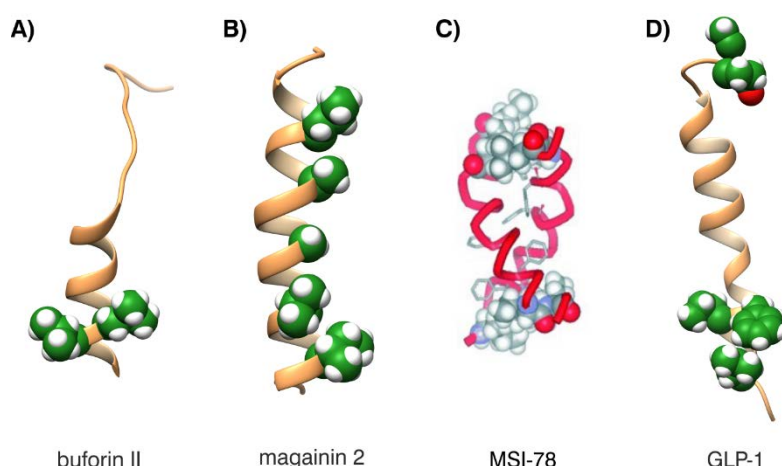
Figure 2.16: Structures and sites of fluorination of different biologically active peptides. **A)** Buforin II series: Leu18 and 19 were substituted with $5^3,5'^3$-F$_6$Leu (PDB code: 2RVQ). **B)** Magainin 2 series: sites of fluorination are residues Leu6, Ala9, Ala13, Val17, and Ile20 (PDB code: 2MAG). **C)** MSI-78 dimer structure with Leu and Ile residues. **D)** GLP-1: Ala8, Glu9, Gly10, Phe28, Ile29, Leu32 were replaced by $5^3,5'^3$-F$_6$Leu (PDB code: 1D0R). (The structure of MSI-78 is reproduced with permission from Gottler *et al*.,[146] Copyright © 2008 WILEY-VCH Verlag GmbH & Co. KGaA, Weinheim)

Gottler *et al.* introduced $5^3,5'^3$-F$_6$Leu into a synthetic analogue of magainin 2, named MSI-78 (Figure 2.16 C). The two Leu and Ile residues of the sequence were substituted with this highly fluorinated amino acid to produce a peptide referred to as fluorogainin-1. Both peptides were then compared for their antimicrobial and hemolytic activity, and proteolytic stability towards trypsin, and chymotrypsin.[146] Neither of the peptide showed any hemolytic activity, while fluorogainin-1 maintained the broad-spectrum antibiotic activity. MSI-78 and its fluorinated analogue were unstructured in the absence of liposomes, whereas in their presence the peptides possessed an α-helical conformation.[146] Interestingly, the incorporation of $5^3,5'^3$-F$_6$Leu residues only protects the resulting peptide almost completely against proteolysis by trypsin and chymotrypsin in the presence of liposomes. Whereas MSI-78 was fully degraded within 30 min, fluorogainin-1 remained intact even after 10 h. In contrast, the fluorous peptide was as rapidly degraded as the nonfluorinated control in the absence of a membrane environment. These findings are in contrast to the observations made for buforin II and magainin 2 described above,[144] where fluorination results in an improved proteolytic stability even in the absence of a membrane. Thus, it is suggested that $5^3,5'^3$-F$_6$Leu introduction itself is not the solely factor responsible for prevention of proteolysis.[146] Here, the interaction of the fluorinated peptide with the membrane rather accounts for the observed resistance, attributable to a formation of a more stable coiled-coil dimer.[146, 149]

The glucagon-like-peptide-1 GLP-1[7-36] (Figure 2.16 D) is a promising therapeutic for treatment of diabetes mellitus type 2, but unfortunately the rapid digestion ($t_{1/2} \approx 2$ min) by the serine dipeptidyl peptidase IV (DPP IV) limits its application substantially.[150-152] Thus, $5^3,5'^3$-F$_6$Leu was site-specifically incorporated into this peptide at positions adjacent to the cleavage site for proteolysis (Ala8-Glu9) with the aim to improve the resistance towards DPP IV.

Furthermore, a double substituted mutant was synthesized, as well as variants containing $5^3,5^{'3}$-F$_6$Leu at the *N*-terminal site of GLP-1 to adjust its binding affinity to the corresponding receptor GLP-1R.[145] The authors showed that the fluorination did not result in structural perturbation as these peptides adopt secondary structures similar to the native GLP-1. It was demonstrated that the substitution of the hydrophobic positions 8, 9 and 10 adjacent to the cleavage site can lead to a complete resistance towards DPP IV digestion. For some sequences no digestion products could be detected even after 24 h. In addition, fluorine introduction left the cleavage site between residues 8 and 9 unchanged.[145]

To summarize, using the highly fluorinated, aliphatic amino acid $5^3,5^{'3}$-F$_6$Leu therapeutically valuable peptides can be generated that display higher proteolytic stability while retaining their activity. Furthermore, the obtained results indicate that large hydrophobic side chains such as that of $5^3,5^{'3}$-F$_6$Leu are well tolerated at different positions within a peptide.

Another extensively fluorinated amino acid that was used to improve proteolytic stability of therapeutically valuable peptides is 4,4,4,4',4',4'-hexafuorovaline. In the 1980s the group Marshall showed that the incorporation of this amino acid at different positions of the angiotensin II peptide enhances the resistance of the gained fluorinated analogues towards proteolytic degradation by the enzymes carboxypeptidase A, hog renal acylase, and α-chymotrypsin.[153-154] Angiotensin II plays an important role in blood pressure regulation and was recently approved by the U. S. Food and Drug Administration (FDA) as a vasoconstrictor for the treatment of low blood pressure resulting from septic shock.[155-156]

Model peptides

$5^3,5^{'3}$-F$_6$Leu was furthermore applied for investigations on the impact of fluorination on the stability of an *de novo* designed model 4-α-helix bundle α$_4$H (Figure 2.17).[157] The Leu residues in the hydrophobic core (three **a**- and three **d**-positions) of this peptide were entirely packed with $5^3,5^{'3}$-F$_6$Leu to produce an extensively fluorinated analogue referred to as α$_4$F$_6$. Both peptides were compared for their ability to resist proteolytic degradation and unfolding by fluorinated and nonfluorinated solvents. α$_4$F$_6$ is more stable towards unfolding by organic solvents than α$_4$H, and ^{19}F-NMR studies demonstrated that this peptide does not exhibit a self-segregating behavior as assumed by the fluorous effect. Although both peptides have several potential cleavage sites for either chymotrypsin or trypsin, α$_4$F$_6$ resists proteolysis by these proteases much better than α$_4$H. The latter was almost completely digested already after 15 min when incubated with trypsin, and in the case of chymotrypsin within 2 h. In contrast, less than 50% of the full-length α$_4$F$_6$ were digested by trypsin after 110 min, and hardly any degradation was detected by chymotrypsin. This is somewhat surprising as introduction of 48 trifluoromethyl groups in α$_4$F$_6$ can be considered quite an extreme modification, also regarding the fact that the side chain of $5^3,5^{'3}$-F$_6$Leu is ~ 30% (32 Å^3) larger than that of Leu[24]. The observed differences might be explained by the greater

hydrophobicity of $5^3,5'^3$-F$_6$Leu,[135] leading to an increased thermodynamic stability of the fluorinated peptide α_4F$_6$ compared to the non-fluorinated parent peptide α_4H, rather than the fluorous effect, or the inability of proteases to accommodate fluorinated substrates.[157] Such thermodynamic stabilizations upon a global substitution of the hydrophobic core of a protein were described previously.[88, 104, 107]
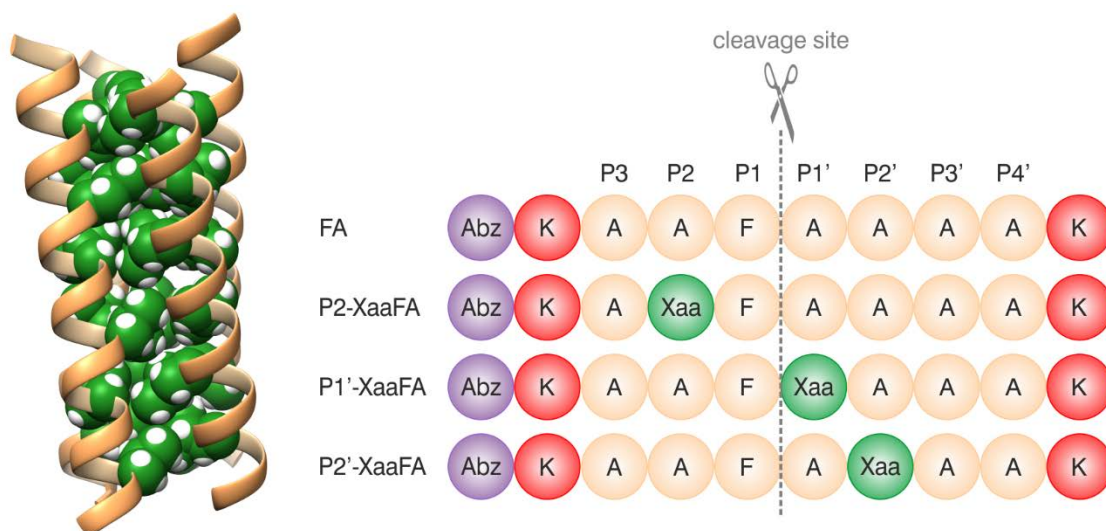
Figure 2.17: Left: Tetrameric structure of α_4H (PDB code: 3TWE). Leu residues are marked in green and were globally substituted with $5^3,5'^3$-F$_6$Leu. **Right:** Primary structures of FA peptide library. Positions are named according to Schechter and Berger nomenclature.[158] Substitution positions Xaa are marked green; with Xaa = Abu, DfeGly, or TfeGly.

The described experiments of fluorine substitution in biologically active peptides suggested that highly fluorinated amino acids such as $5^3,5'^3$-F$_6$Leu generally improve the proteolytic stability rather than reduce it, as there are only a few examples of the latter case.

In order to verify whether small, aliphatic fluorinated amino acids can also enhance the proteolytic stability of peptides, the Koksch group performed systematic studies with the help of a model peptide library.[159-160] Therefore, a model peptide FA was designed that consists of 10 amino acid residues and comprises the substrate specificities of different serine and aspartate proteases. The fluorinated analogues of (*S*)-2-aminobutanoic acid (Abu), 2-amino-4,4-difluorobutanoic acid (DfeGly) and 2-amino-4,4,4-trifluorobutanoic acid (TfeGly), were individually incorporated at the P2, P1', or P2' positions located adjacent to the cleavage site and substitute an Ala residue of the native sequence (Figure 2.17). Comparison to the corresponding peptides containing the hydrocarbon analogue Abu enabled the distinction between the effects resulting from either steric or electronic effects. The proteolytic stability of the resulting peptide library was investigated towards human blood plasma and elastase[159], as well as α-chymotrypsin and pepsin[160] and evaluated using an analytical RP-HPLC assay with fluorescence detection, and cleavage sites were identified by ESI-ToF analysis.

The influence of fluorination on plasma half-lives was observed to be position dependent. While fluorinated Abu analogues in P2 position maintained or decreased the half-life up to 2.3-fold, the substitution of the P1' position resulted in a 1.7- to 2.1-fold increased stability compared to the hydrocarbon analogue Abu. In the case of the P2' substituted peptides, however, fluorination either improved or decreased the half-life of the peptide depending on the fluorine content. In the case of incubation with isolated elastase, this phenomenon was observed for the fluorine substitution in P2, and P1'. Here, incorporation of TfeGly results in an increase in stability whereas DfeGly leads to decreased stability compared to the peptide containing Abu. Noteworthy, the TfeGly containing peptides showed almost completely resistance, only up to 7.5% were degraded after 120 min incubation. The opposite is observed for the impact of fluorination in P2' position. Here, introducing DfeGly slightly increased the stability of the resulting peptide, whereas TfeGly produced a peptide less resistant towards digestion by elastase.[159]

In a second study, these peptides were exposed to α-chymotrypsin and pepsin.[160] When incubated with α-chymotrypsin, fluorine introduction reduced the rate of hydrolysis compared to the corresponding Abu analogue in only one case, that is when DfeGly is positioned in the P2 position of FA. Here, the resistance towards α-chymotrypsin hydrolysis was enhanced by a factor of ~ 2.5. All other fluorinated peptides of this library were more prone to hydrolysis by α-chymotrypsin. The observations made for the P2' substitution correlate with the increase in hydrophobicity for the fluorinated Abu analogues,[50] underpinning the hydrophobic character of the S2' subsite of the enzyme.[161-162] For pepsin digestion the observed effects are different, here TfeGly is able to protect the peptide against digestion in all substitution positions when compared to the non-fluorinated peptide containing Abu in the respective positions. On the contrary, DfeGly effectively stabilized the peptide against pepsin only in P2'. Remarkably, pepsin seems to disfavor the fluorinated side chain in P2' position, as only up to 5% of the peptides are digested within 120 min.[160]

In brief, a significant increase in proteolytic stability towards either α-chymotrypsin or pepsin was observed in only half of the investigated cases. A remarkably increased resistance with a greater than 50% gain in stability was shown for two cases: fluorination at P2' in the context of pepsin digestion.[160] These systematic studies revealed that the impact of fluorine on the proteolytic stability depends on the particular enzyme, the position of the substitution relative to the cleavage site and the fluorine content of the side chain. Moreover small, aliphatic fluorinated amino acids significantly increase the proteolytic stability only in a few cases.

Aromatic, side-chain fluorinated amino acids

In addition to the aliphatic, fluorinated amino acids derivatives, also aromatic fluorinated amino acids have been the subject of studies regarding their impact on peptide proteolysis. These were mainly performed in the context of globular proteins,[163-164] but these class of amino acids found also use in small peptides to modulate stability and potency.[165-167] In this cases, neither a global nor a single substitution with aromatic, fluorinated amino acids is able to increase stability of a globular protein or small peptide towards different proteases, but rather the stability is maintained or reduced. This is in huge contrast to the observations made for highly fluorinated and bulky fluorinated amino acids like $5^3,5'^3$-F$_6$Leu described above that are able to protect a peptide from digestion by various proteases.

Nevertheless, the effect of incorporation of side-chain fluorinated amino acids on resistance towards proteolytic degradation cannot be generalized and is far from being predictable, and consequently needs to be studied always case-by-case. Depending upon the substitution position, the chemical nature and fluorine content of the amino acid side chain, as well as the particular protease used, the proteolytic stability of peptides and proteins can be modified in various ways. Even a single substitution with a minimally fluorinated amino acid bearing a small side chain can have a dramatic effect on proteolytic stability.

3.   HIV-1 and its entry into the host cell

The infection with the **h**uman **i**mmunodeficiency **v**irus (HIV) causes over time **a**cquired **i**mmuno**d**eficiency **s**yndrome (AIDS). The HIV infection leads to a progressive failure of the cellular immune function, and as a consequence AIDS is characterized by increased susceptibility to life-threatening opportunistic infections and a higher incidence of cancers.[9] Due to a global scale-up of antiretroviral therapy, with nowadays ~ 46% of HIV-1 infected people worldwide covered, annual deaths from AIDS-related causes have decreased by 48% from 2003 until 2016.[6-7] In **h**ighly **a**ctive **a**nti**r**etroviral **t**herapy (HAART), first introduced in 1995, three or four antiretroviral therapeutics are combined that target different stages of the retrovirus life-cycle (entry, reverse transcription, integration and maturation). Usually two nucleoside/nucleotide reverse transcriptase inhibitors (NRTI/NtRTI) are applied together with one protease inhibitor or a non-nucleoside reverse transcriptase inhibitor (NNRTI).[9, 168] These drugs can stop ~ 99% of viral replication, changing HIV infection from a deadly to a chronic disease.

Although HAART is generally effective in most patients, severe side effects, resistance development and high costs restrict its efficacy considerably.[9, 168-176] Moreover, there were more than 1.8 million new cases of HIV-1 infection diagnosed worldwide in 2016, which means about 5000 new infections each day.[6-7] Hence, there is still need for further expanding treatment and identifying new drugs that could enhance the efficiency of HAART. Elucidation of the whole machinery underlying the entry process has provided insights into a new type of drugs, which block HIV entry.[168] Such inhibitors of viral fusion target different receptors and proteins involved in the several stages of the entry mechanism (CCR5, CXCR4, gp120 and gp41) and are applicable in combined therapies or when resistance to other antiretroviral drugs appears.[168, 177-178] Moreover, since they act before the virus enters the cell, they could have the same pre-exposure prophylactic potential as vaccine-induced immunity.[169] In this context, especially the development of fusion inhibitors that target the gp41 region of HIV-1 gained widespread interest as gp41 directly mediates fusion of the viral with the host cell's membrane by formation of a 6-HB.[94, 176, 179-182] Aspects regarding this topic will be discussed in the following sections.

3.1   Entry mechanism of HIV-1

The structure of a human immunodeficiency virus (HIV) is depicted in Figure 3.1. For membrane fusion with a target cell only the HIV-1 envelope glycoprotein is required. It is initially generated as the fusion-incompetent precursor gp160, which is extensively glycosylated and proteolytic cleaved to generate two non-covalently associated subunits - a surface subunit gp120 and a transmembrane subunit gp41.[94, 179, 183]
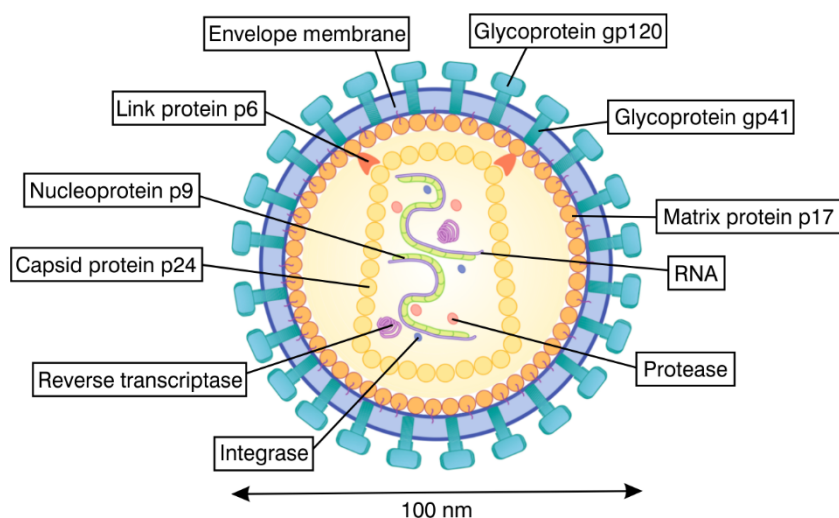
Figure 3.1: Structure of the human immunodeficiency virus (HIV) in cross section. The virus is surrounded by an envelope membrane in which the complex of the viral glycoproteins (gp120/gp41) is embedded. The viral capsid (core) with the genome is located in the interior. It contains two copies of single stranded RNA, which interact with the viral nucleoproteins to form the nucleocapsids, and the viral enzymes protease, reverse transcriptase and integrase. The link protein connects the capsid with the membrane. (Adapted from Löffler.[184] Copyright © 2008, Springer Medizin Verlag, Heidelberg)

The process of HIV entry into the host cell can be divided into three principal events (see Figure 3.2):[176]

(i)   Viral particle attachment to the host cell

(ii) Binding to a seven-transmembrane chemokine co-receptor

(iii) Fusion of the viral and cellular membranes

The entry of HIV into the target cell is initiated by attachment of the envelope glycoprotein gp120 to the cellular receptor CD4 on the target cell surface. Thus, HIV preferably infects cells with strong CD4 expression such as helper T cells and macrophages. The binding to CD4 initiates a structural rearrangement in gp120, leading to the formation and exposure of the co-receptor binding site. In humans, CCR5 or CXCR4, both seven-transmembrane proteins of the chemokine receptor family, act as co-receptors. The co-receptor binding induces further conformational changes in gp120 that result in the exposure of the gp41 and its insertion into the host cellular membrane, leading to viral entry.[94, 176, 179, 183, 185-186]
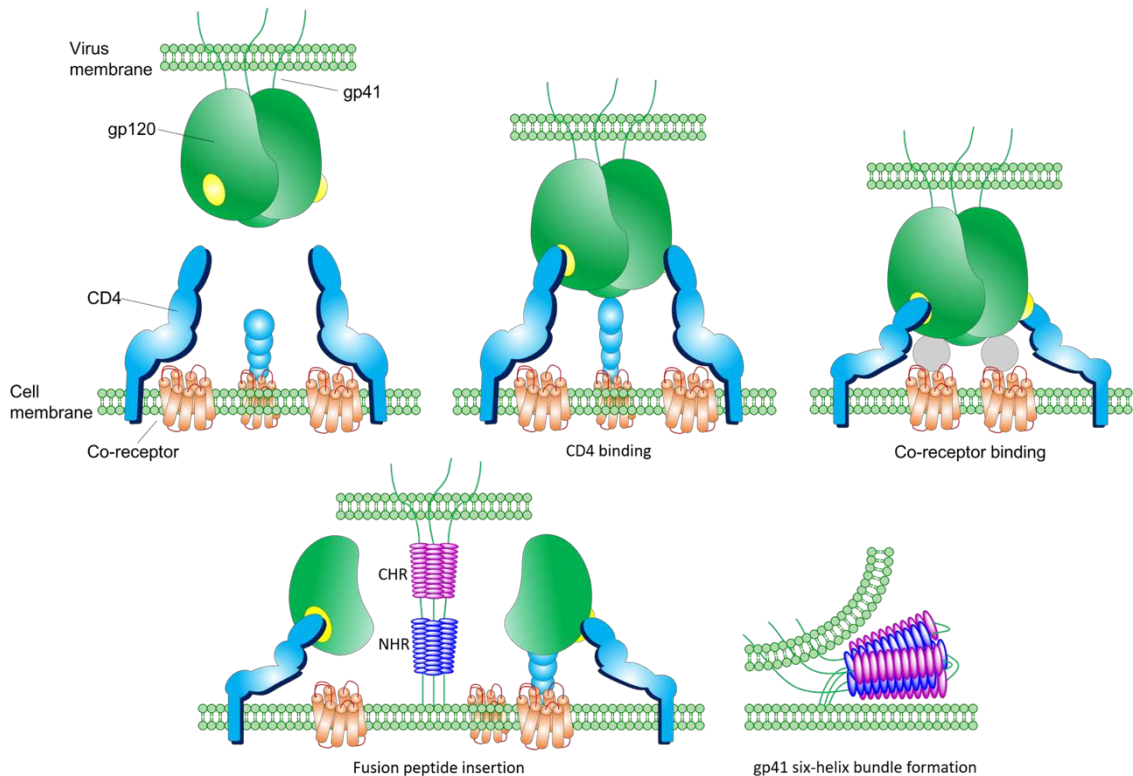
Figure 3.2: Mechanism of HIV entry. HIV entry begins with the attachment of the envelope glycoprotein gp120 to a CD4 molecule (binding site for CD4 is shown in yellow) on a target cell. Binding to CD4 induces conformational changes in gp120 which exposes the V3 loop and co-receptor binding site (gray). Engagement of these CD4-induced epitopes with the chemokine co-receptors initiates further rearrangements leading to the uncovering of the gp41 fusion peptide. Once exposed, the fusion peptide inserts into the host cell membrane leading to destabilization of the lipid bilayer. The *N*-terminal (blue) and *C*-terminal (purple) helices of gp41 form a hairpin structure by folding onto each other, thereby creating a stable six-helix bundle. This leads to the approximation of viral and cellular membranes, which results in membrane fusion. (Adapted with permission from Esté and Telenti,[187] Copyright © 2007 Elsevier Ltd.)

Current models suggest that upon interaction of gp41's amino terminus, referred to as fusion peptide, with the target cell's membrane a pre-hairpin intermediate of gp41 is produced, that spans both viral and cellular membranes.[179, 186-188] This pre-hairpin intermediate then folds into a six-helix bundle (6-HB) core structure by interaction of the *N*-terminal and *C*-terminal heptad repeat regions (NHR and CHR, respectively) of gp41. The formation of this 6-HB presumably induces the membrane fusion as it brings the viral and host cell's membrane in close proximity. As a result, a fusion pore develops that grows rapidly.[176, 186, 189] It is assumed that several fusion proteins may act cooperatively for creation of this pore.[189-190] The viral capsid, containing the genome, is then able to pass through this pore and into the host cell cytoplasm. The 6-HB is extremely stable and probably represents the most thermodynamically favorable structure of gp41. It is likely that the free energy released during this bundle formation overcomes the unfavorable process of putting two phospholipid membranes into close proximity and promotes the pore growth.[179, 191-192]

As the 6-HB structure of gp41 is highly stable, it is unlikely to be disrupted. Therefore, and since it has a relatively long lifetime of several minutes, the pre-hairpin intermediate became an

attractive target for inhibitory peptides (see Section 3.3). Binding of peptides to this pre-hairpin structure inactivates gp41 and prevents its conversion to the fusion-active conformation.[179, 183, 193]

3.2 gp41's core structure

The gp41 subunit is a type I transmembrane protein composed of extracellular and transmembrane region, and a cytoplasmic tail.[176, 194] Its extracellular domain, also denoted as ectodomain, contains different functional regions - a hydrophobic, Gly-rich fusion peptide; an *N*-terminal heptad repeat (NHR) and a *C*-terminal heptad repeat (CHR) that are linked *via* a loop containing a disulfide bond and a Trp-rich region.[194] Over the last decades, several crystallographic studies were performed to determine the exact structure of HIV gp41.[94, 185, 188, 195] The NHR- and CHR-regions associate to form a complex, which was identified as a six-stranded helical bundle that presumably represents the core of the fusion-active state of gp41.[94] This bundle consists of three NHR-helices forming a central parallel, coiled-coil trimer. Three CHR-helices wrap around the outside of this central coiled-coil trimer in an antiparallel orientation (Figure 3.3 A).[94, 185] Thus, the 6-HB can also be described as a trimer of heterodimeric subunits or trimer-of-hairpins.[179]

The overall dimensions of this complex comprise a cylinder measuring ~ 35 Å in diameter and ~ 55 Å in height.[94] The residues at the **a**- and **d**-positions of the *N*-terminal heptad repeat are predominantly hydrophobic, but also a few buried polar interactions are present in the central trimer (Figure 3.3 B).[94] A comparison with the sequence of gp41 in SIV shows that these residues are highly conserved. The characteristic knobs-into-holes packing of coiled coils occurs where the NHR-trimer demonstrates exclusively "acute" packing geometry, similar to that found in the GCN4 isoleucine-zipper trimer.[85, 94]

Residues at the **a**- and **d**-positions of the CHR-derived peptide pack against residues at the **e**- and **g**-positions of the NHR-derived peptide, thereby stabilizing the CHR/NHR-complex through predominately hydrophobic interactions. The central coiled-coil NHR-trimer shows three grooves on its surface, referred to as hydrophobic pocket, where the CHR-helices pack into. The residues lining these grooves, as well as the residues that are projecting into it, are highly conserved as shown by comparison of the HIV-1 and SIV sequence (see Figure 3.3 B). Each groove on the surface of the NHR-trimer has a particularly deep cavity (~ 16 Å long, ~ 7 Å wide, and 5-6 Å deep) and accommodates three hydrophobic residues from the interacting CHR-sequence, Ile635, Trp631, and Trp628. These residues are crucial for stabilizing the helical hairpin structure of the gp41 ectodomain core. In addition to these extensive hydrophobic contacts within the cavity, a salt bridge between Lys574 of NHR and Asp632 of CHR seems also important for the NHR/CHR interaction.[94]
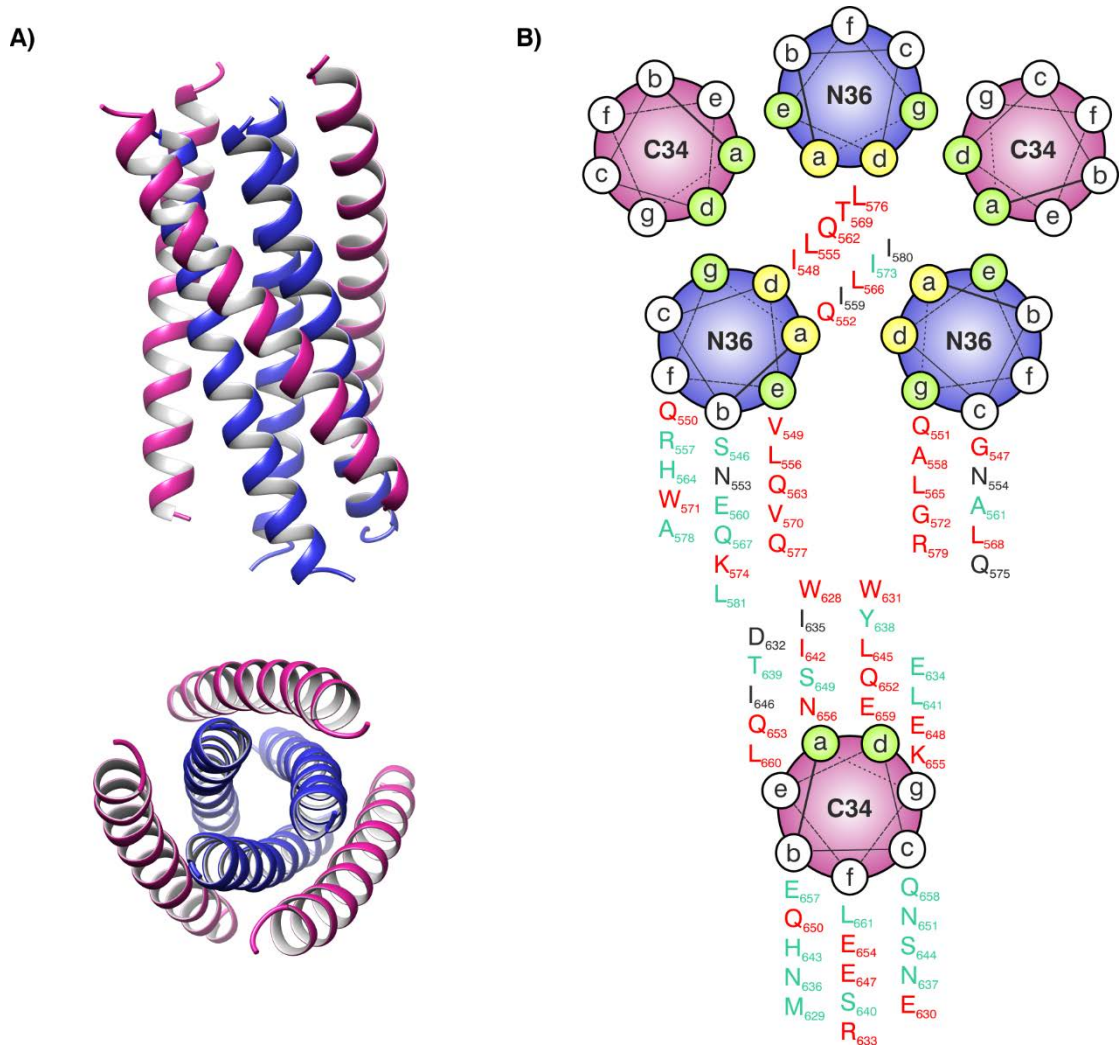
Figure 3.3: A) End-on view (top) and side view (bottom) of the N36/C34 complex of the HIV-1 gp41 six-helix bundle. N36 helices are depicted in blue, the C34 helices in purple. N36 and C34 are peptides derived from the NHR- and CHR-regions of gp41. The amino termini of the N36 helices point toward the top of the page, while those of the C34 helices point toward the bottom. The C34 helices are oblique orientated relative to N36. At the top of the complex, C34 is slightly tilted toward the left N36 helix, while at the bottom of the complex, it is slightly titled toward the right N36 helix. **B)** Helical wheel representation of N36 and C34. The view is from the top of the complex. The residues at each position are colored according to their conservation between HIV-1 (HXB2) and SIV (Mac239): red – identity; black – conservative change; turquoise-green – non-conservative change. The N36 helices interact through knobs-into-holes packing interactions at the **a**- and **d**-positions (colored yellow). Positions of the N36 and C34 helices that occupy the interhelical space between two N36 helices and one C34 helix are marked in green. (Adapted from reference [94], Copyright © 1997 Cell Press, with permission from Elsevier.)

An electrostatic potential map of the central NHR-coiled-coil trimer reveals that its surface is largely uncharged. The grooves responsible for interaction with the CHR-region are predominantly lined by hydrophobic residues, which probably lead to an aggregation of the NHR-peptides upon exposure to solvent. On the contrary, acidic residues on the outside of the CHR-peptide helices result in a much higher charged surface of the 6-HB complex. This explains the enhanced solubility of the heteromeric complex compared to the central coiled-coil trimer.[94]

3.3   Inhibition of cell fusion

As mentioned above gp41 initiates the fusion of HIV and its target cell. Several conformational rearrangements of this protein subunit are involved in the mechanism of cell fusion - a crucial step is the peptide-peptide interaction between the NHR- and CHR-regions forming a coiled-coil 6-HB. During formation of this structure, a pre-hairpin intermediate with a lifetime of many minutes occurs (see Chapter 3.1). Here, the NHR- and CHR-regions are not associated, thus making these regions an attractive target for the development of HIV fusion and entry inhibitors.[94, 179, 183, 193] Synthetic peptides derived from CHR or NHR can inhibit the formation of the fusion-active conformation, and thus, HIV-1 infection in a dominant-negative manner[179, 196-197] by binding to their respective counterpart regions in gp41 at this intermediate stage (Figure 3.4).
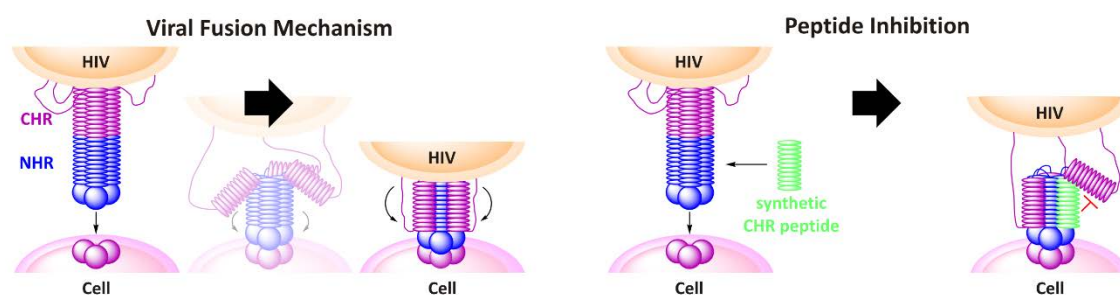
Figure 3.4: Schematic representation of the HIV-1 viral fusion mechanism and its disruption by a decoy CHR-helix shown in green. (Adapted from Bird *et al*.[13])

Since the early 1990s several synthetic peptides derived from the NHR- and CHR-regions of the HIV-1 envelope glycoprotein transmembrane unit gp41 were developed and shown to have potent anti-HIV activity. Most of the investigated fusion inhibitors are CHR-peptides due to their stronger inhibitory potency compared to NHR-peptides, which probably can be attributed to the tendency of NHR-derived sequences to aggregate.[179, 198] Among these, T20 (Fuzeon®, enfuvirtide) and C34 were extensively studied and possess low nanomolar antiretroviral activities.[94, 176, 178, 198-201] T20 is a 36 amino acid peptide and corresponds to the residues 638-673 of gp41 (Figure 3.5).[200] It does not include the pocket-binding sequence 628-635. However, the interaction of this pocket-binding domain (PBD) in the CHR with the pocket-forming domain in the NHR (amino acid residues 565-581) appears to be substantial for stabilization of the 6-HB. Residues Ile635, Trp631 and Trp628 of CHR have been shown to insert into the NHR-pocket making extensive hydrophobic contacts.[94, 193, 202] T20 furthermore contains a highly hydrophobic Trp-rich region at its *C*-terminus, which enables its binding to the lipid membrane of the host cell. Thus, the membrane might serve as a reservoir for the drug and renders the interaction with other segments of gp41 possible, accounting for its high anti-HIV activity.[203-204] C34, a 34 amino acid peptide comprising residues 628-661 of gp41 (Figure 3.5), contains in contrast to T20 the pocket-

binding sequence 628-635, so it can interact with the hydrophobic pocket of the NHR-trimer to form a stable 6-HB complex.[198]
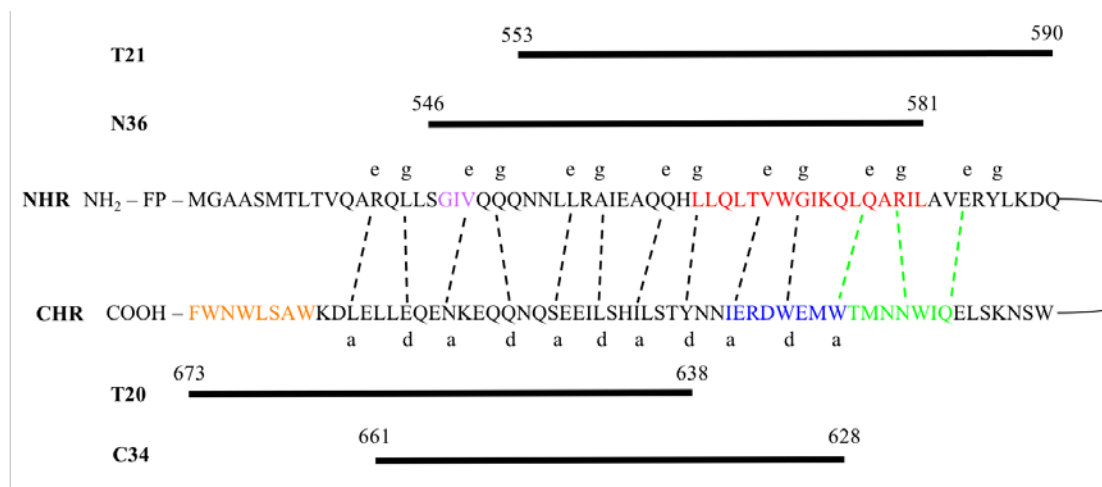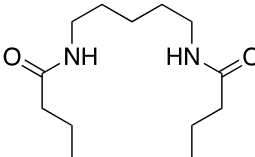
Figure 3.5: Sequence and interaction of the CHR- and NHR-region of gp41. Heptad repeats shown in black. Dashed lines between the NHR- and CHR-regions indicate the interaction between the residues located at the **e**-, **g**- and **a**-, **d**-positions in NHR and CHR, respectively. The interaction of the pocket-binding domain (PBD, in blue) in the CHR with the pocket-forming domain (in red) in the NHR is critical for 6-HB formation. Region immediately adjacent to the PBD (in green) is important for stabilization of the gp41 core structure. This motif may interact with the residues in the pocket-forming domain in the NHR and the downstream motif (AVERY) as shown by the dashed green lines.^{547}GIV^{549} motif (in purple) is responsible for development of drug resistance. The Trp-rich domain (in orange) has a tendency to bind to lipid membranes. The regions of peptides derived from the NHR- or CHR-region are shown above or below the sequence, respectively. (Adapted from He *et al.*)[199]

In 2003 T20 was approved as the first and currently only peptide-based HIV-1 fusion inhibitor used in clinic.[199, 205-207] Unfortunately, its application has been limited as acquired resistance is possible. The development of drug resistance can be attributed to mutations in a 10 amino acid region between residues 547 and 556 within the gp41 NHR-region that forms part of the binding site for T20, with the ^{547}GIV^{549} motif playing a predominant role.[194, 208-212] In addition, the manufacturing procedure of T20 is expensive and complex,[213-214] and *in vivo* proteolysis of T20 is rapid. The latter is limiting bioavailability and thus high subcutaneous injections with high dosages are required twice daily.[9, 13, 215] C34 displays both potent anti-HIV activity as well as reduced susceptibility to the evolution of resistant viruses. However, its poor solubility under physiological conditions might prevent its use as a promising drug candidate.[216] Therefore a new generation of fusion inhibitors with improved antiviral activity and pharmacokinetic profile needs to be developed.

Nearly all CHR-derived peptides reported to date correspond to residues 628-673 of gp41.[181-182, 194, 202] Especially the PBD (residues 628-635) is important for the inhibitory activity of CHR-derived peptides as the residues Trp628, Trp631, and Ile635 contribute substantially to the stability of the 6-HB.[193, 217-218] Moreover, salt bridges between Asp632 of CHR and Lys574 of NHR, as well as Ile642 are critical for viral entry and inhibition.[196, 217, 219-221] Thus, and due to the lack of the PBD in T20, C34 has been widely used as a template for engineering CHR-derived

fusion inhibitors with enhanced pharmacokinetics. Table 3.1 summarizes some of these peptides that possess potent antiretroviral activity, also against virus mutants resistant to T20 or C34.

Table 3.1: Examples of peptides derived from the CHR-region of gp41 that possess highly potent inhibitory activity against HIV-1 fusion.[181-182] Peptides are generally acetylated at the *N*-terminus and amidated at the *C*-terminus to enhance stability. Bold letters indicate substitutions for native residues, and lower-case letters indicate D-amino acids. The pocket-binding domain (PBD) residues are marked in red, and residues of the lipid-binding domain (LBD or MPER) are highlighted in blue.[181-182]

peptide	sequence	gp41 residues	references
T20, enfuvirtide	YTSLIHS LIEESQN QQEKNEQ ELLELDK WASLWNWF	638-673	[200-201]
C34	WMEWDRE INNYTSL IHSLIEE SQNQQEK NEQELL	628-661	[198]
MT-C34	MTWMEWD REINNYT SLIHSLI EESQNQQ EKNEQELL	626-661	[222]
C34M2	WMEWDRE INNYTSL IHSLIEE SQNQQeK NEkELL	628-661	[223]
C34M3	WeEWDRE INNYTSL IHSLIEE SQNQQeK NEkELL	628-661	[223]
sifuvirtide	SWETWER EIENYTR QIYRILE ESQEQQD RNERDLLE	117-115 a)	[224]
SJ-2176	EWDREIN NYTSLIH SLIEESQ NQQEKNE QEGGC	630-659	[225-226]
C43	INNYTSL IHSLIEE SQNQQEK NEQELLE LDKWASL WNWFNITN	635-677	[227]
C42	NNYTSLI HSLIEES QNQQEKN EQELLEL DKWASLW NWFNITN	636-677	[227]
SC34EK	WZEWDRK IEEYTKK IEELIKK SQEQQEK NEKELK (Z = Nle)	628-661	[228]
SC29EK	WEEWDKK IEEYTKK IEELIKK SEEQQKKN	628-656	[229]
MTSC22	MTWEEWD KKIEEYT KKIEELI KKS	626-649	[230-232]
HP23	EMTWEEW EKKIEEY TKKIEEI LK	625-647	[230-231]
CP621-652	QIWNNMT WMEWDRE INNYTSL IHSLIEE SQNQ	621-652	[194]
CP32M	VEWNEMT WMEWERE IENYTKL IYKILEE SQEQ	621-652	[199]
C14linkmid	 succinimide−MTWQEWDREIQNYT	626-639	[233]
T2635	TTWEAWD RAIAEYA ARIEALI RAAQEQQ EKNEAAL REL	626-663	[234-235]
T2544	MTWEAWD RAIAEYA ARIEALI RAAQEQQ EKNEAAL REL	626-663	[234]
T649	WMEWDRE INNYTSL IHSLIEE SQNQQEK NEQELLEL	628-663	[209, 236-237]
T1249	WQEWEQK ITALLEQ AQIQQEK NEYELQK LDKWASL WEWF	chimeric peptide b)	[178, 235, 238-240]

a) The numbering is according to the gp41 CHR-sequence of HIV-1 subtype E from which sifuvirtide is derived. b) T1249 is composed of sequences derived from HIV-1, HIV-2, and SIV and consists of a PBD, a truncated CHR-region and an LBD.

A key strategy used to improve anti-HIV activity of CHR-derived peptides is the introduction of salt-bridge structures, thereby creating electrostatically constrained peptides like SC34EK, SC29EK, T2635 and sifuvirtide (Table 3.1).[224, 228-229, 234] In such peptides, Glu and Lys pairs are placed in *i* and *i* + 4 positions at the solvent-accessible site of the helical bundle while the residues critical for the interaction with the NHR-region remain unchanged (Figure 3.6). The electrostatic

interactions introduced by Glu/Lys substitutions enhance the α-helicity and water solubility of the peptides. Moreover, a thermal stabilization of the CHR/NHR complex is usually observed.[216, 228-229] The increased α-helical structure is proposed to be a key factor for improving antiviral activity to a low nanomolar range.[228-229] Isolated CHR-derived peptides are generally unstructured in solution, while they adopt nearly full α-helical structures when interacting with the NHR to form a 6-HB.[233, 241] Due to the loss of entropy while generating a fixed helical structure out of an unstructured conformation, binding of CHR to the NHR-region exacts a large energetic penalty.[233] Hence, enhancing the helicity of the peptide fusion inhibitor may improve its antiretroviral potency by increasing its binding affinity to NHR.[216]
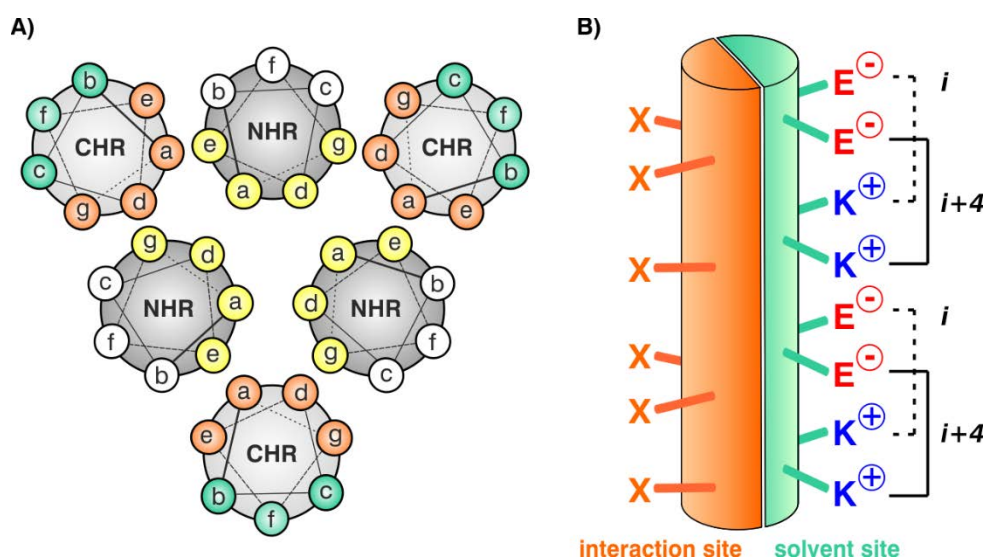
Figure 3.6: A) Helical wheel representation of the 6-HB structure. Amino acid residues at positions **a**, **d**, **e** and **g** of CHR interact with NHR. Residues in solvent-exposed positions of CHR are substituted with Glu or Lys to form salt-bridges. **B)** Design concept of incorporating the Glu/Lys motif at solvent-accessible sites. The α-helical CHR-peptide could be divided into interaction (orange) and solvent (turquoise green) sites. X indicates the original amino acids of the CHR-sequence. Only amino acid residues at solvent exposed positions are substituted with Glu or Lys at i and $i + 4$ position. (Adapted from Nishikawa *et al.*,[228] Copyright © 2009 with permission from Elsevier)

He *et al.* investigated the upstream sequence of the pocket-binding domain (PBD) in the CHR and found that the [621]QIWNNMT[627] motif, immediately adjacent to the PBD, is critical for the formation and stabilization of the gp41 6-HB core.[194] CHR-derived peptides containing this motif, e.g., CP621-652, showed high thermal stabilities and nanomolar anti-HIV activity in a dose-dependent manner, also against T20- and C34-resistant mutants, presumably due to the fact that they target different sequences of the gp41 NHR. As reported before, when positively or negatively charged residues (Lys or Glu, respectively) were introduced additionally at i and $i + 4$ positions into this peptide, promoting the formation of salt-bridges (peptide CP32M, Table 3.1), a much-improved antiviral activity against some T20-resistant viruses, with IC_{50} values in the picomolar range, was observed.[199] More recently, Chong *et al.* showed that Met628 and Thr627 of the [621]QIWNNMT[627] motif are key residues for HIV-1 entry and inhibition.[202] The researchers determined the high-resolution crystal structure of a peptide containing this domain complexed

by NHR and observed that [621]QIWNNMT[627] does not maintain a fully α-helical conformation. Instead, the Met628 and Thr627 form a unique hook-like structure referred to as M-T hook (Figure 3.7). This M-T hook is crucial for stabilizing the interaction between the pocket-binding residues from the CHR and the pocket region on the NHR-trimer. Mutation studies demonstrate that an absence of these hook residues significantly destabilizes the interaction of NHR- and CHR-peptides and reduce the anti-HIV activity of latter. By incorporating the M-T hook residues at the *N*-terminus of known CHR-derived peptides, like C34 or sifuvirtide, the binding affinity and thermostability of the 6-HB core could be enhanced, and these peptides exhibited significantly increased antiviral activity.[222, 242-244] This structure is furthermore promising to overcome drug resistance. Molecular dynamic simulations revealed that the increased affinity and stability of ligands with such a M-T hook structure can be attributed to the formation of more stable hydrogen bonds compared to ligands that do not possess this structural feature.[245]
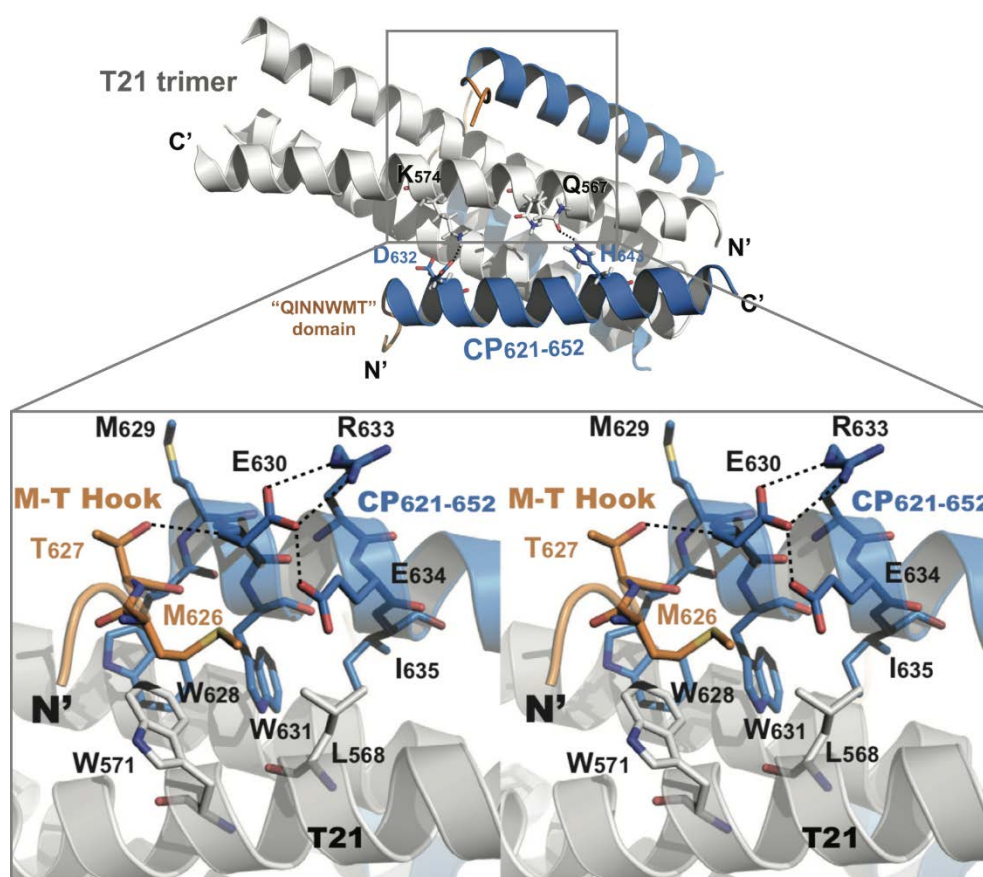
Figure 3.7: Structure of the 6-HB formed by CP621-652 and T21, derived from the CHR- and NHR-region of gp41, respectively (**top**). The T21 trimer is colored light gray, CP621-652 peptides are colored in marine blue, the [621]QIWNNMT[627] motifs of CP621-652 are highlighted in orange. Hydrogen bond interactions observed between Asp632 and Lys574, and between His643 and Gln567 are indicated by dashed lines. A portion of the above 6-HB structure is magnified in the gray box and is illustrated with a wall-eye stereo image. (**bottom**). Residues Thr627 and Met626 form a hook-like structure (highlighted in orange) that stabilizes the interaction between T21 and CP621-652. The Thr627 residue terminates the α-helical conformation of the *N*-terminus of the CP621-652 peptide. The hydroxyl group of the Thr627 side chain accepts a hydrogen bond from the NH-group of Glu630, directing the *N*-terminus of the CP621-652 peptide away from the T21 trimer. The side chain of Met626 caps the hydrophobic pocket on the T21 trimer. Dashed lines indicate the hydrogen bonds between the residues. (Adapted with permission from Chong *et al.*.[202] Copyright © 2012, The American Society for Biochemistry and Molecular Biology)

Gochin *et al.* found that both specific and non-specific interactions can form a basis for inhibitor affinity of CHR-derived peptides.[221] Classic effects such as electrostatic forces, specific van der Waals interactions, entropy, and amphiphilicity all seem to play key roles in binding. However, especially a negative net charge of - 2 or - 3 in combination with non-specific hydrophobic interactions and high helical content is crucial for the affinity of CHR and NHR and thus for the antiretroviral potency.[221] Besides that, the authors also examined the upstream region of the CHR-sequence and found that specific salt-bridges and hydrogen-bond networks may occur in following regions: Arg579 of the NHR could form intermolecular salt-bridges or hydrogen bonds to Glu620 and Asn624 of CHR, respectively, as well as an intramolecular hydrogen bond with Gln575. This underlines the findings of He *et al.* described above that an extended interaction site may be necessary to obtain low nanomolar inhibitory potencies.[194, 199]

Studies by the Gellman group furthermore suggest that the affinity between individual CHR-helices and the complementary groove in NHR depends upon interactions distributed across an extended protein interface.[246] Even though their results showed very high binding affinities within the hydrophobic pocket, also residues downstream (*C*-terminal) of the PBD contribute significantly to the stability of the six-helix assembly.

Peptide drugs have an intrinsic weakness due to rapid proteolysis and thus, limited bioavailability. Unnatural building blocks may be used to overcome this poor *in vivo* stability and might even lead to oral bioavailability. Bird *et al.* inserted backbone crosslinks, referred to as chemical staples, into HIV-1 fusion inhibitors T649 and T20 at *i* and *i* + 4-positions (schematic representation in Figure 3.8).[13] The stapled peptides exhibited improved antiviral activities even against T20 resistant strains and showed remarkable protease resistance. The latter can be attributed to the strengthening of the overall α-helical structure and complete blockage of peptide cleavage at the sites localized within or adjacent to the *i* and *i* + 4-crosslinked regions, which slows down the kinetics of proteolysis.
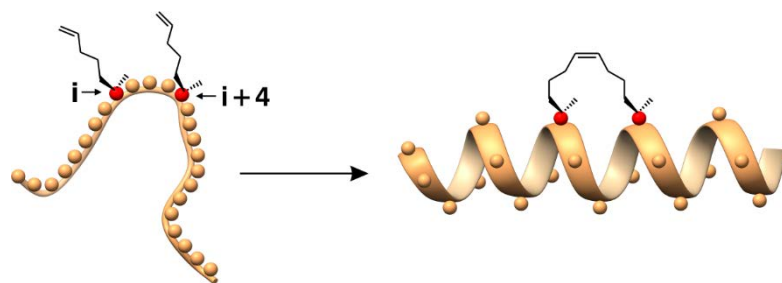
Figure 3.8: Schematic illustration of peptide stapling. α,α-Disubstituted non-natural amino acids containing olefinic side chains are incorporated at two or more *i* and *i* + 4 positions in the peptide chain. Crosslinking occurs by ruthenium-catalyzed ring-closing olefin metathesis, resulting in an increased helicity of the peptide. (From Walensky *et al.*.[247] Adapted with permission from American Association for the Advancement of Science, Copyright © 2004.)

A different chemical crosslink was introduced by the group of Kim to improve the inhibitory potency of short CHR-peptides, whose sequence corresponds to the HIV-1 gp41 residues 626-639.[233] A diaminoalkane crosslinker was used to stabilize the helical conformation of the peptide, yielding C14linkmid (Table 3.1). As expected, the peptides bind to the gp41 hydrophobic pocket and the short linear peptide showed no significant inhibitory activity, while the constrained peptide C14linkmid inhibited HIV fusion at micromolar potency. Additionally, the authors observed that not the peptides with the greatest α-helicity were the most potent inhibitors, but rather those that best balance the changes in binding enthalpy and entropy.

An alternative approach to enhance the resistance to proteolytic degradation is the substitution with D-amino acids. In 1999, Eckert *et al.* used mirror-image phage display to identify peptides composed of D-amino acids that are able to bind to the hydrophobic pocket of gp41 NHR.[197] These peptides additionally contain two Cys residues that form an intramolecular disulfide bond to create a cyclic structure. Therefore, they are practically insensitive to proteolytic digestion. Unfortunately, these D-peptides inhibit HIV-1 entry with only modest potency. Eight years later Welch *et al.* used the consensus sequence C**X₅**EW**X**WLC identified from the phage screen to discover D-peptide pocket-specific inhibitors of entry (PIE) with improved antiviral potency.[248] For this purpose, the researchers developed a constrained library in which the six **X** residues were randomized while the other consensus positions (underlined) were fixed. A family of D-peptides with enhanced potency was identified and surprisingly, the most potent D-peptides found were missing two of the randomized residues (C**X₃**EW**X**WLC). The best inhibitor among these proved to be ~ 15-fold more potent, and a trimeric version of this PIE showed an IC_{50} value of 250 pM, which means an 40,000-fold increase in antiviral potency compared to D-peptides previously reported by Eckert *et al.*. Bahraoui and co-workers site-specifically incorporated D-amino acids into C34, to yield peptides C34M2 and C34M3 containing either two or three D-residues, respectively (Table 3.1).[223] Both peptides are able to inhibit HIV-1 replication with an efficiency similar to that of the native C34 sequence, consisting of solely L-amino acids, while being more resistant to proteolytic degradation. In contrast, an all-D-amino acid containing C34 showed no antiviral activity.

All the results described demonstrate that D-peptides can form specific and high-affinity interactions with gp41.[223, 248] The non-natural D-amino acids are readily accommodated within a peptide sequence without altering its structure and judiciously placed, even only few D-residues may improve inhibitory activity. Unlike natural L-peptides, D-peptides are resistant to proteolytic digestion and have the potential for oral bioavailability, extended persistence in circulation and reduced immunogenicity.[248] Thus, such non-natural building blocks show considerable potential for the development of peptide-based highly potent anti-HIV-1 drugs and other therapeutic agents.[223, 248]

To summarize, several CHR-derived peptide sequences have been generated and those peptides with a length of 30 residues and longer are usually significantly more potent compared to short peptides and small molecules. This fact can be attributed to the large, shallow and hydrophobic intermolecular binding interface of the gp41 fusion complex.[13, 246] However, long peptides are not orally bioavailable and must be administered *via* injection. Furthermore, the length of peptide closely relates to difficulty and cost of its production, thus still making the development of short-peptide inhibitors attractive. Unfortunately, their low binding affinity and poor inhibitory potency creates an obstacle to the development of a small orally bioavailable HIV-1 entry inhibitor,[233] but in the last decade several short peptides with stabilized α-helical conformations and moderate inhibitory efficiency have been reported.[233, 249-250] Hence, the inability of CHR-derived peptide inhibitors to bind to the corresponding NHR-region cannot exclusively be attributed to their sequence length.

Taking all the above described findings into account, a CHR-derived peptide that includes the downstream as well as the upstream region of the PBD was previously designed in the Koksch group (Table 3.2).[251] Its ability to bind to the NHR-derived peptide T21 was investigated by CD spectroscopy and a *N*-PAGE experiment. Gained results suggest hetero-oligomerization and formation of a helical bundle. Moreover, the helical content as well as the thermal stability are considerably increased in comparison to the C34/N36 complex. The highly conserved Trp628-Trp632-Ile635 motif of the PBD constitutes the center of this peptide and was chosen as a starting point for substitution studies carried out in this doctoral thesis (see Section 5.4).

Table 3.2: Sequence of the CHR-derived peptide C31.

peptide	sequence
	620 650
C31	EQIWNNMTWMEWDREINNYTSLIHSLIEESQ

A more recent evolved class of fusion inhibitors are the so-called anchoring inhibitors that target the highly conserved fusion peptide of HIV-1 gp41. While T20 and other CHR-derived peptides inhibit formation of the hairpin which is able to trigger the membrane fusion, anchoring inhibitors directly block the insertion preventing the anchorage of gp41 into the cell membrane, which is the previous stage of the hairpin formation (Figure 3.9). Münch and colleagues screened a comprehensive peptide library generated from human hemofiltrat and identified a 20 residue peptide, referred to as VIRus-Inhibitory Peptide (VIRIP), corresponding to a *C*-proximal cleavage fragment of α1-antitrypsin, the most abundant circulating serine protease inhibitor (Table 3.3).[252] The researchers found that VIRIP is highly potent inhibitor for a wide variety of HIV-1 strains including those resistant to common antiretroviral drugs. This peptide blocks HIV-1 entry by specifically interacting with the gp41 fusion peptide and additionally, the antiretroviral potency of VIRIP was greatly improved by changing specific amino acid side chains and/or

particular structural features such as charge and peptide chain rigidity.[252] An about two orders of magnitude increased anti-HIV-1 activity compared to the natural form was observed for VIRIP derivatives, e.g., VIR-576, containing an intramolecular cyclic motif by a disulfide bond (Table 3.3). For this, a Cys residue was introduced into the VIRIP sequence, resulting in peptides with similar potency as T20. VIR-576 was later selected for clinical development and its safety, pharmacokinetics, and antiviral efficacy were determined in a short-term monotherapy with treatment-naïve HIV-1 patients.[18] VIR-576 was well tolerated and reduced the plasma viral load by more than one order of magnitude. These findings show that inhibitors targeting the fusion peptide, thereby preventing virus particles from anchoring to and infecting host cells, offer great prospects for the development of a new class of antiviral drugs.
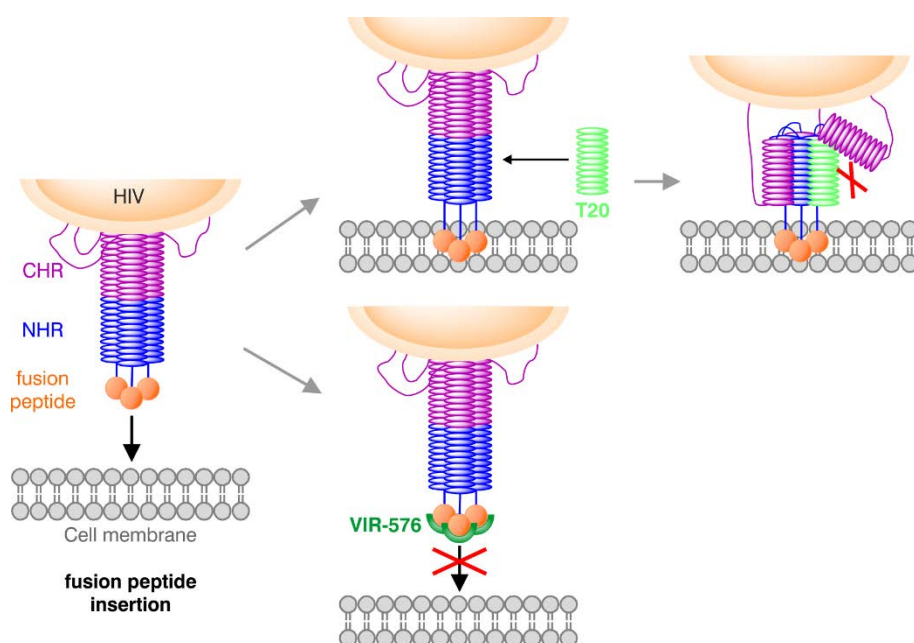
Figure 3.9: Schematic representation of modes of action of T20 in comparison with VIR-576. The fusion inhibitor T20 binds to the NHR-region of HIV-1 gp41 and thereby prevents the formation of the 6-HB hairpin structure required for membrane fusion (**top**). VIR-576 is an anchoring inhibitor that binds to the hydrophobic gp41 fusion peptide and blocks its insertion into the host cell membrane (**bottom**). (From Forssmann *et al.*.[18] Adapted with permission from the American Association for the Advancement of Science.)

Table 3.3: Sequences of the anchoring inhibitors VIRIP and VIR-576.

peptide	sequence
VIRIP	LEAIPMSIPPEVKFNKPFVF
VIR-576	(LAEIP**C**SIPPE**FL**F**G**KPFVF)$_2$

3.4 Multimerization of gp41-derived peptide inhibitors

Multivalent binding is based on multiple simultaneous molecular recognition processes and plays a crucial role in biological processes by establishing strong, but also reversible interactions between two units, such as receptor and ligand or virus and host cell.[253] Here the multiple additive (in some cases cooperative) interactions between a large number of individual, mutually binding partners result in dramatically enhanced binding. In the case of virus infection such interactions initially lead to a stable adhesion since the virus has a high affinity for the multivalent binding sites of the cell surface. In this regard, monovalent drugs can only be effective in very high doses, resulting in a widespread interest for engineering multivalent molecules as drug candidates. Such molecules may allow for strong binding to the recognition sites on the virus or host cell, thereby preventing infection.[253] This section shortly summarizes the research reported in recent years on the development of multimerized HIV-gp41-derived peptides with possible application as fusion inhibitors and vaccines. Especially the trimerization of CHR- or NHR-peptides represents a promising approach as it mimics their native conformation in the pre-hairpin intermediate of gp41.

As already briefly mentioned above, Welch *et al.* observed that trimeric versions of D-peptide pocket-specific inhibitors of entry such as PIE7 show improved antiviral potency compared to the monomeric analogue.[248] The trimer was produced by connecting two PIE7 peptides with the *N*-terminal Lys residue to a central PIE7 peptide with two Lys at the *N*-terminus *via* bis-PEG9 NHS ester crosslinks ($N_9N(PIE7)_3$). More recently, the same research group reported the design and characterization of a new pocket-specific D-peptide, denoted PIE12-trimer.[254] To this end, linker optimization was performed first by relocating Lys to the *C*-terminus of the PIE and using a shorter PEG5 crosslink. This resulted in PIE peptides with a C_5C-linkage, which show enhanced potency compared to the N_9N linkage ($N_9N(PIE7)_3$ *vs* $C_5C(PIE7)_3$; Table 3.4). Second, optimizing the flanking residues of the PIE7 core sequence (CDYPEWQWLC) yielded in peptide PIE12 with improved binding affinity to the gp41 pocket. A combination of these findings yielded the PIE12-trimer $C_5C(PIE12)_3$ that exhibits ~ 100,000-fold enhanced target binding affinity, a significantly broadened inhibitory potency, and a dramatically improved resistance profile compared to that of the previously described D-peptides, as well as those of T20.[254]

Table 3.4: Trimeric D-peptide inhibitors and antiviral potency against HXB2 and JRFL HIV-1 strains. The central peptide of each trimer has an additional Lys residue (not shown).

| peptide | sequence | IC$_{50}$ [nM] | | reference |
		HXB2	JRFL	
$N_9N(PIE7)_3$	(KGA**CDYPEWQWLC**AA)$_3$	0.3	220	[248]
$C_5C(PIE7)_3$	(GA**CDYPEWQWLC**AAGK)$_3$	0.1	6.7	[254]
$C_5C(PIE12)_3$	(HP**CDYPEWQWL**CELGK)$_3$	0.5	2.8	[254]

Francis *et al.* described an optimization of the PIE12-trimer synthesis by using a modular PEG scaffold.[255] This approach greatly improves yield and the scaffold furthermore allows to conjugate the peptide trimer to different membrane-localizing groups, e.g., cholesterol or alkyl chains (Figure 3.10), resulting in up to ~ 160-fold increased potency and retention of PIE12-trimer's resistance profile. Pessi and co-workers used a similar approach and synthesized dimeric cholesterol-tagged fusion inhibitors (Figure 3.10).[256] For this purpose, two Cys-containing C34 peptide chains were conjugated to a maleimide-functionalized core that bears a cholesterol group. The resulting dimer shows highly potent antiviral activity in the picomolar range, while the untagged dimer is not as potent with nanomolar concentrations needed for inhibitory activity.
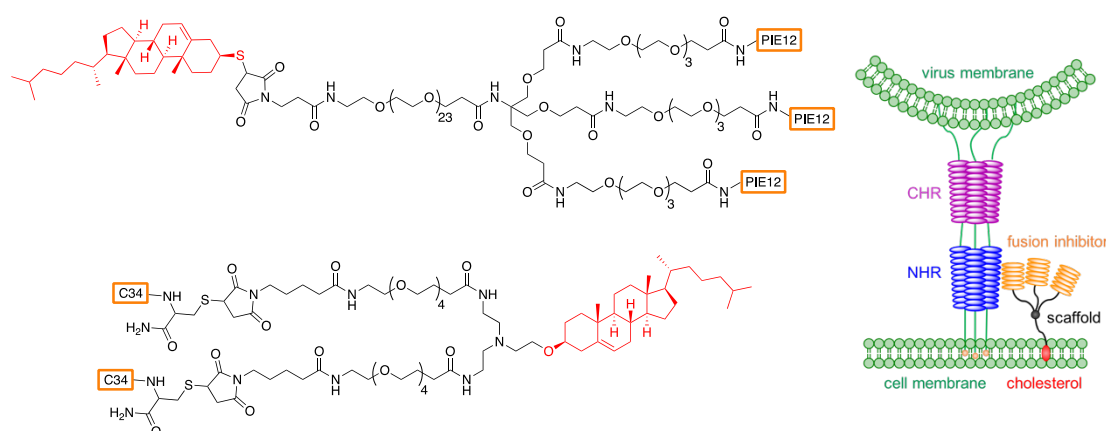
Figure 3.10: A tetrameric conjugate bearing three PIE12 peptide chain and a cholesterol moiety separated by a PEG scaffold (**top left**).[255] A dimeric cholesterol-tagged fusion inhibitor *via* a trivalent scaffold comprising two C34 peptides (**bottom left**).[256] Schematic representation of a cholesterol containing scaffold carrying peptide-based fusion inhibitors (**right**). The peptides can bind to the pre-hairpin intermediate of gp41 thereby preventing the formation of the 6-HB required for membrane fusion. It is assumed that the cholesterol tag as lipophilic moiety interacts with the membrane and facilitates the accumulation of the inhibitor peptide at the fusion site, resulting in improved antiviral potency. (Adapted with permission from Francis *et al.*,[255] Copyright © 2012, American Chemical Society.)

The group of Tamamura designed a novel three-helical bundle mimetic that corresponds to the trimeric form of native N36 and evaluated its inhibitory activity against HIV-1 infection.[257] The trimer triN36e (Figure 3.11 A) was synthesized by conjugating N36, containing a Cys residue at the *N*-terminus, to a three-armed aldehyde scaffold using thiazolidine ligation. TriN36e showed only modest anti-HIV-1 activity, however the potency was threefold higher than that of unconjugated N36. The same researchers also reported an trimeric from of C34, denoted triC34e (Figure 3.11 B), which shows a 100 times improved inhibitory potency compared to the corresponding C34 monomer.[258] In this approach, a Gly thioester was added to the *C*-terminus of C34 and the resulting C34 strands were coupled to a three-armed Cys scaffold *via* native chemical ligation. The authors also generated a C34 dimer by using the same template with a three-armed cysteine scaffold.[259] In this case, unprotected C34 thioester was coupled, stoichiometrically to the template, followed by carboxymethylation of the free thiol groups with iodoacetamide to produce the dimer diC34e (Figure 3.11 C). The anti-HIV activity of diC34e is

approximately equal to that of the trimer triC34e. In the same manner, also dimeric and trimeric variants of T20 were synthesized that also showed increased fusion inhibitory activity compared to the corresponding monomeric T20.[259]
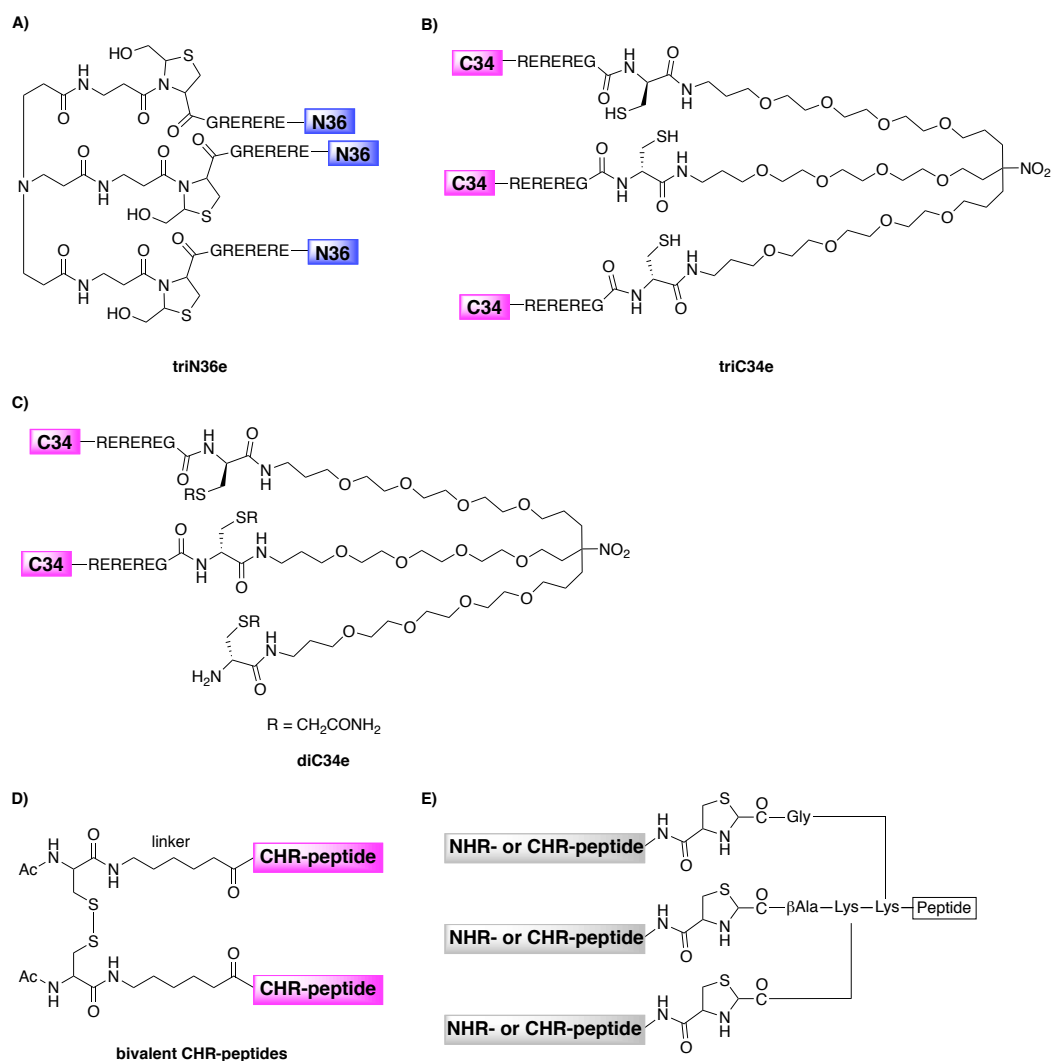
Figure 3.11: Structures of dimers or trimers of CHR- or NHR-derived peptides.[257] **A)** Trimeric N36, triN36e. **B)** Trimeric C34 conjugate triC34e.[258] **C)** C34-derived dimer diC34e. The thiol groups were capped by iodoacetamide (R = CH$_2$CONH$_2$).[259] **D)** Bivalent CHR-peptides. 6-aminohexanoic acid, alanine or triethylene glycol were used as linker.[260] **E)** Structure of three-helix bundles mimicking the HIV membrane fusion-state proteins. NHR or CHR are N36, C34 or T20.[261]

Ling *et al.* reported other dimeric CHR-derived peptides as fusion inhibitors using an bivalent drug design approach.[260] First, the CHR-derived peptides were modified *N*-terminally with a linker and Cys residue and two CHR-domains were afterwards crosslinked *via* a disulfide bond (Figure 3.11 D). The crosslinked, bivalent peptides showed improved inhibitory activity against HIV-1 fusion compared to the respective monomer and in few cases the determined values are close to one of the high active peptidic fusion inhibitor C34. Tam and Yu described a facile ligation approach to prepare trimeric NHR- and CHR-peptides of gp41 as fusion-state protein mimetics that may be useful as inhibitors and vaccine candidates for blocking HIV infection.[261] In this approach thiazolidine ligation is used to couple chemo-selectively NHR- or CHR-derived

peptides, which contain a Cys residue at the *N*-terminus, to an three-armed aldehyde scaffold. This resulted in different three-helix bundle fusion-state protein mimetics (Figure 3.11 E), but their antiviral potency was not determined within the reported study. The peptide scaffold also enables to incorporate T helper epitopes for synthetic vaccines or other peptide cargoes for testing other biological functions.

The group of Kim designed a small protein, denoted 5-Helix, which should bind tightly and specifically to the CHR-region of gp41.[262] It is composed of five of the six helices that form the 6-HB core of gp41 connected with short peptide linkers (Figure 3.12 A). The 5-Helix lacks the third CHR-peptide and thus indeed binds to the CHR-region of gp41 with high affinity, resulting in potent, nanomolar inhibitory activity against diverse HIV-1 strains. In contrast, a control protein, in which six helices form the entire trimer-of-hairpins structure, does not bind CHR-peptides and displays no appreciable inhibitory activity.
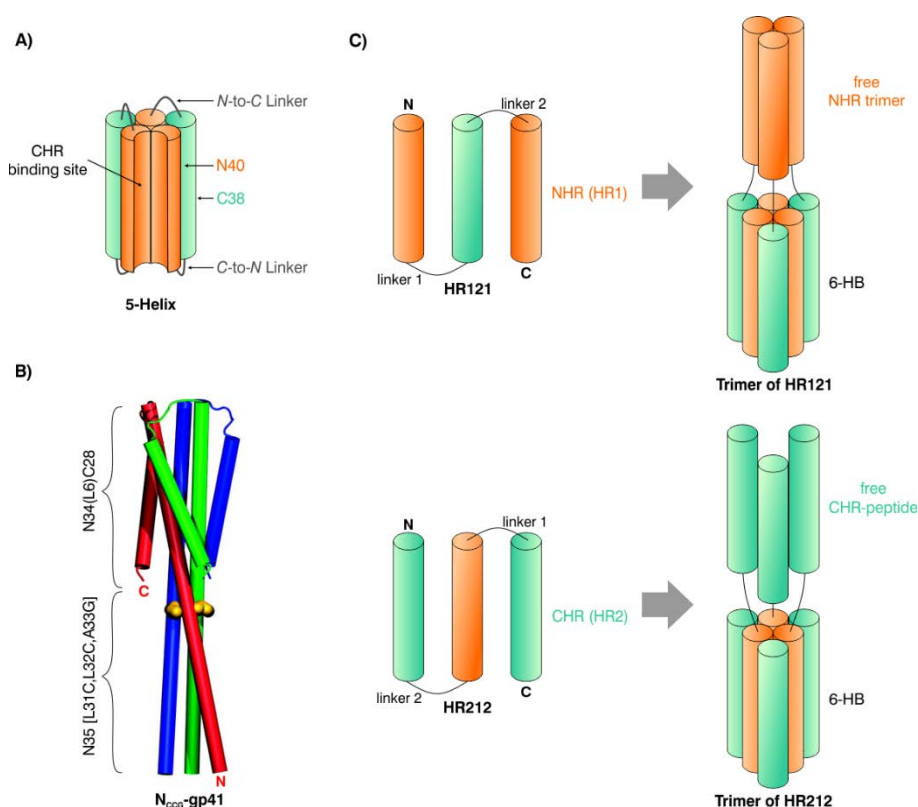
Figure 3.12: A) A schematic model of the 5-Helix protein. Three NHR-derived (N40, orange) and two CHR-derived peptide segments (C38, turquoise green) are alternately linked (N40-C38-N40-C38-N40) using short Gly/Ser peptide sequences (gray loops). N40 corresponds to residues 543-582 of gp41 and C38 is derived from residues 625-662. The sequences of the linkers are: *N*-to-*C* linker, GGSGG; and *C*-to-*N* linker, GSSGG. (Adapted from Root *et al.*[262] with permission from The American Association for the Advancement of Science, Copyright © 2001.) **B)** Structure of N$_{\text{CCG}}$-gp41 with exposed N35 portion. By linking N35 to the *N*-terminus of N34(L6)C28 and substituting Leu576, Gln577 and Ala578 of N35 with Cys, Cys and Gly, respectively, three molecules of N34(L6)C28 segments in N$_{\text{CCG}}$-gp41 can form a 6-HB, while the three N35 molecules form a helical trimer which is stabilized by three intermolecular disulfide bonds. (Reprinted with permission from Louis *et al.*[263] Copyright © 2001.) **C)** HR121 and HR212 constructs and schematic models of the trimers. The sequences of NHR (HR1) and CHR (HR2) for constructing HR121 and HR212 are peptides N34 (residues 546-579 of HIV-1 gp41) and C34 (residues 628-661), respectively. (Adapted from Ni *et al.*[264] with permission from Elsevier, Copyright © 2005.)

Louis *et al.* reported the design and characterization of a chimeric protein, referred to as N$_{CCG}$-gp41, derived from the ectodomain of HIV-1 gp41 (Figure 3.12 B).[263] This molecule features an exposed trimeric coiled-coil structure of N35 derived from the NHR-region of gp41 (residues 546-580). The helical, trimeric conformation is stabilized by fusion to the *N*-terminus of the minimal thermostable ectodomain N34(L6)C28 of gp41 and three engineered intermolecular disulfide bridges. N34(L6)C28 consists of N34 (residues 546-579 of HIV-1 gp41) and C28 (residues 628-655) that are covalently linked by L6, a six-residue loop with the sequence SGGRGG.[195, 265] The exposed trimeric coiled-coil domain of N$_{CCG}$-gp41 targets the CHR-region of gp41 in its pre-hairpin intermediate and possesses potent inhibitory activity at nanomolar concentrations against HIV-1 envelope-mediated cell fusion.

Ni and co-workers designed two recombinant proteins, denoted HR121 and HR212 (Figure 3.12 C).[264, 266] HR121 consists of two N34 molecules derived from the NHR (also referred to as HR1) region of gp41, and one molecule of C34 derived from the gp41 CHR- (or HR2) region. These peptide sequences are linked in the order NHR-CHR-CHR. The other peptide HR212 contains two C34 and one N34 peptide connected in the order CHR-NHR-CHR. In this design three heptad repeats (two NHR- and one CHR-peptide or one NHR- and two CHR-peptides) are linked by flexible linkers so that the NHR- and CHR-peptides in each protein are able to associate and form a hairpin structure.[266] Consequently, three molecules of the protein can form a stable 6-HB with three free NHR- or CHR-peptides exposed (Figure 3.12 C). These exposed peptides can bind to the counterpart regions in HIV-1 gp41, thus inhibiting gp41-mediated membrane fusion. Both proteins HR121 and HR212 showed potent inhibitory activity with IC$_{50}$ values in low nanomolar range, comparable to the potency of T20. Other advantages of this recombinant proteins are that they could be abundantly expressed and easily purified, which may reduce the cost of production compared to the synthetic peptides.

In conclusion, with the different strategies to obtain multimerization of CHR- or NHR-derived described above, e.g., flexible PEG spacers, disulfide bonds, three-armed cysteine-scaffolds, short peptide linkers or recombinant protein expression, binding affinities and antiretroviral activities can be significantly improved. The obtained findings may serve as basis for the design of novel peptide-based anti-HIV-1 therapeutics, and trimeric C34 and N36 derivatives may additionally be applied in the development of HIV-1 vaccines.[257, 267-268] Recently is was also shown that multimerization strategies can be applied to enhance the potency of small molecule gp41 inhibitors.[269]

4.   Aim of the study

The aim of the current study is the design of novel active peptides that specifically bind to the gp41 region of the envelope protein of HIV-1 and thereby prevent the fusion of viral and cellular membrane. Therefore, peptide C31, previously developed in our group and derived from the CHR-region of the wild type sequence of the gp41 core of HIV-1, which was previously shown to interact with the corresponding NHR-region, will be substituted with different fluorinated amino acids at a central position. Specifically, the three fluorinated amino acids difluoroethylglycine (DfeGly), 5,5,5-trifluoroisoleucine (5^3-F$_3$Ile) and 5,5,5,5',5',5'-hexafluoroleucine ($5^3,5'^3$-F$_6$Leu) will replace an Ile residue, and the peptides are to be synthesized *via* solid phase peptide synthesis. Subsequently, their folding characteristics and thermal stabilities are to be investigated *via* CD spectroscopy to determine the influence of the fluorination on the interaction with the NHR-derived counterpart. Also, ITC measurements will be carried out to determine the thermodynamic parameters of the peptide/peptide interaction. Furthermore, for a more detailed investigation on the binding kinetics of the new CHR-peptide analogues, an SPR-based assay will be conducted. To this end, a hetero-tetrameric scaffold will be designed and synthesized, which on the one hand effectively presents the NHR-derived peptide as a trimer and on the other hand enables immobilization on the surface of an SPR chip.

To gain insights into how sterically demanding, highly fluorinated amino acids behave and how they influence the stability of peptides when it comes to single amino acid substitutions, initial studies should be performed using two well established model systems to evaluate both thermal stability and stability towards proteolytic digestion.

5.   Results and Discussion

Parts of the results presented in this chapter were published in the following peer-reviewed reports:

- H. Erdbrink, E. K. Nyakatura, S. Huhmann, U. I. M. Gerling, D. Lentz, B. Koksch, C. Czekelius, Synthesis of enantiomerically pure (2*S*,3*S*)-5,5,5-trifluoroisoleucine and (2*R*,3*S*)-5,5,5-trifluoro-allo-isoleucine. *Beilstein J. Org. Chem.* **2013**, *9*, 2009-2014. **(Section 5.1)**

- J. R. Robalo, S. Huhmann, B. Koksch, A. Vila Verde, The Multiple Origins of the Hydrophobicity of Fluorinated Apolar Amino Acids. *Chem* **2017,** *3*, 881-897. **(Section 5.1)**

- S. Huhmann, E. K. Nyakatura, H. Erdbrink, U. I. M. Gerling, C. Czekelius, B. Koksch, Effects of single substitutions with hexafluoroleucine and trifluorovaline on the hydrophobic core formation of a heterodimeric coiled coil. *J. Fluorine Chem.* **2015,** *175*, 32-35. **(Section 5.2)**

- S. Huhmann, A.-K. Stegemann, K. Folmert, D. Klemczak, J. Moschner, M. Kube, B. Koksch, Position-dependent impact of hexafluoroleucine and trifluoroisoleucine on protease digestion. *Beilstein J. Org. Chem.* **2017,** *13*, 2869-2882. **(Section 5.3)**

Results that are not part of these publications are evaluated and discussed in additional sections.

5.1   Hydrophobicity and α-helix propensity of fluorinated amino acids

The side-chain size, or rather shape and hydrophobicity of an amino acid as well as its intrinsic propensity for a certain secondary structure, e.g., α-helix propensity, are important factors for peptide and protein folding, such as the formation of helical assemblies, and are thus also crucial for the interpretation of the results presented in this thesis. These properties have been extensively studied in our group for side-chain fluorinated amino acids.[50, 134-135, 270] The following section summarizes the results for the fluorinated amino acids used in this study and describes newly gained insights in the multiple origins of the hydrophobicity of these amino acids.

5.1.1   Hydrophobicity of side-chain fluorinated amino acids

The relationship between side-chain volume and hydrophobicity of side-chain fluorinated amino acids was investigated by plotting their retention times from an RP-HPLC experiment against their calculated side-chain van der Waals volumes (Figure 5.1). The non-polar character of the reversed-phase column used in this experiment provides a hydrophobic environment.[271] The accuracy of this method was validated in prior studies by our group.[50, 117]
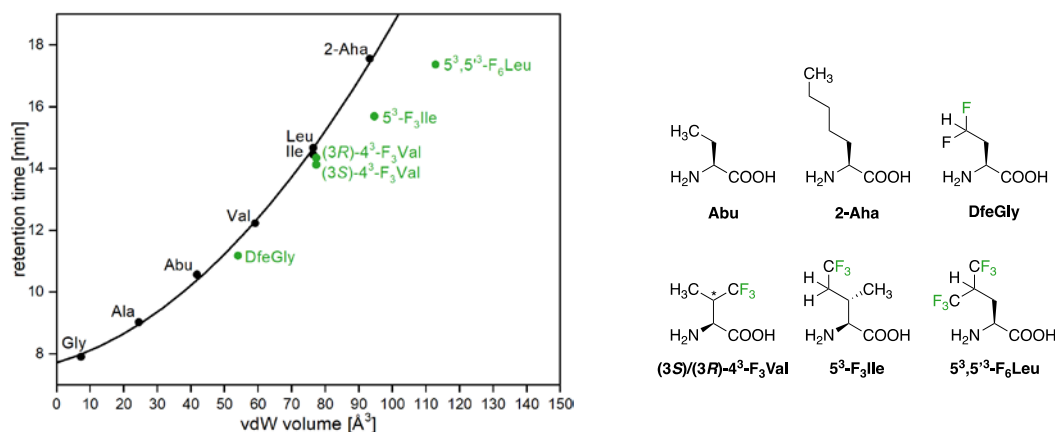
Figure 5.1: Retention times of Fmoc amino acids plotted against the van der Waals volume of their side chains.[50, 134-135] The van der Waals volumes of the amino acid side chains were calculated according to Zhao *et al*.[272] Non-fluorinated amino acids and the correlation between them are depicted in black. Fluorinated amino acids are presented in green. A version of the figure containing all fluorinated amino acids studied by our group is published in reference [31].

The retention time of non-fluorinated aliphatic amino acids increases non-linearly with increasing side-chain volume.[50, 135] As expected, the enlargement of the aliphatic side chain results in an increase of hydrophobicity. The retention times of the fluorinated amino acids do not fit into this correlation.[50, 134-135] A significant increase in the van der Waals volume is observed with each addition of a fluorine atom. The fluorinated amino acids relevant for this thesis are all more hydrophobic (as indicated by the increased retention time) than their native, non-fluorinated analogues. The hydrophobicity and side-chain volume of DfeGly lies in between the values obtained for Abu and Val.[50] (3*S*)-, and (3*R*)-4^3-F$_3$Val are comparable to Leu and Ile with regard to side-chain volume as well as hydrophobicity. A slight difference is determined for both isomers, which might be attributed to the orientation of the side chain.[134] The fluorinated analogue of Ile, 5^3-F$_3$Ile, is similar in size but at the same time much less hydrophobic than 2-Aha.[135] On the contrary, 5^3,5'^{3}-F$_6$Leu is similar to 2-Aha in hydrophobicity while exhibiting a much larger volume.[135]

It has been suggested that there are two effects that determine the overall hydrophobicity of the side-chain fluorinated aliphatic amino acids.[50]

    (i)   The solvent-accessible surface area is increased when a hydrogen atom is substituted by a fluorine atom, leading to an increase in hydration energy.

    (ii) The C-F bond is more polarized than the C-H bond, resulting in energetically more favorable electrostatic interactions of the fluorinated group with the solvent.

Thus, the fluoroalkyl side chains possess two opposing physicochemical properties: hydrophobicity and polarity. The combination of both leaves fluorinated amino acids less hydrophobic than their surface area would suggest.[135] Recently it was shown that this explanation is insufficient.[136] The group of Ana Vila Verde used molecular dynamics simulations and the gained results were compared to the experimental data obtained from the RP-HPLC experiment established by our group. Changes in the surface area of an amino acid upon fluorination have

only a secondary contribution to the changes in the hydrophobicity. Differences in hydration free energy arise primarily from steric hindrance and changes in the number of hydrogen bonds formed between backbone amine and carbonyl groups with water. The total number of backbone-water hydrogen bonds was found to decrease upon fluorination and correlates well with the observed increase in amino acid hydration free energy.[136] The smallest contribution to the free energy comes from changes in the dipole moment. Furthermore, it was found that changes in hydration free energy upon fluorination depend strongly on the identity of the amino acid and the orientation of the fluorinated side chain as in the case of (3S)-, and (3R)-4^3-F$_3$Val. These results are supported by earlier quantum mechanics and molecular dynamics studies that showed that fluoromethylated groups establish hydrogen bonds to water molecules, which are weaker than that of non-fluorinated side chains in native protein environments.[50]

5.1.2 α-helix propensity of side-chain fluorinated amino acids

The α-helix propensity of fluorinated amino acids was determined using methods established by the Cheng group.[273-274] Therefore, the amino acid of interest is incorporated at a guest position (X) of an α-helical alanine-based model peptide with the sequence Ac-YGGKAAAAKAXAAKAAAAK-NH$_2$ (K-X). The helical content of the peptides is then evaluated by CD spectroscopy and the mean residue ellipticity at 222 nm is used to calculate the fraction helix f_{helix} from which the α-helix propensity ω of the amino acids is determined applying modified Lifson-Roig theory (Table 5.1).[275-277]

Table 5.1: Ellipticity [θ] at 222nm from normalized CD data, fraction helix f_{helix} and α-helix propensity ω of K-X peptides for selected natural and fluorinated amino acids.

amino acid	$[\theta]_{222nm}$	f_{helix}	ω
Abu[273]	-18100 ± 200	0.522 ± 0.006	1.22 ± 0.14
Val[270]	-13054 ± 452	0.38 ± 0.01	0.41 ± 0.04
Ile[135]	-13813 ± 156	0.40 ± 0.01	0.52 ± 0.05
Leu[273]	-17400 ± 200	0.502 ± 0.006	1.06 ± 0.12
DfeGly[134]	-13969 ± 569	0.40 ± 0.02	0.497 ± 0.060
(3S)-4^3-F$_3$Val[270]	-2685 ± 526	0.08 ± 0.01	0
(3R)-4^3-F$_3$Val[270]	-3887 ± 547	0.11 ± 0.02	0
5^3-F$_3$Ile[135]	-10776 ± 216	0.31 ± 0.01	0.26 ± 0.03
$5^3,5'^3$-F$_6$Leu[273]	-8720 ± 200	0.251 ± 0.006	0.128 ± 0.023

Chiu *et al.* showed that fluorinated amino acids generally exhibit lower α-helix propensities compared to their hydrocarbon analogues.[273-274] We expanded these studies with other fluorinated amino acids and observed the same trend.[134-135, 270] The introduction of two fluorine atoms into the Abu side chain results in a slightly reduced propensity for an α-helical structure, and the value obtained for DfeGly is comparable to Ile or Val.[134] (3R)- and (3S)-4^3-F$_3$Val does

not display any α-helix propensity at all.[134, 270] Val is known to prefer β-sheet conformations[278] and the fluorination of one of the two β-methyl groups increases this effect even further. The close proximity of the large CF_3-group to the peptide backbone prevents the formation of α-helical structures, and hence explains the absence of a α-helix propensity of the two 4^3-F_3Val diastereomers.[270] This is supported by the findings for $4'^3$-F_3Ile.[270] A complete loss of helix propensity is reported in this case as well, and also here, the β-methyl group is replaced by a CF_3-substituent.[270] In contrast, it was observed that 5^3-F_3Ile, in which the γ-CH_3 group is replaced with CF_3, still exhibits some α-helix propensity, namely half the value for Ile.[135] $5^3,5'^3$-F_6Leu has an 8-fold reduced α-helix propensity compared to Leu.[273]

The dramatic decrease in α-helix propensity of an amino acid upon fluorination is generally attributed to burial of the fluorinated side chain within the unfolded state of the peptide, as solvent exposure of these side chains in the monomeric helical state would be unfavorable due to the hydrophobic nature of the fluorinated amino acids.[273] In addition, the steric demand of the side chains is another factor that must be considered. For instance, amino acids that are branched at the β-carbon atom like Val or Ile have reduced α-helix propensities compared with the β-unbranched Leu as these side-chain atoms come into close proximity with the peptide backbone.[278] This effect is strengthened by the observations made for 4^3-F_3Val and $4'^3$-F_3Ile that carry the voluminous CF_3 group at the β-carbon.[270] Here, the close proximity of this sterically demanding group to the peptide backbone seems to prevent the formation of α-helical structures as these amino acids possess no α-helix propensity.[270]

It remains to be elucidated to what extent the α-helix propensity influences the protein stability at buried positions, e.g., within the hydrophobic cores of proteins, such as the hydrophobic pocket of gp41 of HIV-1, since the observed decrease in α-helix propensity might be caused by unfavorable solvent interactions at exposed positions of the monomeric K-X peptide.

5.2 Effects of hexafluoroleucine and trifluorovaline on the hydrophobic core formation of a heterodimeric coiled coil

The results presented in this section were originally published as:

S. Huhmann, E. K. Nyakatura, H. Erdbrink, U. I. M. Gerling, C. Czekelius, B. Koksch, Effects of single substitutions with hexafluoroleucine and trifluorovaline on the hydrophobic core formation of a heterodimeric coiled coil, *J. Fluorine Chem.* **2015**, *175*, 32-35.

The original paper including supporting information is available at:

Individual contributions

S. Huhmann synthesized the fluorinated VPK peptides, performed CD, and SEC/SLS experiments, and wrote the manuscript. E. K. Nyakatura had the project idea, synthesized the unmodified VPK and VPE peptides, and helped with the analysis of the results. H. Erdbrink, U. I. M. Gerling, and C. Czekelius provided the fluorinated amino acids.

Paper summary

Modifying peptides and proteins with fluorinated amino acids allows for modulation of their biophysical and pharmaceutical properties, and, therefore, biological activity.[21, 31-33] Systematic investigations that are based on model systems, which mimic natural protein-protein interaction domains, for instance the coiled-coil folding motif, can help to provide valuable insights into how side-chain fluorinated amino acids behave in natural protein environments.

Several prior studies focused on the global substitution of the hydrophobic core with fluorinated analogues of hydrophobic amino acid residues, namely Leu and Val, and showed that the resulting coiled-coil systems display increased thermal stabilities. The enhanced stability was primarily attributed to hydrophobic effects.[21, 23-24, 35-36, 87-88, 98, 102-103, 105-106, 108] In contrast, work from the Koksch group placed emphasis on single amino acid substitutions by small, minimally fluorinated building blocks within the hydrophobic core. A coiled-coil model system developed for this purpose, named VPE/VPK, served as the scaffold. It was found that these modifications can lead to thermal destabilization,[79, 114-115] and that the degree of destabilization depends on how efficiently fluorinated residues pack against neighboring side chains.[118-119, 279-280]

The goal of this study was to examine whether single substitutions with sterically demanding, highly fluorinated side chains are able to stabilize the hydrophobic core of such structures. Thus, $5^3,5'^3$-F_6Leu and two different diastereomers of 4^3-F_3Ile were incorporated into the parallel heterodimeric coiled-coil model system VPE/VPK (Figure 5.2) to replace their natural analogues Leu or Val at the hydrophobic core positions **d**19 and **a**16, respectively, within VPK. The effect of these substitutions on coiled-coil structure and stability was evaluated by applying CD

spectroscopy (secondary structure, thermal denaturation), and size exclusion chromatography in combination with static light scattering (oligomerization state).
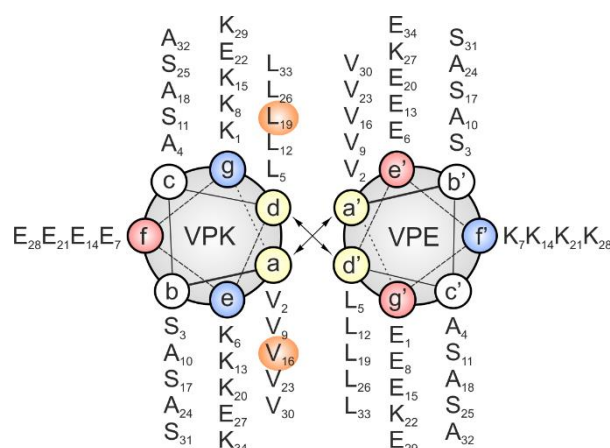
Figure 5.2: Helical wheel representation of the parallel VPE/VPK heterodimeric model system.[79]

The results demonstrate that although fluorinated amino acids generally possess distinctly lower helix propensities than their hydrocarbon counterparts,[134-135, 270, 273-274] the fluorinated VPK peptides form stable α-helical bundles with VPE showing slightly higher helical contents, while maintaining the parental dimeric oligomerization state (Table 5.2). The VPE/VPK-$5^3,5'^3$-F$_6$Leu$_{19}$ dimer exhibits a higher thermal stability (74.4°C *vs.* 70.7°C for the parent VPE/VPK system), while the melting points of the VPE/VPK bundles containing either $(3R)$-4^3-F$_3$Val$_{16}$ or $(3S)$-4^3-F$_3$Val$_{16}$ at position **a**16 are similar or somewhat lower (70.8°C and 67.5°C, respectively). As in the used model system, the fluorinated amino acids exclusively interact with natural residues of VPE, the increase in thermal stability upon $5^3,5'^3$-F$_6$Leu introduction might be attributed to the greater hydrophobicity and efficient packing within the hydrocarbon side chains in the hydrophobic core, resulting in the highly favorable burial of the bulky hydrophobic fluorinated side chain. On the contrary, due to the shorter side chain of the 4^3-F$_3$Val residue, the fluorine content and packing behavior seem to contribute less to hydrophobic core formation.

Table 5.2: Theoretically and experimentally determined molecular weight, helical content f_H, melting temperature T$_M$, and ΔG^Ø values for each VPE/VPK heteromer.

peptide	theoretical dimer mass [Da]	SEC/SLS determined mass [Da]	f_H [%]	T$_M$ [°C]	ΔG^Ø [kcal mol^{-1}]
VPE/VPK	7576	7578 ± 16	64	70.7 ± 0.3	11.1 ± 0.1
VPE/VPK-$5^3,5'^3$-F$_6$Leu$_{19}$	7684	7685 ± 40	69	74.4 ± 0.3	11.9 ± 0.3
VPE/VPK-$(3R)$-4^3-F$_3$Val$_{16}$	7630	7674 ± 121	71	70.8 ± 0.2	11.1 ± 0.2
VPE/VPK-$(3S)$-4^3-F$_3$Val$_{16}$	7630	7634 ± 15	73	67.5 ± 0.3	11.3 ± 0.2

In conclusion, the same principles that underpin the stability of natural proteins, which are efficient packing and hydrophobicity of side chains,[24] appear to determine whether fluorine substitution within a hydrophobic protein environment can enhance the stability of peptide structures. Even single substitutions with highly fluorinated amino acids can expand the hydrophobic core sequence space of coiled-coil based peptides, when correct packing and steric demands are considered.

For copyright reasons, the article is not included in the online version of this thesis.

*An electronic version of the article is availabl*e (DOI: 10.1016/j.jfluchem.2015.03.003).

5.3 Position-dependent effect of sterically demanding, and highly fluorinated amino acids on the proteolytic stability of a model peptide

The results presented in this section were originally published as:

S. Huhmann, A.-K. Stegemann, K. Folmert, D. Klemczak, J. Moschner, M. Kube, B. Koksch, Position-dependent impact of hexafluoroleucine and trifluoroisoleucine on protease digestion, *Beilstein J. Org. Chem.* **2017**, *13*, 2869-2882.

The original paper with supporting information is available at:

https://doi.org/10.3762/bjoc.13.279

Individual contributions

S. Huhmann synthesized the FA peptide, its analogues containing 5^3-F$_3$Ile, and Ile, and performed the enzymatic digestion assay for these peptides. Furthermore, S. Huhmann wrote the main part of the manuscript. K. Folmert synthesized the six Leu and $5^3,5^{'3}$-F$_6$Leu containing peptides, as well as FA, and carried out the enzymatic digestion studies for the Leu/$5^3,5^{'3}$-F$_6$Leu series. J. Moschner synthesized the amino acid Fmoc-$5^3,5^{'3}$-F$_6$Leu. A.-K. Stegemann, D. Klemczak, and M. Kube repeated the enzymatic digestion assay for all peptides and performed the analysis of the cleavage patterns by mass spectrometry during bachelor thesis/research internship in the group of Prof. Dr. B. Koksch under supervision of K. Folmert and the author of this thesis. In addition, A.-K. Stegemann wrote some parts of the publication.

Paper summary

Peptide-based drugs are promising lead structures for the development of new drug candidates typically benefitting from high binding affinity and selectivity for their target. Their application, however, is limited as peptides suffer from rapid digestion by proteases or poor membrane permeability resulting in low bioactivity and poor oral bioavailability.[12, 15-17, 140] Several strategies to overcome these limitation, especially to prolong half-life and enhance resistance towards proteases, are based on the modification of peptides with non-natural building blocks.[15-17] Among these, the incorporation of fluorinated amino acids is of particular interest, since the decoration of small molecules with fluorine substituents is a widespread strategy in medicinal chemistry to modulate numerous molecular properties. Fluorine's high electronegativity, small size, low polarizability and strong inductive effect can lead to changes in

molecule conformation, pK_a values of neighboring functional groups, and, thus, the way in which a molecule interacts with a protein or receptor or permeates a membrane. As a consequence, pharmacokinetics and biological half-life can considerably change.[20, 25, 27-30] In light of these facts, several studies are focused on incorporation of fluorinated building blocks into peptides and proteins with the intention of improving or tuning their properties.[21, 31-33] For example, fluorinated amino acids have been shown to improve the proteolytic stability of peptides and proteins, though this is not always the case.[144-146, 157, 163-164] For a detailed discussion regarding this topic see Section 2.4.

In an attempt to understand fluorine's impact on the proteolytic stability of peptides in more detail, Koksch *et al.* established a systematic study. Therefore, a 10-amino acid model peptide, named FA, was designed comprising substrate specificities of different serine and aspartate proteases.[159-160] In initial studies, Ala residues at the P2, P1' or P2' positions, which are at or adjacent to the cleavage site, were substituted by DfeGly, TfeGly or Abu individually. The proteolytic stability of the resulting peptide library was investigated against human blood plasma and elastase,[159] as well as α-chymotrypsin and pepsin.[160] In only about 25% of all cased a strong increase in proteolytic stability upon introduction of fluorine was observed, while a strong destabilization was determined for almost the same amount of peptide substrates. In all other cases, no or only a small impact on protease resistance was detected, when fluorinated amino acids were introduced into the peptide chain.

The objective of the study presented here, as a follow up to the previous results, was to evaluate the influence of the sterically demanding, highly fluorinated amino acids 5^3-F$_3$Ile and 5^3,$5'^3$-F$_6$Leu on the proteolytic stability of the model peptide FA. As this project was conducted in cooperation with K. Folmert, who studied the 5^3,$5'^3$-F$_6$Leu/Leu containing variants as part of her doctoral thesis,[281] the results for the 5^3-F$_3$Ile/Ile substituted analogues are discussed again separately in the following paragraphs.

5^3-F$_3$Ile and Ile were singly substituted for Ala at positions P2, P1', and P2', yielding six modified FA analogues (Table 5.3). All peptide substrates, including FA as reference, were subjected to degradation by treatment with α-chymotrypsin, pepsin, elastase or proteinase K. The digestion process was followed over a time period of 24 h by an analytical RP-HPLC assay with fluorescence detection, and the cleavage products were identified by ESI-ToF mass spectrometry.

Table 5.3: Names and amino acid sequences of the studied peptides. The substitution positions are marked as Xaa with Xaa = Ile or 5^3-F$_3$Ile. Positions are named according to Schechter and Berger nomenclature.[158]

				P3	P2	P1	P1'	P2'	P3'	P4'
FA	Abz	K	A	A	F	A	A	A	A	K
P2-XaaFA	Abz	K	A	Xaa	F	A	A	A	A	K
P1'-XaaFA	Abz	K	A	A	F	Xaa	A	A	A	K
P2'-XaaFA	Abz	K	A	A	F	A	Xaa	A	A	K

cleavage site ⇓

Both P2 modified peptides were more stable than FA against digestion by α-chymotrypsin (Figure 5.3). Ile seems to be not that preferred as Ala in the P2 position, and the introduction of three fluorine atoms strengthens this effect with a 50% gain in stability towards α-chymotrypsin. The fluorinated P2 peptide was not digested at all after 24 h, suggesting that 5^3-F$_3$Ile is not favored within the S2 pocket of α-chymotrypsin. Substitution of Ala in P1' gave peptides that were more resistant towards proteolytic degradation. Again, fluorine modification led to less efficient degradation. In the case of the P2' modified variants, Ile introduction slightly accelerates proteolysis by α-chymotrypsin compared to FA, while 5^3-F$_3$Ile has a protective effect in this position. Analysis of the cleavage products by ESI-ToF mass spectrometry confirmed that position P1 bearing Phe is the main cleavage site for α-chymotrypsin (Figure 5.5).
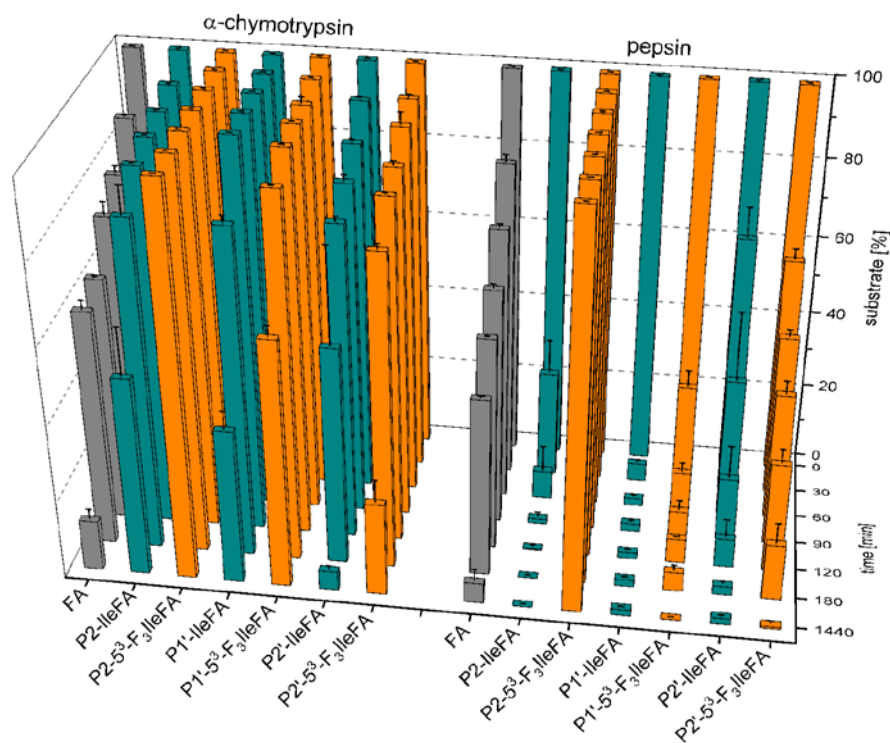
Figure 5.3: Digestion of peptide substrates by α-chymotrypsin and pepsin. The data shown represent the average of three independent measurements. Errors are derived from the standard deviation.

In the pepsin digestion assay, the control peptide FA is almost fully digested after 24 h (Figure 5.3). Except for P2-5^3-F$_3$IleFA, the same holds true for the modified variants as also these peptides are digested completely, even faster than FA. P2-5^3-F$_3$IleFA instead is fully resistant to pepsin, still 100% of the full-length peptide is detected after 24 h. Thus, fluorination shows only a protective effect when introduced *N*-terminal of the cleavage site. Observed digestion products corresponded to the expected cleavage pattern with Phe in the P1 position (Figure 5.5). In addition, for P2'-5^3-F$_3$IleFA two further peptide bonds were found to be cleaved by pepsin.

Substitution of Ala by Ile or 5^3-F$_3$Ile in position P2 results in increased stability towards elastase digestion, while 5^3-F$_3$Ile provides the best protection (Figure 5.4). Introduction of three fluorine atoms into Ile yields an about 35% gain in stability. Also in the P1' position, Ile seems not as preferred as Ala, while 5^3-F$_3$Ile shows a comparable amount of digestion to FA. That means fluorination of the P1' residue does not protect the peptide from digestion by elastase. The opposite is observed for P2' modified peptides. Whereas P2'-IleFA is almost completely degraded by elastase after 24 h, substitution by 5^3-F$_3$Ile slows down the digestion process with an observed stabilization of around 37%. As the peptide substrates have Ala as the main residue present, multiple cleavage fragments are observed, consistent with the substrate specificity of elastase that preferably hydrolyzes peptide bonds *C*-terminal to uncharged non-aromatic amino acids and mainly between Ala-Ala or Ala-Gly bonds.[282-283] Thus, none of the peptide fragments detected corresponded to a Phe in the P1 position.
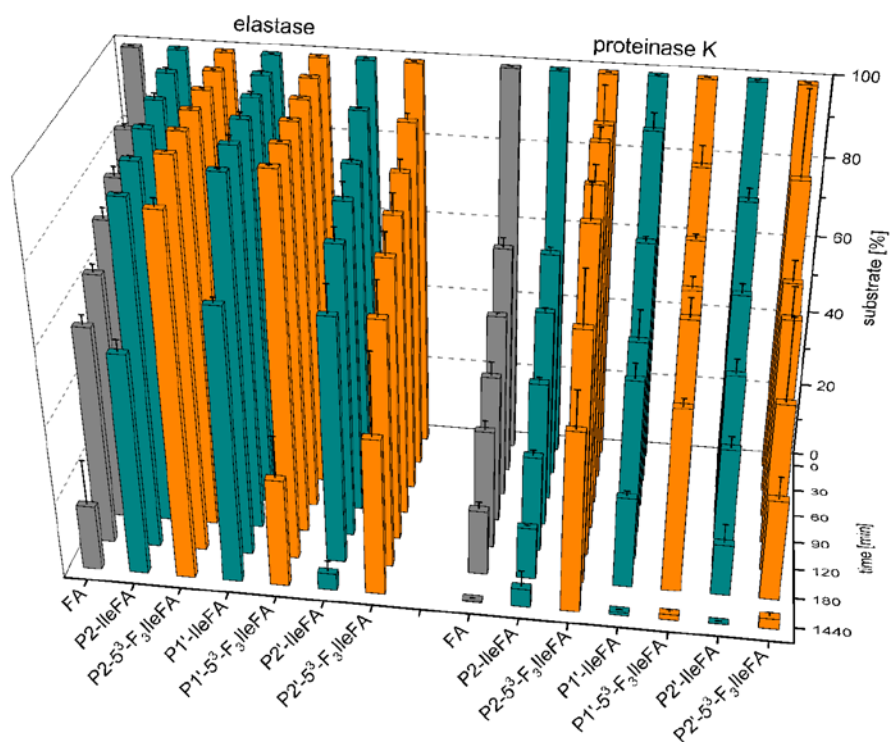
Figure 5.4: Digestion of peptide substrates by elastase and proteinase K. The data shown represent the average of three independent measurements. Errors are derived from the standard deviation.

When incubated with proteinase K all peptides except for one were almost fully digested within 24 h (Figure 5.4). Although fluorination of Ile in either the P2, P1' or P2' positions reduced the reaction velocity, only P2-5^3-F$_3$IleFA was still present in a reasonable amount with 47% of the full-length sequence detectable after 24 h. This is a remarkable observation, as proteinase K possesses a broad substrate specificity, high activity and is able to digest numerous proteins even in the presence of detergents.[284] Due to the enzyme's broad specificity, cleaving peptide bonds *C*-terminal to a number of amino acids, multiple cleavage patterns were detected for the substituted variants (Figure 5.5). As in the case of elastase, cleavage mostly occurred *C*-terminal to Ala.
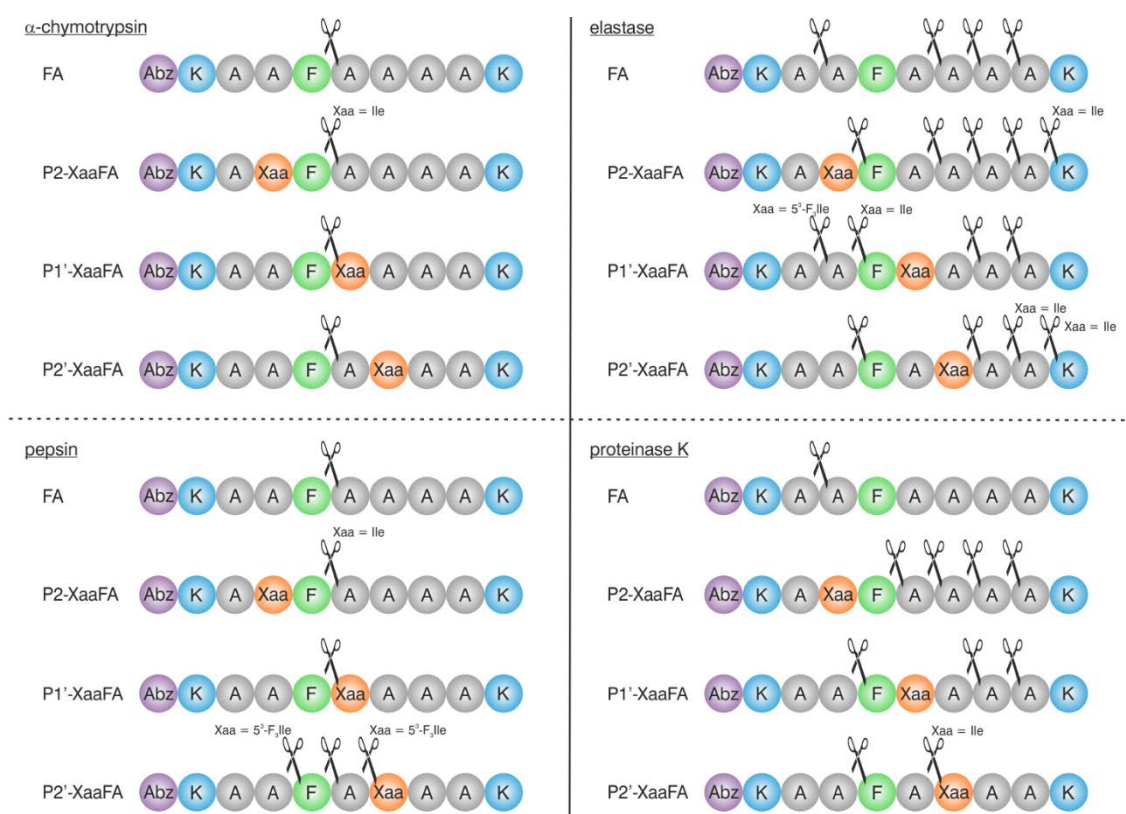
Figure 5.5: Cleavage positions observed in the digestion of peptide substrates. Cleavage sites that are not marked with a certain amino acid were detected in all P2, P1' or P2' modified peptides.

In brief, 5^3-F$_3$Ile introduction helps to protect the peptide against proteolysis by α-chymotrypsin in all modified positions when compared to the Ile containing analogues (Figure 5.6). For the other three enzymes a strong stabilization towards proteolytic digestion is only observed for fluorination of Ile *N*-terminal to the cleavage site. Remarkably, there is only one case (P1'-5^3-F$_3$IleFA for elastase), in which the incorporation of fluorine atoms renders the peptide substrate significantly more prone to degradation. Furthermore, the P2-5^3-F$_3$IleFA peptide is an outstanding example for the protective effect that fluorine introduction can account for. This peptide is the most resistant substrate towards digestion by all the four proteases investigated (see Figures 5.3 - 5.4).
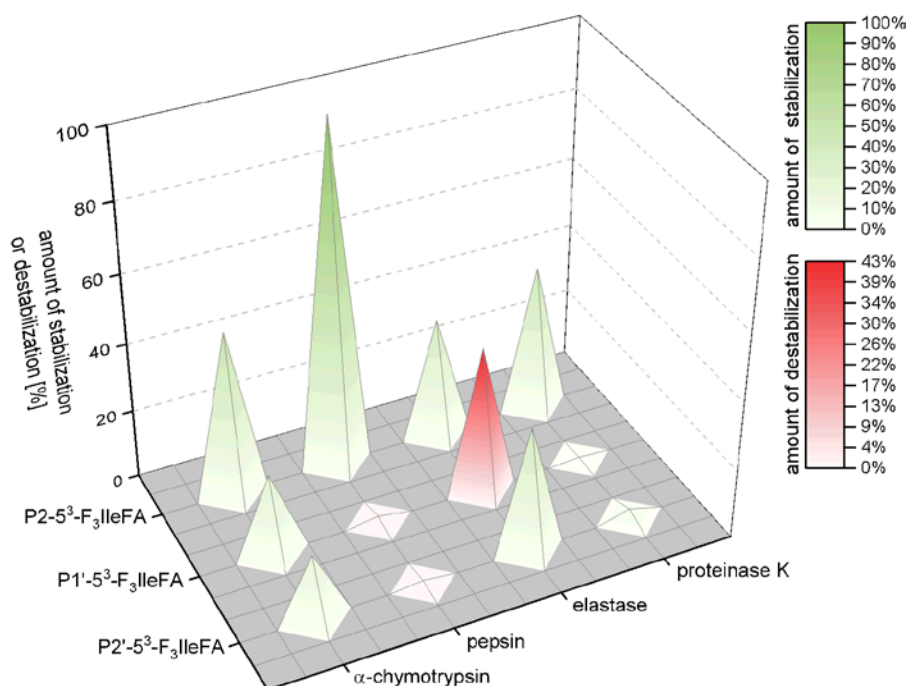
Figure 5.6: Dimension of stabilization or destabilization upon 5^3-F_3Ile incorporation compared to the non-fluorinated analogues containing Ile for all four different enzymes studied and measured after 24 h of incubation.

Although in most cases an increase in proteolytic stability upon the introduction of fluorine into the Ile side chain was observed, the more rapid proteolytic digestion compared to the non-fluorinated control in other cases point to fluorine specific interactions of the substrate with the respective enzyme binding site. Sterically demanding, fluorinated amino acids such as 5^3-F_3Ile are not solely excluded from but can even be well accommodated by the active site. However, the results demonstrate that 5^3-F_3Ile holds potential for engineering proteolytically stable peptide-based drug candidates.

BEILSTEIN JOURNAL OF ORGANIC CHEMISTRY

Position-dependent impact of hexafluoroleucine and trifluoroisoleucine on protease digestion

Susanne Huhmann, Anne-Katrin Stegemann, Kristin Folmert, Damian Klemczak, Johann Moschner, Michelle Kube and Beate Koksch[*]

Full Research Paper

Open Access

Address:
Department of Chemistry and Biochemistry, Freie Universität Berlin, Takustraße 3, 14195 Berlin, Germany

Email:
Beate Koksch[*] - beate.koksch@fu-berlin.de

[*] Corresponding author

Abstract

Rapid digestion by proteases limits the application of peptides as therapeutics. One strategy to increase the proteolytic stability of peptides is the modification with fluorinated amino acids. This study presents a systematic investigation of the effects of fluorinated leucine and isoleucine derivatives on the proteolytic stability of a peptide that was designed to comprise substrate specificities of different proteases. Therefore, leucine, isoleucine, and their side-chain fluorinated variants were site-specifically incorporated at different positions of this peptide resulting in a library of 13 distinct peptides. The stability of these peptides towards proteolysis by α-chymotrypsin, pepsin, proteinase K, and elastase was studied, and this process was followed by an FL-RP-HPLC assay in combination with mass spectrometry. In a few cases, we observed an exceptional increase in proteolytic stability upon introduction of the fluorine substituents. The opposite phenomenon was observed in other cases, and this may be explained by specific interactions of fluorinated residues with the respective enzyme binding sites. Noteworthy is that 5,5,5-trifluoroisoleucine is able to significantly protect peptides from proteolysis by all enzymes included in this study when positioned N-terminal to the cleavage site. These results provide valuable information for the application of fluorinated amino acids in the design of proteolytically stable peptide-based pharmaceuticals.

Introduction

Peptide-based drugs are promising pharmaceuticals since they offer several advantages including high selectivity, specificity, and efficacy for recognizing and binding to their targets [1-6]. However, their application as drugs is often limited due to low oral bioavailability and a short half-life attributable in part to proteases of the digestive system and blood plasma [1-8]. Effi-

2869

cient approaches to overcome these limitations have been developed including the incorporation of non-natural amino acids, such as D-amino acids, backbone-extended or chemically modified amino acids [1]. In this regard, the incorporation of fluorine into amino acids has become a promising strategy. Fluorine's unique properties, namely low polarizability, a strong inductive effect, and high electronegativity, as well as its small size, result in strong, short C–F bonds and perturb the acidity and basicity of adjacent functional groups. Moreover, these changes may strongly influence hydrogen bonding and electrostatic interactions that are crucial for binding to receptors or, in context of protease stability, enzymes. Thus, when introduced in the form of fluorinated amino acids, this unique element can alter the biophysical, chemical and pharmaceutical properties of proteins and peptides including their interaction with proteases [9,10].

Several laboratories have focused on introducing highly fluorinated analogues of hydrophobic amino acids and have studied the effects on stability of the resulting proteins towards thermal and chemical denaturation [9,11-22]. These studies prompted further investigation into the extent to which fluorinated amino acids stabilize peptides and proteins against proteolytic degradation in particular. Meng and Kumar reported that the incorporation of 5,5,5,5',5',5'-hexafluoroleucine (HfLeu) into the antimicrobial peptides magainin 2 amide and buforin enhanced their resistance towards proteolytic degradation by trypsin [23]. They also introduced HfLeu into the glucagon-like-peptide-1 (GLP-1), which is an attractive lead compound for the treatment of diabetes mellitus type 2. Unfortunately, the clinical use of the wild-type peptide is severely hampered due to rapid digestion ($\approx$2 min) by the serine protease dipeptidyl peptidase [24-26]. Satisfyingly, the fluorinated GLP-1 analogues displayed higher proteolytic stability against this enzyme [27].

Usually, the enhanced proteolytic stability of fluorinated peptides is explained by their greater hydrophobicity and altered secondary structure compared to the parent, non-fluorinated peptide. A further reason is the increased steric bulk of the fluorinated amino acid, meaning protection from protease degradation is a result of the steric occlusion of the peptide from the active site [23,28]. In contrast, the Marsh lab found that the introduction of HfLeu into the antimicrobial peptide MSI-78 only renders it more stable towards proteolysis by trypsin and chymotrypsin in the presence of liposomes [29]. In the absence of liposomes, the fluorinated variants were as rapidly degraded as the non-fluorinated control, suggesting that the incorporation of HfLeu is not the only factor that prevents the peptide from being digested by proteases [29]. Fluorinated aromatic amino acids were also investigated regarding their impact on peptide proteolysis. For instance, incorporation of monofluorinated

phenylalanine variants into the histone acetyltransferase protein tGN5 resulted in destabilization in a chymotrypsin digestion assay [30]. Substitution of tryptophan, tyrosine, and phenylalanine residues in a glycosylation-deficient mutant of *Candida antarctica* lipase B, CalB N74D, by their monofluorinated analogues, left the resistance to proteolytic degradation by proteinase K unchanged [31]. Incorporation of α-fluoroalkyl-substituted amino acids can also lead to proteolytically stable peptides, and proteases can even be used to synthesize α-fluoroalkyl-substituted peptides [32-38].

These results indicate that the influence of fluorinated amino acids on the proteolytic stability of peptides and proteins remains difficult to predict. In an attempt to systematically study the influence of fluorinated amino acids on the proteolytic stability of peptides, a 10-amino acid peptide (FA) was previously designed in our group, comprising the substrate specificities of the proteases α-chymotrypsin and pepsin [39,40]. 2-Aminobutanoic acid (Abu) and its fluorinated analogues 2-amino-4,4-difluorobutanoic acid (DfeGly) and 2-amino-4,4,4-trifluorobutanoic acid (TfeGly) were individually incorporated at either the P2, the P1' or the P2' position [41] to give nine different analogues of FA. In prior studies, we observed that the introduction of fluorine atoms into the Abu side chain can significantly improve or dramatically reduce resistance to hydrolysis by different enzymes and human blood plasma, depending upon the fluorine content of the side chain, the position of the substitution relative to the cleavage site and the particular protease [39,40].

Here, we extend these studies to include highly fluorinated, sterically demanding HfLeu, and 5,5,5-trifluoroisoleucine (TfIle) and to investigate their effects on proteolytic stability towards the serine proteases α-chymotrypsin, elastase, and proteinase K, and the aspartate protease pepsin.

Results and Discussion
Peptide design and structure
To elucidate the impact of fluorination on proteolytic stability we previously designed the peptide FA (Figure 1b) that comprises the substrate specificities of α-chymotrypsin and pepsin [39,40]. Consequently, the P1 position is occupied by a phenylalanine residue. Lysine residues were introduced at both ends of the peptide sequence to enhance solubility, and *o*-aminobenzoic acid (Abz) at the N-terminus serves as a fluorescence label. Alanine residues in positions P3, P3', and P4' act as spacers as the peptide binds in an extended conformation to the enzyme's active site [42]. The positions P2, P1' and P2' at or adjacent to the cleavage site [41] carry the key residues for the recognition of the substrate by the protease and serve as substitution sites.

2870

Figure 1: (a) Structures of isoleucine (**1**), leucine (**2**), and their fluorinated analogues 5,5,5-trifluoroisoleucine (**3**, TfIle) and 5,5,5,5',5',5'-hexafluoro-leucine (**4**, HfLeu). The van der Waals volumes given in parentheses correspond to the side chains (starting at α-carbon), and were calculated according to Zhao et al. [43]; (b) Names and amino acid sequences of the studied peptides; the substitution positions are marked as Xaa; Xaa = Leu, HfLeu, Ile or TfIle. Positions are named according to Schechter and Berger nomenclature [41].

The alanines at P2, P1' or P2' positions were substituted individually with either TfIle or HfLeu (Figure 1a). Ile and Leu variants were also included in this study as non-fluorinated controls. This led to a library of 12 FA variants (Figure 1b).

Leu and Ile are larger and more hydrophobic than Ala. The fluorinated amino acids are even larger and more hydrophobic than their hydrocarbon analogues [44,45]. Furthermore, fluorine substitution has been shown to polarize neighboring C–H bonds (here the γ-hydrogens) that could affect noncovalent interactions [9,11]. Since the amino acids used here (Figure 1a) differ in their degree of fluorination, spatial demand and hydrophobicity, it is expected that they will have different impacts on the enzyme's binding pocket, reflected by different behavior in the proteolysis assay.

Determination of proteolytic stability

All peptides were incubated with the four different proteases and their proteolytic degradation was followed over a period of 24 h. Both, α-chymotrypsin [46-49] and pepsin [50-54] are well characterized digestive proteases. They are, together with trypsin, the main enzymes of the human digestive system. Elastase possesses a wide substrate specificity for non-aromatic, neutral side chains [55,56] and is found in the human pancreas and in blood serum. Proteinase K, an enzyme widely used for inactivation and degradation studies of proteins, was included here since it shows a broad substrate specificity and high activity and, thus, is able to digest numerous native proteins, even in the presence of detergents [57]. These four enzymes have different preferences at their subsites, thus providing a broad scope for our investigations.

The course of proteolytic digestion was characterized by an analytical HPLC-assay with fluorescence detection [39,40]. For quantification of substrate degradation, integration of the corresponding HPLC peak was conducted. Cleavage products were identified by ESI–ToF mass spectrometry (see Supporting Information File 1, Tables S4–S7). Figure S2 (Supporting Information File 1) shows the time course of all of the digestion experiments. A detailed description of the results for the individual enzymes is given in the following sections.

Proteolytic stability towards α-chymotrypsin (EC 3.4.21.1)

α-Chymotrypsin is a serine endopeptidase with broad specificity. It preferably cleaves peptide bonds C-terminal to large hydrophobic residues such as phenylalanine, tyrosine, tryptophan, and leucine in the P1 position. Secondary hydrolysis also occurs at the carbonyl end of isoleucine, methionine, serine, threonine, valine, histidine, glycine, and alanine [47,58-60].

The S2 subsite of α-chymotrypsin generally prefers to accommodate hydrophobic residues [59,61]. We observed that the fluorinated P2 variants show a smaller amount of digestion after 120 min compared to their hydrocarbon analogues, while all variants are more stable than the control FA (Figure 2). After 24 h, all P2 peptides except for P2-LeuFA are still more stable than FA. Incorporation of Leu into P2 leads to complete proteolysis compared to FA, in which Ala occupies this position. However, incorporation of six fluorine substituents into Leu (resulting in HfLeu) results in an almost 100% gain in proteolytic stability. Ile is not as highly preferred in P2 as Leu, but also here the introduction of three fluorine substituents leads to a

Figure 2: Percentage of substrate remaining after incubation for 120 min (left) and 24 h (right) with α-chymotrypsin in 10 mM phosphate buffer, pH 7.4, at 30 °C. The data shown represent the average of three independent measurements. Errors are derived from the standard deviation.

50% gain in stability. P2-HfLeuFA and P2-TfIleFA are not digested at all, suggesting that HfLeu and TfIle are not favored within the S2 pocket of α-chymotrypsin.

P1'-substituted peptides are all more stable towards digestion than the control peptide FA, while Leu seems to provide the best protection from proteolysis. Here, introduction of fluorine makes the peptide prone to degradation. The opposite is true for Ile as TfIle leads to less efficient degradation. The S1' subsite of α-chymotrypsin usually accommodates basic residues with long side chains [59,62,63]. Ile, as a branched amino acid, is obviously not well accommodated in this position for steric reasons. A further increase in side chain volume with TfIle exacerbates this effect. In the case of HfLeu, however, fluorine substituents seem to engage in favorable interactions with amino acid residues of the binding site, thus making P1'-HfLeuFA a better substrate than the non-fluorinated Leu peptide. Several such interactions are possible, as described in our previous work [39,40,64].

The S2' subsite of α-chymotrypsin exhibits a hydrophobic character and thus prefers to accommodate hydrophobic residues [59,65]. However, the more hydrophobic peptides P2'-LeuFA, P2'-HfLeuFA, P2'-IleFA, P2'-TfIleFA are more stable against digestion by α-chymotrypsin compared to FA after 120 min of incubation. After 24 h, only the fluorinated analogues are less degraded than the control FA. Full length P2'-HfLeuFA and P2'-TfIleFA are present at percentages up to 44% and 24%, respectively, while substitution by Leu and Ile in P2' position leads to accelerated proteolysis compared to FA. Thus, both HfLeu and TfIle have a protective effect towards proteolysis in this position.

ESI–ToF mass analysis confirms that the position P1 bearing Phe is the main cleavage site for α-chymotrypsin (Figure 3). Cleavage C-terminal to Leu and HfLeu in P1'-LeuFA and P1'-HfLeuFA is also observed (Figure 3, see Supporting Information File 1, Table S4), which means that the cleavage site was shifted towards the C-terminus by one residue. This is likely a consequence of α-chymotrypsin's preference for not only aromatic residues but also bulky hydrophobic residues in the S1 pocket, thus, HfLeu is accepted by the P1 binding pocket of α-chymotrypsin.
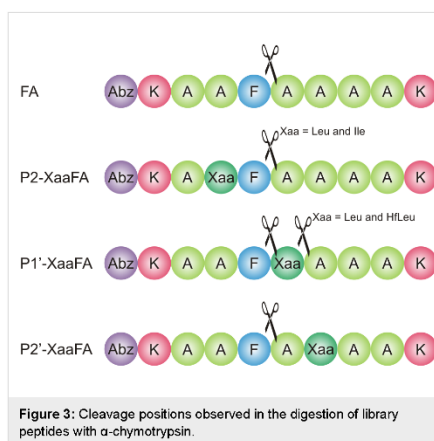
Figure 3: Cleavage positions observed in the digestion of library peptides with α-chymotrypsin.

In summary, the introduction of fluorinated Leu and Ile analogues into a α-chymotrypsin specific peptide sequence can

improve proteolytic stability mainly at the P2 and P2' positions, with the strongest effects observed for the P2 position.

Proteolytic stability towards pepsin (EC 3.4.23.1)

Pepsin is an aspartic endopeptidase and one of the main digestive enzymes in humans. It exhibits specificity for hydrophobic, especially aromatic residues like Phe, Trp, and Tyr at the P1 and P1' positions [50-54]. It has an extended active site that can bind at least seven residues [66,67], and peptide bond cleavage occurs N-terminal to the residue at position P1. The cleavage efficiency heavily depends upon the identity of this amino acid, with Phe and Leu being the most favored residues. At the P1' position aromatic amino acid residues are preferred, however, the influence of the P1' position on proteolytic cleavage is not as significant [68]. Pepsin typically does not cleave at Val, Ala, or Gly linkages [60].

The S2 subsite of pepsin preferentially accommodates hydrophobic residues such as Leu, Ala or norleucine as well as the β-branched species Ile and Val, but can also bind charged residues [69,70]. Except for P2-TfIleFA, we observed that the P2-modified peptides are degraded more rapidly than the control peptide FA and that these peptides are almost or completely degraded after 120 min (Figure 4). For example, whereas after 24 h FA is also almost completely degraded, P2-TfIleFA is still detected at a level of 100%. Incorporation of Leu or Ile leads to complete proteolysis. Remarkably, the introduction of six fluorine atoms into Leu doesn't change this behavior. In sharp contrast yet equally remarkable, the incorporation of three fluorine substituents into Ile results in a 100% gain in proteolytic stability. These results indicate that Leu, HfLeu,

as well as Ile are well accommodated in the S2 subsite of pepsin. In contrast, TfIle, although smaller than HfLeu [44], doesn't appear to fit well into the S2 pocket of pepsin.

To compare the P1' substituted peptides, only P1'-HfLeuFA shows the same persistence after 120 min as the control peptide FA, while all other sequences are digested faster. Here, the introduction of fluorine into Leu seems to stabilize the peptide by about 20%. Interestingly, after 24 h this trend is reversed, and the P1'-HfLeuFA peptide is destabilized to an amount of 17% compared to the hydrocarbon analogue, but both peptides are somewhat more stable than the control FA. The incorporation of TfIle into this position doesn't show a significant impact. Although the fluorine substituents slow down the digestion process (see Supporting Information File 1, Figure S2b), the TfIle containing peptide as well as its hydrocarbon analogue are fully digested after 24 h. The S1' subsite has hydrophobic character and thus prefers to accommodate hydrophobic or aromatic residues [71]. Ile and TfIle are obviously well accommodated in this position, while Leu and HfLeu are not.

The S2' subsite of pepsin favors hydrophobic amino acids, but also accepts charged polar amino acids like Glu and Thr [52,72]. After 120 min peptides P2'-LeuFA, P2'-IleFA and P2'-TfIleFA are degraded faster than the control FA. Instead, P2'-HfLeuFA is only digested up to 5%. This effect is even more pronounced after 24 h. While all other P1' substituted peptides, along with the control peptide FA, are almost or completely digested, P2'-HfLeuFA is still present to about 76%. In this case fluorination leads to protection against proteolysis by pepsin. Hfleu is obviously not well accommodated in this position. As already observed for position P1', the introduction of

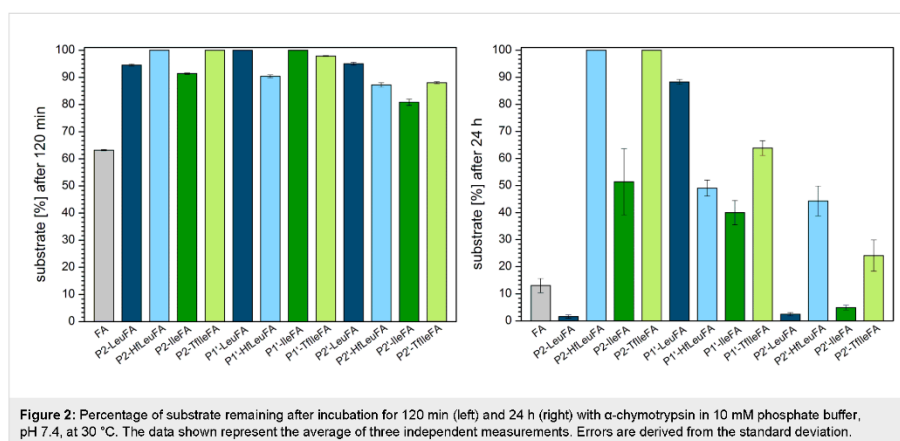**Figure 4:** Percentage of substrate remaining after incubation for 120 min (left) and 24 h (right) with pepsin in 10 mM acetate buffer, pH 4.0, at 30 °C. The data shown represent the average of three independent measurements. Errors are derived from the standard deviation.
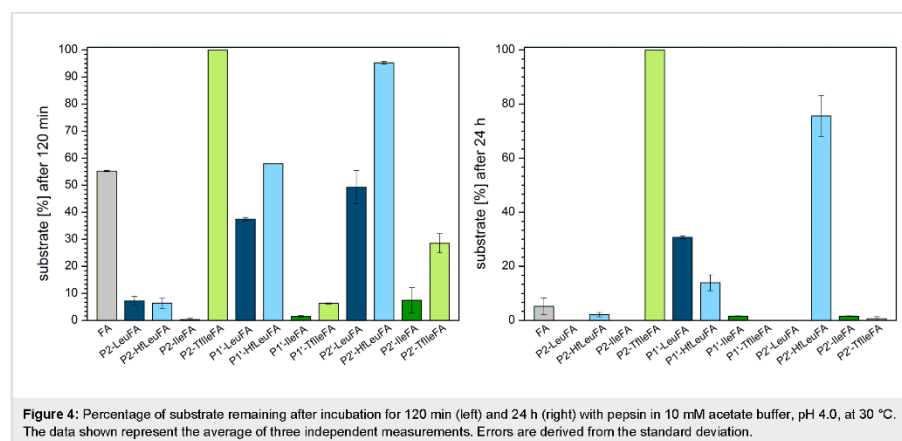
three fluorine atoms into Ile slows down proteolysis, although both peptides are completely digested after 24 h.

For almost all peptides of our library, we observed the expected cleavage pattern with Phe in the P1 position (Figure 5, see Supporting Information File 1, Table S5). Only P2'-HfLeuFA is not hydrolyzed at the designed cleavage site, instead cleavage occurs exclusively N-terminal to the HfLeu residue, thus demonstrating that HfLeu occupies the P1' position. In the case of P2'-TfIle we found two further peptide bonds that are cleaved by pepsin, namely N-terminal cleavage to TfIle and to Phe. These findings indicate that the S1' subsite accommodates bulky hydrophobic residues more readily than does the S2' site of pepsin. For P1'-LeuFA and P1'-HfLeuFA we found an addi-

tional cleavage site at which the peptide bonds $Leu^{P1'}$-$Ala^{P2'}$, and $HfLeu^{P1'}$-$Ala^{P2'}$ are hydrolyzed, respectively, which means that the cleavage site was shifted towards the C-terminus by one residue. This cleavage pattern was also detected for α-chymotrypsin before, and indicates that HfLeu is well accepted by pepsin in its S1 binding site. Furthermore, we identified a second cleavage site for P2-HfLeuFA at which the peptide bond N-terminal to Phe is proteolytically cleaved as well. This means that the cleavage site is shifted such that HfLeu occupies the P1 and Phe the P1' position. However, this perfectly matches the specificity of pepsin that prefers bulky hydrophobic and aromatic amino acids both up- and downstream of the scissile bond.

In summary, the introduction of fluorinated Leu into a pepsin specific peptide sequence can improve the proteolytic stability at the P2' position, whereas the incorporation of a fluorinated Ile into the P2 position shows the strongest effect in protection from proteolysis.

Proteolytic stability towards elastase (EC 3.4.21.36)

Elastase is a serine endopeptidase, and has a wide specificity for non-aromatic uncharged side chains. It preferentially cleaves peptide bonds C-terminal to small uncharged non-aromatic amino acid residues such as glycine, alanine and serine, but also valine, leucine, isoleucine [56,73]. Its binding site extends over eight subsites (S5 to S1, and S1' to S3') [74].

The fact that in this study larger and more hydrophobic amino acids [44,45] were introduced may explain why degradation of most of the variants during the first 120 min of incubation with elastase is hardly observed (Figure 6). Only P2'-LeuFA, P2'-
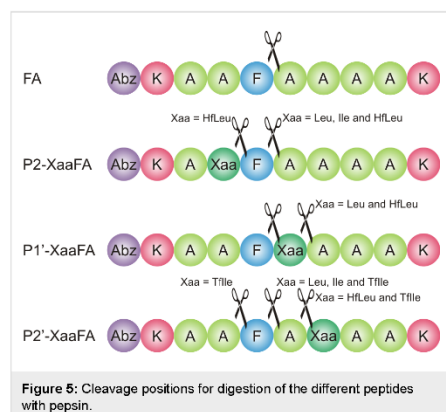
Figure 5: Cleavage positions for digestion of the different peptides with pepsin.

Figure 6: Percentage of substrate remaining after incubation for 120 min (left) and 24 h (right) with elastase in 100 mM Tris/HCl buffer, pH 8.4, at 37 °C. The data shown represent the mean of three independent measurements. Errors are derived from the standard deviation.

2874

IleFA, and P2'-TflIleFA were somewhat digested during this time, however, all of the modified peptides are more stable than the control FA.

After 24 h all P2 peptide variants are more stable than the control FA (Figure 6), while TfIle provides the best protection from elastase digestion. Leu and Ile are not quite as preferred in P2 position as is Ala. Fluorination of Leu leads to an increase in stability of around 19%. With 35% this effect is even higher when three fluorine atoms are introduced into Ile.

Modification of the P1' postion renders P1'-HfLeuFA and P1'-IleFA more stable than the control peptide FA, while P1'-TflIleFA is comparably stable. Incorporation of Leu into P1' leads to complete digestion. However, introducing six fluorine atoms into Leu results in an 85% gain in stability. The opposite is observed for Ile, where TfIle accelerates enzymatic degradation.

Except for P2'-IleFA, all P2' modified variants are more stable compared to the control peptide FA after 24 h. Leu is not as preferred in this position as is Ala. Introduction of fluorine strengthens this effect and effectively doubles the stability. In contrast, introduction of Ile leads to almost complete proteolysis. However, substitution by TfIle slows down the degradation rate and results in a stabilization of around 37%. In P2', fluorination shows in both cases a protective effect towards hydrolysis by elastase.

Elastase preferably hydrolyses peptide bonds C-terminal to uncharged non-aromatic amino acids and mainly between Ala–Ala and Ala–Gly bonds [56,73]. Since Ala is the main residue present in the peptides studied here, we observed various cleavage products in the ESI–ToF analysis (Figure 7, see Supporting Information File 1, Table S6). For none of the peptides were fragments with Phe in the P1 position observed. Since elastase has a constricted S1 pocket, the binding of aromatic amino acids at P1 is deleterious [75]. Here, we also observed that Leu appears to never occupy the P1 position, although it is known to occupy this position in other substrates [73]. Interestingly, the larger fluorinated variant was found in the P1 position in one case, while Ile and its fluorinated analogue occupy this position in two of the three peptide analogues.

The S2' subsite of elastase has a marked specificity for Ala, and can accommodate bulkier residues only with some difficulty [74]. Thus, we did not find the fluorinated amino acids HfLeu and TfIle binding to the S2' subsite of the enzyme as expected, whereas for the Leu and Ile variants this was observed only in one case each.
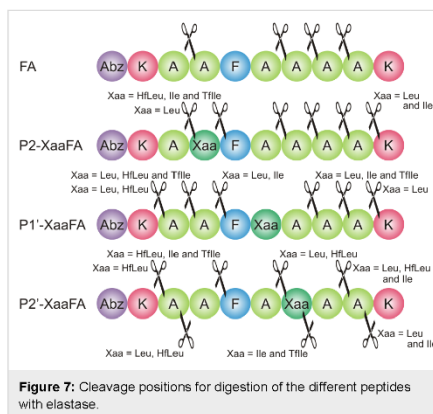
Figure 7: Cleavage positions for digestion of the different peptides with elastase.

The S1' subsite usually prefers Lys residues, and to a lesser extent Ala or Glu [74,76]. Indeed, we found a fragment cleaved off corresponding to a Lys in P1', but primarily detected fragments with Ala in P1' and also Phe that was even more favored than Lys. We observed that Ile as well as its fluorinated analogue TfIle are not accommodated in this subsite, probably due to their β-branched topology.

The S3' pocket in elastase is known to have a high aromatic specificity [74]. Interestingly, in our cases Phe in P3' was less favored. Instead, mainly Lys occupied this position.

Ala is favored in P2. Its carboxyl group can form a hydrogen bond with the amide nitrogen of Gly193 in the S2 pocket, and Ala's methyl group faces the solvent [76].

Occupation of the S4 subsite is important for efficient catalysis [76,77]. Thus elastase might not easily split the first three bonds at the amino terminus of a peptide chain, since interactions of a residue with S4 is necessary [77]. Indeed, we only observed a low amount of cleavage proximal to the N-terminus, while most of the hydrolysis occurred at the C-terminal end of the peptides. The S3 subsite seems to accommodate bulkier hydrophobic amino acids well, as we observed cleavage products containing Ile and Leu in P3 position for all the peptides modified with these residues, as well as their fluorinated analogues for two of the three substituted peptides each.

In summary, introduction of HfLeu in different positions of a peptide can enhance the proteolytic stability up to 85% compared to the corresponding Leu analogues. Replacing Ile with TfIle can increase the stability against elastase as well, although not as efficiently as HfLeu.

2875

8

Proteolytic stability towards proteinase K (EC 3.4.21.64)

Proteinase K is a non-specific serine endopeptidase and the main proteolytic enzyme produced by the fungus *Tritirachium album Limber* [78]. It has a broad substrate specificity, cleaving peptide bonds C-terminal to a number of amino acids, however, prefers aromatic or aliphatic hydrophobic amino acids in position P1 [57,78]. Furthermore, Ala is favored in position P2 and enhances cleavage efficiency [79,80]. Proteinase K possesses a very high proteolytic activity [79]. Its active center contains an extended binding region consisting of several subsites, at least four or five subsites on the N-terminal side of the scissile bond (S1 to S4/S5) and three subsites C-terminal to the scissile bond (S1' to S3') [81-83]. The "bottom" of substrate recognition site is predominantly hydrophobic and there is evidence that not the sequence of the substrate is of importance in the recognition but only the volume of the side chains [84].

Substitution of Ala in position P2 with Ile and Leu leads to a greater or comparable amount of degradation after 120 min. Introducing fluorine atoms in both cases slows down the digestion process, most pronounced for P2-TfIleFA with a gain of 60% in stability compared to its non-fluorinated analogue. Ile is not preferred to the extent that Leu is, and the introduction of fluorine enhances this effect. While all other peptides are almost completely or entirely degraded after 24 h, P2-TfIleFA is the only peptide that is still left after 24 h of incubation (Figure 8).

Introduction of Leu at the P1' position leads to an amount of digestion comparable to FA after 120 min. Fluorination of the Leu side chain leads to a small acceleration in digestion. Ile at

this position is not as preferred as is Leu and this enhances the stability to a small extent compared to FA. Introducing three fluorine atoms at the Ile side chains strengthens the stability against proteinase K even further.

As already observed for the other two Leu containing peptides, also substitution of Ala at position P2' with Leu does not change the resistance against proteinase K significantly. Interestingly, when six fluorine atoms are introduced, the digestion process is faster and P2'-HfLeuFA is almost completely degraded after 120 min. The opposite is observed for the fluorination of Ile. While P2'-IleFA is as stable as FA, P2'-TfIleFA shows a small gain in stability of around 12%.

Thus, in the case of P1' as well as P2' peptide variants, only fluorination of Ile leads to a slower digestion by proteinase K, while introducing even more fluorine atoms into the Leu side chain leads to more rapid hydrolysis compared to the non-fluorinated analogues. Ile seems in all investigated cases not as preferred as Leu, since less efficient digestion is observed. Introduction of three fluorine atoms even enhances this protective effect.

Based on the wide substrate specificity of proteinase K and its preference for alanine, and since our studied peptides have a high number of alanine residues present, there are multiple cleavage sites possible in addition to the designed site between Phe[P1] and Xaa[P1']. Indeed, multiple cleavage patterns are observed, especially cleavage C-terminal to Ala (Figure 9, see Supporting Information File 1, Table S7). Thus, Ala mainly occupies the S1 subsite, but is also found to bind to the S2 site
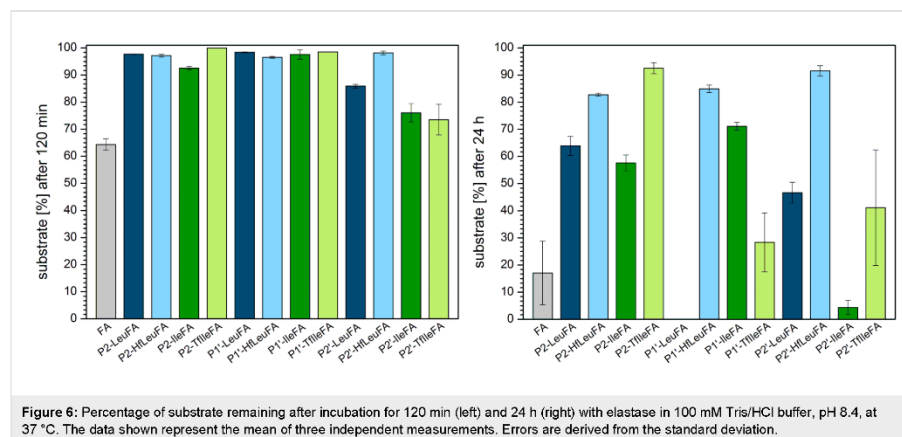

Figure 8: Percentage of substrate remaining after incubation for 120 min (left) and 24 h (right) with proteinase K in 50 mM Tris/HCl buffer, containing 10 mM CaCl$_2$ pH 7.5, at 37 °C. The data shown represent the mean of three independent measurements. Errors are derived from the standard deviation.

2876

Figure 9: Cleavage positions found with proteinase K.
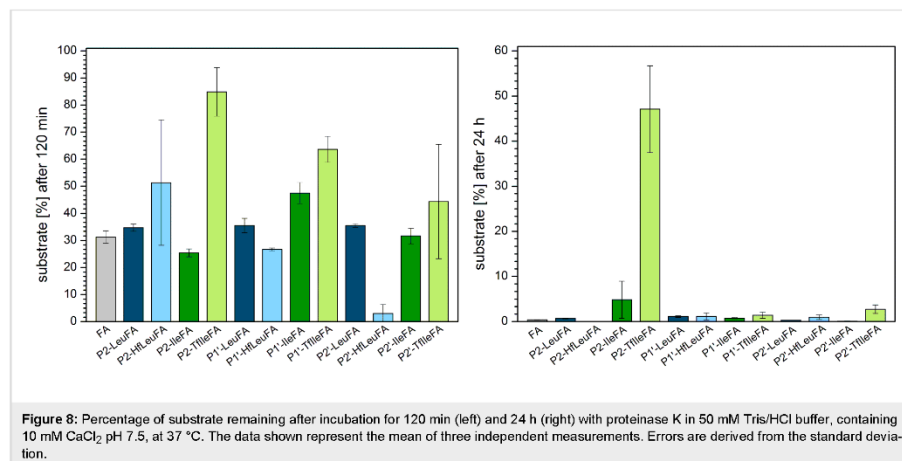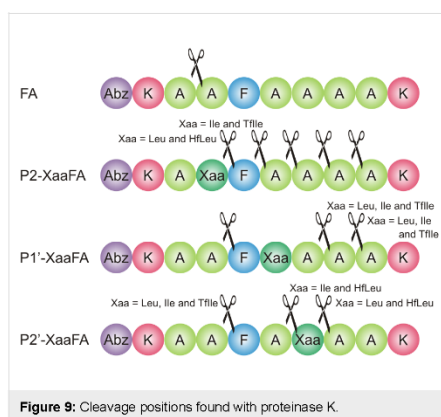
to a greater extent. Ala is most effective in P2 [80] as the S2 subsite is a small and narrow cleft, which limits the possibilities for effective side chain substitutions [79]. However, Ile and TfIle are well accepted here. A negative or positive charge at S2 is not preferred and hampers the formation of the enzyme substrate complex [82]. Thus, it can be concluded that Lys is poorly accepted at this position. HfLeu, the most sterically bulky amino acid investigated here, is not observed to occupy the S2 subsite. Instead, HfLeu is mainly found to bind to the S1 pocket. Leu is also found to occupy the S1 site of proteinase K, which is large and has mainly hydrophobic character [82,83,85]. It does not impose too strong steric limitations on the amino acid side chain but prefers hydrophobic and aromatic residues, with a specificity for Ala [78,81,83,86]. Charged side chains of Glu and Lys are very poorly accepted, as are β-branched functional groups, because the entrance to the S1 subsite is too narrow to allow their passage [79]. Thus, Lys is not observed to occupy the S1 subsite. Neither Ile nor TfIle can be accommodated by the S1 pocket due to their β-branching. Phe is found in S1 in only two cases in our study, and mainly occupies the S3 and S1' pockets. The S3 pocket has a wide specificity due to its location at the protein surface, but exhibits preference for aromatic side chains in P3 (Trp, Phe) [79]. S1' shows a slight preference for smaller residues like Ala and Gly, but also bulkier residues such as Phe and Leu are hydrolyzed to a significant extent [81]. In this study Leu apparently does not bind to the S1' site at all, and this is also true of TfIle. Additionally, Lys is not well accommodated here. Phe is also found to occupy S4 to a great extent, and this subsite is known to have an affinity for aromatic groups, especially a marked preference for Phe [79]. S4–P4 interactions are primarily hydrophobic in nature [79], which might explain why we observed that Lys is only poorly accepted in this position. The S3 subsite cannot be

defined as a "cleft" or "pocket" [79]. The P3 residue of the peptide substrate lies on the protein surface and the side chain of P3 should be directed toward the solvent [79]. This arrangement might explain the broad specificity of S3 [79]. We observed that all the residues used in this study can occupy the P3 position, mainly Phe and Lys. Leu, Ile and TfIle are also found to a great extent in P3.

In summary, fluorination of an Ile residue N-terminal to the cleavage site can help to protect a peptide against proteolysis by proteinase K. Due to its broad specificity and high activity, proteinase K typically digests peptides quickly [57]. This was also observed in this work in experiments in which all peptides, except for P2-TfIleFA, a remarkably stable species, were completely degraded after an incubation time of 24 h.

Conclusion

The bulky side-chain fluorinated amino acids HfLeu and TfIle have the power to significantly stabilize peptides against proteolytic degradation. The impact of their incorporation on the proteolytic stability of peptides does not follow a general trend but rather depends on a combination of factors including the nature of the fluorinated amino acid, the substitution position relative to the cleavage site and the studied protease. Also, in contrast to proteolytic studies published before [23,27,28], the expectation of a general increase in proteolytic stability as a result of steric occlusion of the peptide from the active site upon incorporation of sterically demanding fluorinated amino acids could not be verified based on the results of our current study. We found a significant stabilization towards proteolysis in 13 of a total of 24 peptides of the library studied here upon introduction of either HfLeu or TfIle (Figure 10). However, we observed that even these sterically demanding fluorinated amino acids show in some cases favorable interactions with the enzymes binding sites resulting in a more rapid digestion as the non-fluorinated control.

The introduction of fluorinated Leu and Ile analogues into P2 and P2' position improved the proteolytic stability towards α-chymotrypsin. When introduced in the P1' position a stabilization was still observed for TfIle, while incorporation of HfLeu made the peptide more prone to proteolytic digestion compared to the non-fluorinated control. Incorporation of HfLeu had a significantly stabilizing effect towards hydrolysis by pepsin only in P2' position, while TfIle develops a protective effect only when incorporated in P2 position.

As both, elastase and proteinase K possess a broad specificity, preferring C-terminal cleavage to Ala, we observed here a rather unspecific cleavage pattern for both enzymes with multiple cleavage products, in which the intended designed

Figure 10: Dimension of stabilization or destabilization upon TfIle or HfLeu incorporation compared to the non-fluorinated analogues containing Ile or Leu, respectively, for all four different enzymes studied here and measured after 24 h of incubation.
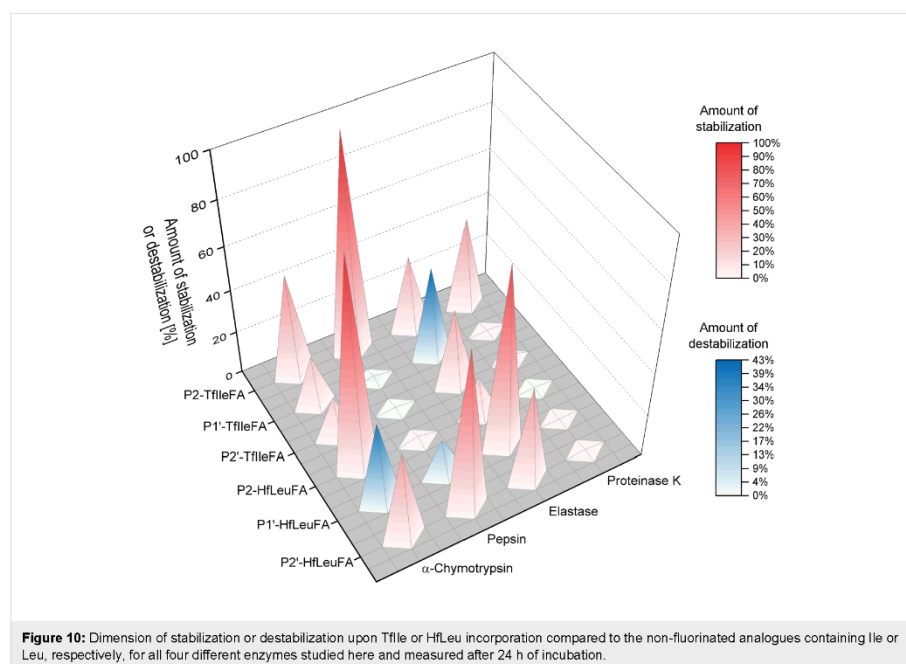
cleavage site with Phe in P1 position wasn't affected. However, we observed that the introduction of HfLeu has a general protective effect against degradation by elastase, whereas the effect of TfIle depends on the substitution position. Although the introduction of fluorine substituents generally affected the rate of hydrolysis by proteinase K, only fluorination of an Ile residue N-terminal to the cleavage site effectively protected the peptide from digestion. Particularly noteworthy is the effect of fluorination of the Ile side chain in P2 position. The P2-TfIleFA peptide was the most resistant substrate towards proteolysis by all four proteases applied in this study. In contrast, destabilization due to fluorination was only observed when TfIle and HfLeu were incorporated into the P1' position.

In future studies, we will focus on a more precise characterization of the interaction of fluorinated substrates with proteolytic enzymes to which multiple factors contribute. The steric demand or conformation of the side chain, hydrophobicity, fluorine induced polarity and significant pK_a-value changes of neighboring groups [9,10] can lead to fluorine-specific interactions between substrate and enzyme binding sites as well as to an exclusion of the cleavage-relevant peptide bonds from the active site.

Furthermore, our investigations show that fluorine's impact on proteolytic stability needs to be investigated always case-by-case as there is no general trend to be concluded. Nevertheless, the results of this current study provide valuable knowledge on how bulky fluorinated amino acids can help to increase the proteolytic stability of peptides, and show that upon smart design, these fluorinated amino acids can be used to engineer peptide drug candidates.

Experimental
Materials

Fmoc-L-amino acids were purchased from ORPEGEN Peptide Chemicals GmbH (Heidelberg, Germany). Fmoc-Lys(Boc)Wang resin was from Novabiochem (Merck Chemicals GmbH, Darmstadt, Germany). All solvents were used from VWR (Darmstadt, Germany) without further purification. All other chemicals were bought from Acros (Geel, Belgium), abcr GmbH (Karlsruhe, Germany), fluorochem (Hadfield, United Kingdom), VWR (Darmstadt, Germany) or Merck (Darmstadt, Germany) at highest commercially available purity and used as such. A detailed synthetic strategy for Fmoc-TfIle-OH is described in literature [44]. For the synthesis of Fmoc-HfLeu-OH see Supporting Information File 1.

2878

Peptide synthesis, purification and characterization

Peptides were synthesized manually in a 0.05 mmol scale on a solid support by means of an Fmoc/*tert*-butyl protecting group strategy on a preloaded Fmoc-Lys(Boc)Wang resin (0.57 mmol/g loading) using 10 mL polypropylene reactors. HfLeu containing peptides were synthesized with an Activo-P11 automated peptide synthesizer (Activotec, Cambridge, United Kingdom). Couplings of non-fluorinated amino acids were performed in dimethylformamide (DMF) with the Fmoc-L-amino acid, 1-hydroxybenzotriazole (HOBt) and *N,N'*-diisocarbodiimide (DIC) in an eight-fold excess with respect to the resin amount. In order to ensure completion of the reaction the couplings were performed twice for 1 h each. The fluorinated amino acids and coupling reagents 1-hydroxy-7-azabenzotriazole (HOAt)/DIC were used in 1.2-fold excess, and the coupling was carried out manually one time overnight. In the case of an insufficient coupling, the coupling was repeated for 3 h with 0.5 equivalents. Prior to the Fmoc deprotection of the fluorinated amino acids, free N-termini were capped by adding a mixture of acetic anhydride (Ac_2O, 10% (v/v)) and *N,N*-diisopropylethylamine (DIPEA, 10% (v/v)) in DMF (3 × 10 min). Fmoc deprotection was achieved by treatment with 20% (v/v) piperidine in DMF (3 × 10 min). All peptides were N-terminally labeled with *o*-aminobenzoic acid (Abz) to enable photometric detection. The resin was washed between each step with DMF and dicholoromethane (DCM, 3 × 2 mL each). After the synthesis, the peptides were cleaved from the resin by treatment with a solution (2 mL) containing triisopropylsilane (TIS, 10% (v/v)), water (1% (v/v)), and trifluoroacetic acid (TFA) (89% (v/v)) for 3 h. The resin was washed twice with TFA (1 mL) and DCM (1 mL) and excess solvent was removed by evaporation. The crude peptide was precipitated with ice-cold diethyl ether (80 mL), and after centrifugation dried by lyophilization. Purification of the synthesized peptides was performed on a LaPrepΣ low-pressure HPLC system (VWR, Darmstadt, Germany) using a Kinetex RP-C18 endcapped HPLC column (5 µM, 100 Å, 250 × 21.2 mm, Phenomenex®, USA). A Security GuardTM PREP Cartridge Holder Kit (21.20 mm, ID, Phenomenex®, USA) served as pre-column. As eluents deionized water (Milli-Q Advantage® A10 Ultrapure Water Purification System, Millipore®, Billerica, MA, USA) and acetonitrile (ACN), both containing 0.1% (v/v) TFA were used. HPLC runs were performed starting with an isocratic gradient of 5% ACN over 5 min, flow rate: 10 mL/min, continuing with a linear gradient of 5–70% ACN over 25 min, flow rate: 20.0 mL/min. UV-detection occurred at 220 nm. Data analysis was performed with an EZChrom Elite-Software (Version 3.3.2 SP2, Agilent Technologies, Santa Clara, CA, USA). The fractions containing pure peptide were combined, reduced in vacuo and lyophilized to give the peptides as a white

powder. The purity of the peptides was controlled by analytical HPLC (LUNA™ C8 (2) column, 5 µm, 250 × 4.6 mm, Phenomenex®, Torrance, CA, USA), and the products were identified by high-resolution ESI–ToF–MS (see Supporting Information File 1).

Protease digestion assay

All peptides employed in the degradation studies were used as the TFA salts obtained after lyophilization. Stock solutions of α-chymotrypsin (from bovine pancreas, EC 3.4.21.1, ≥40.0 units/mg of protein, Sigma Aldrich, St. Louis, MO, USA), and pepsin (from porcine stomach mucosa, EC 3.4.23.1, ≥250 units/mg of protein, Sigma Aldrich, St. Louis, MO, USA) were prepared at concentrations of 1 mg/mL in phosphate buffer (10 mM, pH 7.4), or in acetate buffer (10 mM, pH 4.0), respectively. For proteinase K (from tritirachium album, EC 3.4.21.64, ≥30 units/mg of protein, Sigma Aldrich, St. Louis, MO, USA) and elastase (from porcine pancreas, EC 3.4.21.36, 6.2 units/mg of protein, Sigma Aldrich, St. Louis, MO, USA) stock solutions were prepared also at concentrations of 1 mg/mL in tris/HCl (50 mM) + $CaCl_2$ (10 mM) buffer (pH 7.5), or in tris/HCl buffer (100 mM, pH 8.4), respectively. Peptides (0.002 mmol) were prepared as stocks in DMSO (100 µL) and incubated with the respective enzyme at 30 °C (for α-chymotrypsin and pepsin) or 37 °C (for proteinase K and elastase) with shaking at 300 rpm in a thermomixer over a period of 24 h. The reaction mixture consisted of DMSO (15 µL), corresponding buffer (25 µL), peptide solution (5 µL) and the corresponding enzyme solution (5 µL). The concentration of enzyme was optimized so that the hydrolysis of the control peptide FA was about 40% after 120 min. Aliquots of 5 µL were taken at fixed time points (0, 15, 30, 60, 90, 120 min as well as 3 h and 24 h) and either quenched with ACN containing 0.1% (v/v) TFA (95 µL), in the case of α-chymotrypsin, proteinase K and elastase, or 2% aqueous ammonia (95 µL), in the case of pepsin. All samples were subjected to analytical HPLC on a LaChrom-ELITE-HPLC-System equipped with a fluorescence detector (VWR International Hitachi, Darmstadt, Germany). A monolithic reversed-phase C8 Chromolith® Performance HPLC column (100 × 4.6 mm, Merck KGaA, Darmstadt, Germany) was used to resolve and quantify the products of digestion. The used system and gradients are described in detail in Supporting Information File 1. Detection based on the Abz label was carried out using a fluorescence detector with λ_{ex} = 320 nm and λ_{em} = 420 nm. In all cases, the peaks corresponding to the starting materials (full-length peptides) or the N-terminal fragments (products) were integrated and used to determine the velocity of the reaction (see Supporting Information File 1). The FA peptide was used as a reference. Each fragment cleaved from the full-length peptide was identified by ESI–ToF mass analysis on an Agilent 6220 ESI–ToF–MS spec-

2879

trometer (Agilent Technologies, Santa Clara, CA, USA, see Supporting Information File 1). All experiments were performed in triplicate.

Supporting Information

Supporting Information File 1

Characterization and identification of synthesized peptides, characterization of the enzymatic digestion reactions, and identification of proteolytic cleavage products, HPLC methods, and synthesis protocol for Fmoc-HfLeu-OH.
[http://www.beilstein-journals.org/bjoc/content/supplementary/1860-5397-13-279-S1.pdf]

References

1. Vlieghe, P.; Lisowski, V.; Martinez, J.; Khrestchatisky, M. *Drug Discovery Today* **2010**, *15*, 40–56. doi:10.1016/j.drudis.2009.10.009
2. Sato, A. K.; Viswanathan, M.; Kent, R. B.; Wood, C. R. *Curr. Opin. Biotechnol.* **2006**, *17*, 638–642. doi:10.1016/j.copbio.2006.10.002
3. Albericio, F.; Kruger, H. G. *Future Med. Chem.* **2012**, *4*, 1527–1531. doi:10.4155/fmc.12.94
4. Uhlig, T.; Kyprianou, T.; Martinelli, F. G.; Oppici, C. A.; Heiligers, D.; Hills, D.; Calvo, X. R.; Verhaert, P. *EuPa Open Proteomics* **2014**, *4*, 58–69. doi:10.1016/j.euprot.2014.05.003
5. Fosgerau, K.; Hoffmann, T. *Drug Discovery Today* **2015**, *20*, 122–128. doi:10.1016/j.drudis.2014.10.003
6. Santos, G. B.; Ganesan, A.; Emery, F. S. *ChemMedChem* **2016**, *11*, 2245–2251. doi:10.1002/cmdc.201600288
7. Jäckel, C.; Koksch, B. *Eur. J. Org. Chem.* **2005**, 4483–4503. doi:10.1002/ejoc.200500205
8. Latham, P. W. *Nat. Biotechnol.* **1999**, *17*, 755–757. doi:10.1038/11686
9. Salwiczek, M.; Nyakatura, E. K.; Gerling, U. I. M.; Ye, S.; Koksch, B. *Chem. Soc. Rev.* **2012**, *41*, 2135–2171. doi:10.1039/C1CS15241F
10. Berger, A. A.; Völler, J.-S.; Budisa, N.; Koksch, B. *Acc. Chem. Res.* **2017**, *50*, 2093–2103. doi:10.1021/acs.accounts.7b00226
11. Salwiczek, M.; Samsonov, S.; Vagt, T.; Nyakatura, E.; Fleige, E.; Numata, J.; Cölfen, H.; Pisabarro, M. T.; Koksch, B. *Chem. – Eur. J.* **2009**, *15*, 7628–7636. doi:10.1002/chem.200802136
12. Huhmann, S.; Nyakatura, E. K.; Erdbrink, H.; Gerling, U. I. M.; Czekelius, C.; Koksch, B. *J. Fluorine Chem.* **2015**, *175*, 32–35. doi:10.1016/j.jfluchem.2015.03.003
13. Marsh, E. N. G. Designing Fluorinated Proteins. In *Methods in Enzymology*; Vincent, L. P., Ed.; Academic Press, 2016; Vol. 580, pp 251–278. doi:10.1016/bs.mie.2016.05.006

14. Vukelić, S.; Moschner, J.; Huhmann, S.; Fernandes, R.; Berger, A. A.; Koksch, B. Synthesis of Side Chain Fluorinated Amino Acids and Their Effects on the Properties of Peptides and Proteins. In *Modern Synthesis Processes and Reactivity of Fluorinated Compounds*; Leroux, F. R.; Tressaud, A., Eds.; Elsevier, 2017; pp 427–464. doi:10.1016/B978-0-12-803740-9.00015-9
15. Buer, B. C.; Meagher, J. L.; Stuckey, J. A.; Marsh, E. N. G. *Protein Sci.* **2012**, *21*, 1705–1715. doi:10.1002/pro.2150
16. Buer, B. C.; Meagher, J. L.; Stuckey, J. A.; Marsh, E. N. G. *Proc. Natl. Acad. Sci. U. S. A.* **2012**, *109*, 4810–4815. doi:10.1073/pnas.1120112109
17. Jäckel, C.; Salwiczek, M.; Koksch, B. *Angew. Chem., Int. Ed.* **2006**, *45*, 4198–4203. doi:10.1002/anie.200504387
18. Tang, Y.; Tirrell, D. A. *J. Am. Chem. Soc.* **2001**, *123*, 11089–11090. doi:10.1021/ja016652k
19. Tang, Y.; Ghirlanda, G.; Petka, W. A.; Nakajima, T.; DeGrado, W. F.; Tirrell, D. A. *Angew. Chem., Int. Ed.* **2001**, *40*, 1494–1496. doi:10.1002/1521-3773(20010417)40:8<1494::AID-ANIE1494>3.0.CO;2-X
20. Tang, Y.; Ghirlanda, G.; Vaidehi, N.; Kua, J.; Mainz, D. T.; Goddard, W. A., III; DeGrado, W. F.; Tirrell, D. A. *Biochemistry* **2001**, *40*, 2790–2796. doi:10.1021/bi0022588
21. Yoder, N. C.; Kumar, K. *Chem. Soc. Rev.* **2002**, *31*, 335–341. doi:10.1039/b201097f
22. Bilgiçer, B.; Xing, X.; Kumar, K. *J. Am. Chem. Soc.* **2001**, *123*, 11815–11816. doi:10.1021/ja016767o
23. Meng, H.; Kumar, K. *J. Am. Chem. Soc.* **2007**, *129*, 15615–15622. doi:10.1021/ja075373f
24. Deacon, C. F.; Nauck, M. A.; Toft-Nielsen, M.; Pridal, L.; Willms, B.; Holst, J. J. *Diabetes* **1995**, *44*, 1126–1131. doi:10.2337/diab.44.9.1126
25. Holst, J. J.; Deacon, C. F. *Curr. Opin. Pharmacol.* **2004**, *4*, 589–596. doi:10.1016/j.coph.2004.08.005
26. Drucker, D. J. *Curr. Pharm. Des.* **2001**, *7*, 1399–1412. doi:10.2174/1381612013397401
27. Meng, H.; Krishnaji, S. T.; Beinborn, M.; Kumar, K. *J. Med. Chem.* **2008**, *51*, 7303–7307. doi:10.1021/jm8008579
28. Akçay, G.; Kumar, K. *J. Fluorine Chem.* **2009**, *130*, 1178–1182. doi:10.1016/j.jfluchem.2009.09.002
29. Gottler, L. M.; Lee, H.-Y.; Shelburne, C. E.; Ramamoorthy, A.; Marsh, E. N. G. *ChemBioChem* **2008**, *9*, 370–373. doi:10.1002/cbic.200700643
30. Voloshchuk, N.; Zhu, A. Y.; Snydacker, D.; Montclare, J. K. *Bioorg. Med. Chem. Lett.* **2009**, *19*, 5449–5451. doi:10.1016/j.bmcl.2009.07.093
31. Budisa, N.; Wenger, W.; Wiltschi, B. *Mol. BioSyst.* **2010**, *6*, 1630–1639. doi:10.1039/c002256j
32. Bordusa, F.; Dahl, C.; Jakubke, H.-D.; Burger, K.; Koksch, B. *Tetrahedron: Asymmetry* **1999**, *10*, 307–313. doi:10.1016/S0957-4166(98)00508-4
33. Koksch, B.; Sewald, N.; Burger, K.; Jakubke, H.-D. *Amino Acids* **1996**, *11*, 425–434. doi:10.1007/BF00807946
34. Koksch, B.; Sewald, N.; Hofmann, H.-J.; Burger, K.; Jakubke, H.-D. *J. Pept. Sci.* **1997**, *3*, 157–167. doi:10.1002/(SICI)1099-1387(199705)3:3<157::AID-PSC94>3.0.CO;2-W
35. Smits, R.; Koksch, B. *Curr. Top. Med. Chem.* **2006**, *6*, 1483–1498. doi:10.2174/156802606777951055
36. Thust, S.; Koksch, B. *J. Org. Chem.* **2003**, *68*, 2290–2296. doi:10.1021/jo020613p

2880

37. Thust, S.; Koksch, B. *Tetrahedron Lett.* **2004**, *45*, 1163–1165. doi:10.1016/j.tetlet.2003.12.007

38. Sewald, N.; Hollweck, W.; Mütze, K.; Schierlinger, C.; Seymour, L. C.; Gaa, K.; Burger, K.; Koksch, B.; Jakubke, H. D. *Amino Acids* **1995**, *8*, 187–194. doi:10.1007/BF00806491

39. Asante, V.; Mortier, J.; Schlüter, H.; Koksch, B. *Bioorg. Med. Chem.* **2013**, *21*, 3542–3546. doi:10.1016/j.bmc.2013.03.051

40. Asante, V.; Mortier, J.; Wolber, G.; Koksch, B. *Amino Acids* **2014**, *46*, 2733–2744. doi:10.1007/s00726-014-1819-7

41. Schechter, I.; Berger, A. *Biochem. Biophys. Res. Commun.* **1967**, *27*, 157–162. doi:10.1016/S0006-291X(67)80055-X

42. Davies, D. R. *Annu. Rev. Biophys. Biophys. Chem.* **1990**, *19*, 189–215. doi:10.1146/annurev.bb.19.060190.001201

43. Zhao, Y. H.; Abraham, M. H.; Zissimos, A. M. *J. Org. Chem.* **2003**, *68*, 7368–7373. doi:10.1021/jo034808o

44. Erdbrink, H.; Nyakatura, E. K.; Huhmann, S.; Gerling, U. I. M.; Lentz, D.; Koksch, B.; Czekelius, C. *Beilstein J. Org. Chem.* **2013**, *9*, 2009–2014. doi:10.3762/bjoc.9.236

45. Samsonov, S. A.; Salwiczek, M.; Anders, G.; Koksch, B.; Pisabarro, M. T. *J. Phys. Chem. B* **2009**, *113*, 16400–16408. doi:10.1021/jp906402b

46. Blow, D. M.; Birktoft, J. J.; Hartley, B. S. *Nature* **1969**, *221*, 337–340. doi:10.1038/221337a0

47. Blow, D. M. The Structure of Chymotrypsin. In *The Enzymes;* Paul, D. B., Ed.; Academic Press, 1971; Vol. 3, pp 185–212. doi:10.1016/S1874-6047(08)60397-2

48. Derewenda, Z. S.; Derewenda, U.; Kobos, P. M. *J. Mol. Biol.* **1994**, *241*, 83–93. doi:10.1006/jmbi.1994.1475

49. Polgár, L. *Cell. Mol. Life Sci.* **2005**, *62*, 2161–2172. doi:10.1007/s00018-005-5160-x

50. Fruton, J. S. The Specificity and Mechanism of Pepsin Action. In *Advances in Enzymology and Related Areas of Molecular Biology;* Nord, F. F., Ed.; John Wiley & Sons, Inc., 1970; Vol. 33, pp 401–443. doi:10.1002/9780470122785.ch9

51. Fruton, J. S. Pepsin. In *The Enzymes;* Paul, D. B., Ed.; Academic Press, 1971; Vol. 3, pp 119–164. doi:10.1016/S1874-6047(08)60395-9

52. Dunn, B. M. *Chem. Rev.* **2002**, *102*, 4431–4458. doi:10.1021/cr010167q

53. Antonov, V. K. New Data on Pepsin Mechanism and Specificity. In *Acid Proteases:Structure, Function, and Biology;* Tang, J., Ed.; Springer US: Boston, MA, 1977; pp 179–198. doi:10.1007/978-1-4757-0719-9_11

54. Powers, J. C.; Harley, A. D.; Myers, D. V. Subsite Specificity of Porcine Pepsin. In *Acid Proteases:Structure, Function, and Biology;* Tang, J., Ed.; Springer US: Boston, MA, 1977; Vol. 92, pp 141–157. doi:10.1007/978-1-4757-0719-9_9

55. Largman, C.; Brodrick, J. W.; Geokas, M. C. *Biochemistry* **1976**, *15*, 2491–2500. doi:10.1021/bi00656a036

56. Shotton, D. M. Elastase. *Methods in Enzymology;* Academic Press, 1970; Vol. 19, pp 113–140. doi:10.1016/0076-6879(70)19009-4

57. Sweeney, P. J.; Walker, J. M. Proteinase K (EC 3.4.21.14). In *Enzymes of Molecular Biology;* Burrell, M. M., Ed.; Humana Press: Totowa, NJ, 1993; pp 305–311. doi:10.1385/0-89603-234-5:305

58. Czapinska, H.; Otlewski, J. *Eur. J. Biochem.* **1999**, *260*, 571–595. doi:10.1046/j.1432-1327.1999.00160.x

59. Hedstrom, L. *Chem. Rev.* **2002**, *102*, 4501–4524. doi:10.1021/cr000033x

60. Sweeney, P. J.; Walker, J. M. Proteolytic Enzymes for Peptide Production. In *Enzymes of Molecular Biology;* Burrell, M. M., Ed.; Humana Press: Totowa, NJ, 1993; pp 277–303. doi:10.1385/0-89603-234-5:277

61. Brady, K.; Abeles, R. H. *Biochemistry* **1990**, *29*, 7608–7617. doi:10.1021/bi00485a010

62. Schellenberger, V.; Jakubke, H.-D. *Biochim. Biophys. Acta, Protein Struct. Mol. Enzymol.* **1986**, *869*, 54–60. doi:10.1016/0167-4838(86)90309-2

63. Schellenberger, V.; Turck, C. W.; Rutter, W. J. *Biochemistry* **1994**, *33*, 4251–4257. doi:10.1021/bi00180a020

64. Ye, S.; Loll, B.; Berger, A. A.; Mülow, U.; Alings, C.; Wahl, M. C.; Koksch, B. *Chem. Sci.* **2015**, *6*, 5246–5254. doi:10.1039/C4SC03227F

65. Antal, J.; Pál, G.; Asbóth, B.; Buzás, Z.; Patthy, A.; Gráf, L. *Anal. Biochem.* **2001**, *288*, 156–167. doi:10.1006/abio.2000.4886

66. Sampath-Kumar, P. S.; Fruton, J. S. *Proc. Natl. Acad. Sci. U. S. A.* **1974**, *71*, 1070–1072. doi:10.1073/pnas.71.4.1070

67. Fruton, J. S. *Acc. Chem. Res.* **1974**, *7*, 241–246. doi:10.1021/ar50080a001

68. Hamuro, Y.; Coales, S. J.; Molnar, K. S.; Tuske, S. J.; Morrow, J. A. *Rapid Commun. Mass Spectrom.* **2008**, *22*, 1041–1046. doi:10.1002/rcm.3467

69. Rao, C.; Dunn, B. M. Evidence for Electrostatic Interactions in the S2 Subsite of Porcine Pepsin. In *Aspartic Proteinases: Structure, Function, Biology, and Biomedical Implications;* Takahashi, K., Ed.; Springer US: Boston, MA, 1995; pp 91–94. doi:10.1007/978-1-4615-1871-6_10

70. Fujinaga, M.; Chernaia, M. M.; Mosimann, S. C.; James, M. N. G.; Tarasova, N. I. *Protein Sci.* **1995**, *4*, 960–972. doi:10.1002/pro.5560040516

71. Kageyama, T. *Cell. Mol. Life Sci.* **2002**, *59*, 288–306. doi:10.1007/s00018-002-8423-9

72. Dunn, B. M.; Hung, S.-H. *Biochim. Biophys. Acta, Protein Struct. Mol. Enzymol.* **2000**, *1477*, 231–240. doi:10.1016/S0167-4838(99)00275-7

73. Naughton, M. A.; Sanger, F. *Biochem. J.* **1961**, *78*, 156–163. doi:10.1042/bj0780156

74. Renaud, A.; Lestienne, P.; Hughes, D. L.; Bieth, J. G.; Dimicoli, J. L. *J. Biol. Chem.* **1983**, *258*, 8312–8316.

75. Qasim, M. A. *Protein Pept. Lett.* **2014**, *21*, 164–170. doi:10.2174/09298665113206660093

76. Atlas, D. *J. Mol. Biol.* **1975**, *93*, 39–48. doi:10.1016/0022-2836(75)90358-7

77. Atlas, D.; Levit, S.; Schechter, I.; Berger, A. *FEBS Lett.* **1970**, *11*, 281–283. doi:10.1016/0014-5793(70)80548-8

78. Ebeling, W.; Hennrich, N.; Klockow, M.; Metz, H.; Orth, H. D.; Lang, H. *Eur. J. Biochem.* **1974**, *47*, 91–97. doi:10.1111/j.1432-1033.1974.tb03671.x

79. Georgieva, D.; Genov, N.; Voelter, W.; Betzel, C. *Z. Naturforsch., C: J. Biosci.* **2006**, *61*, 445–452. doi:10.1515/znc-2006-5-623

80. Morihara, K.; Tsuzuki, H. *Agric. Biol. Chem.* **1975**, *39*, 1489–1492. doi:10.1080/00021369.1975.10861790

81. Brömme, D.; Peters, K.; Fink, S.; Fittkau, S. *Arch. Biochem. Biophys.* **1986**, *244*, 439–446. doi:10.1016/0003-9861(86)90611-9

82. Kraus, E.; Femfert, U. *Hoppe-Seyler's Z. Physiol. Chem.* **1976**, *357*, 937–947. doi:10.1515/bchm2.1976.357.2.937

83. Betzel, C.; Singh, T. P.; Visanji, M.; Peters, K.; Fittkau, S.; Saenger, W.; Wilson, K. S. *J. Biol. Chem.* **1993**, *268*, 15854–15858.

84. Wolf, W. M.; Bajorath, J.; Müller, A.; Raghunathan, S.; Singh, T. P.; Hinrichs, W.; Saenger, W. *J. Biol. Chem.* **1991**, *266*, 17695–17699.

85. Betzel, C.; Bellemann, M.; Pal, G. P.; Bajorath, J.; Saenger, W.; Wilson, K. S. *Proteins: Struct., Funct., Genet.* **1988**, *4*, 157–164. doi:10.1002/prot.340040302

86. Kraus, E.; Kiltz, H.-H.; Femfert, U. F. *Hoppe-Seyler's Z. Physiol. Chem.* **1976,** *357,* 233–237. doi:10.1515/bchm2.1976.357.1.233

Supporting Information

for

Position-dependent impact of hexafluoroleucine and trifluoroisoleucine on protease digestion

Susanne Huhmann[1], Anne-Katrin Stegemann[1], Kristin Folmert[1], Damian Klemczak[1], Johann Moschner[1], Michelle Kube[1] and Beate Koksch*[1]

Address: [1]Department of Chemistry and Biochemistry, Freie Universität Berlin, Takustraße 3, 14195 Berlin, Germany

Email: Beate Koksch - beate.koksch@fu-berlin.de

* Corresponding author

Characterization and identification of synthesized peptides, characterization of the enzymatic digestion reactions, and identification of proteolytic cleavage products, HPLC methods, and synthesis protocol for Fmoc-HfLeu-OH

S1

Synthesis of Fmoc-HfLeu-OH

General information

All reactions were run under an argon atmosphere unless otherwise indicated. Room temperature refers to 22 °C. Reagents and anhydrous solvents were transferred *via* oven-dried syringe or cannula. Flasks were flame-dried under vacuum and cooled under a constant stream of argon. Reactions were monitored by thin layer chromatography using Merck KGaA silica gel 60 F_{254} TLC aluminium sheets and visualized with ceric ammonium molybdate, vanillin staining solution or potassium permanganate staining solution. Chromatographic purification was performed as flash chromatography on Macherey-Nagel GmbH & Co. KG silica gel 60 M, 0.04–0.063 mm, using a forced flow of eluent (method of Still). Concentration under reduced pressure was performed by rotary evaporation at 40 °C at the appropriate pressure. Yields refer to chromatographically purified and spectroscopically pure compounds. NMR measurements were recorded on a JEOL-ECX400 (operating at 400 MHz for ^{1}H NMR, 101 MHz for ^{13}C NMR and 376 MHz for ^{19}F NMR). Chemical shifts δ are reported in ppm with the solvent resonance as the internal standard. Coupling constants *J* are given in Hertz (Hz). Multiplicities are classified by the following abbreviations: s = singlet, d = doublet, t = triplet, q = quartet, br = broad or m = multiplet and combinations thereof. High resolution mass spectra were obtained on an Agilent ESI-ToF 6220 (Agilent Technologies, Santa Clara, CA, USA).

Scheme S1: Synthesis of Fmoc-HfLeu-OH **9**.
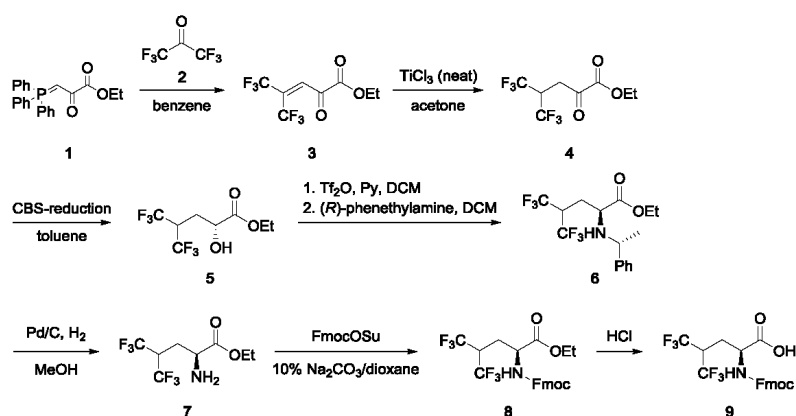
Compounds **3** to **7** were synthesized according to literature [1,2]. Obtained NMR data (^{1}H, ^{13}C, and ^{19}F) are consistent with literature [1,2].

Synthesis of Fmoc-HfLeu-OEt (**8**)

(*S*)-**7** (1.04 g, 3.89 mmol) was dissolved in 10% Na_2CO_3, aq (4 mL) and cooled to 0°C. Dioxane (1 mL) was added and the suspension was stirred for 15 min at 0 °C after which FmocOSu (1.44 g, 4.28 mmol) was added. The mixture was stirred for 3 h at 0 °C and at room temperature overnight. The reaction was diluted with H_2O (50 mL) and extracted with Et_2O (4 x 25 mL). The combined organic layers were concentrated in vacuo and the residue was subjected to column chromatography (*n*-hexane/Et_2O, 3:1) to give (*S*)-**8** (1.12 g, 2.29 mmol, 59%) as a waxy solid.

TLC: R_f = 0.45 (*n*-hexane/Et_2O, 5:1).

^{1}H-NMR (400 MHz, $CDCl_3$): δ = 7.77 (d, *J* = 7.5, 2H); 7.58 (d, *J* = 7.2, 2H); 7.40 (t, *J* = 7.5, 2H); 7.32 (t, *J* = 7.0, 2H); 5.40 (d, *J* = 7.50, 1H); 4.47 (dt, *J* = 20.0; 13.40, 3H); 4.32 – 4.18 (m, 3H); 3.18 (s, 1H); 2.40 (d, *J* = 14.5, 1H); 2.05 (d, *J* = 10.0, 1H); 1.30 (t, *J* = 7.1, 3H).

^{13}C-NMR (101 MHz, $CDCl_3$) δ = 170.68, 143.75, 143.53, 141.45, 141.44, 140.84, 130.32, 127.92, 127.90, 127.19, 127.17, 125.07, 124.98, 120.32, 120.15, 120.11, 67.29, 62.53, 51.96, 47.21, 37.15, 27.27, 14.13.

^{19}F-NMR (376 MHz, $CDCl_3$): δ = -67.27 – -67.44 (m), -67.63 – -67.79 (m).

HRMS calculated for $C_{23}H_{31}F_6NNaO_4$ [M+Na]$^+$: 512.1267; observed: 512.1294.

Synthesis of Fmoc-HfLeu-OH (**9**)

A solution of (*S*)-**8** (55.0 mg, 11.2 mmol) in HCl_{conc} (2 mL) was stirred at room temperature for 24 h. The crude product was lyophilized and purified via a LaPrepΣ low-pressure HPLC system (VWR, Darmstadt, Germany) using a Kinetex RP-C18 endcapped HPLC-column (5 µM, 100 Å, 250 × 21.2 mm, Phenomenex$^®$, USA). Deionized water and acetonitrile (ACN), both containing 0.1% (v/v) TFA served as eluents. A linear gradient of 30–100% ACN + 0.1% (v/v) TFA over 18 min with a flow rate of 20.0 mL/min was applied. UV-detection occurred at 280 nm. This gave (*S*)-**9** (36.3 mg, 7.87 mmol, 70%) as a white powder.

^{1}H-NMR (400 MHz, DMSO-D_6): δ = 7.82 (d, *J* = 7.6, 2H); 7.77 (d, *J* = 8.7, 1H); 7.63 (d, *J* = 7.5, 2H); 7.36 (t, *J* = 7.4, 2H); 7.26 (t, *J* = 7.4, 2H); 4.35 – 4.23 (m, 2H); 4.17 (t, *J* = 6.7, 1H); 4.04 (br, 1H); 2.30 – 2.17 (m, 1H); 2.13 – 2.01 (m, 1H).

S3

^{13}C-NMR (101 MHz, DMSO-D$_6$): δ = 175.95 (s); 158.87 (s); 144.17 (s); 144.10 (s); 141.23 (s); 141.22 (s); 128.27 (s); 128.25 (s); 127.62 (s); 127.61 (s); 125.69 (s); 125.69 (s); 125.63 (s); 125.61 (s); 120.65 (s); 120.61 (s); 66.23 (s); 51.54 (s); 47.11 (s); 29.52 (s); 26.34 (s).

^{19}F-NMR (376 MHz, DMSO-D6): δ = -65.91 – -66.13 (m); -66.38 – -66.62 (m).

HRMS calculated for C$_{21}$H$_{17}$F$_6$NO$_4$ [M+Na]$^+$: 484.0954; observed: 484.0942.

Peptide synthesis, purification and characterization

Peptide synthesis

Peptides containing HfLeu were synthesized on an Activo P11 Automated Peptide Synthesizer (Activotec, Cambridge, United Kingdom) working under nitrogen atmosphere. All other peptides, either non-fluorinated or TfIle containing, were synthesized manually under standard conditions.

Peptide characterization

High resolution mass spectra were recorded on an Agilent 6220 ESI–ToF LC–MS spectrometer (Agilent Technologies Inc., Santa Clara, CA, USA) to identify the pure peptide products. The samples were dissolved in a 1:1 mixture of water and acetonitrile containing 0.1% (v/v) TFA and injected directly into the spray chamber by a syringe pump using a flow rate of 10 μL min^{-1}. A spray voltage of 3.5 kV was used, the drying gas glow rate was set to 5 L min^{-1} and the nebulizer to 30 psi. The gas temperature was 300 °C.

To verify purity of the synthesized peptides analytical HPLC was carried out on a Chromaster 600 bar DAD-System with CSM software (VWR/Hitachi, Darmstadt, Germany). The system works with a low-pressure gradient containing a HPLC-pump (5160) with a 6-channel solvent degasser, an organizer, an autosampler (5260) with a 100 μL sample loop, a column oven (5310) and a diode array flow detector (5430). A LUNA^{TM} C8 (2) column (5 μm, 250 × 4.6 mm, Phenomenex$^®$, Torrance, CA, USA) was used. As eluents water and ACN, both containing 0.1% (v/v) TFA were used, the flow rate was adjusted to 1 mL/min and the column was heated to 24 °C. The used gradient method is shown in Table S1. The UV-detection of the peptides occurred at 220 nm. The data were analyzed with EZChrom Elite software (version 3.3.2, Agilent Technologies, Santa Clara, CA, USA).

S4

Table S1: Used linear gradient for the purity determination of the synthesized peptides.

Time [min]	Water + 0.1% (v/v) TFA [%]	ACN + 0.1% (v/v) TFA [%]
0	95	5
18	30	70
19	0	100
21	0	100
21.5	95	5
24	95	5

Table S2: Identification of the synthesized peptides by ESI–ToF mass spectrometry and analytical RP-HPLC.

Peptide	Retention time [min]	Charge	m/z calculated	m/z observed
FA	10.597	+1	967.5364	967.5396
		+2	484.2721	484.2736
P2-LeuFA	12.500	+1	1009.5463	1009.5849
		+2	505.2956	505.2970
P2-HfLeuFA	12.393	+1	1117.4622	1117.5306
		+2	559.2573	559.2691
P2-IleFA	12.137	+1	1009.5463	1009.5849
		+2	505.2956	505.2971
P2-TfIleFA	12.493	+1	1063.4622	1063.5576
		+2	532.2814	532.2845
P1'-LeuFA	11.773	+1	1009.5463	1009.5863
		+2	505.2956	505.7982
P1'-HfLeuFA	11.917	+1	1117.4622	1117.5272
		+2	559.2573	559.2684
P1'-IleFA	11.370	+1	1009.5463	1009.5858
		+2	505.2956	505.2975
P1'-TfIleFA	11.870	+1	1063.4622	1063.5556
		+2	532.2814	532.2816
P2'-LeuFA	11.847	+1	1009.5463	1009.5866
		+2	505.2956	505.2981
P2'-HfLeuFA	12.197	+1	1117.4622	1117.5305
		+2	559.2573	559.2693
P2'-IleFA	11.557	+1	1009.5463	1009.5864
		+2	505.2956	505.2980
P2'-TfIleFA	12.283	+1	1063.4622	1063.5576
		+2	532.2814	532.2835
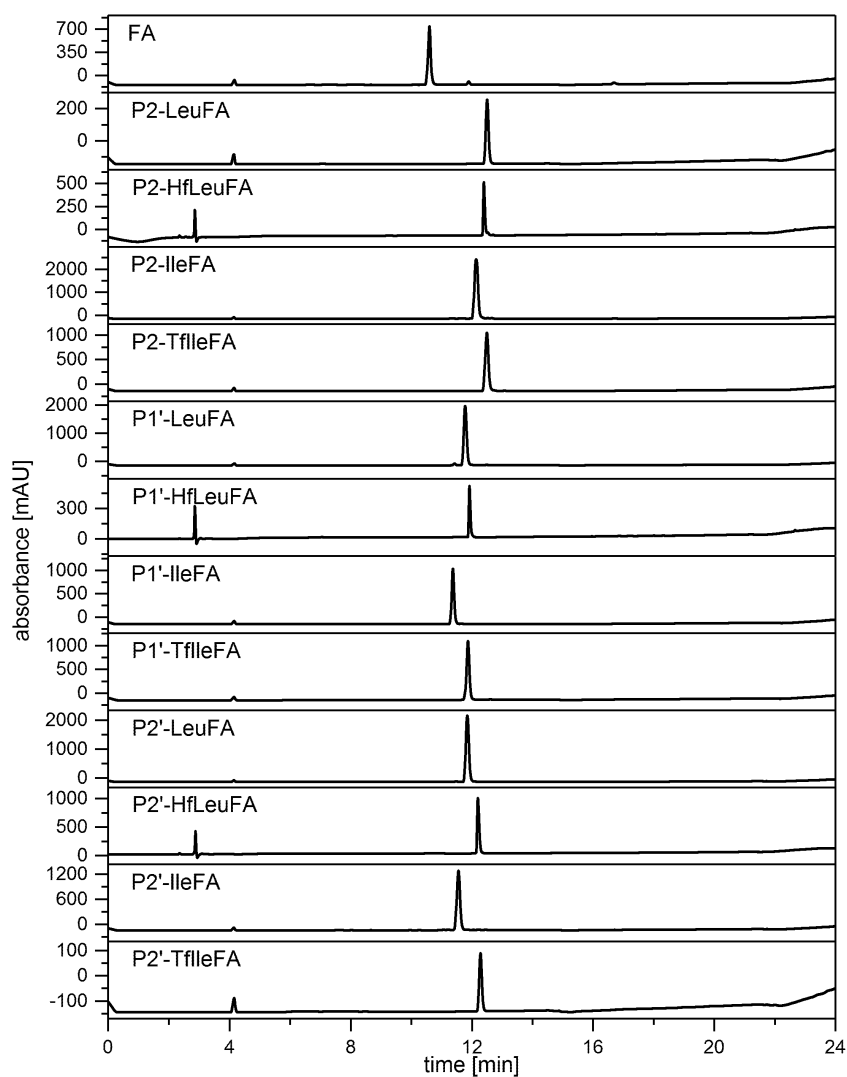
Figure S1: Analytical HPLC chromatograms of purified peptides; column: Luna™C8 (5 µM, 250 × 4.6 mm, Phenomenex®); Solvent A was H₂O, solvent B was acetonitrile, both containing 0.1% (v/v) TFA. The flow rate was 1 mL/min; linear gradient from 5% B to 70% B over 18 min (see Table S1).

Enzymatic digestion studies

Characterization of the enzymatic digestion reactions was carried out via analytical HPLC on a LaChrom-ELITE-HPLC-System from VWR International Hitachi (Darmstadt, Germany). The system contains an organizer, two HPLC-pumps (L-

S6

98

2130) with solvent degasser, an autosampler (L-2200) with a 100 μL sample loop, a diode array flow detector (L-2455), a fluorescence detector (L-2485) and a high pressure gradient mixer. As eluents water and ACN, both containing 0.1% (v/v) TFA were used, and a flow rate of 3 mL/min was applied. The used linear gradients are shown in Table S3. For the non-fluorinated peptides method A was used to follow the digestion process, and for the fluorinated peptides method B was applied. For chromatograms where an insufficient baseline separation was observed, measurements were repeated using methods C [FA (pepsin), P2-LeuFA (proteinase K), P2-IleFA (pepsin), P2-IleFA (proteinase K), P1'-LeuFA (elastase), P1'-LeuFA (proteinase K), P1'-IleFA (proteinase K)] or D [P2-HfleuFA (proteinase K), P2-TflleFA (pepsin), P2-TflleFA (proteinase K), P1'-TflleFA (elastase), P2'-TflleFA (proteinase K)]. The obtained data were analyzed with EZChrom Elite software (version 3.3.2, Agilent Technologies, Santa Clara, CA, USA).

Table S3: Used linear gradients to follow the digestion process by FL-RP-HPLC.

Method	Time [min]	Water + 0.1% (v/v) TFA [%]	ACN + 0.1% (v/v) TFA [%]
A	0	95	5
	5	70	30
	5.5	70	30
	6	95	5
	9	95	5
B	0	95	5
	5	60	40
	5.5	60	40
	6	95	5
	9	95	5
C	0	95	5
	15	70	30
	15.5	70	30
	16	95	5
	17	95	5
D	0	95	5
	15	55	45
	15,5	55	45
	16	95	5
	17	95	5
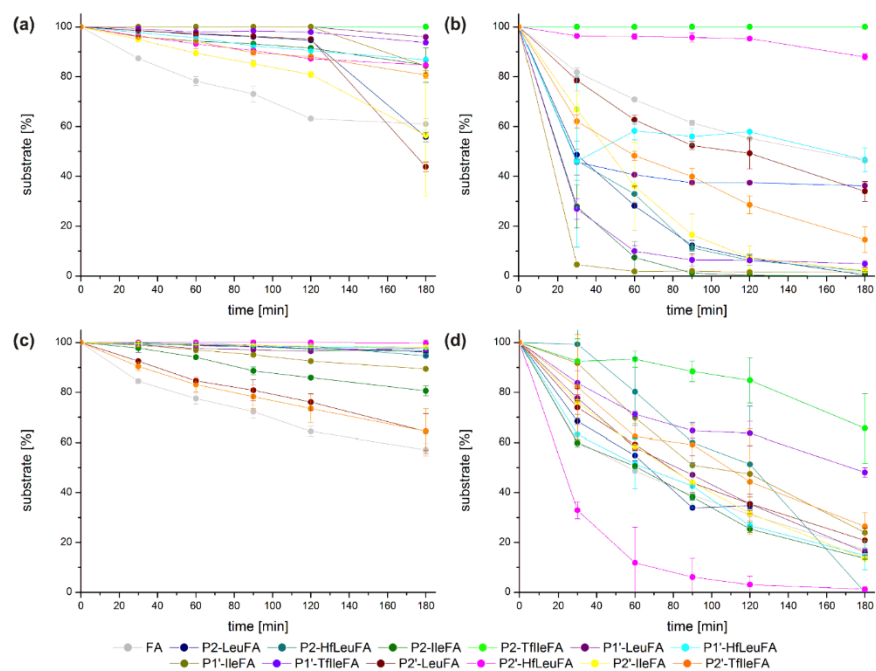
Figure S2: Chronological sequence of the substrate amount [%] over an incubation time of 180 min with **(a)** α-chymotrypsin, **(b)** pepsin, **(c)** elastase, and **(d)** proteinase K. The depicted values represent the mean of three independent measurements.

Identification of the proteolytic cleavage products (Table S4–S7) occurred according to the mass-to-charge ratios determined with an Agilent 6220 ESI–ToF–MS instrument (Agilent Technologies, Santa Clara, CA, USA). For this, the quenched peptide-enzyme-solutions after 120 min and 24 h incubation were analyzed. The solutions were injected directly into the spray chamber using a syringe pump with a flow rate of 10 µL min^{-1}. Spray voltage was set to 3.5 kV, a drying gas flow rate of 5 L min^{-1} was used, the nebulizer was set to 30 psi, and the gas temperature to 300 °C. The fragmentor voltage was 200 V. Not all corresponding fragments could be detected.

Table S4: Identification of the cleavage products of the different peptides by ESI–ToF mass spectrometry after digestion with α–chymotrypsin.

Peptide	Fragment	[M + H]$^{1+}$ calculated	[M + H]$^{1+}$ observed
FA	Abz-KAAFAAAAK	967.5364	967.5376
	Abz-KAAF	555.2559	555.2938
	AAAAK	431.2617	431.2627
P2-LeuFA	Abz-KALeuFAAAAK	1009.5463	1009.5883
	Abz-KALeuF	597.3029	597.2609

S8

100

	AAAAK	431.2617	431.2617
P2-HfLeuFA	Abz-KAHfLeuFAAAAK	1117.4622	1117.5298
P2-IleFA	Abz-KAIleFAAAAK	1009.5463	1009.5851
	Abz-KAIleF	597.3029	597.3435
	AAAAK	431.2617	431.2647
P2-TfIleFA	Abz-KATfIleFAAAAK	1063.4622	1063.5577
P1'-LeuFA	Abz-KAAFLeuAAAK	1009.5463	1009.5866
	Abz-KAAFLeu	668.3400	668.3760
	Abz-KAAF	555.2559	555.2907
	LeuAAAK	473.3087	473.3087
	AAAK	360.2246	360.2239
P1'-HfLeuFA	Abz-KAAFHfLeuAAAK	1117.4622	1117.5280
	Abz-KAAFHfLeu	776.2559	776.3214
	HfLeuAAAK	581.2246	581.2246
	Abz-KAAF	555.2559	555.2934
	AAAK	360.2246	360.3630
P1'-IleFA	Abz-KAAFIleAAAK	1009.5463	1009.5825
	Abz-KAAF	555.2559	555.2951
	IleAAAK	473.3087	473.3104
P1'-TfIleFA	Abz-KAAFTfIleAAAK	1063.4622	1063.5604
	Abz-KAAF	555.2559	555.2954
	TfIleAAAK	527.2246	527.2827
P2'-LeuFA	Abz-KAAFALeuAAK	1009.5463	1009.5872
	Abz-KAAF	555.2559	555.2922
	ALeuAAK	473.3087	473.3087
P2'-HfLeuFA	Abz-KAAFAHfLeuAAK	1117.4622	1117.5331
	AHfLeuAAK	581.2246	581.2550
	Abz-KAAF	555.2559	555.2965
P2'-IleFA	Abz-KAAFAIleAAK	1009.5463	1009.5875
	Abz-KAAF	555.2559	555.2943
	AIleAAK	473.3087	473.3112
P2'-TfIleFA	Abz-KAAFATfIleAAK	1063.4622	1063.5575
	Abz-KAAF	555.2559	555.2945
	ATfIleAAK	527.2246	527.2822

Table S5: Identification of the cleavage products of the different peptides by ESI–ToF mass spectrometry after digestion with pepsin.

Peptide	Fragment	[M + H][1+] calculated	[M + H][1+] observed
FA	Abz-KAAFAAAAK	96.5364	967.5434
	Abz-KAAF	555.2559	555.2967
	AAAAK	431.2617	431.2617
P2-LeuFA	Abz-KALeuFAAAAK	1009.5463	1009.5895
	Abz-KALeuF	597.3029	597.3438
	AAAAK	431.2617	431.2642
P2-HfLeuFA	Abz-KAHfLeuFAAAAK	1117.4622	1117.5302
	Abz-KAHfLeuF	705.2188	705.2870
	FAAAAK	578.3301	578.3327
	AAAAK	431.2617	431.2636
P2-IleFA	Abz-KAIleFAAAAK	1009.5463	1009.5916
	Abz-KAIleF	597.3029	597.3442
	AAAAK	431.2617	431.2647
P2-TfIleFA	Abz-KATfIleFAAAAK	1063.4622	1063.5639
P1'-LeuFA	Abz-KAAFLeuAAAK	1009.5463	1009.5926

S9

Peptide	Fragment	[M + H]$^{1+}$ calculated	[M + H]$^{1+}$ observed
	Abz-KAAFLeu	668.3400	668.3820
	Abz-KAAF	555.2559	555.2971
	LeuAAAK	473.3087	473.3126
	AAAK	360.2246	360.2271
P1'-HfLeuFA	Abz-KAAFHfLeuAAAK	1117.4622	1117.5325
	Abz-KAAFHfLeu	776.2559	776.3236
	HfLeuAAAK	581.2246	581.2553
	Abz-KAAF	555.2559	555.2956
	AAAK	360.2246	360.2273
P1'-IleFA	Abz-KAAFIleAAAK	1009.5463	1009.5908
	Abz-KAAF	555.2559	555.2969
	IleAAAK	473.3087	437.3087
P1'-TfIleFA	Abz-KAAFTfIleAAAK	1063.4622	1063.5634
	Abz-KAAF	555.2559	555.2969
	TfIleAAAK	527.2246	527.2843
P2'-LeuFA	Abz-KAAFALeuAAK	1009.5463	1009.5905
	Abz-KAAF	555.2559	555.2963
	ALeuAAK	473.3087	473.3117
P2'-HfLeuFA	Abz-KAAFAHfLeuAAK	1117.4622	1117.5307
	Abz-KAAFA	626.2930	626.3344
	HfLeuAAK	510.1875	510.2170
P2'-IleFA	Abz-KAAFAIleAAK	1009.5463	1009.5889
	Abz-KAAF	555.2559	555.2970
	AIleAAK	473.3087	473.3121
P2'-TfIleFA	Abz-KAAFATfIleAAK	1063.4622	1063.5627
	FATfIleAAK	674.2930	674.3530
	Abz-KAAFA	626.2930	626.3333
	Abz-KAAF	555.2559	555.2969
	ATfIleAAK	527.2246	527.2845
	TfIleAAK	456.1875	456.2462

Table S6: Identification of the cleavage products of the different peptides by ESI–ToF mass spectrometry after digestion with elastase.

Peptide	Fragment	[M + H]$^{1+}$ calculated	[M + H]$^{1+}$ observed
FA	Abz-KAAFAAAAK	967.5364	967.5352
	Abz-KAAFAAA	768.3672	768.4080
	Abz-KAAFAA	697.3301	697.3690
	AFAAAAK	649.3673	648.2935
	Abz-KAAFA	626.2930	626.3308
	AAAK	360.2246	360.2238
	AAK	289.1875	289.1872
P2-LeuFA	Abz-KALeuFAAAAK	1009.5463	1009.5871
	Abz-KALeuFAAAA	881.4513	881.4831
	Abz-KALeuFAAA	810.4142	810.4831
	Abz-KALeuFAA	739.4116	739.4116
	LeuFAAAAK	691.4142	691.4116
	Abz-KALeuFA	668.3404	668.3745
	AAAAK	431.2617	430.0496
	AAAK	360.2246	360.2205
	AAK	289.1875	289.1858
P2-HfLeuFA	Abz-KAHfLeuFAAAAK	1117.4622	1117.5325
	Abz-KAHfLeuFAAA	918.3301	918.3980
	Abz-KAHfLeuFAA	847.2930	847.3610

	Abz-KAHfLeuFA	776.2559	776.2559
	FAAAAK	578.3301	578.2440
P2-IleFA	Abz-KAIleFAAAAK	1009.5463	1009.5884
	Abz-KAIleFAAAA	881.4513	881.4960
	Abz-KAIleFAAA	810.4142	810.4960
	Abz-KAIleFAA	739.3771	739.4176
	Abz-KAIleFA	668.3400	668.3787
	FAAAAK	578.3301	578.3322
	AAAK	360.2246	360.2256
	AAK	289.1875	289.1880
	AK	218.1504	218.1505
P2-TfIleFA	Abz-KATfIleFAAAAK	1063.4622	1063.5576
	Abz-KATfIleFAAA	864.3301	864.4210
	Abz-KATfIleFAA	793.2930	793.3844
	Abz-KATfIleFA	722.2559	722.3470
	FAAAAK	578.3301	578.3271
	AAAK	360.2246	360.224
P1'-LeuFA	Abz-KAAFLeuAAAK	1009.5463	1009.5887
	Abz-KAAFLeuAAA	881.4513	881.4815
	Abz-KAAFLeuAA	810.4142	810.4472
	AAFLeuAAAK	762.4513	762.4458
	Abz-KAAFLeuA	739.3771	7394120
	AFLeuAAAK	691.4142	691.4142
	FLeuAAAK	620.3771	620.3783
	Abz-KAA	408.1875	408.1875
	Abz-KA	337.1504	337.1504
	AAK	289.1504	289.1858
P1'-HfLeuFA	Abz-KAAFHfLeuAAAK	1117.4622	1117.5330
	Abz-KAAFHfLeuAA	918.3301	918.3982
	AAFHfLeuAAAK	870.3673	870.3975
	AFHfLeuAAAK	799.3301	799.3600
	Abz-KA	337.1504	337.1864
P1'-IleFA	Abz-KAAFIleAAAK	1009.5463	1009.5853
	Abz-KAAFIleAA	810.4142	810.4500
	Abz-KAAFIleA	739.3771	739.4144
	FIleAAAK	620.3771	620.3747
P1'-TfIleFA	Abz-KAAFTfIleAAAK	1063.4622	1063.5578
	Abz-KAAFTfIleAA	864.3301	864.4205
	Abz-KAAFTfIleA	793.2930	793.3844
	AFTfIleAAAK	745.3301	745.3814
	AAK	289.1875	289.1857
	AK	218.1504	218.1483
P2'-LeuFA	Abz-KAAFALeuAAK	1009.5463	1009.5894
	Abz-KAAFALeuAA	881.4513	881.4938
	Abz-KAAFALeuA	810.4142	810.4938
	AFALeuAAK	691.4142	691.4168
	Abz-KAAFA	626.2930	626.3324
	LeuAAK	402.2716	402.2730
	Abz-KA	337.1504	337.1872
P2'-HfLeuFA	Abz-KAAFAHfLeuAAK	1117.6622	1117.5330
	Abz-KAAFAHfLeu	918.3301	918.4349
	AAFAHfLeuAAK	870.3673	870.4001
	AFAHfLeuAAK	799.3301	799.3612

S11

	FAHfLeuAAK	728.2930	728.3229
	Abz-KAAFA	626.2930	626.3230
	Abz-KAAFA	408.1875	408.2262
P2'-IleFA	Abz-KAAFAIleAAK	1009.5463	1009.5866
	Abz-KAAFAIleAA	881.4513	881.4910
	Abz-KAAFAIleA	810.4142	810.4539
	Abz-KAAFAIle	739.3771	739.4171
	FAIleAAK	620.3771	620.3687
	Abz-KAA	408.1875	408.2252
P2'-TfIleFA	Abz-KAAFATfIleAAK	1063.4622	1063.5530
	Abz-KAAFATfIle	793.2930	793.3851
	FATfIleAAK	674.2930	674.3441
	Abz-KAA	408.1875	408.2233
	AAK	289.1875	289.1855

Table S7: Identification of the cleavage products of the different peptides by ESI–ToF mass spectrometry after digestion with proteinase K.

Peptide	Fragment	[M + H]$^{1+}$ calculated	[M + H]$^{1+}$ observed
FA	Abz-KAAFAAAAK	967.5364	967.5376
	AFAAAAK	649.3673	649.2762
P2-LeuFA	Abz-KALeuFAAAAK	1009.5463	1009.5863
	Abz-KALeuFAAA	810.4142	810.4536
	Abz-KALeuFAA	739.4116	739.4179
	Abz-KALeuFA	668.3404	668.3816
	Abz-KALeu	450.2345	450.2719
	AAK	289.1504	289.1880
P2-HfLeuFA	Abz-KAHfLeuFAAAAK	1117.4622	1117.5298
	Abz-KAHfLeuFAAA	918.3301	918.3970
	Abz-KAHfLeuFAA	847.2930	847.3608
	Abz-KAHfLeuFA	776.2559	776.3233
	Abz-KAHfLeu	558.1504	558.2168
	AAK	289.1875	289.1884
P2-IleFA	Abz-KAIleFAAAAK	1009.5463	1009.5872
	Abz-KAIleFAAA	810.4142	810.4551
	Abz-KAIleFAA	739.3771	739.4192
	Abz-KAIleFA	668.3400	889.3806
	Abz-KAIleF	597.3029	597.3422
	AAK	289.1875	289.1891
P2-TfIleFA	Abz-KATfIleFAAAAK	1063.4622	1063.5604
	Abz-KATfIleFAAA	864.3301	864.4204
	Abz-KATfIleFAA	793.2930	793.3895
	Abz-KATfIleFA	722.2559	722.3512
	Abz-KATfIleF	651.2188	651.3140
	AAAAK	431.2617	430.0513
	AAK	289.1875	289.1888
P1'-LeuFA	Abz-KAAFLeuAAAK	1009.5463	1009.5877
	Abz-KAAFLeuAA	810.4142	810.4552
	Abz-KAAFLeuA	739.3771	739.4182
	FLeuAAAK	620.3771	620.3813
	Abz-KAA	408.1875	408.2276
	AAK	289.1504	2891885
P1'-HfLeuFA	Abz-KAAFHfLeuAAAK	1117.4622	1117.5271
	FHfLeuAAAK	728.2930	728.3226

S12

104

	Abz-KAA	408.1875	408.2261
P1'-IleFA	Abz-KAAFIleAAAK	1009.5463	1009.5878
	Abz-KAAFIleAA	810.4142	810.4545
	Abz-KAAFIleA	739.3771	739.4169
	FIleAAAK	620.3771	620.3795
	Abz-KAA	408.1875	408.2265
	AAK	289.1504	289.1891
P1'-TfIleFA	Abz-KAAFTfIleAAAK	1063.4622	1063.5580
	Abz-KAAFTfIleAA	864.3301	864.4253
	Abz-KAAFTfIleA	793.2930	793.3853
	FTfIleAAAK	647.2930	674.3504
	Abz-KAA	408.1875	408.2260
	AAK	289.1875	289.1880
	AK	218.1504	218.1508
P2'-LeuFA	Abz-KAAFALeuAAK	1009.5463	1009.5845
	Abz-KAAFALeu	739.3771	739.4166
	FALeuAAK	620.3771	620.3782
	Abz-KAA	408.1875	408.2252
	AAK	289.1875	289.1883
P2'-HfLeuFA	Abz-KAAFAHfLeuAAK	1117.4622	1117.5304
	Abz-KAAFAHfLeu	847.2930	847.3603
	HfLeuAAK	510.1875	510.2172
	AAK	289.1875	268.1885
P2'-IleFA	Abz-KAAFAIleAAK	1009.5463	1009.5854
	Abz-KAAFA	626.2930	626.338
	FAIleAAK	620.3771	620.3791
	Abz-KAA	408.1875	408.2260
P2'-TfIleFA	Abz-KAAFATfIleAAK	1063.4622	1063.5563
	FATfIleAAK	674.2930	674.3496
	Abz-KAA	408.1875	408.2239

Reference

1. Chiu, H.-P.; Cheng, R. P. *Org. Lett.* **2007,** *9* (26), 5517-5520.
2. Zhang, C.; Ludin, C.; Eberle, M. K.; Stoeckli-Evans, H.; Keese, R. *Helv. Chim. Acta* **1998,** *81* (1), 174-181.

S13

5.4 Towards fluorinated, peptide-based HIV-1 fusion inhibitors

5.4.1 Rationale of the study

CHR-derived peptide C31 was previously developed in our group,[251] and was used for substitution studies with fluorinated amino acids. Here, the three fluorinated amino acids difluoroethylglycine (DfeGly), 5,5,5-trifluoroisoleucine (5^3-F$_3$Ile) and 5,5,5,5',5',5'-hexafluoro-leucine (5^3,$5'^3$-F$_6$Leu) (Figure 5.7) were applied to substitute the Ile16 residue in the center of the C31 sequence. This Ile is, together with Trp631 and Trp628 of the natural sequence, a highly conserved residue in the pocket binding domain of CHR and crucial for interaction with NHR (see Chapter 3.2).
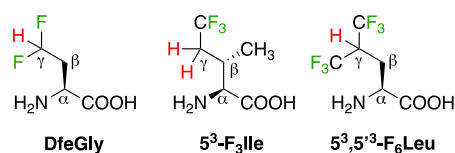
C31: Ac-EQIWNNMTWMEWDREINNYTSLIHSLIEESQ-NH$_2$

Figure 5.7: Structures of fluorinated amino acids and the C31 sequence.

As described in Section 2.2 fluorinated aliphatic amino acids have been demonstrated to be effective in stabilizing protein structures like coiled coils. Furthermore, it was also found that the remaining hydrogen of tetrafluorinated phenylalanines has an increased partial positive charge and it was shown that an accurate positioning of these highly, but not fully, fluorinated aromatic molecules can enhance protein stability due to greater CH···π interactions.[113] Such interactions are common in protein structures,[121] and taking a detailed look at the crystal structure of the pocket binding domain of HIV-1 gp41,[94] a CH···π interaction might formed between the γ-methylene group of Ile635 and the aromatic ring of Trp631 (Figure 5.8).
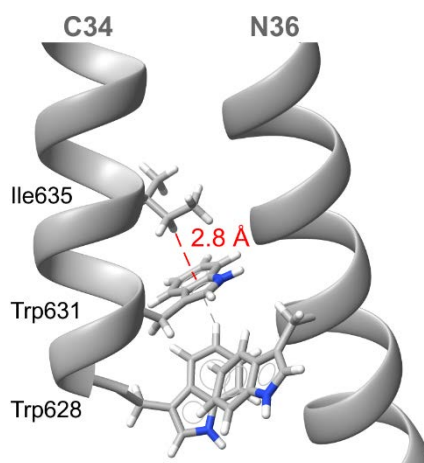
Figure 5.8: Crystal structure of C34/N36 (PDB code: 1AIK). Only one asymmetric unit consisting of one NHR- and CHR-strand each is depicted.

In organic molecules, the distance from the hydrogen atom to the aromatic π-plane in CH$\cdots\pi$ interactions typically varies from 2.0 Å to 3.5 Å, and the distance obtained from the crystal structure here is around 2.8 Å.[125, 285-287]

The hydrophobicity of the fluorinated amino acids is increased in comparison to their non-fluorinated analogues,[50, 135-136] while the fluorination of the side chains likely results in polarization of the adjacent CH bonds. As a consequence, the electrostatic potential of the corresponding hydrogens, here the γ-hydrogens (see Figure 5.7 marked in red) should be greater in the fluorinated side chain. This polarization might furthermore lead to a stabilization of the CH$\cdots\pi$ interaction and thus may result in a stabilization of the helical peptide structure. With the different fluorinated peptides, the impact of the CH$\cdots\pi$ interaction on coiled-coil structure and stability can be investigated. Moreover, site-specific substitution of an aliphatic residue within the pocket binding domain with fluorinated amino acids of different side-chain volume and polarity can elucidate their optimal packing and binding specificities at hydrophobic interfaces.

5.4.2 Peptide synthesis

Peptides were generated by means of solid phase peptide synthesis (SPPS). The CHR-derived peptides C31, its fluorinated analogues and C34, as well as the NHR-derived peptides T21 and N36 were synthesized (Figure 5.9).
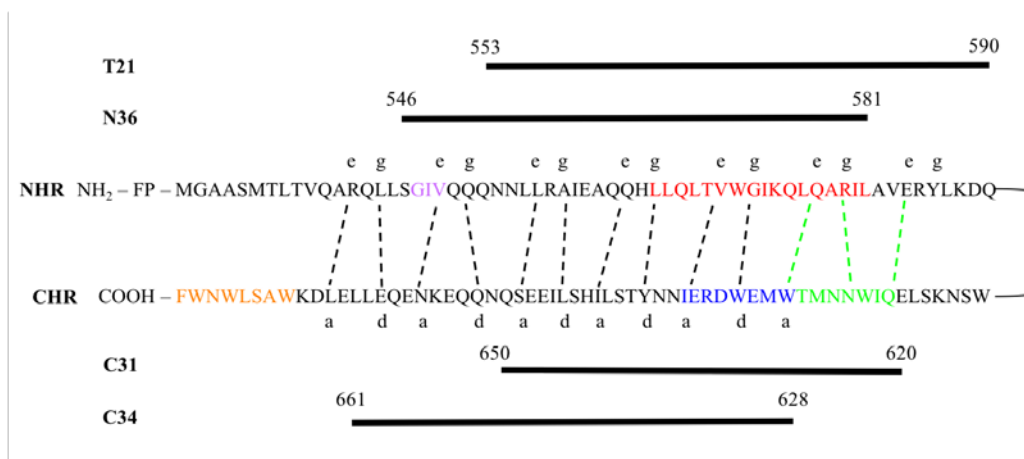
Figure 5.9: Sequence of gp41 and the peptides T21 and N36, as well as C31 and C34 derived from the NHR- or CHR-region, respectively.

Especially the synthesis of the C31 peptides is quite challenging as described previously.[288] Numerous deletion products, as well as an oxidation of the Met residues were observed, and a peptide fragment was detected that corresponds to the Fmoc protected sequence 17-31 (Fmoc-NNYTSLIHSLIEESQ-NH$_2$). The deprotection of the Asn17 residue appears to be very difficult; the protecting group remains during the further synthesis and this fragment can still be found after peptide synthesis for the remainder of the population is complete. The many

byproducts also result in a very difficult purification of the peptides in the end, leading to peptides with only up to 75% purity.[288]

First of all, the deprotection step of the Asn17 residue must to be optimized. This is also the last residue before the substitution position and thus its efficient deprotection is of great interest. Figure 5.10 shows the HPLC chromatograms of the C31_aa17-31 fragment.
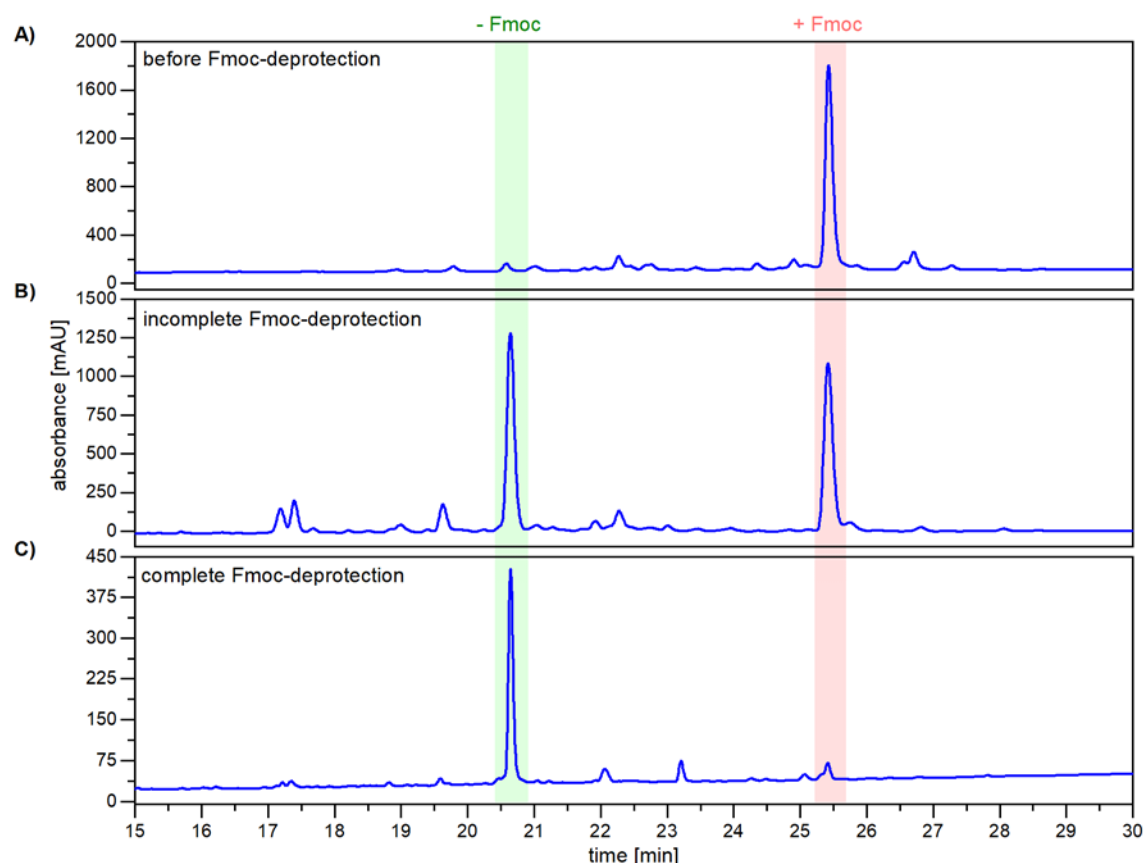
Figure 5.10: HPLC spectra of C31_aa17-31 fragment (NH$_2$-NNYTSLIHSLIEESQ-NH$_2$) at 220 nm. **A)** Before Fmoc deprotection of Asn17, **B)** Incomplete Fmoc deprotection, and **C)** almost fully Fmoc-deprotection. HPLC system: LaChrom ELITE®; column: Luna® C8(2); eluent: A = H$_2$O, B = ACN both containing 0.1% (v/v) TFA; gradient: 5% → 70% B over 30 min. The spectra are depicted from 15 to 30 min.

Under the standard conditions applied for Fmoc deprotection (3 × 10 min 2% (v/v) Pip + 2% (v/v) DBU in DMF or 3 × 10 min 20% (v/v) Pip in DMF) only 73% or 49% of the batch was deprotected (Table 5.4, entry 1-2), respectively. Thus, different Fmoc cleavage solutions were prepared and tested (Table 5.4, entry 3-18). Addition of DBU seems to enhance the deprotection efficiency compared to using solely piperidine in DMF; in contrast, longer reaction times alone do not lead to enhanced Fmoc-deprotection. Furthermore, slight improvement of the Fmoc deprotection was observed when a chaotropic agent such as NaClO$_4$ was added or when ultrasonication as well as higher temperatures were applied. This suggests that aggregation may prevent the *N*-Fmoc group of Asn17 from being accessible to the deprotection reagents.

Table 5.4: Different conditions tested for the Fmoc-deprotection of the Asn17 residue. The percentage of Fmoc removed or still attached to the peptide fragment was calculated by determination of the area under the corresponding peaks in the HPLC spectra at 222 nm. No temperature given refers to room temperature. If not mentioned otherwise, the reactions were performed manually.

entry	conditions		Fmoc off [%]	Fmoc on [%]
1	2% (v/v) Pip + 2% (v/v) DBU in DMF 3 × 10 min		73.4	26.6
2	20% (v/v) Pip in DMF 3 × 10 min		48.7	51.3
3	20% (v/v) Pip + 2% (v/v) DBU in DMF 3 × 10 min		44.6	55.4
4	40% (v/v) Pip + 2% (v/v) DBU in DMF 3 × 10 min		72.6	27.4
5	2% (v/v) Pip + 2% (v/v) DBU in NMP 3 × 10 min		77.0	23.0
6	20% (v/v) Pip + 2% (v/v) DBU in DMF 6 × 5 min		68.5	31.5
7	20% (v/v) Pip + 5% (v/v) DBU in DMF 6 × 5 min	40°C water bath	81.04	18.96
8	40% (v/v) Pip + 5% (v/v) DBU in DMF 8 × 5 min additional 6 × 5 min	45°C water bath	83.8 81.5	16.2 18.5
9	2% (v/v) Pip + 2% (v/v) DBU in DMF 2 × 5 min + 2 × 10 min	40°C Activo-P11	46.7	53.3
10	20% (v/v) Pip in DMF 2 × 5 min + 2 × 10 min	40°C water bath	51.9	48.1
11	20% (v/v) Pip in DMF 1 × 16 h	40°C (1 h), then rt	51.7	48.3
12	20% (v/v) Pip + 5% (v/v) DBU in DMF 1 × 6 h		42.6	57.4
13	40% (v/v) Pip + 5% (v/v) DBU in DMF 6 × 5 min		48.4	51.6
14	40% (v/v) Pip + 5% (v/v) DBU in DMF 6 × 5 min	45°C water bath	53.3	46.7
15	40% (v/v) Pip + 5% (v/v) DBU in DMF 6 × 5 min	60°C water bath	56.4	43.6
16	40% (v/v) Pip + 5% (v/v) DBU in DMF 12 × 5 min	40°C ultrasonication	57.3	42.7
17	40% (v/v) Pip + 5% (v/v) DBU in DMF + 0.8 M NaClO$_4$ 3 × 10 min	40°C ultrasonication	62.3	37.7
18	40% (v/v) Pip + 5% (v/v) DBU in DMF + 0.8 M NaClO$_4$ 6 × 10 min	60°C ultrasonication	57.1	42.9
19	20% (v/v) Pip in DMF 2 × 3 min	60°C MW heating	75.2	24.8
20	20% (v/v) Pip in DMF 1 × 15 min	60°C MW heating	75.2	24.8
21	40% (v/v) Pip in DMF 1 × 15 min	60°C MW heating	78.6	21.4
22	20% (v/v) Pip + 5% (v/v) DBU in DMF + 0.5 M NaClO$_4$ 1 × 15 min	60°C MW heating	76.4	23.6
23	20% (v/v) Pip in DMF 1 × 15 min	80°C MW heating	74.7	25.3

Table 5.4: (continued)

entry	conditions		Fmoc off [%]	Fmoc on [%]
24	20% (v/v) Pip in DMF (v/v DBU in DMF 2 × 2 min	75°C Liberty Blue™ MW synthesizer	97.5	2.5
25[a)]	20% (v/v) Pip in DMF 3 × 7 min		96.7	3.3

a) Tyr19-Thr20 was incorporated as pseudoproline dipeptide building block Fmoc-L-Tyr(ᵗBu)-L-Thr[PSI(Me,Me)Pro]-OH.

Due to aggregation that is thought to be caused primarily from intermolecular hydrogen bonding the reactive end of the growing peptide chain may be inaccessible for the reaction, hence leading to poor deprotection and coupling yields.[289-290] In addition, incomplete reaction steps during the synthesis lead to deletion sequences that exacerbate purification problems as the desired peptide is difficult to separate from the impurities. This was also observed for the purification of the C31 peptide during initial studies.[288]

In recent years, microwave irradiation has become a useful tool in SPPS and has been shown to dramatically increase the efficiency of the process overall.[291-293] It is speculated that microwaves can interact directly with the polar peptide backbone, leading to an alignment with the alternating electric field from the microwave. Thus, this mechanism can help to prevent aggregation of the peptide chain, allowing for better access of the reactive end and thereby improved reaction rates (schematically represented in Figure 5.11).[291, 294] In contrast, it is also hypothesized that the beneficial effect of microwave heating can be attributed to the precise nature of this type of heating, rather than a peptide-specific microwave effect.[292]
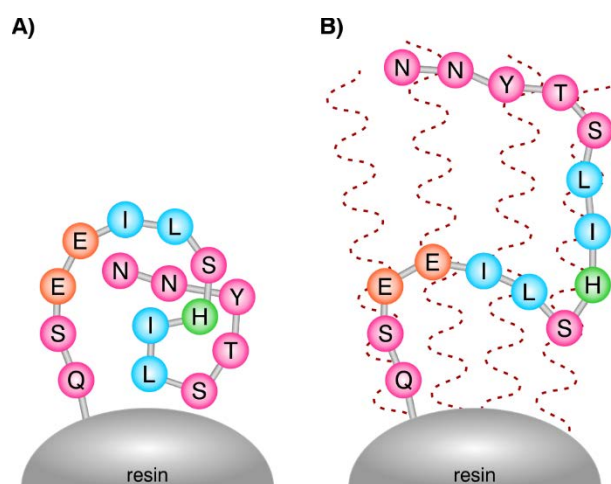
Figure 5.11: Microwave energy helps to break up aggregation through dipole rotation of the polar peptide backbone within the alternating electric field of the microwave.(Adapted with permission from Palasek, Cox, and Collins,[291] Copyright © 2006, European Peptide Society and John Wiley & Sons, Ltd.)

In the case of the deprotection efficiency of Asn17 MW irradiation was also observed to be promising (Table 5.4, entries 19-23). Using only short reaction times (2×3 min or 1×15 min) up to 79% of the peptide fragment could be deprotected, even in the absence of DBU or NaClO$_4$. As the used MW system in these cases was not optimized for solid phase synthesis, the reaction was thought to be further improved by using a system developed for the needs of SPPS. Thus, a microwave assisted automated peptide synthesizer (CEM Liberty Blue™ MW synthesizer) was used. Applying twice a deprotection cycle of 2 min with MW heating at 75°C using 20% (v/v) Pip in DMF, almost a complete Fmoc-deprotection step was observed (Table 5.4, entry 24).

Encouraged by these results, also the synthesis of the entire native C31 sequence was tested under MW conditions. Typically, under standard SPPS conditions, long coupling times and high excesses of reagents are needed, e.g. the Asn17-18 residues were coupled for 2×6 h using 10 eq. amino acid and activating agents (HOAt/DIC).[288] Manual MW synthesis was conducted using a 10-fold excess of amino acid, and HOAt, as well as DIC for activation. The coupling reaction was performed twice for 30 min each. Fmoc deprotection occurred only once for 15 min with 20% (v/v) Pip in DMF. Both synthetic steps were carried out at 60°C with MW. Satisfyingly, automated synthesis with MW needed only 5-fold excess of amino acid, as well as activating agents. Here, DIC and Oxyma were used. At 95°C 2×2 min couplings (3×5 min for Asn residues), and 1×1 min deprotection (2×1 min for Asn17) with 20% (v/v) Pip in DMF occurred. Unfortunately, racemization was observed. Thus, the temperature was reduced to 75°C while prolonging the reaction time for couplings to 2×5 min (3×5 min for Asn residues) and for Fmoc deprotection to 1×2 min (2×2 min for Asn17). For Arg a special protocol was applied using single coupling of 25 min at room temperature without MW irradiation followed by 2 min with MW irradiation at 75°C to prevent γ-lactam formation. 20% (v/v) Pip in DMF were used as Fmoc deprotection solution, and 0.1 M HOBt needed to be added to avoid aspartimide formation. This shows that MW heating can be applied to dramatically increase the efficiency of both deprotection and coupling, resulting in a higher purity of the crude peptide mixture (see Figure 5.12 A *vs* B).
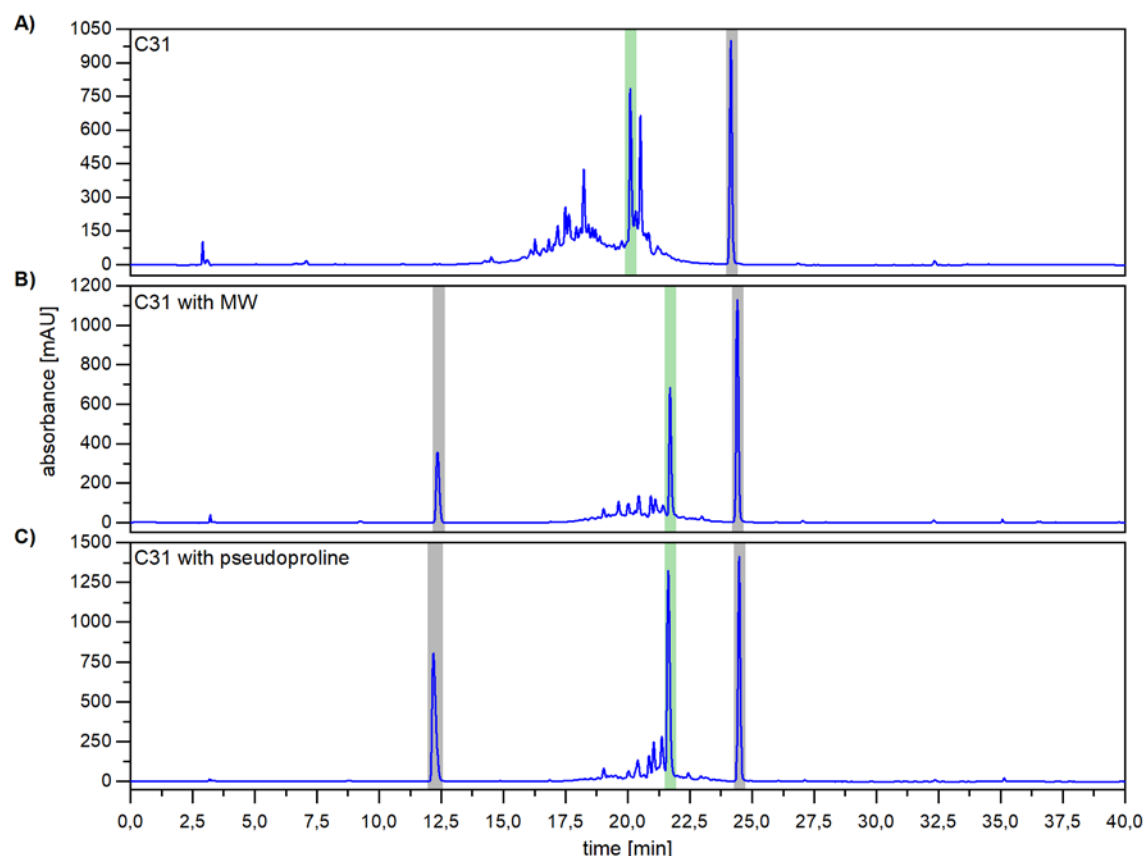
Figure 5.12: HPLC chromatograms of crude C31. **A)** Synthesis without MW or pseudoproline, **B)** synthesis under MW irradiation, and **C)** synthesis with incorporation of one pseudoproline unit. The peak corresponding to the desired peptide sequence is highlighted in green. Peaks with a gray background do not belong to peptide sequences and originate from thioanisole and phenol that are components of the cleavage cocktail. The HPLC data were collected on the LaChrom ELITE® system using a Luna® C8(2) (A)) or a Kinetex® C18 (B) and C)) column. Eluents were H_2O and ACN, both containing 0.1% (v/v) TFA. A linear gradient of 10% → 80% ACN over 30 min was applied.

Another strategy that is frequently used for the synthesis of "difficult" peptides is the incorporation of pseudoprolines.[290, 295-301] Developed originally by Mutter *et al*. in the 1990s,[302-303] the serine, threonine derived oxazolidines and cysteine derived thiazolidines can be readily cleaved by TFA.[304-305] This makes them suitable for standard Fmoc-SPPS, and a large number of pseudoproline building blocks is nowadays commercially available (Figure 5.13).

Fmoc-L-*Xaa*-L-Thr[PSI(Me,Me)Pro]-OH Fmoc-L-*Xaa*-L-Ser[PSI(Me,Me)Pro]-OH Fmoc-L-*Xaa*-L-Cys[PSI(Me,Me)Pro]-OH

R = any AA side chain
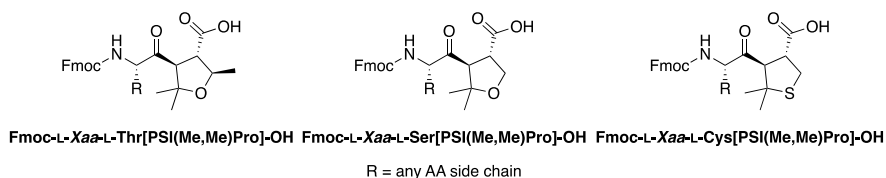
Figure 5.13: Different *N*-Fmoc protected pseudoproline dipeptide building blocks that are commercially available. *Xaa* = canonical amino acid.

The presence of such proline ring structures within the peptide sequence causes as "kink" in the peptide backbone, originating from the preference for a *cis* amide bond conformation and a restricted Φ dihedral angle.[306] Thus, peptide aggregation, self-association and β-sheet structure formation is prevented, resulting in improved solvation and coupling kinetics in the peptide

assembly (Figure 5.14).[304-305] In addition, the incorporation of a dipeptide building block serves one coupling step. These factors lead to an improved SPPS process giving higher purity of the crude peptides, and thus also simplifies HPLC purification. This is not only applicable for long and difficult peptides, but also for short peptides by incorporating just one single pseudoproline unit.[307-308]
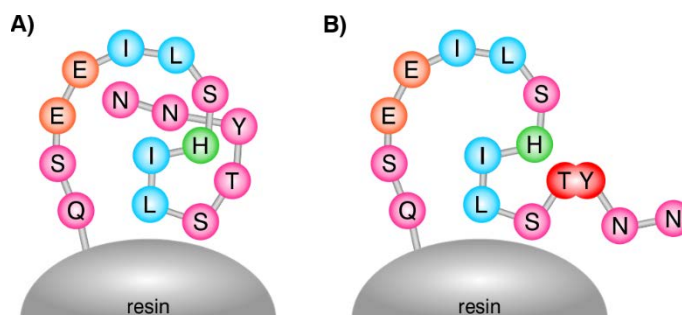
Figure 5.14: Schematic representation of the influence of a pseudoproline dipeptide building block (marked in red). It induces a "kink" conformation in the polyamide backbone of the peptide (**B**), thus interrupting the structure and avoiding peptide aggregation (**A**). This makes the *N*-terminal reactive end more accessible for subsequent reactions.

This structure disrupting property of the pseudoproline dipeptides was also taken advantage of in the synthesis of the C31 peptides. Here, the Fmoc-L-Tyr(^{t}Bu)-L-Thr[Psi(Me,Me)Pro]-OH pseudoproline dipeptide was incorporated at position 19-20 (Figure 5.15).

Ac-EQIWNNMTWMEWDREINN YT SLIHSLIEESQ-NH$_2$

Fmoc-L-Tyr(^{t}Bu)-L-Thr[PSI(Me,Me)Pro]-OH
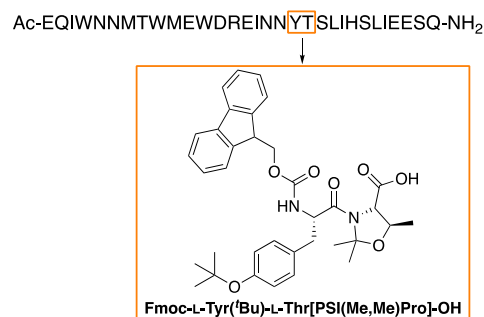
Figure 5.15: Sequence of C31 and structure of the dipeptide building block incorporated.

After incorporating the pseudoproline unit, the subsequent residues are added to the growing peptide chain without any difficulty. The coupling step of the Asn17 and Asn18 residues was shortened from 2×6 h to 2×1 h using an 8-fold excess of amino acids and activating agents. Furthermore, with this approach also the challenging Fmoc-deprotection step of the Asn17 residue was improved dramatically. Treatment of the peptide with 20% (v/v) Pip in DMF for 3×7 min (Table 5.4, entry 25) results in almost complete deprotection. Thus, also the coupling efficiency of the subsequent residue 16, either native Ile or fluorinated amino acids DfeGly, 5^3-F$_3$Ile, and 5^3,$5'^3$-F$_6$Leu, was quite high. The second part of the sequence could further be

synthesized exploiting standard procedures (see Chapter 7.4) resulting in the desired C31 sequence with higher crude peptide purity compared to the synthesis without using the pseudoproline dipeptide building block (Figure 5.12 A *vs* C).

In summary, the introduction of one single pseudoproline unit improves the synthesis of the C31 peptides considerably, leading to better crude purity and thus simpler downstream purification. This strategy was used to synthesize the fluorinated C31 peptides, as well as the native analogue containing Ile at position 16. These peptides were then further characterized by means of CD-spectroscopic measurements and ITC studies to gain insights into their interactions with the NHR-derived peptide T21. These results are described in the following sections.

5.4.3   CD-spectroscopic studies and thermal stabilities

To investigate the structures and thermal stabilities of the different complexes and the influence of fluorination upon the conformation of the peptides, CD measurements were carried out. First the non-fluorinated peptide C31 was studied and its interaction with the NHR-derived peptides N36 and T21 was examined. For comparison, also C34 was included, as the C34/N36 six-helix bundle (6-HB) is considered to be a core structure of the fusion active conformation of gp41 and typically assessed when bundle formation is investigated.[94, 194, 196, 220, 309] Thus, the C34/N36 bundle serves as a positive control.

The CD spectra show that the CHR-derived peptides C31 and C34 possess are unstructured, whereas the NHR-derived peptides T21 and N36 reveal a helical structure as indicated by the minima at 208 nm and 222 nm (Figure 5.16). In the case of N36 the minima are not clearly visible, and the signal intensity is low, which is due to the low solubility of the peptide that may be caused by aggregation (this is known for the NHR-derived peptide[241, 265]). To investigate the binding to the NHR-region of the gp41 to form a 6-HB, equimolar mixtures of the CHR-peptides with either N36 or T21 were incubated at 37°C for 30 min. Subsequently, the mixtures were analyzed *via* CD spectroscopy (Figure 5.16). All 1:1 mixtures indicate 6-HB formation as evidenced by the two distinct minima observed that indicate α-helical structures. The C34/N36 complex seems to possess a higher helical content than C31/T21. The C31/N36 mixture shows less helicity, due to the lower overlap of the interaction region between both peptides (see Figure 5.9), leading to unstructured peptide ends.
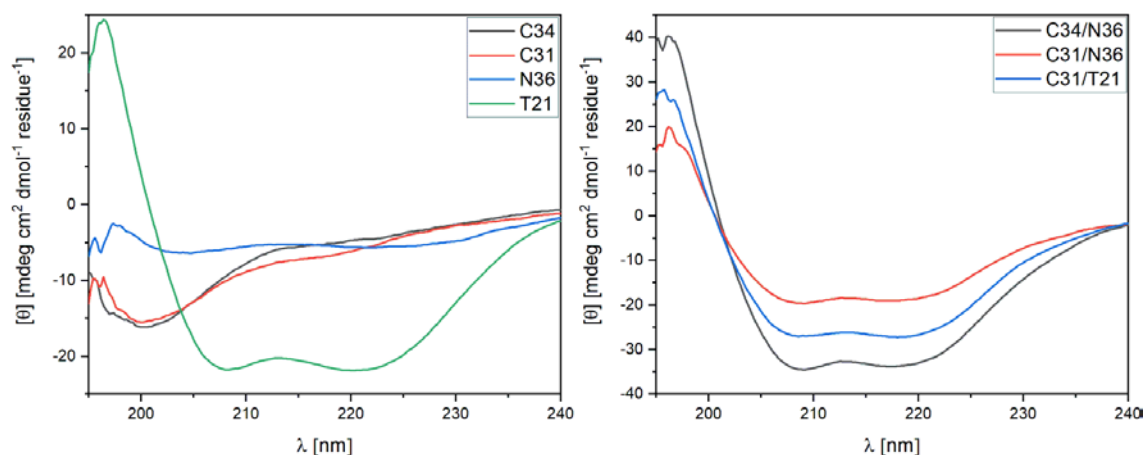
Figure 5.16: CD spectra of the CHR- and NHR-derived peptides alone (**left**) and in equimolar mixtures (**right**). The spectra were recorded at pH 7.4 and 37°C in 50 mM phosphate buffer containing 150 mM NaCl with an overall peptide concentration of 20 μM. The depicted spectra are normalized and represent the mean of three independent measurements.

This is also observed in the thermal denaturation experiments conducted to further characterize complex formation (Figure 5.17). Therefore, the CD signal of the 1:1 mixtures at 222 nm was measured in the range of 25°C to 100°C. The melting temperature (T_M) is defined as the temperature at which the unfolded fraction is 0.5 and this value is given in the figure legend.
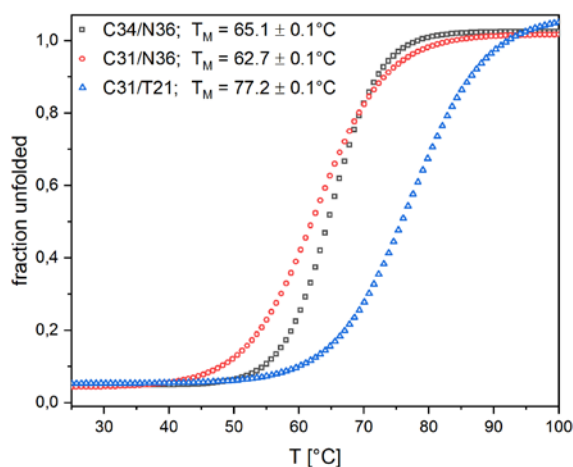
Figure 5.17: Thermal denaturation curves represented as fraction unfolded of the equimolar mixtures of CHR- and NHR-derived peptides. The spectra were recorded at pH 7.4 in 50 mM phosphate and 150 mM NaCl buffer with a peptide concentration of 20 μM. The depicted spectra represent the mean of at least three independent measurements.

Here, the complex of C31/N36 shows the lowest melting point (62.7°C). In contrast, the C21/T21 showed the highest melting point (77.2°C). The thermal stability for the wild-type C34/N36 complex was determined with 65.1°C, which is consistent with previous results from our group and from other literature reports.[194, 251]

As the C31 peptide bears a larger interacting region with T21 than with N36 (see Figure 5.9), also supported by the CD results, the fluorinated C31 peptide analogues were investigated together with only the T21 peptide. All fluorinated C31 peptides are unstructured as well

(Figure 5.18) and only small differences are observed upon introduction of the fluorinated amino acid, suggesting that the substitution of Ile for DfeGly, 5^3-F_3Ile or 5^3,$5'^3$-F_6Leu has no influence on the conformation of the peptide.

CD analysis of the 1:1 mixtures of T21 and one C31 peptide indicate 6-HB formation as α-helical structures are observed (Figure 5.18). As in the case of the single peptides, there seems to be virtually no difference in conformation when the different C31 peptides are mixed with the NHR-peptide T21. Interestingly, the helical content of all fluorine containing C31/T21 complexes is slightly increased in comparison to the non-fluorinated, parent C31/T21 mixture.
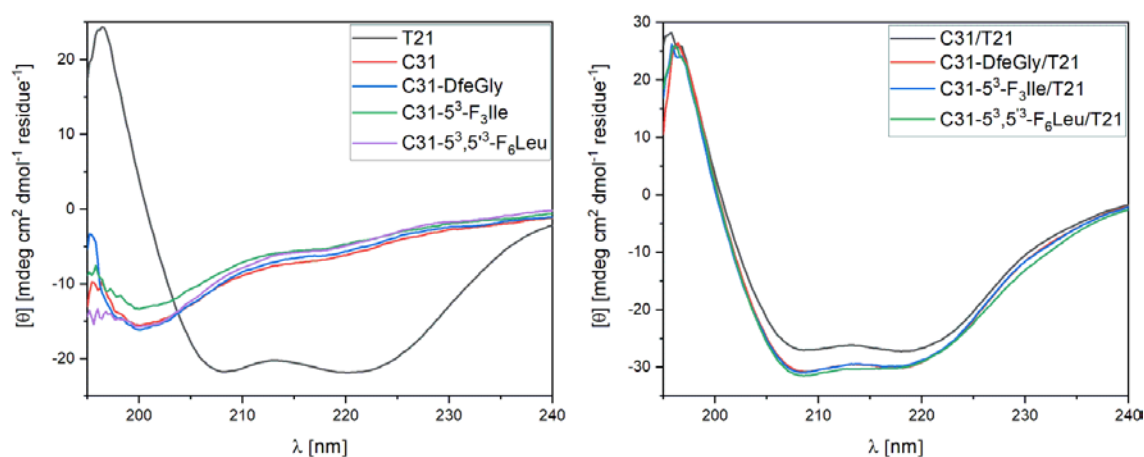
Figure 5.18: CD spectra of the C31 peptides and T21 alone (**left**) and in equimolar mixture (**right**). The spectra were recorded at pH 7.4 and 37°C in 50 mM sodium phosphate with 150 mM NaCl. The overall peptide concentration was 20 µM. The depicted spectra are normalized and represent the mean of three independent measurements.

Thermal denaturation curves for the C31/T21 complexes are shown in Figure 5.19. The non-fluorinated native C31/T21 has the highest melting point (77.2°C). The results for the fluorinated derivatives demonstrate a decrease in the thermal stability of up to ~ 9°C for all mixtures in comparison to the non-fluorinated analogue. Here, the 5^3-F_3Ile containing derivative is the most stable with a melting point of 73.6°C. C31-DfeGly/T21 shows almost the same stability ($T_M = 72.5$°C). Unexpected is that the incorporation of 5^3,$5'^3$-F_6Leu leads to the most unstable complex. This is in contrast to observations made before in which the incorporation of just one single 5^3,$5'^3$-F_6Leu residue results in a more stable coiled-coil bundle compared to the non-fluorinated analogue (see Section 5.2).[310]
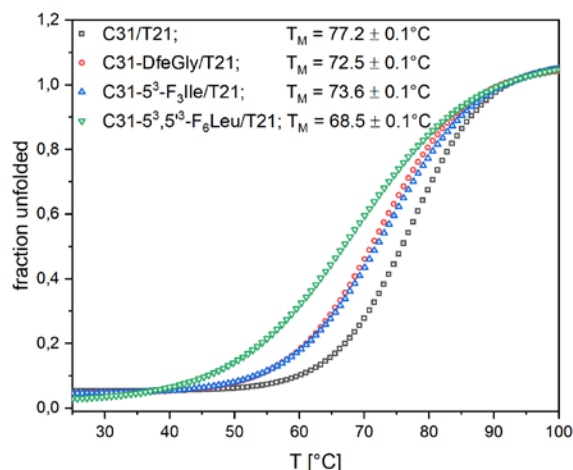
Figure 5.19: Thermal denaturation curves of the equimolar mixtures of C31 peptides with T21. These spectra were recorded at pH 7.4 in 50 mM phosphate and 150 mM NaCl buffer with an overall peptide concentration of 20 μM. The spectra are depicted in terms of fraction unfolded and represent the mean of at least three independent measurements.

5.4.4 ITC measurements

Isothermal titration calorimetry (ITC) is a method routinely used to characterize protein-protein interactions. ITC measures the binding equilibrium by determination of the heat evolved in binding of a ligand to its partner, yielding the thermodynamic properties in terms of binding constant (K), stoichiometry (N) and enthalpy of binding (ΔH). The entropy (ΔS) and free energy of binding can then be calculated from these parameters.[311-314]

ITC measurements were performed with the C31 peptides and T21. The studies were conducted at 25°C since at 37°C a bad signal to noise ratio was observed. Thus, CD studies were repeated at 25°C beforehand to investigate whether the change in temperature has a pronounced effect on the structure of the peptides itself, as well as the helical bundle assembly of the mixtures. As shown in Figure 5.20 the C31 peptides are still unstructured while the NHR-derived peptide T21 shows a helical conformation. Mixtures of the C31 peptides with T21 exhibit a helical content, where the fluorinated derivatives show slightly higher helicity than the parent C31/T21 mixture. This is in agreement with the results obtained at 37°C (see Figure 5.18).
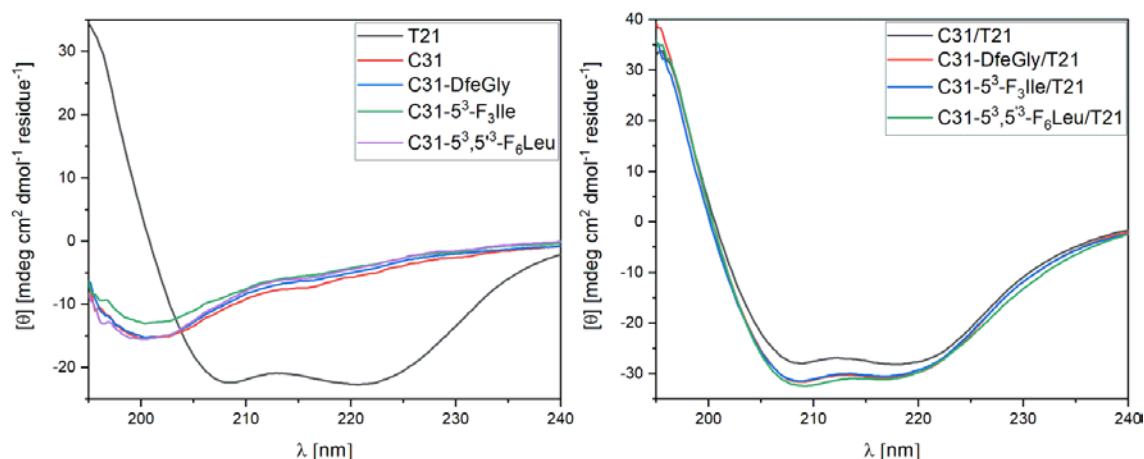
Figure 5.20: CD spectra of the C31-peptides and T21 alone (left) and in equimolar mixture (right). The spectra were recorded at pH 7.4 and 25°C in 50 mM phosphate and 150 mM NaCl buffer with a peptide concentration of 20 μM. The depicted spectra are normalized and represent the mean of three independent measurements.

For ITC measurements, the C31 peptide or its fluorinated analogues were injected into the T21 peptide solution. Upon injection, the heat that is either released or absorbed when the C31 peptide binds to T21 is measured and depicted in μcal/sec (Figure 5.21, top graphs). Integration of the resulting peaks and fitting using the one-set of sites model, in which all the binding sites are considered to be identical (Figure 5.21, lower panels) give the following parameters: (i) number of sites N, (ii) binding constant K, and (iii) heat change ΔH. The entropy change ΔS is afterwards determined from ΔH and K (Table 5.5). In addition, these parameters can be used to calculate the Gibbs free energy ΔG of the binding process (Table 5.6).
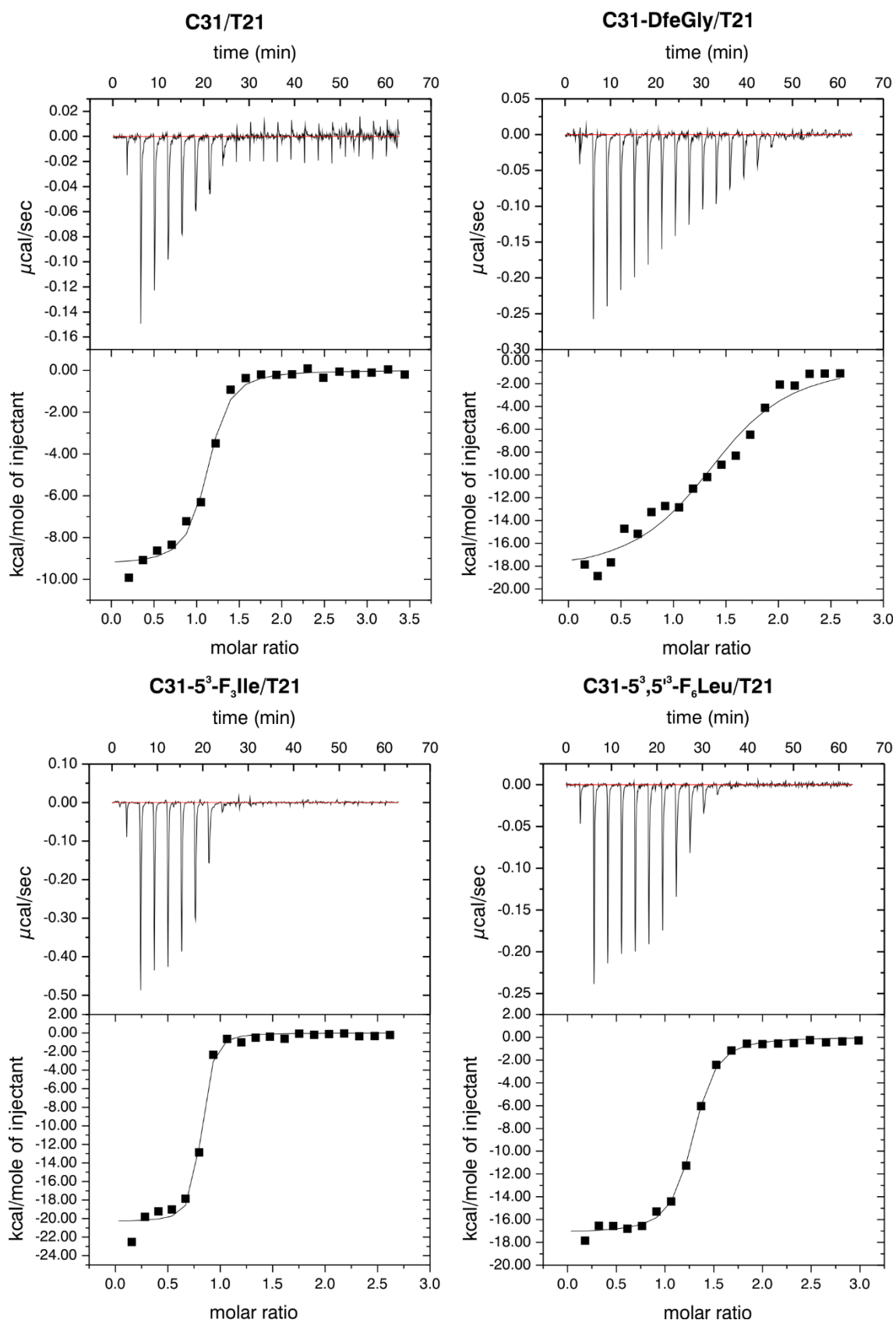
Figure 5.21: ITC assay of C31 peptides with T21. 100 µM of C31 peptide was injected into the chamber containing 10 µM T21, both dissolved in 50 mM sodium phosphate and 150 mM NaCl (pH 7.4). The experiments were carried out at 25°C. The top graph displays raw data of the heat flows (power) resulting from each injection in terms of µcal/sec plotted against time, after the integration baseline has been subtracted. The bottom graph shows the normalized integration data of each spike of the corresponding upper panel in terms of kcal/mole of injectant plotted against molar ratio, yielding the heat (enthalpy) exchanged after each injection.

Table 5.5: Kinetic parameters obtained for the binding of C31 peptides to T21 from ITC measurements, and compared to the C34/N36 bundle formation.

	N [sites]	K [10^6 M^{-1}]	ΔH [kcal mol^{-1}]	ΔS [cal mol^{-1} deg^{-1}]
C31/T21	1.07 ± 0.0167	9.35 ± 2.27	-9.30 ± 0.21	0.715
C31-DfeGly/T21	1.43 ± 0.0519	1.18 ± 0.34	-18.8 ± 0.97	-35.2
C31-5^3-F$_3$Ile/T21	0.763 ± 0.00885	22.3 ± 7.86	-20.3 ± 0.40	-34.5
C31-5^3,5'^{3}-F$_6$Leu/T21	1.23 ± 0.00774	13.5 ± 1.67	-17.2 ± 0.17	-25.0
C34/N36[222]	0.846 ± 0.0344	0.55 ± 0.27	-14.9 ± 0.92	-23.7

Table 5.6: Calculated ΔG values for the binding of interaction of C31 peptides to T21 from kinetic parameters (Table 5.5) determined by ITC and compared to values for C34/N36.

	TΔS [kcal mol^{-1}]	ΔG [kcal mol^{-1}]
C31/T21	0.21	-9.3
C31-DfeGly/T21	-10.5	-8.3
C31-5^3-F$_3$Ile/T21	-10.3	-10
C31-5^3,5'^{3}-F$_6$Leu/T21	-7.5	-9.7
C34/N36[222]	-7.1	-7.8

As indicated by the negative peaks in the ITC graph (Figure 5.21, upper panels), all C31 peptides bind in an exothermic fashion to the T21 peptide. The raw data also show that binding of C31 and C31-5^3-F$_3$Ile to T21 reaches the equilibrium faster and at much lower concentrations than binding of C31-5^3,5'^{6}-F$_6$Leu or C31-DfeGly. This is somewhat reflected by the binding affinity: C31-DfeGly exhibits the lowest binding affinity with a binding constant of $(1.18 \pm 0.34) \times 10^6$ M^{-1}, whereas the highest affinity with a binding constant of $(22.3 \pm 7.86) \times 10^6$ M^{-1} was determined for C31-5^3-F$_3$Ile, followed by C31-5^3,5'^{3}-F$_6$Leu and the non-fluorinated control C31 with K values of $(13.5 \pm 1.67) \times 10^6$ M^{-1} and $(9.35 \pm 2.27) \times 10^6$ M^{-1}, respectively (Table 5.5). Interestingly, this does not correlate with the thermal stability of the bundles as shown previously for other gp41 derived peptides.[196, 222] Compared to the C34/N36 complex, all C31 peptides, either the native peptide or its fluorinated analogues, possess ∼ 2- to 40-fold higher binding constants than that of C34 binding to N36 (K = $(0.55 \pm 0.27) \times 10^6$ M^{-1})[222], pointing towards significantly greater binding affinities of the C31 peptides binding to T21 than C34 binding to N36.

The titration experiments revealed that the number of binding sites N for the interaction between C31 and T21 is 1.07, indicating a 1:1 binding stoichiometry as expected, whereas for the fluorinated variants different values are observed (Table 5.5). Binding of C31-DfeGly and C31-5^3,5'^{3}-F$_6$Leu to T21 gave a higher stoichiometry of 1.43 and 1.23, respectively. In contrast, for C31-5^3-F$_3$Ile reduced stoichiometry with a value of 0.763 was determined. The lower value than expected might be explained by the tendency of NHR-derived peptides to aggregate.[241, 265] Therefore, T21 may be present in multiple forms, e.g. monomers, trimers, and aggregates.

Although aggregates in the peptide solutions should be formed to a small extent as only a low concentration is used, there may still be some microaggregates present, which may not be able to interact with C31. This results in an actual concentration of the active T21 peptide that can interact with C31 lower than expected, explaining why the measured stoichiometry for the binding of C31 to T21 is lower than 1. A higher stoichiometry than 1 can be explained by a C31 concentration that is lower than expected, so that the number of binding sites needed to be occupied to reach the equilibrium is reached slower. Another possibility is that the simple one-set of binding sites model is inappropriate. Taking a more detailed look at the integration data for the C31-DfeGly titration against T21 (Figure 5.21) there might be actually two different binding sites involved in the interaction of C31-DfeGly with T21.

The change in enthalpy ΔH is higher for the fluorinated peptides compared to the native C31 peptide. Around two times more energy is released when a fluorine-containing peptide binds to the counterpart T21. Again, the highest value is observed for C31-5^3-F_3Ile. Compared to C34/N36, the fluorinated C31 peptides still show a higher change in enthalpy of binding, although not that pronounced. The negative heat capacity change observed is consistent with a burial of hydrophobic residues upon binding.[315] The observations made for ΔH are somehow compensated by the entropically disfavored binding of the fluorinated peptides to T21. This is in contrast to an expected positive ΔS value for classical hydrophobic interactions.[315] The non-fluorinated C31 shows a 25.7 to 35.9 cal mol^{-1} deg^{-1} more favorable entropic contribution for binding to T21, leading to free energies of binding ΔG with only small differences. A ΔG of -10 kcal mol^{-1} is observed for C31-5^3-F_3Ile binding to T21, whereas this value is slightly reduced to -9.7 and -9.3 kcal mol^{-1} for C31-5^3,$5'^3$-F_6Leu or C31, respectively. C31-DfeGly has an even more reduced value of -8.3 kcal mol^{-1}. However, all C31 peptides show a more negative ΔG compared to the binding of C34 to N36. As all values are negative, the binding process is exergonic and binding of the different CHR-derived peptides to T21 or N36 occurs spontaneously at 25°C. ΔG of the C31/T21 binding is almost completely enthalpy driven, as ΔH contributes to nearly 100% to ΔG.

To summarize, C31-5^3-F_3Ile and C31-5^3,$5'^3$-F_6Leu seem to bind more tightly to T21 than C31, whereas C31-DfeGly is not a very strong binder. The C31/T21 unit seems to bind more tightly than the C34/N36 part of gp41, which correlates with their T_M values (Figure 5.19). All fluorinated peptides have a greater enthalpic (ΔH) release of energy upon binding to T21. The entropy change upon binding was less favorable for fluorinated C31 peptides than for non-fluorinated C31, with quite large differences caused by only one single amino acid substitution. Such large changes in entropy upon formation of a helical bundle were also observed for single alterations of the N36 peptide.[196]

A less favorable entropic contribution to the free energy of binding can be attributed to several factors. Usually, the unfavorable negative entropy change is explained by the loss of

conformational entropy when the CHR-derived peptides bind to its counterpart of gp41 as these peptides go from an unstructured, flexible conformation to a rigid, well-defined helical assembly. This has been observed by others as well.[222, 233, 242, 315] Other reasons include: (i) an altered configuration of water molecules surrounding the unbound peptides caused by a different hydrophobicity of the incorporated residues (5^3-F_3Ile and $5^3,5^{'3}$-F_6Leu are more hydrophobic than Ile,[135] whereas DfeGly is less hydrophobic[50]); (ii) less degrees of freedom of the modified peptide once it is bound to its interaction partner, because the fluorinated amino acid might fit better into the hydrophobic grooves than the natural one, and (iii) a reduced number of carbon bonds for rotation in the side chain, which would be the case for DfeGly compared to Ile.[222, 316-317]

However, that peptides show a large gain of binding enthalpy while also possessing a large loss of binding entropy (enthalpy-entropy compensation) is a general phenomenon observed in many biomolecular interactions.[233, 315-316, 318-322]

5.5 Development of a hetero-tetrameric linker for trimeric presentation of a peptide for SPR studies

5.5.1 Rationale of the study

To enable the efficient application of the CHR-derived peptides, the determination of kinetic binding parameters (e.g. k_{on}, k_{off}, ΔG^{ϕ}) is of particular interest. Over the last few decades, surface plasmon resonance (SPR) has emerged as a powerful tool to characterize and quantify the kinetics of various macromolecular interactions as well as high- and low-affinity small molecule interactions and is nowadays frequently used to study protein-protein interactions.[323-326] Advantages of the SPR technique are the following: it offers direct and rapid, as well as highly-sensitive determination of binding kinetics, labelling of the samples is not required, and only small quantities of material are needed for the assay (often nM concentrations).[323-324, 326] It furthermore enables the analysis of association and dissociation individually, and with this rate and affinity constants of the binding reaction can be determined.[323] Thus, the SPR technique has potential to provide crucial information on the molecular interaction of the peptidic inhibitor with its ligand, i.e. the NHR-region of gp41 from HIV-1.

Current SPR assays, that are applied to study interactions of gp120 or gp41 of HIV-1 as well as inhibition of 6-HB formation, usually rely on a monomeric immobilization of the NHR-peptides on the SPR chip.[248, 252, 327-332] This means that the trimer formation of the NHR-peptide on the surface is not ensured (see Figure 5.22 A). In the described cases, mostly amine coupling chemistry, and to a lesser extent the biotin/streptavidin interaction is used to immobilize the peptide onto the sensor chips surface. However, as proteins and peptides usually contain not only one functional group, amine coupling can give rise to heterogenous surfaces due to covalent bond formation at random sites leading to arbitrary orientations of the immobilized biomolecules. This in turn can lead to limited conformational flexibility and impaired function of the protein giving rise to a loss in activity and complexity in binding interactions. Therefore, it is advantageous to use other approaches that may allow for a site-directed surface immobilization and are useful in preparing more homogenous ligand surfaces, e.g., thiol or biotin-streptavidin coupling chemistries.[325, 333]
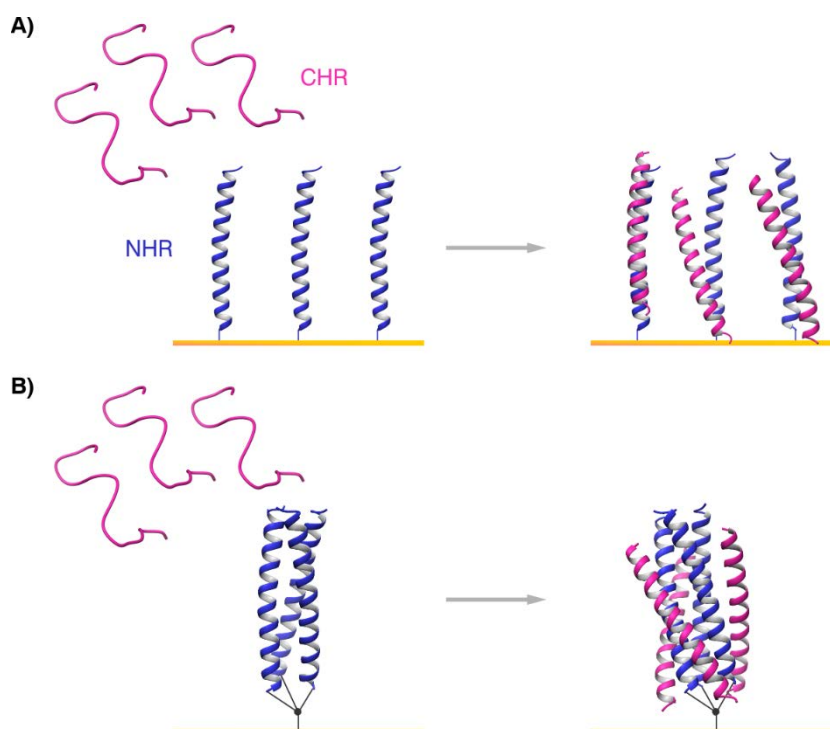
Figure 5.22: Schematic representation of the possibilities for the immobilization of NHR-peptides. **A)** Trimerization of NHR on the surface is not ensured and **B)** the trimerization of NHR by immobilization on an appropriate scaffold.

With the intent to optimize the NHR-peptide immobilization, we aimed for the development of a hetero-tetrameric linker that presents the NHR-peptide in its trimeric conformation and enables a site-specific binding to the SPR surface (see Figure 5.22 B). Therefore, a linker that provides the spatial constraint for the trimerization of NHR should be designed. Tris(hydroxymethyl)aminomethane (Tris) should serve as hetero-tetrameric scaffold that can bind three NHR-peptides on the one hand, and on the other hand allows for a second modification to immobilize the trimeric presented NHR-peptide on the SPR chip (Figure 5.23). Due to its branched structure and the two different reactive sites, Tris is also frequently used in the synthesis of dendrimers that can further be functionalized for the multivalent presentation of oligosaccharides or DNA.[334-340]
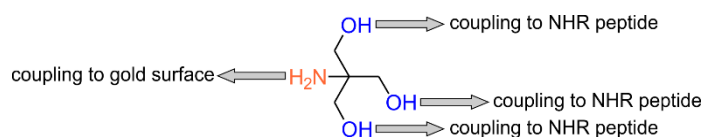
Figure 5.23: Hetero-tetrameric scaffold of tris(hydroxymethyl)-aminomethane (Tris) for presentation of an NHR-trimer. The three hydroxy groups are used for coupling of the NHR-peptide and the amino group for coupling of, e.g., a thiol-containing compound that enables immobilization on the gold surface of the SPR chip.

A detailed description of the efforts that were made to achieve this objective is given in the next sections.

5.5.2 Synthesis of an ethylene glycol linker and coupling to the NHR-peptide on solid phase

Linker synthesis

A synthesis strategy that was previously proposed for initial studies by our group is shown in Scheme 5.1.[341]
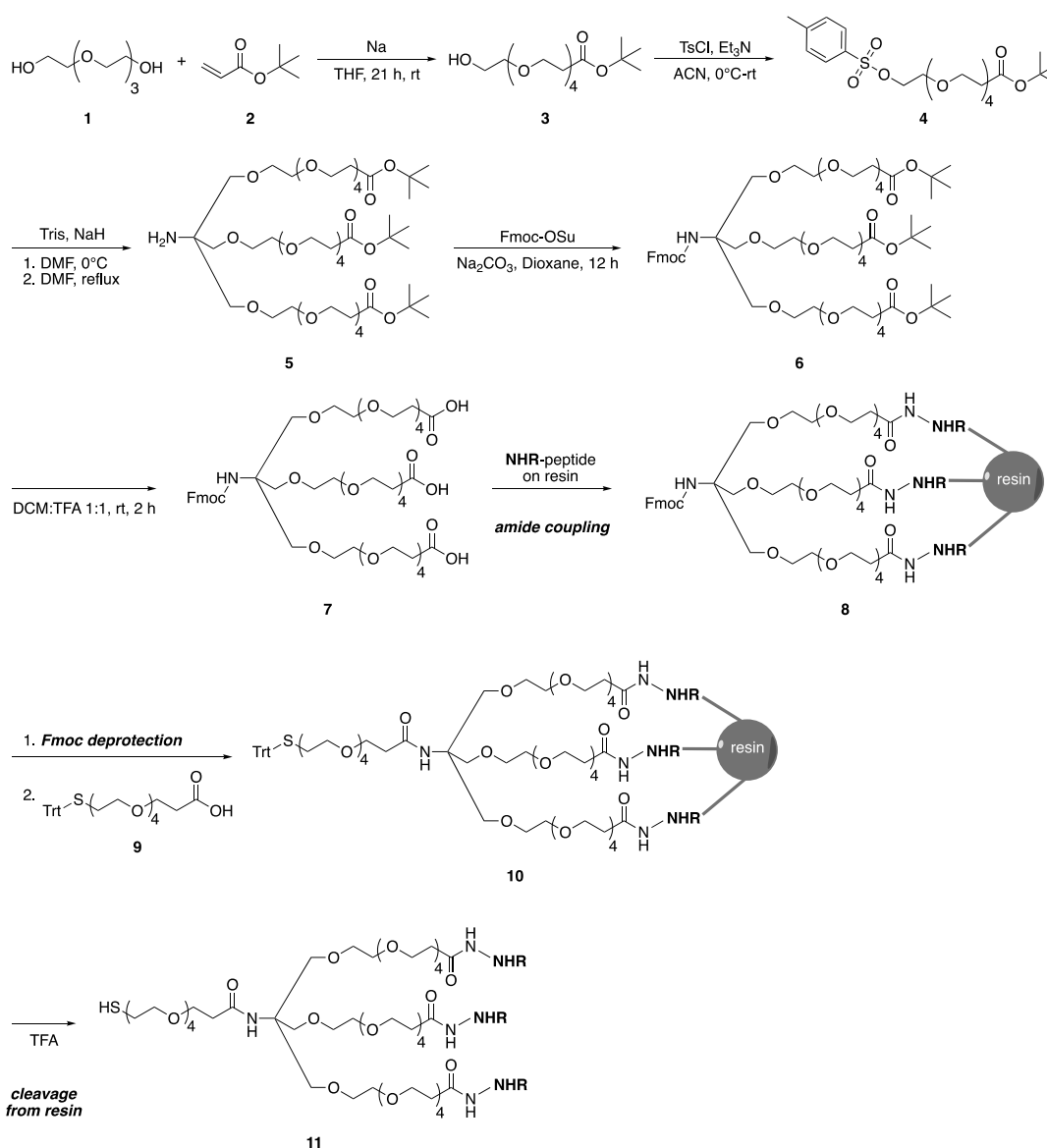
Scheme 5.1: Synthesis strategy for the ethylene glycol linker **7** and the immobilization of the NHR-derived peptide on it.

The synthesis of scaffold **7** is based on ethylene glycol **1** and Tris. Here, the PEG moiety serves as spacer between the branched site of the Tris scaffold and the peptide chain and allows for a not that rigid structure. The coupling of the NHR-derived peptide to this scaffold occurs on solid support *via* amide coupling reaction between the carboxyl group of **7** and the *N*-terminal amino group of the peptide.

The first two steps of this approach could be performed without problems. First, *tert*-butyl-1-hydroxy-3,6,9,12-tetraoxapentadecan-15-oate **3** was synthesized by a 1,4-addition of tetra-ethylene glycol **1** with *tert*-butyl acrylate **2** in the presence of 1 mol% sodium according to procedures described by Seitz and Kunz (Scheme 5.2).[342]
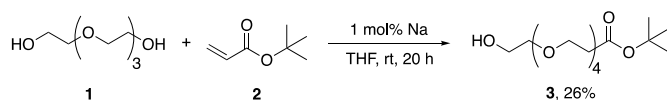
Scheme 5.2: Synthesis of *tert*-butyl-1-hydroxy-3,6,9,12-tetraoxapentadecan-15-oate **3**.

tert-Butyl-1-hydroxy-3,6,9,12-tetraoxapentadecan-15-oate **3** could be obtained in 26% yield and this step was followed by tosylation of the remaining free hydroxy group to give the corresponding tosylate **4** (Scheme 5.3).[343] After purification *via* flash column chromatography, compound **4** was obtained in 72% yield.
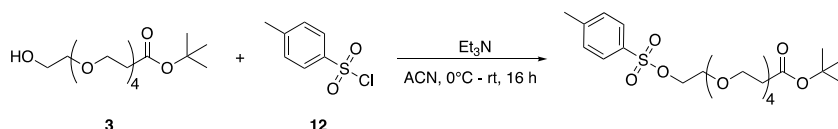
Scheme 5.3: Synthesis of *tert*-butyl-1-(tosyloxy)-3,6,9,12-tetraoxapentadecan-15-oate **4**.

The tosyl group is a good leaving group and should thus enhance the rate of the nucleophilic substitution with Tris **13** in the subsequent reaction (Scheme 5.4).
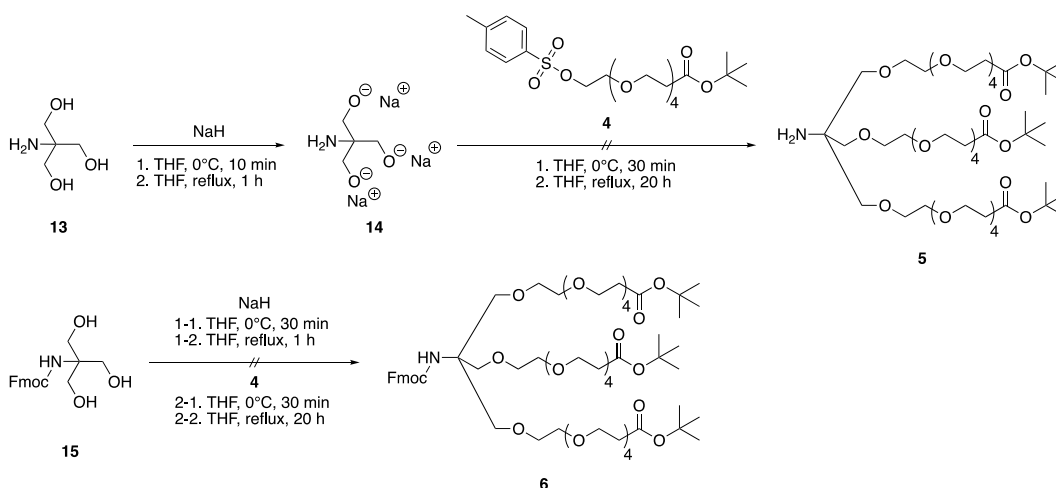
Scheme 5.4: Synthesis of di-*tert*-butyl 18-amino-18-(19,19-dimethyl-17-oxo-2,5,8,11,14,18-hexaoxaicosyl)-4,7,10,13,16, 20,23,26,29,32-decaoxapentatriacontanedioate **5** (**top**), and *N*-Fmoc protected derivative **6** (**bottom**).

Adapting known procedures,[344] Tris **13** was reacted with NaH in THF under inert conditions, TsO-PEG(4)-COO*t*Bu **4** was added, and the mixture was refluxed for 20 h. Unfortunately, the desired product could not be obtained. Only the starting material **4** could be detected. The same reaction using *N*-Fmoc protected Tris **15** to avoid possible side reaction on the free amino group

was not successful as well (Scheme 5.4). Here, the starting material, as well as the product with only one molecule **4** coupled to Tris **13** could be detected.

As this synthetic approach was not successful, a new strategy was pursued, in which the PEG moiety is first coupled to the peptide on the resin, before the hetero-tetrameric scaffold is introduced (Scheme 5.5).
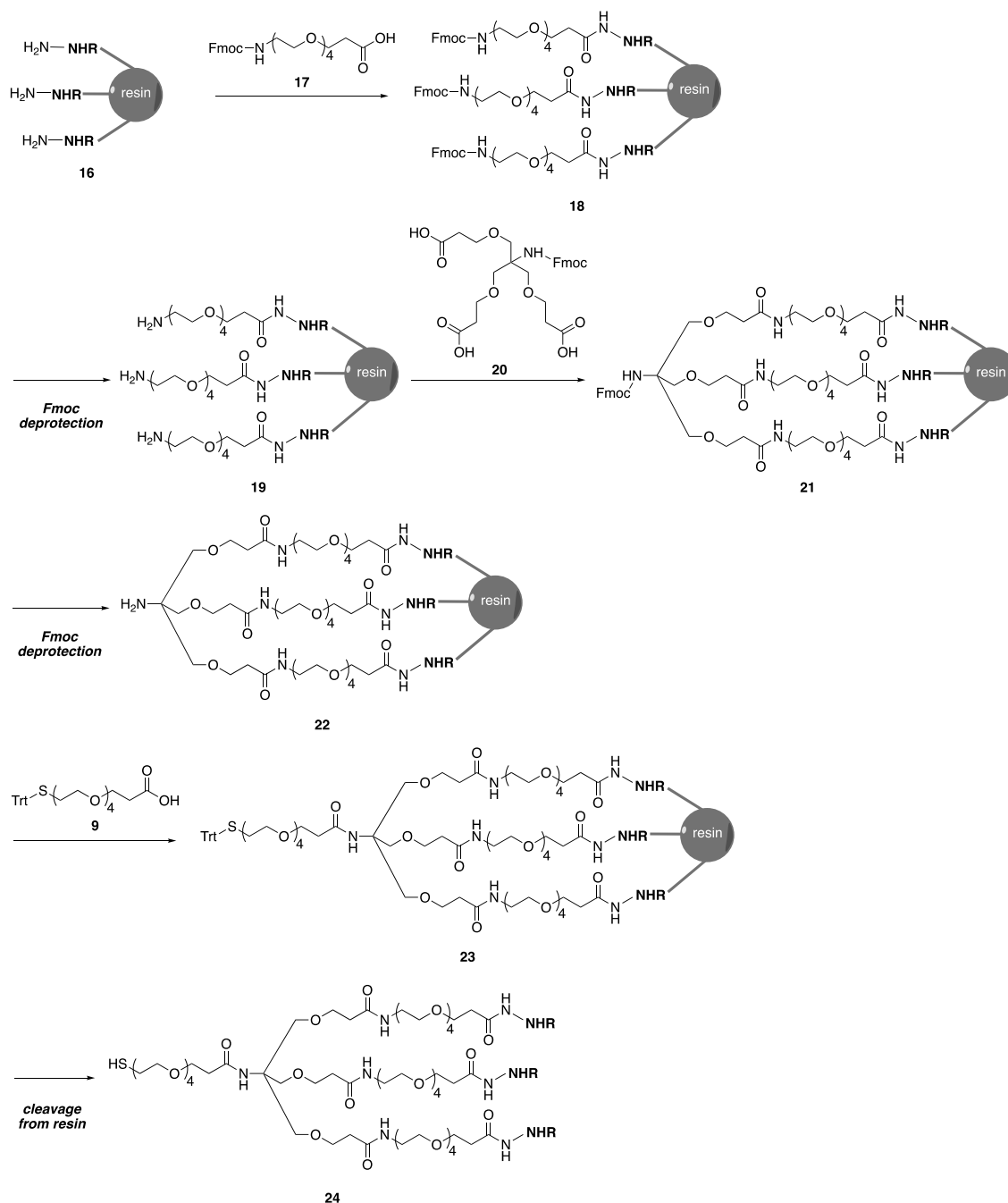
Scheme 5.5: New synthetic approach for the presentation of trimeric NHR-peptide on a hetero-tetrameric scaffold **20**.

The carboxyl containing Tris derivative **20** can be easily obtained following literature procedures.[335, 339, 345-346] Two different strategies are depicted in Scheme 5.6 and Scheme 5.7.
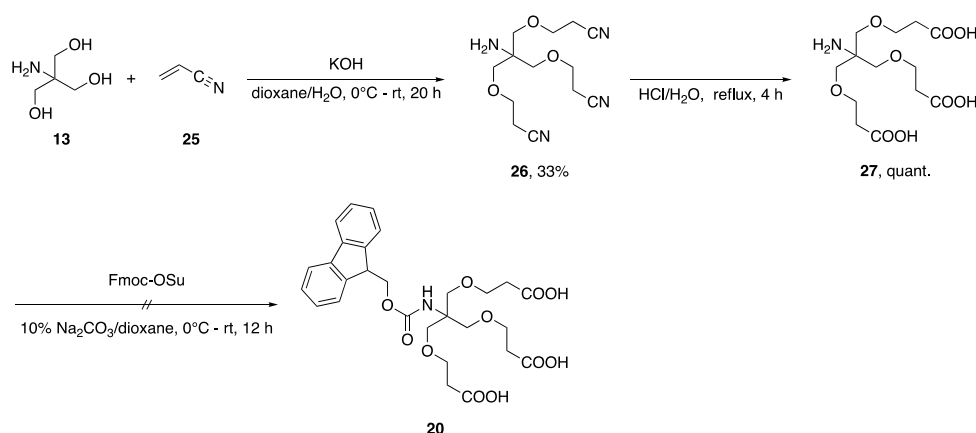
Scheme 5.6: First strategy for the synthesis of 3,3'-((2-(((((9H-fluoren-9-yl)methoxy)carbonyl)amino)-2-((2-carboxyethoxy)methyl)propane-1,3-diyl)bis(oxy))dipropionic acid **20**.
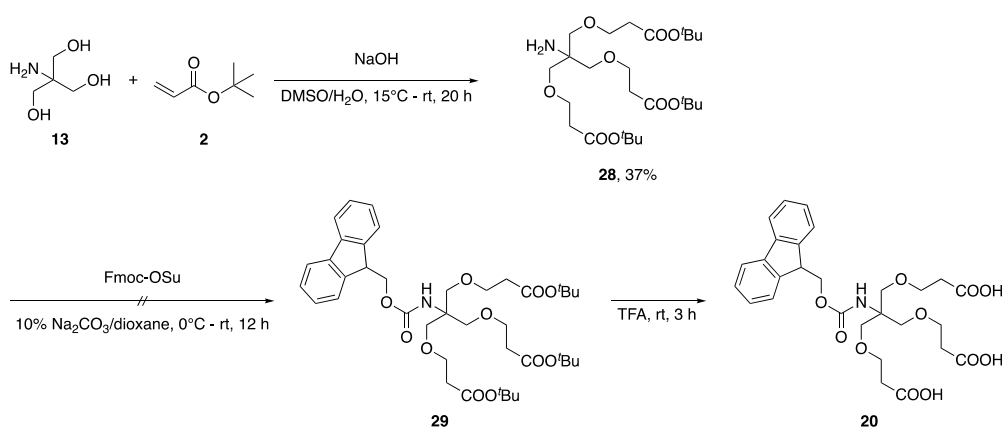
Scheme 5.7: Second strategy for the synthesis of 3,3'-((2-(((((9H-fluoren-9-yl)methoxy)carbonyl)amino)-2-((2-carboxyethoxy)methyl)propane-1,3-diyl)bis(oxy))dipropionic acid **20**.

In the first approach Tris-nitrile **26** is obtained by cyanoethylation, a special type of Michael addition, of Tris **13** with acrylonitrile **25**.[336, 345] Subsequent acid hydrolysis converts the nitrile into the corresponding carboxylic acid compound **27**.[346]

In the second approach (Scheme 5.7) Tris **13** is reacted with *tert*-butyl acrylate **2** in the presence of 5 M NaOH to give Tris-*tert*-butyl propionate **28** in 37% yield.[335] In both cases the Fmoc protection step of either **27** or **28** using Fmoc-OSu was unsuccessful. Thus, Fmoc-OSu was replaced by Fmoc-Cl, adapting the method described by Kostiainen *et. al.*.[339] With this **28** was converted into the desired *N*-Fmoc-protected derivative **29**, which could be obtained in reasonable yield after purification *via* preparative RP-HPLC (Scheme 5.8).
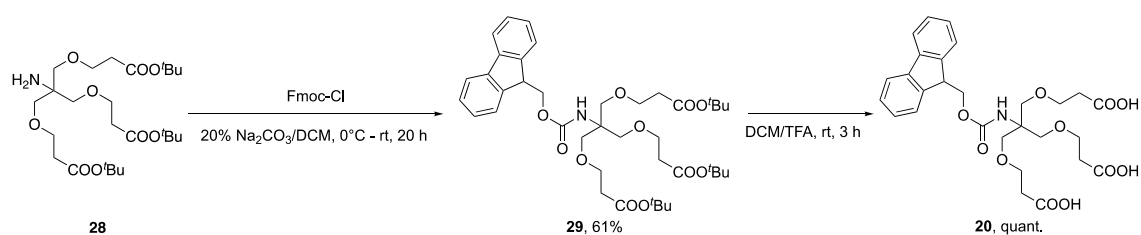
Scheme 5.8: Synthesis of 3,3'-((2-(((((9H-fluoren-9-yl)methoxy)carbonyl)amino)-2-((2-carboxyethoxy)methyl)-propane-1,3-diyl)bis(oxy))dipropionic acid **20**.

Removal of the *tert*-butyl group in TFA/DCM resulted in the carboxyl functionalized compound **20** with quantitative yield. This carboxyl groups should be activated to enable the amide bond formation with the *N*-terminal amino group of the NHR-derived peptide (see following section).

Coupling of the linker to the NHR-peptide on solid support

Coupling of the scaffold **20** with the NHR-peptide was tested using different activation methods (Table 5.7). First, the NHR-peptide was modified with a PEG moiety acting as spacer. Therefore, the commercially available Fmoc-NH-PEG(4)-COOH building block **17** was coupled to the NHR-peptide on resin using HCTU/DIPEA activation until complete coupling could be detected.

After Fmoc removal, the Tris scaffold **20** was to be reacted with the free *N*-terminal amino group (Scheme 5.9).
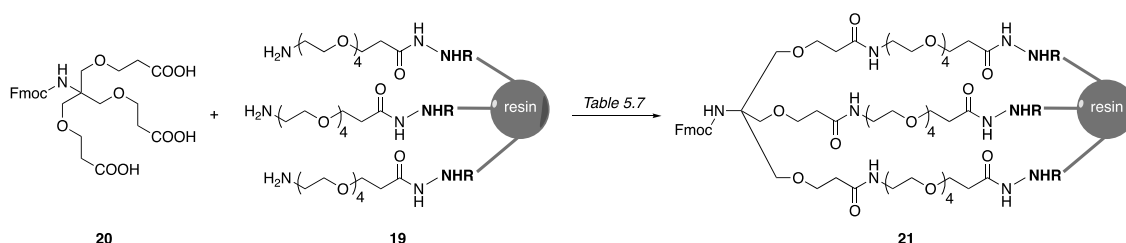
Scheme 5.9: Coupling of scaffold **20** to NHR-PEG(4) **19** peptide on resin.

Different conditions were applied to couple the NHR-derived peptide to the scaffold and are presented in Table 5.7. The coupling reaction was tested using different activation methods such as HCTU/DIPEA or HOBt/DIC. Reactions were shaken overnight, and reaction control occurred *via* test cleavage from the resin and characterization by RP-HPLC and mass spectrometry.

Table 5.7: Coupling reactions of scaffold **20** to different peptides. Reactions were performed on 0.005 mmol scale.

entry	peptide	conditions	observation
1	N36-PEG(4) (3.00 eq.)	1.00 eq. **20**, 3.00 eq. HCTU, and 6.00 eq. DIPEA in 1:1 DCM:DMF containing 0.5 M NaClO$_4$ 20 h	- only free N36-PEG(4) peptide detected - degradation of scaffold **20** (decarboxylation?)
2	T21-PEG(4) (3.00 eq.)	0.90 eq. **20**, 2.70 eq. HCTU, and 5.40 eq. DIPEA in DCM:DMF (1:1) 16 h	- only free T21-PEG(4) peptide detected - degradation scaffold **20**
3	N36-PEG(4) (3.00 eq.)	1.00 eq. **20**, 3.00 eq. HOBt, and 3.00 eq. DIC in 1:1 DMF:DCM (7 min pre-activation) 20 h	- 2 peptide strains coupled to the scaffold [M+5H]$^{5+}$ calcd. 1852.24, obs. 1853.58 - many other products - broad and overlapping peaks in the HPLC spectrum
4	T21-PEG(4) (3.00 eq)	0.90 eq. **20**, 2.70 eq. HOAt, and 2.70 eq. DIC in 1:1 DCM:DMF (7 min pre-activation) 20 h	- probably one peptide chain coupled to the scaffold with still one HOAt molecule is attached [M+4H]$^{4+}$ calcd. 1347.99, obs. 1352.02 [M+5H]$^{5+}$ calcd. 1078.59, obs. 1081.81 - non separable peaks in the HPLC spectrum

Activation of the carboxylic acid function HCTU/DIPEA was unsuccessful, as a decomposition of the scaffold was observed, and only uncoupled peptide could be detected. Coupling using HOBt/DIC as activating agents seemed promising as in mass spectrometric analysis a species was observed that possesses a mass in the range of two peptide strands coupled to the scaffold. However, the HPLC chromatogram contains broad and overlapping peaks regardless of the used method, precluding purification. In the case of HOAt/DIC activation, a mass was observed that is within the range of one peptide chain coupled to the scaffold, but some smaller molecule seems to be coupled in addition. The determined difference might correspond to a HOAt active ester still formed. Also here, the HPLC spectrum reveals broad and overlapping peaks, complicating purification.

Another activation method was tested by utilizing the NHS ester of **20**. NHS activation occurred with DSC **30** in the presence of triethylamine to convert the carboxyl groups into the NHS ester (Scheme 5.10). Purification by RP-HPLC gave the product **31** in good yield.
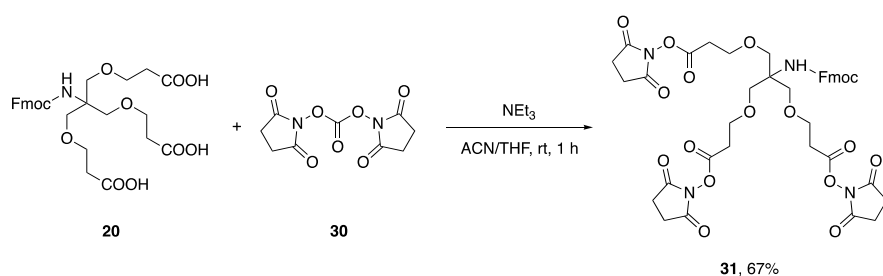
Scheme 5.10: NHS activation of **20**.

Coupling of the NHS ester **31** to the NHR-peptide on resin was tested using slightly basic conditions by adding triethylamine or DIPEA (Table 5.8).

Table 5.8: Different conditions tested for the coupling of scaffold **31** to NHR-derived peptide N36-PEG(4). Reactions were performed on 0.005 mmol scale.

entry	peptide	conditions	observation
1	N36-PEG(4) (3.00 eq.)	0.90 eq. **31** 10.8 eq. DIPEA (4.00 eq. per NHS) in DMF 10 h	- only free N36-PEG(4) peptide detected - scaffold **31** seems to be degraded
2	N36-PEG(4) (3.00 eq.)	0.90 eq. **31** 13.5 eq. NEt₃ (5.00 eq. per NHS) in DMF 10 h	- free N36-PEG(4) detected - degradation of PEG(4) moiety - scaffold **31** seems to be decomposing

In neither case was coupling of the peptide to the linker detected. Only the uncoupled, free N36-PEG(4) peptide was found. In addition, the scaffold **31** seems to be degraded under the applied conditions, and in the case of triethylamine also the PEG(4) moiety on the NHR-peptide seems to be decomposing.

Francis *et al.* described the design of a tetrameric scaffold for the synthesis of membrane-localized D-peptide inhibitors of HIV-1 entry.[255] The authors used a hetero-tetrameric scaffold **32** containing three arms with NHS ester groups for addition of peptides, and a fourth PEG arm functionalized with maleimide for addition of thiol-containing cargo. Peptide coupling occurred in DMAC buffered with triethylamine (Scheme 5.11).
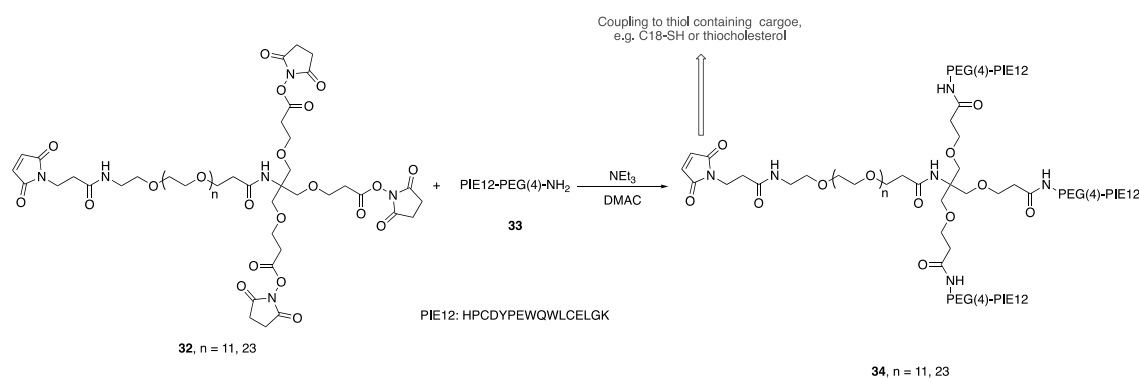
Scheme 5.11: Coupling of peptide PIE12 **33** to hetero-tetrameric scaffold **32** according to Francis *et al.*.[255]

Sanders *et al.* recently reported the solid-phase synthesis of self-assembling multivalent π-conjugated peptides.[347] The researchers synthesized for example a porphyrin containing peptide tetramer **37** *via* amidation on solid phase (Scheme 5.12). Therefore, 4,4',4'',4'''-(porphyrin-5,10,15,20-tetrayl)tetrabenzoic acid **35** was mixed with PyBOP and DIPEA in NMP and added to the resin-bound peptide suspended in DCM.
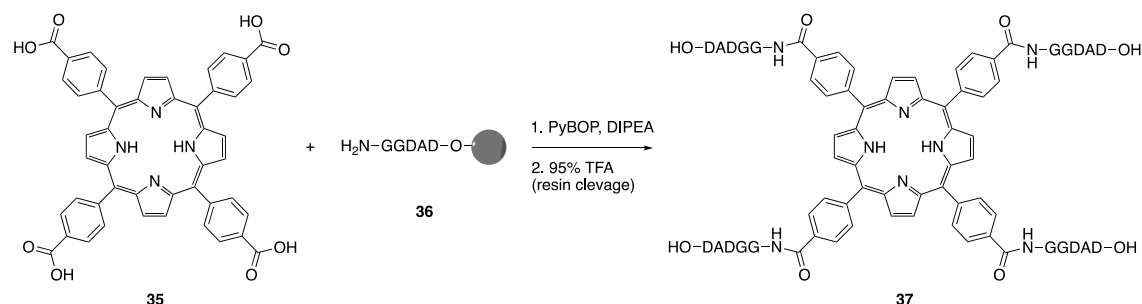
Scheme 5.12: Coupling of porphyrin derivative **35** to peptide **36** on solid support.

These two methods were adapted to bind either scaffold **20** or **31** to the resin-bound NHR-peptide. Unfortunately, all reactions tested were unsuccessful, yielding the unreacted, free peptide and degraded scaffold (Table 5.9).

Table 5.9: Conditions tested for the coupling of scaffold **20** or **31** to NHR-derived peptides. Reactions were performed on 0.005 mmol scale.

entry	scaffold	peptide	conditions	observation
1	**20** (1.00 eq.)	N36 (3.30 eq.)	3.30 eq. PyBOP 45.0 eq. DIPEA in NMP 20 h	- free N36 peptide detected - degradation of scaffold
2	**31** (1.00 eq.)	N36 (3.30 eq.)	66.0 eq. NEt$_3$ in DMAC 20 h	- free N36 detected - scaffold gets degraded
3	**20** (1.00 eq.)	T21-PEG(4) (3.30 eq.)	3.30 eq. PyBOP 45.0 eq. DIPEA in NMP 20 h	- uncoupled T21-PEG(4) peptide detected - PEG(4) moiety seems to decompose - degradation of used scaffold
4	**31** (1.00 eq.)	T21-PEG(4) (3.30 eq.)	66.0 eq. NEt$_3$ in DMAC 20 h	- uncoupled T21-PEG(4) peptide detected - PEG(4) moiety seems to decompose - degradation of used scaffold

5.5.3 Coupling of NHR-peptide with the scaffold in solution

As the coupling of the hetero-tetrameric scaffold to the NHR-peptide for a trimeric presentation was not successful on solid support, the coupling reaction was also tested in solution. The main advantage of this method is that the peptide can be purified before the coupling of the hetero-tetrameric scaffold occurs. This means that only the desired peptide sequence reacts, presumably leading to a simplified purification of the final peptide-linker conjugate, as in the case of the synthesis on solid support also deletion sequences might still react with the scaffold as well.

As the method by Francis *et al.* described above works in solution,[255] the coupling of the NHS activated scaffold **31** was tested also with an NHR-peptide, that is cleaved from the resin beforehand. To avoid side reactions on reactive groups of the amino acid side chains (e.g. ε-NH$_2$ of Lys), the peptide must be synthesized on a resin that allows the cleavage under mild acidic conditions so that the peptide can be obtained in protected form. With this, only the *N*-terminal amino group of the peptide chain is available for reaction with the scaffold.

Thus, N36-PEG(4) was synthesized on a NovaSyn® TGT resin and cleaved of in protected from by treatment with TFE/DCM (2:8). Following the literature procedure,[255] the coupling reaction of the side-chain protected N36-PEG(4) peptide with the NHS modified scaffold **31** was tested by mixing **31** (1.00 eq) with the peptide (3.30 eq.) in DMAC containing triethylamine (pH 7-8). After shaking for 1 h at room temperature, the reaction was stopped, and the outcome was characterized by RP-HPLC and mass spectrometry. The reaction was unsuccessful. The PEG(4) spacer or the peptide itself as well as the scaffold **31** are degraded and no coupling product was detected.

Another solution phase approach that was tested is the native chemical ligation (NCL).[348-349] NCL can be performed using completely unprotected peptide fragments, which is favorable as fully protected peptide sequences often display poor solubility, are more difficult to purify, as well as tend to aggregate due to their high hydrophobic character.[350-351] In the NCL reaction, a peptide fragment containing a thioester at the α-carboxyl group is reacted with a second peptide possessing a Cys residue at the *N*-terminal end (Scheme 5.13). The formed thioester undergoes a rapid intramolecular $S \rightarrow N$ acyl shift involving a 5-membered ring intermediate to give a native peptide bond at the ligation site.

Scheme 5.13: NCL reaction.
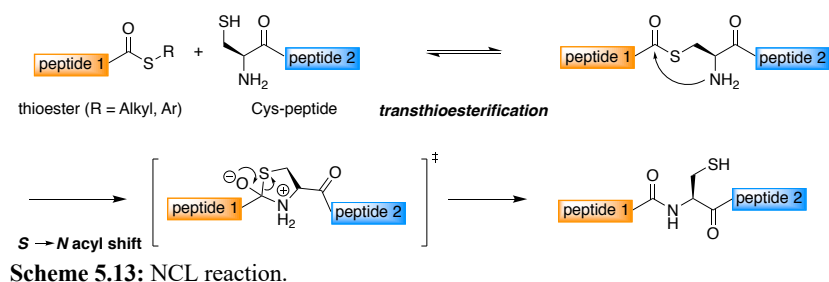
For testing this method, the carboxylic acid scaffold **20** was converted into the thioester variant **39** (Scheme 5.14). Therefore, **20** was reacted with *p*-acetamidothiophenol **38** *via* PyBOP/DIPEA activation to give the corresponding thioester **39** in 28% yield.

Scheme 5.14: Synthesis of a thioester scaffold **39**.
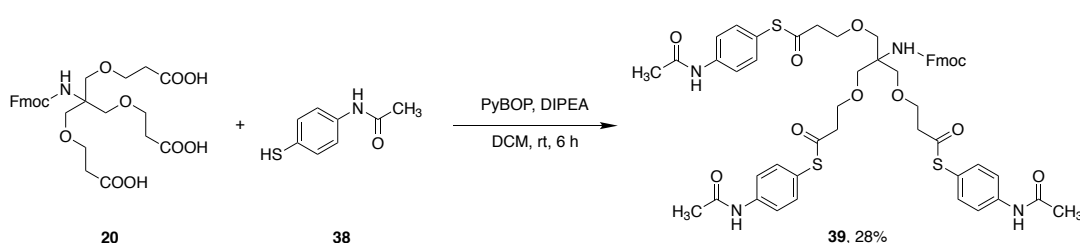
In addition, the NHR-peptide was *N*-terminally modified with a Cys residue. Here, T21-PEG(4)-Cys and T21-Cys were synthesized to investigate the NCL reaction. NCL was then conducted in 50 mM MPAA, 20 mM TCEP, 6 M GndHCl, and 0.1 M Na_2HOP_4 buffer at pH 7.0.

T21-PEG(4)-Cys or T21-Cys (3.30 eq. each) and the thioester scaffold **39** (1.00 eq.) were reacted for 6 h (Scheme 5.15). The total peptide concentration was 1 mM. The reaction progress was followed by analytical RP-HPLC. Formation of the desired product could not be detected. Using a higher concentration of the peptide (3 mM) also did not prove to be successful. Analysis by mass spectrometry reveals that the peptide does not react at all with the thioester scaffold. In addition, a fragment was detected that shows a mass of 166 Da higher than the free, unreacted peptide. This might correspond to a reaction of the peptide with the 4-mercaptophenylacetic acid (MPAA) from the buffer. However, this fragment could have also been detected due to the fact that the sample was not desalted before analysis, so that the MPAA simply stuck to the peptide.
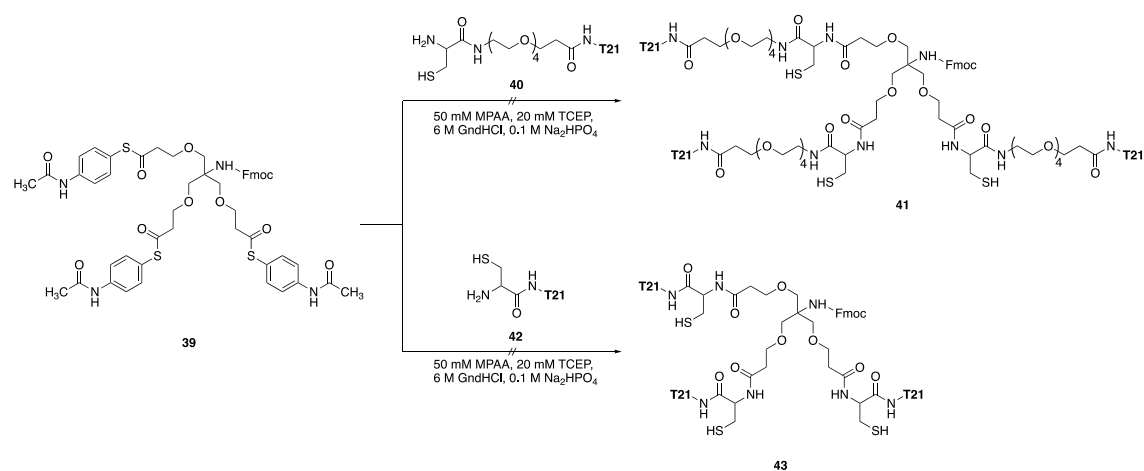
Scheme 5.15: NCL reaction of thioester scaffold **39** with T21 peptides **40**, and **42**.

Unfortunately, all of the tested approaches described above were unsuccessful, thus a new synthetic strategy must be pursued. Possible synthetic alternatives are outlined in the outlook (Chapter 6).

6.   Summary and Outlook

Systematic characterization of the effects of fluorinated amino acids on the formation and stability of peptide structures, e.g., the coiled-coil folding motif, or on proteolytic resistance, provides valuable insights for their specific applications in peptide engineering. The aim of this study was to apply sterically demanding, highly fluorinated amino acids to develop fluorinated peptide-based HIV-1 fusion inhibitors targeting the envelope protein subunit gp41. Moreover, in preliminary studies, initial insights were gained into how these amino acids behave in natural peptide environments and help protect peptides from being digested by proteases.

The following sections summarize individually the different studies performed in the course of this thesis.

Stabilizing a coiled-coil structure by single fluorinated amino acid substitutions within the hydrophobic core

Summary: Crucial factors for the formation of secondary structures in peptides and proteins include size, hydrophobicity, and the propensity of a given amino acid for adopting a certain secondary structure. Fluorinated amino acids are larger than their hydrocarbon analogues and their hydrophobicity is generally greater. This observation can primarily be attributed to a reduced number of hydrogen bonds between water and both the backbone's amine groups and carbonyl groups with fluorination that correlates with the amino acid hydration free energy rather than a change in the solvent-accessible surface area or an alternation in the dipole moment. Also, upon fluorination the α-helix propensity of the resulting amino acid is generally reduced compared to its natural analogue. Despite the latter finding, fluorinated amino acids are readily accommodated within the α-helical coiled-coil folding motif, the motif represented by the VPE/VPK system studied within this thesis. Incorporation of $5^3,5'^3$-F$_6$Leu and 4^3-F$_3$Val within central hydrophobic core positions enables retention of the dimeric and α-helical structure of the parent system as revealed by SEC/SLS studies as well as CD spectroscopy, and results in increased helicity. Thermal denaturation studies showed that a single substitution with $5^3,5'^3$-F$_6$Leu even enhances the overall stability of the coiled-coil model system by 0.8 kcal mol^{-1} residue^{-1}. This is in agreement with observations made by others, in which a stabilization upon $5^3,5'^3$-F$_6$Leu introduction by 0.31-0.83 kcal mol^{-1} residue^{-1} was found.[88, 104, 106-107, 273] In contrast, replacement with either (3*R*)- or (3*S*)-4^3-F$_3$Val does not lead to an increase in stability even though 4^3-F$_3$Val is more hydrophobic than Val. Thus, it seems that besides hydrophobicity also efficient packing of the side chains helps to overcome the less favorable α-helix propensity of the fluorinated amino acid and is responsible for enhancement in the stability of peptide structures upon fluorine introduction within the hydrophobic core. $5^3,5'^3$-F$_6$Leu preserves the shape of the Leu side chain and is thus well accommodated within the hydrophobic core of a coiled coil, showing only

minimal structural perturbations. On the contrary, 4^3-F_3Val substitution results in unfavorable steric clashes between the large β-CF_3 group and the backbone. Hence, these results suggest that upon a careful design that takes correct packing as well as steric demands into account, highly fluorinated amino acids can expand the hydrophobic core sequence space of coiled-coil peptides even with a single substitution.

Outlook: In future studies, X-ray crystallography of the VPE/VPK peptide dimers should be exploited to determine the optimal packing geometry of the fluorinated side chains within the native peptide environment of the hydrophobic core of such a coiled-coil folding motif.

Improving resistance of peptides towards proteolytic digestion with fluorinated amino acids

Summary: The second part of this study was an extensive investigation of the influence of sterically demanding, highly fluorinated amino acids on the proteolytic stability of peptides. Improving resistance towards protease digestion is a crucial factor in the development of peptide therapeutics as their applications are usually limited by low oral bioavailability and short half-lives that can partly be attributed to proteases of the digestive system and blood plasma.

Here, the previously established peptide FA served as a model to systematically substitute Ala residues adjacent to the protease cleavage site by either 5^3-F_3Ile or $5^3,5'^3$-F_6Leu. All peptides were incubated with the proteases α-chymotrypsin, pepsin, elastase, and proteinase K in turn. Their proteolytic degradation was followed over a period of 24 h and characterized by means of an analytical HPLC-assay with fluorescence detection. All cleavage products were identified using ESI-ToF mass spectrometry.

It was observed that sterically demanding and highly fluorinated amino acids such as 5^3-F_3Ile and $5^3,5'^3$-F_6Leu can be used to tune the proteolytic stability of peptides. The assumption that bulky fluorinated amino acids generally enhance proteolytic stability as a result of steric occlusion of the peptide from the active site was not supported. In fact, an even faster digestion compared to the non-fluorinated counterpart was detected for some peptides, although only in a few cases, e.g., P1'-5^3-F_3Ile in the presence of elastase. This suggests favorable interactions between the enzyme and the fluorinated substrate. However, in the case of 5^3-F_3Ile substitution mostly a significant increase in proteolytic stability was observed, especially when this residue was positioned *N*-terminal to the cleavage site. For example, the P2-5^3-F_3IleFA peptide was the most resistant substrate and found to be stable towards all four enzymes. Thus, 5^3-F_3Ile seems to be a promising amino acid that can be used to engineer stable peptide-based drug candidates. However, it should be noted that fluorine's impact on proteolytic stability must always be evaluated case-by-case as there is no general rule suggested by the described study.

Outlook: Future studies should focus on a more precise characterization of the factors that might be involved in the interaction of the fluorinated peptide substrates with the respective enzyme and should reveal whether fluorine-specific interactions between the substrate and the enzyme binding

site, or exclusion of the cleavage-relevant peptide bond from the active site, are responsible for the observed outcomes. Such investigations could include combinations of molecular dynamics simulations, NMR studies, and X-ray crystallographic methods.

Towards fluorinated, peptide--based HIV-1 fusion inhibitors

Summary: Another project within this thesis focused on the synthesis and characterization of fluorinated peptide-based HIV-1 fusion inhibitors. A key step in the fusion of the virus with the host cell is the formation of a stable six-helix bundle (6-HB) between the CHR- and NHR-regions of the viral gp41 protein. Inhibition of this bundle formation with synthetic NHR- or CHR-peptide derivatives can thus block the viral infection of host cells. In the current investigation the previously developed C31 peptide, derived from the CHR-region of gp41, served as a starting point for substitution studies. The Ile16 residue that is located in the middle of the C31 sequence and a highly conserved residue within the pocket binding domain of the CHR-region was replaced by DfeGly, 5^3-F$_3$Ile, or 5^3,$5'^3$-F$_6$Leu to probe a potential CH$\cdots\pi$ interaction. The synthesis of C31 was challenging as a difficult Fmoc-deprotection of the Asn17 residue resulted in poor yields and low crude peptide purity of the desired sequence. Using either MW irradiation or pseudoproline dipeptide building blocks the efficiency of the SPPS process was dramatically improved and the C31 peptide as well as its fluorinated analogues containing either DfeGly, 5^3-F$_3$Ile, or 5^3,$5'^3$-F$_6$Leu at the Ile16 position were successfully synthesized.

CD-spectroscopic investigation of the C31 peptides clearly suggested the formation of hetero-assemblies upon interaction with the NHR-derived peptide T21. While the C31 peptides are unstructured in their isolated forms, the minima in the CD spectra of equimolar mixtures with the NHR-derived peptide T21 clearly verify a helical structure. Moreover, the helical content of the fluorinated mixtures is increased in comparison to the non-fluorinated complex. All fluorinated C31/T21 complexes exhibit a lower thermal stability compared to the parent, non-fluorinated analogue, presumably explainable with steric effects as the C31-5^3,$5'^3$-F$_6$Leu/T21 complex was observed to be the least stable. However, their stabilities are still increased in comparison to C34/N36 that is considered to be a core structure of the 6-HB formation of gp41.

ITC was used to determine the thermodynamic parameters of the interaction between the C31 peptides and T21. The binding is enthalpy-driven, and a large amount of heat is released especially for the fluorinated derivatives. However, for the fluorinated C31 peptide variants this is somewhat opposed by a negative entropy change. This enthalpy-entropy compensation is characteristic for various intermolecular interactions in biological processes. Compared to native C31, the K values of C31-5^3,$5'^3$-F$_6$Leu and C31-5^3-F$_3$Ile are increased 1.5-, and 2.4-fold, respectively, indicating an increased binding affinity for these peptides to T21. In contrast, the K value for C31-DfeGly is reduced about 8-fold, suggesting weaker binding for this peptide to the T21 trimer.

Outlook: Further improvement to the synthesis of the gp41-derived peptides may be achieved when combining MW techniques and pseudoproline incorporation. Furthermore, using 10% (w/v) piperazin in NMP/EtOH (9:1) for Fmoc deprotection in the MW approach might further help to avoid side reactions such as aspartimide formation during this step. Initial attempts towards this combination of different advantageous approaches are currently being conducted in our group with even more complicated sequences. Also, different types of resin should be used in MW synthesis that were specially developed for this purpose, e.g., ProTide Rink amide resin, as the TGR resins used in this study are not suitable for MW conditions.

To further verify the helix bundle formation of the different C31 peptides with T21, N-PAGE experiments could be applied. In this gel electrophoresis setup, peptide sequences or complexes are run in their native state and separated according to their charge and size. As no chemical denaturant is added, the molecules preserve their higher-order structure.

In addition, competitive binding experiments *via* ITC could be carried out to characterize the binding of the fluorinated C31 peptides to T21 more precisely. Here, a strongly binding ligand A (one C31 peptide) is injected into a solution that contains the target molecule (T21 trimer) and the competing ligand B (second C31 peptide). If the ligands behave competitively, the binding constant for ligand A will decrease in the presence of the ligand B compared to the value when present alone.

Another important experiment that should to be conducted is the determination of the oligomerization state of the C31/T21 complexes. The ITC studies described above already indicated binding stoichiometries differing from 1:1 that would be the case if a 6-HB is formed. However, for the determination of the N value *via* ITC it is assumed that all binding sites are identical and independent, that the protein and ligand are pure, that the given protein and ligand concentrations are correct, and that all protein molecules are correctly folded and active.[352-353] This typically cannot be ensured as the concentration determination depends on the accuracy of the method of determination, and extinction coefficients are not always absolutely accurate. Furthermore, not all of the peptides may be correctly folded, which might be the case for the T21 peptide, as NHR-derived peptides are known to aggregate. These factors could result in determined stoichiometries that differ from the expected or actual value. Thus, determination of oligomerization should be performed by SEC/SLS techniques.

Furthermore, the proteolytic stability of the C31 analogues should be investigated in order to verify whether the single substitution with fluorinated amino acids can improve their resistance towards proteolysis, as shown in project 2 above for model substrates.

Another strategy that one can think of in regard to overcome the entropically disfavored binding process would be to make use of so-called stapled peptides. Here α-methyl-α-pentenylglycine, also in combination with bis-(4-pentenyl)glycine, could be incorporated to enable intrahelical crosslinks *via* ring-closing olefin metathesis, thereby increasing the α-helicity

of the peptide. Another advantage of such stapled peptides is their increased metabolic stability.[354-355] As the peptides are thus somewhat preorganized in a helical conformation, the entropic penalty should be decreased in comparison to the unstapled peptides, likely leading to a more favored binding process. Incorporation should here occur at solvent exposed positions of the *C*-terminal side of the C31 peptide. This would result in a new peptide library that would have to be characterized as described above.

Designing a hetero-tetrameric scaffold for presentation of a peptide in a trimeric conformation

Summary: In order to analyze the efficacy of the new C31 analogues, kinetic parameters of the C31 interaction with relevant NHR-counterparts should be determined by applying SPR techniques. In this end, this final part of this thesis work addressed the development of a linker for SPR studies that was designed with the intent to pre-organize the NHR-peptides on the surface of a SPR chip. Therefore, the hetero-tetrameric scaffold 3,3'-((2-((((9H-fluoren-9-yl)methoxy)-carbonyl)amino)-2-((2-carboxyethoxy)-methyl)propane-1,3-diyl)bis(oxy))dipropionic acid **20** was synthesized successfully. It enables presentation of NHR-derived peptides in their trimeric conformation and in addition bears a second functional group for the surface immobilization of the peptide-scaffold conjugate. Coupling of this scaffold to different modified NHR-derived peptides was tested in both the solid and the solution phase. Activation of the carboxylic acid function of the scaffold with HCTU/DIPEA, HOBt/DIC, HOAt/DIC, or PyBOP/DIPEA were unsuccessful. Furthermore, NHS activation was tested, which also did not lead to the desired conjugate. In addition, the scaffold was activated as the thioester and the NHR-peptide was *N*-terminally modified with either Cys or PEG(4)-Cys to enable an NCL reaction between the peptide and the scaffold. However, this method was also unsuccessful. In almost all cases, uncoupled peptide was detected, and degradation of the scaffold was observed.

Outlook: In future work, the synthesis for effectively presenting a trimeric NHR-peptide for SPR studies would have to be further optimized. The coupling reaction of the peptide with the scaffold should therefore be done in solution as several modern ligation techniques offer great flexibility in reaction conditions. For example, a new synthesis approach could make use of a copper(I) catalyzed alkyne-azide 1,3-dipolar cycloaddition reaction (CuAAC; "click" chemistry) by linking a alkyne scaffold **49** to the NHR-derived peptides appropriately modified with an azide-containing residue (Scheme 6.1). This ligation reaction has been used to conjugate sterically demanding oligosaccharides to a similar dendrictic skeleton based on tris(hydroxymethyl)aminomethane **13** as well.[337] The proposed synthetic strategy is depicted in the scheme below.
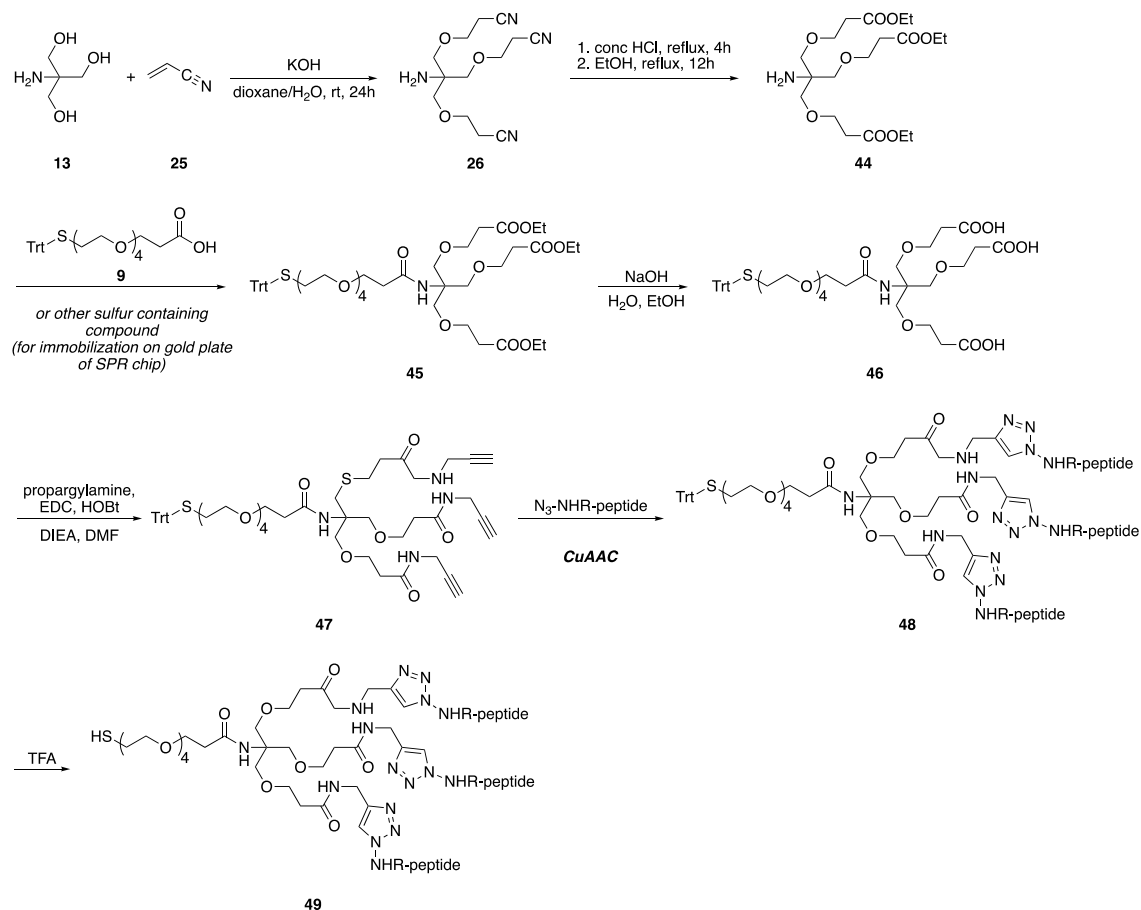
Scheme 6.1: Syntheses of a hetero-tetrameric scaffold **47** and conjugation of azide-functionalized NHR-peptide to this scaffold by CuAAC reaction.

In addition, immobilization on the SPR chip could also be carried out using other methods besides the thiol-gold interaction, as several different surface chemistries are available,[323] e.g., a streptavidin modified surface can be used for binding to a biotinylated molecule. Once the NHR-trimer on the hetero-tetrameric scaffold were to be in hand, SPR could be used to determine the kinetic binding parameters of the C31 peptides. This powerful technique enables systematic evaluation of the influence of fluorinated building blocks on the kinetics and thermodynamics of the 6-HB formation. Thus, insights into the molecular interactions of non-natural amino acids in a native peptide environment would be gained. Moreover, these observations would likely clarify the optimal arrangement and binding specificity of fluorinated amino acids with different side-chain volumes and polarities inside the hydrophobic core of gp41.

7. Materials and Methods

7.1 General experimental conditions

7.1.1 Reagents and solvents

All syntheses involving air- and moisture-sensitive compounds were carried out using standard Schlenk technique under an atmosphere of argon. Prior to use the glassware was flame-dried under vacuum and cooled under flushing with argon. Air- and moisture sensitive compounds were added under argon counterflow or with the help of septa using oven-dried syringe or cannula. Solvents were dried with the solvent purification system MB-SPS 800 from M. Braun (M. Braun Inertgas-Systeme GmbH, Garching, Germany). Room temperature refers to 22°C.

Reactions were monitored by thin-layer chromatography (TLC) using Merck KGaA silica gel 60 F254 TLC aluminum sheets (0.25 mm thickness, Merck KGaA, Darmstadt, Germany) and visualized with ceric ammonium molybdate, vanillin staining solution, potassium permanganate staining solution, ninhydrin solution staining, iodine staining or UV light. Flash chromatography was carried out using Silica 60 M (0.040−0.063 mm) from Macherey-Nagel GmbH & Co. KG (Düren, Germany), using a forced flow of eluent (method of Still)[356] Concentration under reduced pressure was performed by rotary evaporation at 40°C at the appropriate pressure. Yields refer to chromatographically purified and spectroscopically pure compounds.

Resins for solid phase peptide synthesis where purchased from Novabiochem® (Merck KGaA, Darmstadt, Germany). Canonical Fmoc- and orthogonal side-chain protected amino acids were obtained from ORPEGEN Peptide Chemicals GmbH (Heidelberg, Germany). Pseudoproline dipeptide and PEGylation building blocks were bought from Iris Biotech GmbH (Marktredwitz, Germany), and Boc-Abz-OH from Bachem (Bachem AG, Bubendorf, Switzerland). Coupling reagents came from Novabiochem® (Merck KGaA, Darmstadt, Germany), Carbolution (Carbolution Chemicals GmbH, St. Ingbert, Germany) or Sigma-Aldrich® (Merck KGaA, Darmstadt, Germany). Solvents for peptide synthesis were purchased as synthesis grade from Fisher Scientific (Schwerte, Germany), Acros Organics (Thermo Fisher Scientific, Geel, Belgium), VWR (VWR International GmbH, Darmstadt, Germany) or Merck (Merck Chemicals GmbH, Darmstadt, Germany). Solvents for peptide purification were obtained as HPLC or spectroscopy grade from Fisher Scientific (Schwerte, Germany) or Merck (Merck Chemicals GmbH, Darmstadt, Germany).

Deionized water used for HPLC or to prepare buffers was obtained using a Milli-Q® Advantage A10 Ultrapure Water Purification System (Merck KGaA, Darmstadt, Germany).

All other chemicals and solvents were purchased from Acros Organics (Thermo Fisher Scientific, Geel, Belgium), abcr GmbH (Karlsruhe, Germany), chemPUR (Karlsruhe., Germany), Fluorochem (Hadfield, United Kingdom), VWR (Darmstadt, Germany), Merck (Darmstadt,

Germany), Sigma-Aldrich® (Merck KGaA, Darmstadt, Germany), Alfa Aesar (Thermo Fisher (Kandel) GmbH, Karlsruhe, Germany), Novabiochem® (Merck KGaA, Darmstadt, Germany), or Roth (Carl Roth GmbH + Co. KG, Karlsruhe, Germany) at highest commercially available purity.

All reagents and solvents were used without further purification. Acetic anhydride (Grüssing GmbH Analytika, Filsum, Germany) and triethylamine (99%, Acros Organics, Geel, Belgium) were freshly distilled prior to use.

Fluorinated amino acids were obtained as described in Section 7.2.

7.1.2   Solid phase peptide synthesis

If not mentioned otherwise, the syntheses of the peptides were carried out using the fully automatic parallel peptide synthesizer Syro XP (Multi-SynTech GmbH, Witten, Germany) according to the standard protocol in Table 7.7 or with the Activo-P11 Automated Peptide Synthesizer (Activotec, Cambridge, United Kingdom) according to the standard protocol in Table 7.8.

Test approaches for microwave assisted peptide synthesis were performed on the CEM Liberty Blue™ Automated Microwave Peptide Synthesizer (CEM Corporation, Matthews, NC, USA) or with the Biotage® Initiator+ Microwave System (Biotage AB, Uppsala, Sweden) (Section 7.5).

7.1.3   Preparative HPLC

Purification of the synthesized peptides was performed on a LaPrepΣ HPLC system (VWR International GmbH, Darmstadt, Germany), comprising a LaPrepΣ LP 1200 preparative solvent pump with 100 mL titanium pump head, a ternary low-pressure gradient, a dynamic mixing chamber, a 6-port-3-channel injection valve with an automated preparative 10 mL sample loop, a LaPrepΣ LP 3101 1-channel UV-detector, a LaPrepΣ semi-preparative flow cell with 0.5 mm path length and a LaPrepΣ LP2016 17-port/1-channel fractionation valve. A Kinetex® C18 RP-HPLC-column with TMS endcapping (5 µm, 100 Å, 250×21.2 mm, Phenomenex®, Torrance, CA, USA) or a Luna® C8(2) column (10 µm, 100 Å, 250×21.2 mm, Phenomenex®, Torrance, CA, USA) was used. A SecurityGuard™ PREP Cartridge Holder Kit (21.20 mm ID, Ea, Phenomenex®, Torrance, CA, USA) either holding a C18 or C8 cartridge (15×21.2mm, Phenomenex®, Torrance, CA, USA) served as pre-column. As eluents deionized water and ACN, both containing 0.1% (v/v) TFA were applied. HPLC runs were performed according to the methods given in Table 7.1. Data analysis occurred with an EZChrom *Elite* software (Version 3.3.2 SP2, Agilent Technologies, Santa Clara, CA, USA).

Table 7.1: Gradient methods used for preparative HPLC. Eluents: A = water + 0.1% (v/v) TFA, B = ACN + 0.1% (v/v) TFA.

	time [min]	A [%]	B [%]	flow [mL/min]	λ [nm]		time [min]	A [%]	B [%]	flow [mL/min]	λ [nm]
P1	0	70	30			**P2**	0	70	30		
	20	0	100				18	0	100		220
	22	0	100	20	280		21	0	100	15	or
	23	70	30				22	70	30		280
	26	70	30				25	70	30		
P3	0	95	5			**P4**	0	95	5		
	18	0	100		260		30	30	70		220
	21	0	100		or		32	0	100		or
	22	95	5	20	280		35	0	100	20	320
	25	95	5				36	95	5		
							40	95	5		
P5	0	95	5	10		**P6**	0	90	10		
	5	95	5	10			18	20	80		
	30	30	70				19	0	100		
	32	0	100		220		22	0	100	15	220
	35	0	100				23	90	10		
	36	95	5	20			26	90	10		
	40	95	5								
P7	0	90	10			**P8**	0	90	10		
	5	90	10				30	20	80		
	7	50	50				31	0	100		
	20	50	50	10	220		34	0	100	15	220
	22	90	10				36	90	10		
	25	90	10				40	90	10		
P9	0	90	10			**P10**	0	60	40		
	30	20	80				5	60	40		
	32	0	100				30	40	60		
	35	0	100	20	220		32	0	100	20	220
	37	90	10				35	0	100		
	40	90	10				36	60	40		
							40	60	40		
P11	0	60	40			**P12**	0	90	10	10	
	30	30	70				5	90	10	10	
	32	0	100				30	20	80		
	35	0	100	20	220		32	0	100		220
	37	60	40				35	0	100		
	40	60	40				36	90	10	20	
							40	90	10		

7.1.4 Analytical HPLC

Semi-micro Chromaster HPLC system (fixer Fritz)

Analytical HPLC was carried out on a VWR-Hitachi Chromaster HPLC 600 bar system (VWR International GmbH, Darmstadt, Germany) that works with a low-pressure gradient. The system contains a 5160 pump with a 6-channel solvent degaser, an organizer, a 5260 autosampler with a 20 µL sample loop, a 5310 column oven and a 5430 diode array detector with a high pressure semi-micro flow cell (5 mm). A Purospher® STAR RP-C18 endcapped UHPLC column (2 µM, 120 Å, 50 × 2.1 mm, Merck, Deutschland) was used. As eluents deionized water and ACN, both

containing 0.1% (v/v) TFA, were applied. A flow rate of 0.6 mL/min was used and the column was heated to 24°C. The UV-detection occurred at 220 nm (unlabeled peptides), 280 nm (peptides containing Tyr and/or Trp residues) or 320 nm (Abz-labeled peptides) and a linear gradient of ACN + 0.1% (v/v) TFA according to the methods given in Table 7.2 was applied. The data were analyzed with EZChrom *Elite* software (version 3.3.2, Agilent Technologies, Santa Clara, CA, USA).

Table 7.2: Gradient methods used for analytical HPLC on a semi-micro Chromaster HPLC system. Eluents: A = water + 0.1% (v/v) TFA, B = ACN + 0.1% (v/v) TFA.

	time [min]	A [%]	B [%]		time [min]	A [%]	B [%]
A1	0	70	30	A2	0	95	5
	7	0	100		9	0	100
	8	0	100		10.5	0	100
	8.5	70	30		11	95	5
	11	70	30		14	95	5
A3	0	95	5	A4	0	90	10
	6	30	70		6	20	80
	6.5	0	100		6.1	0	100
	7	0	100		7	0	100
	7.1	95	5		7.1	90	10
	10	95	5		10	90	10

Chromaster HPLC system (slow Fritz)

The VWR-Hitachi Chromaster HPLC 600 bar system (VWR International GmbH, Darmstadt, Germany) works with a low-pressure gradient, and comprises a 5160 pump with a 6-channel solvent degaser, an organizer, a 5260 autosampler with a 100 μL sample loop, a 5310 column oven and a 5430 diode array detector with a standard flow cell (10 mm optical path length). A Luna® C8(2) column (5 μm, 100 Å, 250 × 4.6 mm, Phenomenex®, Torrance, CA, USA) or a Kinetex® C18 column (5 μm, 100 Å, 250 × 4.6 mm, Phenomenex®, Torrance, CA, USA), was used. A SecurityGuard™ Cartridge Kit (Ea, Phenomenex®, Torrance, CA, USA) with either a C8 or C18 SecurityGuard™ cartridge (4 × 3.0 mm, Phenomenex®, Torrance, CA, USA) served as pre-column. Deionized water and ACN, both containing 0.1% (v/v) TFA, served as eluents. The flow rate was adjusted to 1 mL/min and the column was heated to 24°C. UV-detection of the peptides occurred at 220 nm (unlabeled peptides and peptide fragments, and purity control of the final peptides), 280 nm (peptides containing Tyr and/or Trp residues) or 320 nm (Abz-labeled peptides) while running a linear gradient of ACN + 0.1% (v/v) TFA according to methods shown in Table 7.3. in either 18 min or 30 min was applied. Data analysis was performed with EZChrom *Elite* software (version 3.3.2, Agilent Technologies, Santa Clara, CA, USA).

Table 7.3: Gradient methods used for analytical HPLC on a Chromaster HPLC system. Eluents: A = water + 0.1% (v/v) TFA, B = ACN + 0.1% (v/v) TFA.

	time [min]	A [%]	B [%]		time [min]	A [%]	B [%]
A5	0	70	30	A6	0	95	5
	18	0	100		18	0	100
	20	0	100		20	0	100
	22	70	30		21	95	5
	25	70	30		24	95	5
A7	0	95	5	A8	0	90	10
	18	30	70		30	20	80
	19	0	100		32	0	100
	21	0	100		36	0	100
	21.5	95	5		37	90	10
	24	95	5		40	90	10

LaChrom ELITE® HPLC system (Rosi)

Analytical HPLC was carried out on a LaChrom ELITE®-HPLC-System from VWR-Hitachi (VWR International GmbH, Darmstadt, Germany). The system contains an organizer, two HPLC-pumps (L-2130) with solvent degaser, an autosampler (L-2200) with a 100 µL sample loop, a diode array flow detector (L-2455), and a high pressure gradient mixer. A Luna® C8(2) column (5 μm, 100 Å, 250 × 4.6 mm, Phenomenex®, Torrance, CA, USA)or a Kinetex® C18 column (5 μm, 100 Å, 250 × 4.6 mm, Phenomenex®, Torrance, CA, USA) was used. A SecurityGuard™ Cartridge Kit (Ea, Phenomenex®, Torrance, CA, USA) holding a C8 or C18 SecurityGuard™ cartridge (4 × 3.0 mm, Phenomenex®, Torrance, CA, USA), respectively, served as pre-column. A flow rate of 1.0 mL/min was applied with deionized water and ACN, both containing 0.1% (v/v) TFA, as eluents. The used gradient methods are shown in Table 7.4, and the UV-detection occurred at 220 nm (unlabeled peptides and peptide fragments, as well as purity control of the final peptides), 280 nm (peptides containing Tyr and/or Trp residues) or 320 nm (Abz-labeled peptides).

For RP-HPLC with fluorescence detection a fluorescence detector (L-2485) was added to the system, and a monolithic reversed-phase C8 Chromolith® Performance HPLC column (100 × 4.6 mm, Merck KGaA, Darmstadt, Germany) was used. The flow rate was set to 3 mL/min, and the used linear gradients are given in Table 7.5. The fluorescence detection occurred based on the Abz label of the peptides using the fluorescence detector with $\lambda_{ex} = 320$ nm and $\lambda_{em} = 420$ nm.

Obtained data were analyzed with EZChrom *Elite* software (version 3.3.2, Agilent Technologies, Santa Clara, CA, USA).

Table 7.4: Gradient methods used for analytical HPLC on a LaChrom ELITE® HPLC system. Eluents: A = water + 0.1% (v/v) TFA, B = ACN + 0.1% (v/v) TFA.

	time [min]	A [%]	B [%]		time [min]	A [%]	B [%]
A9	0	70	30	**A10**	0	70	30
	18	0	100		16	0	100
	20	0	100		19	0	100
	21	70	30		20	70	30
	25	70	30		24	70	30
A11	0	95	5				
	18	0	100				
	20	0	100				
	21	95	5				
	24	95	5				
A12	0	95	5	**A13**	0	90	10
	30	30	70		30	20	80
	32	0	100		31	0	100
	35	0	100		35	0	100
	36	95	5		36	90	10
	40	95	5		40	90	10

Table 7.5: Gradient methods used for analytical HPLC with fluorescence detection on a LaChrom ELITE® HPLC system. Eluents: A = water + 0.1% (v/v) TFA, B = ACN + 0.1% (v/v) TFA.

	time [min]	A [%]	B [%]		time [min]	A [%]	B [%]
FL1	0	95	5	**FL2**	0	95	5
	5	70	30		5	60	40
	5.5	70	30		5.5	60	40
	6	95	5		6	95	5
	9	95	5		9	95	5
FL3	0	95	5	**FL4**	0	95	5
	15	70	30		15	55	45
	15.5	70	30		15.5	55	45
	16	95	5		16	95	5
	17	95	5		17	95	5

Graphical representation of the spectra occurred with the program OriginPro 2018b version 9.55 (OriginLab Corporation, Northampton, MA, USA).

7.1.5 Lyophilization

To lyophilize synthesized compounds a laboratory freeze dryer ALPHA 1-2 LD (Christ Gefriertrocknungsanlagen GmbH, Osterode am Harz, Germany) was used. A chemistry hybrid pump RC 6 (Vacuubrand GmbH + Co KG, Wertheim, Germany) was connected.

7.1.6 Mass spectrometry

High resolution mass spectrometry was conducted on an Agilent 6220 ESI-ToF LC-MS spectrometer (Agilent Technologies Inc., Santa Clara, CA, USA). Mass-to-charge ratios were also determined on an Agilent Technologies 6230 TOF LC/MS instrument with ESI-injector (Agilent Technologies Inc., Santa Clara, CA, USA). The samples were dissolved in a 1:1 mixture of water

and ACN containing 0.1% (v/v) TFA, DCM or MeOH and injected directly into the spray chamber using a syringe pump with a flow rate of 10 μL/min. Parameters were optimized for maximal abundance of $[M + H]^+$, $[M + Na]^+$ or $[M - H]^-$. Exact settings are given in Table 7.6.

For the depiction and analysis of the data the MassHunter Workstation software version B.02.00 or version B.08.00 (Agilent Technologies, Santa Clara, CA, USA) was used. Calculated molar masses and mass to charge residues were obtained from either the ChemDraw Professional software Version 16.0.1.4 (Perkin Elmer Informatics, Inc., Waltham, MA, USA) or from the Peptide Mass Calculator v3.2 (http://rna.rega.kuleuven.be/masspec/pepcalc.htm).

Table 7.6: Settings for high resolution mass spectrometry.

setting	instrument	parameter
A	6220	spray voltage: 3.5 kV nebulizer: 30 psi drying gas flow rate: 5 L/min gas temperature: 300°C fragmentor voltage: 200 V
B	6220	spray voltage: 4 kV nebulizer: 15 psi drying gas flow rate: 5 L/min gas temperature: 300°C fragmentor voltage: 250 V
C	6230	spray voltage: 3.5 kV nebulizer: 20 psi drying gas flow rate: 5 L/min gas temperature: 325°C fragmentor voltage: 250 V

7.1.7 NMR spectroscopy

^{1}H-, ^{13}C- und ^{19}F-NMR spectra were recorded at room temperature using a JEOL ECX400 (^{1}H-NMR: 400 MHz, ^{13}C: 101 MHz, ^{19}F: 376 MHz, JEOL, Tokyo, Japan), a JEOL ECP500 (^{1}H-NMR: 500 MHz, ^{13}C-NMR: 126 MHz, JEOL, Tokyo, Japan) or a Bruker AVANCE III 700 (^{1}H-NMR: 700 MHz, ^{13}C-NMR: 176 MHz, BRUKER, Billerica, MA, USA). The depiction and analysis of the spectra occurred with the program MestReNova version 7.1.2 (Mestrelab Research S. L., Santiago de Compostela, Spain).

The chemical shifts (δ) are given in parts per million (ppm). The ^{1}H- and ^{13}C-NMR chemical shifts were referenced against the internal solvent (CDCl$_3$ δ(^{1}H) = 7.26 ppm, δ(^{13}C) = 77.16 ppm; Aceton-D$_6$ δ(^{1}H) = 2.05 ppm,   δ(^{13}C) = 29.84 ppm;   DMSO-D$_6$ δ(^{1}H) = 2.50 ppm, δ(^{13}C) = 39.52 ppm) and given to trimethylsilane as internal standard (δ = 0.00 ppm).[357] The ^{19}F-NMR chemical shifts are given relative to CFCl$_3$ as external reference.

^{13}C-NMR-spectra were recorded ^{1}H decoupled. The attributions of the chemical shifts were determined by means of COSY and HMQC experiments.

The order of citation in parentheses is a) multiplicity (s = singlet, d = doublet, t = triplet, m = multiplet, br = broad, and combinations thereof), b) coupling constant J, c) number of nuclei, and d) assignment.

7.1.8 UV spectroscopy

UV-spectra were measured using a Varian Cary 50 spectrophotometer (Varian Medical Systems, Palo Alto, CA, USA) and half micro polymethylmethacrylate cuvettes (10 mm path length, 1.5 mL, Plastibrand®, VWR International GmbH, Darmstadt, Germany) for wavelength > 300 nm or quartz cuvettes (10 mm path length, 1.5 mL, Hellma Analytics, Müllheim, Germany) for wavelengths < 300 nm.

7.1.9 CD spectroscopy

CD spectroscopy was carried out on a Jasco J-810 spectropolarimeter (JASCO Deutschland GmbH, Pfungstadt, Germany) equipped with a Jasco PTC-423S Peltier temperature control system and a HAAKE WKL water recirculator (Thermo Electron GmbH, Karlsruhe, Germany) for tempering the samples. Data analysis occurred with the software J-700 (JASCO Deutschland GmbH, Pfungstadt, Germany).

The processing and depiction of the spectra was performed using the program OriginPro 2018b version 9.55 (OriginLab Corporation, Northampton, MA, USA).

7.2 Synthesis of fluorinated amino acids

(2*S*,3*S*)-, and (2*S*,3*R*)-Boc-4^3-F$_3$Val (TfVal), Boc-5^3,5'^{3}-F$_6$Leu (HfLeu), Boc-5^3-F$_3$Ile (TfIle), and the precursor (*S*)-3-((2*S*,3*S*)-2-[*tert*-Butoxycarbonyl]amino-5,5,5-trifluoro-3-methylpentanoyl)-4-benzyloxazolidin-2-one were synthesized according to literature and kindly provided by Dr. Holger Erdbrink and Prof. Dr. Constantin Czekelius.[135, 270] Fmoc-(*S*)-DfeGly was synthesized according to Winkler and Burger,[358] and kindly provided as crude product by members of the AG Koksch. Fmoc-(*S*)-5^3,5'^{3}-F$_6$Leu-OEt was synthesized according to literature procedures and kindly provided by Dr. Johann Moschner.[274, 359-360]

7.2.1 (2*S*,3*S*)-2-((*tert*-butoxycarbonyl)amino)-5,5,5-trifluoro-3-methylpentanoic acid (Boc-5^3-F$_3$Ile)

According to Erdbrink *et al.*[135] (*S*)-3-((2*S*,3*S*)-2-[*tert*-Butoxycarbonyl]amino-5,5,5-trifluoro-3-methylpentanoyl)-4- benzyloxazolidin-2-one (250 mg, 0.563 mmol, 1.00 eq.) was dissolved in a 3:1 mixture of THF/H$_2$O (5.6 mL) at 0°C. A precooled (0°C) solution of LiOH (40.5 mg, 1.69 mmol, 3.00 eq.) and 30% H$_2$O$_2$ (104 µL, 3.38 mmol, 6.00 eq.) in THF/H$_2$O 3:1 (1.75 mL) was added. The reaction was stirred at 0°C for 2.5 h, and a 1 M aq. Na$_2$SO$_3$ solution (3.72 mL, 3.72 mmol, 6.60 eq.) was slowly added. The mixture was allowed to warm to rt, THF was

removed under reduced pressure, and the aqueous residue was washed with DCM (3×5.0 mL). The aqueous phase was carefully acidified with 1 M HCl to pH $\approx$ 3 and extracted with ethyl acetate (4×10 mL). Combined organic layers were dried over sodium sulfate, filtered, and the solvent was removed *in vacuo* to afford 157 mg (0.550 mmol, 98%) of Boc-5^3-F$_3$Ile as white solid. The compound was used without further purification.

^{1}H-NMR (400 MHz, Acetone-D$_6$): δ = 6.28 (s, 1H, NH), 4.27 (d, J = 4.8 Hz, 1H, C$\underline{H}$NHBoc), 2.47-2.36 (m, 2H, CH$_2$CF$_3$, C$\underline{H}$CH$_3$), 2.31-2.18 (m, 1H, CH$_2$CF$_3$), 1.41 (s, 9H, COOC(C$\underline{H}_3$)$_2$), 1.12 (d, J = 6.8 Hz, 3H, CH$_3$).
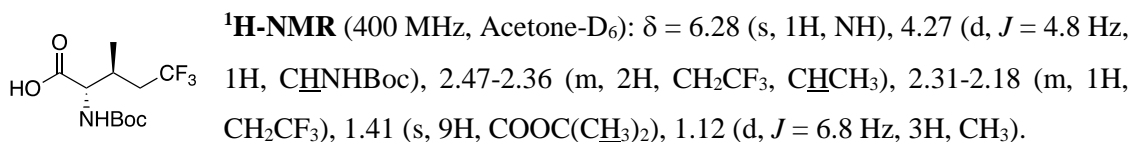
MS (-ESI, ACN/H$_2$O, setting **C**): m/z = 284.1124 obs. [M - H]$^-$ calcd. 284.1115, 591.2131 obs. [2M - 2H + Na]$^-$ calcd. 591.2123.

The presented spectroscopic data are consistent with literature.[135]

7.2.2 Fmoc protection of *N*-Boc protected amino acids

Boc deprotection and Fmoc protection was performed according to the following general procedure using argon atmosphere:

The *N*-Boc protected amino acid was dissolved in a 1:1 mixture of DCM/TFA and stirred at rt for 3 h. The solvent was then removed *in vacuo*. The remaining residue was dissolved in 10% aq. Na$_2$CO$_3$ and dioxane and 1.1 eq. Fmoc-OSu were added at 0°C. The mixture was stirred for 1 h at 0°C, then allowed to warm to rt and stirred overnight. The reaction was quenched by the addition of water (30 mL) and washed with diethyl ether (1×50 mL). The aqueous layer was acidified with HCl to pH = 2 and extracted with DCM (4×50 mL). The combined organic layers were dried over sodium sulfate, filtered and concentrated *in vacuo*. The crude product was dissolved in ACN + 0.1% (v/v) TFA, and purified by reversed-phase preparative HPLC on a LaPrepΣ low-pressure HPLC system (Section 7.1.3). Linear ACN/H$_2$O gradients containing 0.1% (v/v) TFA according to method **P1** for 4^3-F$_3$Val, and method **P2** (see Table 7.1) for 5^3-F$_3$Ile, and 5^5,$5'^3$-F$_6$Leu were applied. UV-detection occurred at 280 nm. For 4^3-F$_3$Val the Luna® C8(2) column, and for 5^3-F$_3$Ile, as well as 5^5,$5'^3$-F$_6$Leu, the Kinetex® C18 RP-HPLC-column was used. Before injection the solution of crude *N*-Fmoc protected amino acid was filtered over 0.45 µm Acrodisc® syringe filters with GHP membrane (Pall Corporation, Port Washington, NY, USA) Around 60-80 mg of the crude Fmoc-amino acid in maximal 4.0 mL ACN + 0.1% (v/v) TFA were injected per run. Collected fractions were checked *via* analytical HPLC on the semi-micro Chromaster system (Section 7.1.4) using method **A1** (see Table 7.2). Fractions containing pure product were combined, ACN was removed *in vacuo*, and the aqueous residue was freeze-dried to give the pure *N*-Fmoc protected amino acids. Identification was carried out by ESI-ToF MS according to setting **B** for 4^3-F$_3$Val, and C for 5^3-F$_3$Ile, and 5^5,$5'^3$-F$_6$Leu (see Section 7.1.6, Table 7.6) and NMR spectroscopy.

7.2.2.1 (2S,3S)-2-((((9H-fluoren-9-yl)methoxy)carbonyl)amino)-5,5,5-trifluoro-3-methyl-pentanoic acid (Fmoc-5³-F₃Ile)

According to the general procedure described above, Boc-5³-F₃Ile (152 mg, 0.533 mmol, 1.00 eq) was stirred in 1:1 DCM/TFA (6.0 mL) for 3 h at rt. The solvent was removed *in vacuo*, and 10% aq. Na₂CO₃ (2.5 mL) and dioxane (1.0 mL) were used to dissolve the residue. Fmoc-OSu (197 mg, 0.584 mmol, 1.10 eq.) was added and the mixture was stirred overnight. Subsequent workup, and purification gave 184 mg (0.452 mmol, 85%) Fmoc-5³-F₃Ile as white solid.
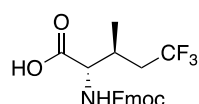
Obtained spectroscopic data (^{1}H-, ^{13}C-. ^{19}F-NMR) are consistent with literature.[135]

MS (-ESI, ACN/H₂O): *m/z* = 406.1246 obs. [M - H]⁻ calcd. 406.1272, 813.2581 obs. [2M - H]⁻ calcd. 813.2616.

MS (+ESI, ACN/H₂O): *m/z* = 430.1255 obs. [M +Na]⁺ calcd. 430.1237, 446.0991 obs. [M + K]⁺ calcd. 446.0976.

HPLC (LaChrom ELITE® system, Kinetex® C18 column, method **A9**): rt = 15.160 min

7.2.2.2 (S)-2-((((9H-fluoren-9-yl)methoxy)carbonyl)amino)-5,5,5-trifluoro-4-(trifluoro-methyl)-pentanoic acid (Fmoc-5³,5'³-F₆Leu)

Corresponding to the general procedure given in Section 7.2.2, *N*-Boc protected 5³,5'³-F₆Leu (80.0 mg, 0.236 mmol, 1.00 eq) was stirred for 3 h at rt in DCM/TFA (2.0 mL/2.0 mL). The solvent was removed under reduced pressure, and the residue dissolved in 10% aq. Na₂CO₃ (2.0 mL) and dioxane (1.0 mL). Fmoc-OSu (87.7 mg, 0.260 mmol, 1.10 eq) was added and the mixture was stirred overnight. After workup, and purification 70.3 mg (0.152 mmol, 64%) Fmoc-5³,5'³-F₆Leu were obtained as white solid.
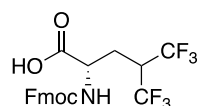
Spectroscopic data of ^{1}H-, ^{13}C-, and ^{19}F-NMR measurements are in accordance with literature.[135, 273-274]

MS (-ESI, ACN/H₂O): *m/z* = 460.1047 obs. [M - H]⁻ calcd. 460.0989, 921.2095 obs. [2M - H]⁻ calcd. 921.2051, 1382.3048 obs. [3M - H]⁻ calcd. 1382.3113.

HPLC (LaChrom ELITE® system, Kinetex® C18 column, method **A10**): rt = 14.893 min

7.2.2.3 (2S,3S)-2-((((9H-fluoren-9-yl)methoxy)carbonyl)amino)-4,4,4-trifluoro-3-methyl-butanoic acid (Fmoc-(3S)-4³-F₃Val)

Following the described general procedure, Boc-(2S,3S)-4³-F₃Val (150 mg, 0.553 mmol, 1.00 eq.) was stirred in 1:1 DCM/TFA (6.0 mL) for 3 h at rt before the solvents was removed *in vacuo*. The resulting residue was dissolved in 10% aq. Na₂CO₃ (5.0 mL) and dioxane (1.0 mL), cooled to 0°C, and Fmoc-OSu (205 mg, 0.608 mmol, 1.10 eq.) was added. After stirring of the reaction mixture, subsequent workup and purification, 92.3 mg (0.235 mmol, 43%) of *N*-Fmoc protected amino acid was obtained as white solid.
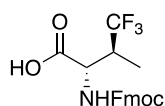
^{1}H, ^{13}C, and ^{19}F-NMR spectroscopic data are consistent with literature.[270]

MS (-ESI, ACN/H$_2$O): m/z = 392.1218 obs. [M - H]$^-$ calcd. 392.1115, 785.2545 obs. [2M - H]$^-$ calcd. 785.2303.

HPLC (LaChrom ELITE® system, Luna® C8(2) column, method **A10**): rt = 15.120 min

7.2.2.4 (2*S*,3*R*)-2-(((9*H*-fluoren-9-yl)methoxy)carbonyl)amino)-4,4,4-trifluoro-3-methyl-butanoic acid (Fmoc-(3*R*)-4^3-F$_3$Val)

According to the general procedure, Boc-(2*S*,3*R*)-4^3-F$_3$Val (150 mg, 0.553 mmol, 1.00 eq.) was stirred in DCM/TFA (3.0 mL/3.0 mL) at rt for 3 h. The solvent was removed *in vacuo*, and the remaining residue was cooled with ice and dissolved in 10% aq. Na$_2$CO$_3$ (5.0 mL). Dioxane (1.0 mL) and Fmoc-OSu (205 mg, 0.608 mmol, 1.10 eq) were added, and the reaction mixture was stirred over night at rt. Workup and purification gave 148 mg (0.376 mmol, 68%) of the corresponding *N*-Fmoc protected amino acid as white solid.
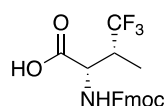
Obtained ^{1}H, ^{13}C, and ^{19}F-NMR spectra are in accordance with literature.[270]

MS (-ESI, ACN/H$_2$O): m/z = 392.1401 obs. [M - H]$^-$ calcd. 392.1115, 785.2678 obs. [2M - H]$^-$ calcd. 785.2303.

HPLC (LaChrom ELITE® system, Luna® C8(2) column, method **A10**): rt = 15.147 min

7.2.3 Fmoc-5^3,5'^{3}-F$_6$Leu from ethyl (*S*)-2-((((9*H*-fluoren-9-yl)methoxy)carbonyl)-amino)-5,5,5-trifluoro-4-(trifluoromethyl)-pentanoate (Fmoc-5^3,5'^{3}-F$_6$Leu-OEt)

Fmoc-5^3,5'^{3}-F$_6$Leu-OEt (300 mg, 0.613 mmol, 1.00 eq) was dissolved in conc. HCl (12 mL) and dioxane (12 mL) and stirred at rt for 7 days. The crude product was lyophilized and purified as described in Section 7.2.2. Before injection, the pH of the solution of the crude product in ACN + 0.1% (v/v) TFA was adjusted to ≈ 5 with 1 M NaOH. 264 mg (0.572 mmol, 93%) of pure Fmoc-5^3,5'^{3}-F$_6$Leu were obtained as white powder.
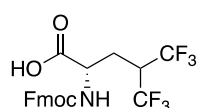
^{1}H, ^{13}C, and ^{19}F-NMR data are consistent with literature.[135, 273-274]

MS (-ESI, ACN/H$_2$O): m/z = 460.0980 obs. [M - H]$^-$ calcd. 460.0989, 574.0904 obs. [M - H + TFA]$^-$ calcd. 574.0918, 596.0726 obs. [M - 2H + TFA + Na]$^-$ calcd. 596.0737, 921.2031 obs. [2M - H]$^-$ calcd. 921.2051.

MS (+ESI, ACN/H$_2$O): m/z = 484.0876 obs. [M + Na]$^+$ calcd. 484.0954, 506.0693 obs. [M + 2Na]$^+$ calcd. 506.0773.

HPLC (LaChrom ELITE® system, Kinetex® C18 column, method **A9**): rt = 15.653 min

7.2.4 (*S*)-2-(((((9*H*-fluoren-9-yl)methoxy)carbonyl)amino)-4,4-difluorobutanoic acid (Fmoc-DfeGly)

Purification of crude Fmoc-DfeGly occurred on a LaPrepΣ low-pressure HPLC system (Section 7.1.3) equipped with the Kinetex® C18 RP-HPLC-column using method **P2** (UV detection at 280 nm, Table 7.1). The crude amino acid was dissolved in ACN + 0.1% (v/v) TFA (80.0 mg in 4.0 mL per HPLC run) and filtered (0.45 µm Acrodisc® syringe filters with GHP membrane, Pall Corporation, Port Washington, NY, USA) before injection. Collected fractions were checked with the semi-micro Chromaster HPLC system (Section 7.1.4) using method **A1** (see Table 7.2). Fractions containing pure product were combined, ACN was removed in vacuo, and the aqueous residue was freeze-dried to yield 494 mg (1.37 mmol) of pure Fmoc-DfeGly as white powder. Identification was carried out by ESI-ToF MS according to setting **B** (Section 7.1.6, Table 7.6) and NMR spectroscopy.
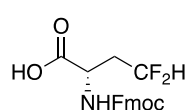
Obtained ^{1}H, ^{13}C, and ^{19}F-NMR spectra are in accordance with literature.[358]

MS (-ESI, ACN/H$_2$O): m/z = 360.1077 obs. [M - H]$^-$ calcd. 360.1053, 721.2191 obs. [2M - H]$^-$ calcd. 721.2179.

HPLC (Chromaster system, Kinetex® C18 column, method **A5**): rt = 11.370 min

7.3 Synthesis of a hetero-tetrameric linker for a SPR assay

7.3.1 *tert*-butyl 1-hydroxy-3,6,9,12-tetraoxapentadecan-15-oate 3[342]

To a solution of tetraethylene glycol **1** (25.0 mL, 145 mmol, 2.85 eq.) in anhydrous THF (100 mL) were added sodium pieces (33.3 mg; 1.45 mmol, 1 mol%) 34.5 mg). After this was completely dissolved, *tert*-butyl acrylate **2** was added (7.39 mL, 50.9 mmol, 1.00 eq.) and the solution was stirred for 20 h. 1 M HCl (~ 1.50 mL) was used to neutralize the reaction mixture and excess solvent was removed *in vacuo* to give a yellow oil. The residue was resuspended in brine (~ 50.0 mL) and extracted with ethyl acetate (3 × 50.0 mL). The combined organic layers were washed with brine (1 × 20.0 mL), then with water (1 × 20.0 mL), and finally dried over sodium sulfate. The solvent was removed under reduced pressure and the crude product was purified by flash column chromatography (SiO$_2$, DCM : MeOH 98:2) to yield 4.18 g (13.0 mmol, 26%) of **3** as light yellow oil.
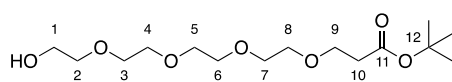
^{1}**H-NMR** (400 MHz, CDCl$_3$): δ = 3.77-3.43 (m, 18H, -C$\underline{H}_2$-O-), 2.82 (s, 1H, -O$\underline{H}$), 2.46 (t, *J* = 6.6 Hz, 2H, -C$\underline{H}_2$-COO^{t}Bu), 1.40 (s, 9H, -C(C$\underline{H}_3$)$_3$).

^{13}**C-NMR** (101 MHz, CDCl$_3$): δ = 170.95 (C-11), 80.55 (C-12), 72.60 (C-2), 70.65, 70.60, 70.53, 70.40, 70.38 (C-3 - C-8), 66.93 (C-9), 61.74 (C-1), 36.28 (C-10), 28.13 (-C(C$\underline{H}_3$)$_3$).

Obtained ^{1}H- and ^{13}C-NMR spectra are consistent with literature.[361]

7.3.2 *tert*-butyl 1-(tosyloxy)-3,6,9,12-tetraoxapentadecan-15-oate 4[343]

tert-butyl 1-hydroxy-3,6,9,12-tetraoxapentadecan-15-oate **3** (1.00 g, 3.10 mmol, 1.00 eq.) was dissolved in ACN (10.0 mL) and triethylamine (0.516 mL, 3.72 mmol, 1.20 eq.) was added at 0°C. Tosylchloride **12** (0.709 g; 3.72 mmol; 1.2 eq.) dissolved in ACN (10.0 ml) was slowly added over a time period of 30 min at 0°C. The mixture was then allowed to warm to room temperature and stirred overnight. The solvent was removed *in vacuo* and the residue redissolved in ethyl acetate (10.0 mL). The resulting precipitate was filtered off, and the filtrate was concentrated *in vacuo*. Purification by flash column chromatography over silica (5% ethyl acetate in hexane, followed by neat ethyl acetate) gave 1.06 g (2.22 mmol, 72%) of **4** as light yellow oil.
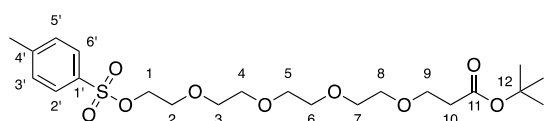
¹H-NMR (400 MHz, CDCl₃): δ = 7.75 (d, *J* = 8.2 Hz, 2H, H-2', H-6'), 7.30 (d, *J* = 8.2 Hz, 2H, H-5', H-3'), 4.12 (t, *J* = 6.0 Hz, 2H, H-1), 3.68-3.63 (m, 4H, H-2, H-9), 3.58-3.54 (m, 12H, H-3–H-8), 2.45 (t, *J* = 6.5 Hz, 2H, H-10), 2.41 (s, 3H, -CH₃), 1.40 (s, 9H, -C(CH₃)₃).

¹³C-NMR (101 MHz, CDCl₃): δ =170.90 (C-11), 144.81 (C-4'), 133.07 (C-1'), 129.86 (C-3', C-5'), 127.99 (C-2', C-6'), 80.49 (C-12), 70.75, 70.63, 70.59, 70.54, 70.51, 70.38 (C-3 – C-8), 69.28 (C-2), 68.69 (C-9), 66.91 (C-1), 36.30 (C-10), 28.12 (-C(CH₃)₃), 21.65 (-CH₃).

The NMR data are in agreement with the literature.[343]

7.3.3 3,3'-((2-amino-2-((2-cyanoethoxy)methyl)propane-1,3-diyl)bis(oxy))-di-propanenitrile 26[345]

Tris(hydroxymethyl)aminomethane **13** (2.00 g, 16.5 mmol, 1.00 eq.) was dissolved in dioxane (4.00 mL) and aq. KOH (100 mg, 1.78 mmol, ~ 10 mol%, in 0.50 mL H₂O) was added. The reaction mixture was stirred for 10 min and cooled to 0°C. Acrylonitrile **25** (3.46 mL, 52.8 mmol, 3.20 eq.) was added and the reaction solution stirred overnight at room temperature. The solvent was removed *in vacuo* and the yellow residue redissolved in CH₂Cl₂ (20.0 mL). After washing with water (3× 20.0 mL), the organic layer was dried over sodium sulfate and the solvent was removed under reduced pressure. Flash column chromatography (SiO₂, MeOH : DCM 1:10) yielded 1.53 g (5.46 mmol, 33%) of **26** as yellow oil.
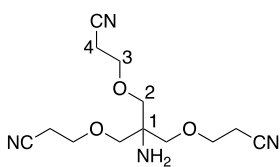
¹H-NMR (400 MHz, CDCl₃): δ = 3.65 (t, *J* = 6.0 Hz, 6H, H-3), 3.40 (s, 6H, H-2), 2.58 (t, *J* = 6.0 Hz, 6H, H-4), 1.64 (br s, 2H, -NH₂).

¹³C-NMR (101 MHz, CDCl₃): δ =118.07 (CN), 72.49 (C-2), 65.73 (C-3), 56.08 (C-1), 18.81 (C-4).

MS (+ESI, MeOH, setting **B**): *m/z* = 281.1621 obs. [M + H]⁺ calcd. 281.1608, 303.1437 obs. [M + Na]⁺ calcd. 303.1428.

Obtained NMR data are consistent with literature.[336, 345-346]

7.3.4 3,3'-((2-amino-2-((2-carboxyethoxy)methyl)propane-1,3-diyl)bis(oxy))di-propionic acid 27[346]

Above cyano derivative **26** (1.30 g, 4.64 mmol, 1.00 eq) was refluxed for 4 h in conc. HCl (4.00 mL). The mixture was allowed to cool to room temperature and water (20.0 ml) was added. The water was removed by lyophilization and 1.60 g (4.74 mmol, quant.) of **27** was obtained as colorless viscous oil that was used without further purification.
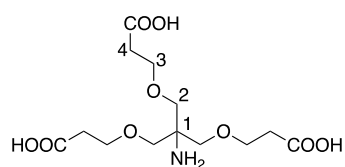
1H-NMR (400 MHz, DMSO-D$_6$): δ = 8.09 (br s, 2H, -NH$_2$), 3.58 (t, J = 6.3 Hz, 6H, H-3), 3.42 (s, 6H, H-2), 2.44 (t, J = 6.3 Hz, 6H, H-4).

13C-NMR (101 MHz, DMSO-D$_6$): δ =173.13 (COOH), 75.38 (C-2), 67.51 (C-3), 59.39 (C-1), 34.82 (C-4).

MS (-ESI, MeOH, setting **B**): m/z = 366.1363 obs. [M - H]$^-$ calcd. 336.1300.

1H-, and 13C-NMR data are in accordance with literature.[346]

7.3.5 Di-*tert*-butyl 3,3'-((2-amino-2-((3-(*tert*-butoxy)-3-oxopropoxy)methyl)-propane-1,3-diyl)bis(oxy))dipropionate 28[335]

Tris(hydroxymethyl)aminomethane **13** (1.21 g, 10.0 mmol, 1.00 eq.) was dissolved in DMSO (2.00 mL) and cooled to 15°C. 5 M NaOH (200 µL) was added and afterwards *tert*-butylacrylate **2** (4.94 mL; 34.0 mmol, 3.40 eq.) was added dropwise under stirring. The reaction mixture was allowed to warm to room temperature and left stirring overnight. The solvent was removed under high vacuum applying gentle heat (40°C). Purification *via* flash column chromatography (SiO$_2$, ethyl acetate : hexane 2:1 to 100% ethyl acetate) gave 1.89 g (3.74 mmol, 37%) of **28** as yellow oil.
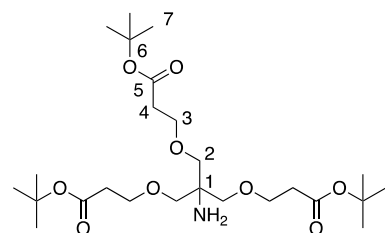
1H-NMR (400 MHz, CDCl$_3$): δ = 3.62 (t, J = 6.4 Hz, 6H, H-3), 3.29 (s, 6H, H-2), 2.43 (t, J = 6.4 Hz, 6H, H-4), 1.42 (s, 27H, -C(CH$_3$)$_3$).

13C-NMR (101 MHz, CDCl$_3$): δ = 171.04 (C-5), 80.53 (C-6), 72.91 (C-2), 67.22 (C-3), 56.08 (C-1), 36.41 (C-4), 28.20 (C-7).

MS (+ESI, MeOH, setting **B**): m/z = 506.3371 obs. [M + H]$^+$ calcd. 506.3324, 1011.6608 obs. [2M + H]$^+$ calcd. 1011.6574.

Obtained spectroscopic data are comparable to literature.[335, 362]

7.3.6 di-*tert*-butyl 3,3'-((2-(((((9*H*-fluoren-9-yl)methoxy)carbonyl)amino)-2-((3-(*tert*-butoxy)-3-oxopropoxy)methyl)propane-1,3-diyl)bis(oxy))dipropionate 29 [339]

28 (100 mg, 0.198 mmol, 1.00 eq.) was dissolved in DCM and 20% Na_2CO_3 (2.5:1, 3.00 mL). Fmoc-Cl (154 mg, 0.594 mmol, 3.00 eq.), dissolved in DCM (0.5 mL), was added dropwise under stirring, and the mixture was kept stirred overnight. DCM was removed *in vacuo* and the aqueous layer was dried *via* lyophilization. Purification occurred on a LaPrepΣ low-pressure HPLC system (Section 7.1.3) equipped with the Kinetex® C18 RP-HPLC-column using method **P3** (UV detection at 280 nm, Table 7.1). The crude compound was dissolved in 1:1 H_2O: ACN, both containing 0.1% (v/v) TFA, (100 mg in 5.0 mL per HPLC run) and filtered over a 0.45 µm Acrodisc® syringe filter (GHP membrane, Pall Corporation, Port Washington, NY, USA) before injection. Collected fractions were checked with the semi-micro Chromaster HPLC system (Chapter 7.1.4) using method **A2** (Table 7.2). Fractions containing pure product were combined, ACN was removed *in vacuo*, and the aqueous residue was freeze-dried to yield 88.0 mg (0.121 mmol, 61%) of **29** as colorless oil.
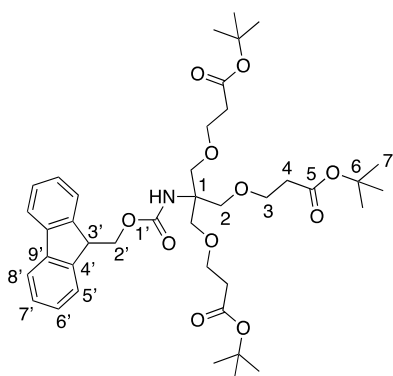
^{1}H-NMR (400 MHz, CDCl$_3$): δ = 7.76 (d, *J* = 7.5 Hz, 2H, H-8'), 7.62 (d, *J* = 7.4 Hz, 2H, H-5'), 7.39 (t, *J* = 7.4 Hz, 2H, H-7'), 7.31 (t, *J* = 7.4 Hz, 2H, H-6'), 5.38 (br s, 1H, NH), 4.37-4.22 (br m, 2H, H-2'), 4.20 (t, *J* = 6.8 Hz, 1H, H-3'), 3.82-3.54 (br m, 12H, H-3, H-2), 2.60-2.35 (br m, 6H, H-4), 1.44 (s, 27H, -C(C$\underline{H}_3$)$_3$).

^{13}C-NMR (101 MHz, CDCl$_3$): δ = 170.97 (C-5), 144.22 (C-4'), 141.37 (C-9'), 127.71 (C-6'), 127.17 (C-7'), 125.30 (C-5'), 120.01 (C-8'), 80.57 (C-6), 70.83 (C-2'), 69.43 (C-2), 67.17 (C-3), 58.90 (C-1), 47.33 (C-3'), 36.33 (C-4), 28.21 (C-7)).

MS (+ESI, DCM/MeOH, setting **B**): *m/z* = 728.4031 obs. [M + H]$^+$ calcd. 728.4004, 750.3863 obs. [M + Na]$^+$ calcd. 750.3824, 766.3599 obs. [M + K]$^+$ calcd. 766.3563.

HPLC (LaChrom ELITE® system, Kinetex® C18 column, method **A11**): rt = 23.013 min
Spectroscopic data comparable to literature.[339]

7.3.7 3,3'-((2-(((((9*H*-fluoren-9-yl)methoxy)carbonyl)amino)-2-((2-carboxyethoxy)-methyl)propane-1,3-diyl)bis(oxy))dipropionic acid 20

FmocTrisCOO^{t}Bu **29** (88.0 mg, 0.121 mmol, 1.00 eq.) was stirred for 3 h in 1:1 DCM:TFA (6.00 mL) at room temperature. The solvent was removed *in vacuo* to obtain 70.7 mg of **20** (0.126 mmol, quant.) as light yellow oil. The product was used without further purification.
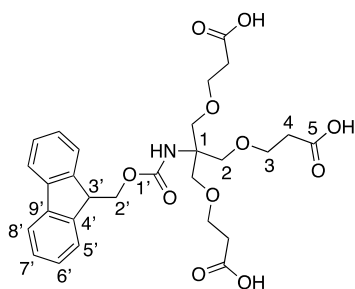
^{1}H-NMR (500 MHz, CDCl$_3$): δ = 7.75 (d, *J* = 7.5 Hz, 2H, H-8'), 7.58 (d, *J* = 7.4 Hz, 2H, H-5'), 7.38 (t, *J* = 7.4 Hz, 2H, H-7'), 7.31 (t, *J* = 7.4 Hz, 2H, H-6'), 4.39-4.26 (br m, 2H, H-2'), 4.21 (t, *J* = 5.7 Hz, 1H, H-3'), 3.77-3.55 (br m, 10H, H-aliph.), 2.60-2.41 (br m, 8H, H-aliph.).

^{13}C-NMR (126 MHz, CDCl$_3$): δ = 144.14 (C-5), 141.63 (C-arom.), 141.50 (C-arom.), 127.85 (C-arom.), 127.28 (C-arom.), 120.46 (C-arom.), 120.14 (C-arom.), 69.59 (C-2), 66.57 (C-3), 58.86 (C-2'), 47.27 (C-3'), 34.89 (C-4).

MS (+ESI, ACN, setting **B**): *m/z* = 560.2151 obs. [M + H]$^+$ calcd. 560.2126, 582.1971 obs. [M + Na]$^+$ calcd. 582.1946, 598.1688 obs. [M + K]$^+$ calcd. 598.1685, 1119.4211 [2M + H]$^+$ calcd. 1119.4180, 1141.4043 obs. [2M + Na]$^+$ calcd. 1141.3999, 1157.3746 obs. [2M + K]$^+$ calcd. 1157.3739.

MS (-ESI, ACN, setting **B**): *m/z* = 558.2112 obs. [M - H]$^-$ calcd. 558.1981, 672.2057 obs. [M - H + TFA]$^-$ calcd. 672.1909, 1117.4249 obs. [2M - H]$^-$ calcd. 1117.4034.

HPLC (LaChrom ELITE® system, Kinetex® C18 column, method **A11**): rt = 14.260 min

7.3.8 NHS-activation of FmocTrisCOOH 20 (31)

FmocTrisCOOH **20** (10.0 mg, 0.018 mmol, 1.00 eq.) and *N,N'*-Disuccinimidyl carbonate (DSC) **30** (41.5 mg, 0.162 mmol, 9.00 eq.) were dissolved in a 1:1 mixture of THF:ACN (4.00 mL) and freshly distilled triethylamine (37.6 µL, 0.270 mmol, 15.00 eq.) was added. The mixture was stirred at room temperature, and the reaction progress was followed by RP-HPLC (LaChrom ELITE® system, Kinetex® C18 column, method A11). After 1 h the solvent was removed under reduced pressure. Purification occurred on a LaPrepΣ low-pressure HPLC system (Section 7.1.3) using the Kinetex® C18 RP-HPLC-column, and method **P3** with UV detection at 280 nm (Table 7.1). The crude compound was dissolved in 3.0 mL 1:1 H$_2$O:ACN, both containing 0.1% (v/v) TFA, and filtered over a 0.45 µm Acrodisc® syringe filter (GHP membrane, Pall Corporation, Port Washington, NY, USA) before injection. Collected fractions were checked with the semi-micro Chromaster HPLC system (Chapter 7.1.4) using method **A2** (Table 7.2). Fractions containing pure product were combined, ACN was removed *in vacuo*, and the aqueous residue was freeze-dried to give 10.5 mg (0.012 mmol, 67%) of **31** as white solid.
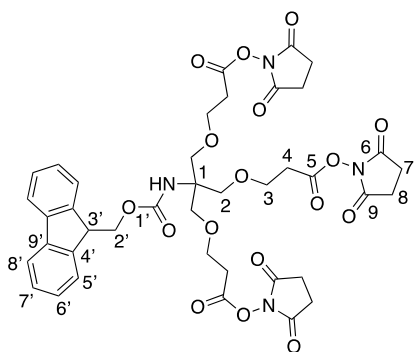
¹H-NMR (500 MHz, CDCl₃): δ = 7.76 (d, *J* = 7.4 Hz, 2H, H-8'), 7.64 (d, *J* = 7.5 Hz, 2H, H-5'), 7.39 (t, *J* = 7.4 Hz, 2H, H-7'), 7.31 (t, *J* = 7.5 Hz, 2H, H-6'), 4.38-4.22 (br m, 2H, H-2'), 4.21 (t, *J* = 6.8 Hz, 1H, H-3'), 3.89-3.65 (br m, 12H, H-3, H-2), 2.88-2.82 (m, 6H, H-4), 2.81-2.75 (m, 12H, H-7, H-8).

¹³C-NMR (126 MHz, CDCl₃): δ = 169.21 (C-6, C-9), 167.02 (C-5), 144.37 (C-1'), 134.44 (C-arom.), 133.98 (C-arom.), 127.79 (C-arom.), 127.75 (C-arom.), 120.77 (C-arom.), 120.06 (C-arom.), 69.25 (C-2), 65.87 (C-3), 47.41 (C-2'), 32.25 (C-4), 25.73 (C-7, C-8).

MS (+ESI, DCM/MeOH, setting **B**): *m/z* = 851.2660 obs. [M + H]⁺ calcd. 851.2618, 1701.5212 obs. [2M + H]⁺ calcd. 1701.5163.

HPLC (LaChrom ELITE® system, Kinetex® C18 column, method **A11**): rt = 17.387 min

7.3.9 Thioester-activation of FmocTrisCOOH 20 (39)

FmocTrisCOOH **20** (10.0 mg, 0.018 mmol, 1.00 eq.), *p*-acetamidothiophenol **38** (45.2 mg, 0.270 mmol, 15.0 eq.) and PyBOP (140.5 mg, 0.270 mmol, 15.00 eq.) were dissolved in 1.00 mL DCM. DIPEA (44.6 µL, 0.270 mmol, 15.0 eq.) was added, and the mixture was stirred at room temperature for 6 h. After the solvent was removed *in vacuo*, the crude mixture was purified by RP-HPLC using the LaPrepΣ low-pressure system (Chapter 7.1.3). The Kinetex® C18 RP-HPLC-column was used while applying method **P3** (Table 7.1). UV detection occurred at 260 nm. Therefore, the crude residue was dissolved in 3.0 mL 2:1 ACN:H₂O, both containing 0.1% (v/v) TFA, and filtered over a 0.45 µm Acrodisc® syringe filter (GHP membrane, Pall Corporation, Port Washington, NY, USA) before injection. Collected fractions were checked with the semi-micro Chromaster HPLC system (Section 7.1.4) using method **A2** (Table 7.2). Fractions containing pure product were combined, ACN was removed *in vacuo*, and the aqueous residue was freeze-dried to give 5.1 mg (0.005 mmol, 28%) of **39** as white solid.
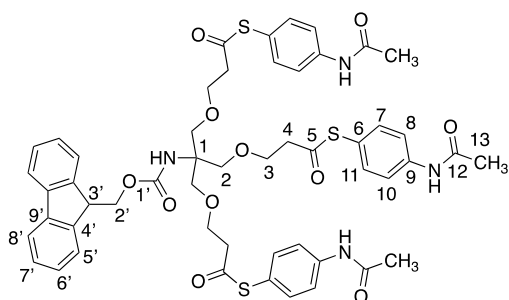
¹H-NMR (500 MHz, CDCl₃): δ = 7.84-7-70 (m, 6H, H-arom.), 7.58-7.48 (m, 2H, H-arom.(Fmoc)), 7.48-7.40 (m, 4H, H-arom.(Fmoc)), 7.40-7.35 (m, 2H, H-arom.(Fmoc)), 7.35-7.23 (m, 6H, H-arom.) 4.32-3.96 (br m, 7H, H-aliph.), 3.82-3.60 (br m, 9H, H-aliph.), 2.93-2.72 (m, 5H, H-aliph.), 2.15 (s, 9H, -CH₃).

A ¹³C-NMR spectrum could not be analyzed, presumably due to the low concentration of the sample measured. Although the measurement was performed for 14 h (25000 scans) no reasonable intensity was obtained.

MS (+ESI, H$_2$O/ACN, setting **B**): m/z = 1007.3023 obs. [M + H]$^+$ calcd. 1007.3024, 1029.2809 obs. [M + Na]$^+$ calcd. 1029.2843, 1045.2571 obs. [M + K]$^+$ calcd. 1045.2583.

HPLC (Chromaster system, Kinetex® C18 column, method **A6**): rt = 16.953 min

7.4   Solid phase peptide synthesis

All peptides were synthesized from the *C*-terminal to the *N*-terminal end on solid phase according to standard Fmoc/^{t}Bu protecting group strategy.[363] If not stated otherwise, synthesis occurred in 0.05 mmol scale.

The following protected derivatives of the standard canonical amino acids were used: Fmoc-L-Ala-OH × H$_2$O, Fmoc-L-Arg(Pbf)-OH, Fmoc-L-Asn(Trt)-OH, Fmoc-L-Asp(O^{t}Bu)-OH, Fmoc-L-Cys(Trt)-OH, Fmoc-L-Gln(Trt)-OH, Fmoc-L-Glu(O^{t}Bu)-OH × H$_2$O, Fmoc-Gly-OH, Fmoc-L-His(Trt)-OH, Fmoc-L-Ile-OH, Fmoc-L-Leu-OH, Fmoc-L-Lys(Boc)-OH, Fmoc-L-Met-OH, Fmoc-L-Phe-OH, Fmoc-L-Ser(^{t}Bu)-OH, Fmoc-L-Thr(^{t}Bu)-OH, Fmoc-L-Trp(Boc)-OH, Fmoc-L-Tyr(^{t}Bu)-OH, Fmoc-L-Val-OH.

The following pseudoproline dipeptides, PEGylation agents and non-natural building blocks were used for the synthesis: Fmoc-L-Tyr(^{t}Bu)-L-Thr[PSI(Me,Me)Pro]-OH, Fmoc-L-Leu-L-Thr[PSI(Me,Me)Pro]-OH, Fmoc-NH-PEG(4)-COOH, and Boc-2-Abz-OH.

The following fluorinated amino acids were used: Fmoc-(S)-DfeGly, Fmoc-($2S,3R$)-4^3-F$_3$Val, Fmoc-($2S,3S$)-4^3-F$_3$Val, Fmoc-(S)-5^3-F$_3$Ile, Fmoc-(S)-5^3,5'^{3}-F$_6$Leu (for synthesis see Chapter 7.2).

7.4.1   Loading of the resin

Gp41 peptides were synthesized on a NovaSyn®TGR-resin (loading capacity: 0.250 mmol/g), which had to be preloaded with the *C*-terminal amino acid Fmoc-L-Leu-OH in case of C34 and N36, and Fmoc-L-Gln(Trt)-OH for the C31 peptides and T21.

First the resin was swelled in DMF for 2 × 30 min (5.0 mL for 500 mg resin). Five equivalents of the amino acid were pre-activated with HOBt and DIC, each five equivalents, in DMF (4.0 mL per 500 mg resin) for 7 min and then added to the resin. After three hours the resin was washed with DMF, DCM and MeOH (each 3 × 5.0 mL) and dried *in vacuo*.

The loading of the resin was determined *via* UV-detection of the Fmoc protecting group according to the procedure of Gude *et al.*.[364] Approximately 30.0 mg of each loaded resin were swelled in 20.0 mL DMF for 30 min. Then 400 μL DBU were added and it was shaken for another 30 min. Subsequently, the reaction was quenched by adding ACN to a total volume of 100 mL. 2.0 mL of this solution were then diluted with ACN to a volume of 25.0 mL. With this solution, the UV-detection was carried out. The absorption was measured at 294 nm and 304 nm in 1 cm quartz glass cuvettes and performed in triplicate. The spectra were recorded with baseline

correction through a blank sample containing only the reference that was prepared in the same manner but without addition of the resin. The resin loading was calculated according to the following equations:[364]

$$\text{loading} \left[\text{mmol}/\text{g} \right]_{294\text{nm}} = \frac{\text{absorbance} \times 142.14}{m_{\text{resin}}[\text{mg}]} \qquad (7.1)$$

$$\text{loading} \left[\text{mmol}/\text{g} \right]_{304\text{nm}} = \frac{\text{absorbance} \times 163.96}{m_{\text{resin}}[\text{mg}]} \qquad (7.2)$$

For the Fmoc-L-Leu-OH loaded resin a loading of 0.250 mmol/g and for the Fmoc-L-Gln(Trt)-OH loaded resin a loading of 0.230 mmol/g was determined.

Potentially unreacted NH$_2$-groups on the resin surface were capped afterwards by treatment with a solution containing 10% acetic anhydride and 10% DIPEA in DMF (5.0 mL per 500 mg resin) three times for 10 min. The resin was then washed with DMF, DCM and MeOH (each 3×5.0 mL) and dried *in vacuo*.

7.4.2 Automated peptide synthesis

The peptides described in this thesis were almost completely synthesized *via* automated peptide synthesis.

Synthesis on a MultiSynTech Syro XP fully automated, parallel peptide synthesizer (MultiSynTech GmbH, Witten, Germany) occurred according to the protocol shown in Table 7.7. The coupling of the amino acids was carried out using TBTU/HOBt/DIPEA activation. Therefore, four or five equivalents of the corresponding amino acid, TBTU and HOBt, as well as eight or ten equivalents DIPEA in DMF were added to the resin. Furthermore, the coupling mixture contained sodium perchlorate (0.23 M) to prevent on-resin aggregation during synthesis. After 30 min to one hour, the resin was washed with 2.5 mL DMF and the coupling was repeated under the same conditions. Fmoc deprotection was achieved by treatment of the resin with 2% (v/v) piperidine and 2% (v/v) DBU in DMF, 20% (v/v) piperidine in DMF, or 20% (v/v) piperidine + 0.1 M HOBt in DMF (4×5 min) after washing three times with 2.5 mL DMF. Then the resin was washed six times with 2.5 mL DMF. Prior to the synthesis the resin was swelled two times in 2.5 mL DMF for 15 min.

Table 7.7: Protocol for the automated solid phase peptide synthesis with 0.05 mmol scale on a MultiSynTech Syro XP peptide synthesizer.

	process step	reagents	reaction time
Start	Swelling	2.5 mL DMF	2×15 min
	Fmoc-deprotection	2% piperidine, 2% DBU in DMF, 20% piperidine in DMF or 20% piperidine + 0.1 M HOBt in DMF	4×5 min
	Washing	2.5 mL DMF	6×1 min
Double coupling	Amino acid coupling	4 or 5 eq. Fmoc-X-OH and HOBt in DMF 4 or 5 eq. TBTU in DMF 8 or 10 eq. DIPEA in NMP	30 or 60 min
	Washing	2.5 mL DMF	1 min
	Amino acid coupling	4 or 5 eq. Fmoc-X-OH and HOBt in DMF 4 or 5 eq. TBTU in DMF 8 or 10 eq. DIPEA in NMP	30 or 60 min
	Washing	2.5 mL DMF	3×1 min
	Fmoc-deprotection	2% piperidine, 2% DBU in DMF, 20% piperidine in DMF or 20% piperidine + 0.1 M HOBt in DMF	4×5 min
	Washing	2.5 mL DMF	6×1 min

Synthesis was also performed on an Activo-P11 Automated Peptide Synthesizer (Activotec, Cambridge, United Kingdom) following the protocol given in Table 7.8. The coupling of the amino acids was carried out using HOAt/DIC activation. Therefore, 8 or 10 equivalents HOAt, 8 or 10 equivalents DIC and 8 or 10 equivalents of the corresponding amino acid in 1.6 mL DMF were added to the resin. Furthermore, the coupling solution contained sodium perchlorate (0.25 M) to prevent aggregation on the resin during synthesis. After 1-2 hours the coupling was repeated under the same conditions. After washing five times with 2.0 mL DMF, Fmoc deprotection was achieved by treatment of the resin with 2.0 mL of either 2% (v/v) piperidine and 2% (v/v) DBU in DMF, 20% (v/v) piperidine in DMF, or 20% (v/v) piperidine + 0.1 M HOBt in DMF for 2×5 min and 2×10 min, or 4×5 min. Then the resin was washed six times with 2.0 mL DMF. Prior to the synthesis the resin was swelled two times in 2.0 mL DMF for 15 min. At the end of the synthesis the resin was washed three times for 2 min with 2.0 mL of DCM.

Coupling steps were performed also *via* HATU/DIPEA activation (Table 7.9). Here, 5 eq. amino acid, 4.9 eq. HATU and 10 eq. DIPEA in 1.6 mL DMF were added to the resin. The coupling solution also contained 0.25 M NaClO$_4$ to prevent on-resin aggregation. This reaction step was performed two times for 45 min.

All coupling and deprotection steps were carried out at 40°C. Coupling of His-residues occurred at room temperature to avoid racemization, and for Met-residues the temperature was slightly reduced to 35°C. The washing steps were conducted at ambient temperature.

Table 7.8: Protocol for the automated solid phase peptide synthesis with 0.05 mmol scale on the Activo-P11 Automated Peptide Synthesizer using HOAt/DIC activation.

process step		reagents	reaction time
Start	Swelling	2.0 mL DMF	2 × 15 min
	Fmoc-deprotection	2.0 mL 2% piperidine, 2% DBU in DMF, 20% piperidine in DMF or 20% piperidine + 0.1 M HOBt in DMF	2 × 5 min + 2 × 10 min or 4 × 5min
	Washing	2.0 mL DMF	6 × 1 min
Double coupling	Amino acid coupling	8 or 10 eq. Fmoc-X-OH, 8 or 10 eq. HOAt and 8 or 10 eq. DIC in 1.6 mL DMF	2 × 1-2 h
	Washing	2.0 mL DMF	5 × 1 min
	Fmoc-deprotection	2.0 mL 2% piperidine, 2% DBU in DMF, 20% piperidine in DMF or 20% piperidine + 0.1 M HOBt in DMF	2 × 5 min + 2 × 10 min or 4 × 5min
	Washing	2.0 mL DMF	6 × 1 min

Table 7.9: Protocol for the automated solid phase peptide synthesis with 0.05 mmol scale on the Activo-P11 Automated Peptide Synthesizer using HATU/DIPEA activation.

process step		reagents	reaction time
Start	Swelling	2.0 mL DMF	2 × 15 min
	Fmoc-deprotection	2.0 mL 20% piperidine in DMF	4 × 5min
	Washing	2.0 mL DMF	6 × 1 min
Double coupling	Amino acid coupling	5 eq. Fmoc-X-OH, 4.9 eq. HATU and 10 eq. DIPEA in 1.6 mL DMF	2 × 45 min
	Washing	2.0 mL DMF	5 × 1 min
	Fmoc-deprotection	2.0 mL 20% piperidine in DMF	4 × 5min
	Washing	2.0 mL DMF	6 × 1 min

7.4.3 Manual peptide synthesis

Peptide synthesis carried out manually followed the procedure described in Table 7.10 using 10 mL polypropylene reactors. The reaction cycles started with the Fmoc deprotection. For this the resin was treated with a 2.0 mL mixture of 20% (v/v) piperidine in DMF three times for 7 min. After washing with DMF and DCM, each three times, the amino acid coupling was performed. Eight equivalents of the canonical *N*-Fmoc-protected amino acid were mixed with eight equivalents of DIC and HOAt in 2.0 mL DMF containing 0.4 M NaClO$_4$ and pre-activated for 7 min. Instead of HOAt, also HOBt can be used. The resulting mixture was added to the resin. After shaking for 60 min, the resin was washed once with 5 mL DMF and the coupling was repeated another time under the same conditions. Finally, the resin was washed with DCM and DMF. Prior to the synthesis the resin was swelled two times for 15 min in 5.0 mL DMF.

Table 7.10: Protocol for manual solid phase peptide synthesis (0.05 mmol scale). HOAt can also be replaced by HOBt

process step	reagents	reaction time
Swelling	5.0 mL DMF	2×15 min
Fmoc-deprotection	2.0 mL 20% piperidine DMF	3×7 min
Washing	5.0 mL DMF 5.0 mL DCM	3×1 min 3×1 min
Amino acid coupling	8 eq. Fmoc-X-OH, 8 eq. HOAt and 8 eq. DIC in 2.0 mL DMF	2×1 h
Washing	5.0 mL DMF 5.0 mL DCM	3×1 min 3×1 min

Coupling of fluorinated amino acids and other non-natural building blocks also occurred manually under the conditions that are described in the next section.

7.4.3.1 Coupling of non-natural building blocks, and *N*-terminal capping

Coupling of the fluorinated amino acids

Fluorinated amino acids as well as the first subsequent amino acid were activated by DIC/HOAt 1:1. For fluorine-containing residues a single coupling step was carried out with a molar excess of the amino acid and coupling reagents of 1.2-fold relative to the resin loading in 2.0 mL DMF containing 0.4 M $NaClO_4$. These couplings were performed for 12 h. If insufficient coupling was detected (test cleavage, see Section 7.6.1), another 0.5 eq. of amino acid and coupling reagents (DIC/HOAt) were added to the resin and shaken for 12 h. Prior to the Fmoc deprotection of the fluorinated amino acids possibly free *N*-termini were capped by adding a mixture of acetic anhydride (10% (v/v)) and DIPEA (10% (v/v)) in DMF (2.0 mL; 3×10 min). The resin was washed with DMF and DCM (3×5.0 mL each). The amino acid that is immediately following the fluorinated one was also coupled manually according to the protocol in Table 7.10 using 8-fold excess of amino acid and coupling reagents (DIC/HOAt).

Coupling of Pseudoproline Dipeptides

Coupling of pseudoproline dipeptide building blocks occurred manually with HCTU/DIPEA activation. 1.5 eq pseudoproline and 1.5 eq HCTU were dissolved in 2.0 mL DMF + 0.4 M $NaClO_4$, and 3.0 eq DIPEA were added. The mixture was added to the resin without pre-activation and then shaken for 12 h. Afterwards, the resin was washed with DMF and DCM (both 3×5.0 mL). If an incomplete coupling was observed, another 0.8 eq. pseudoproline together with 0.8 eq. HCTU and 1.6 eq. DIPEA in 2.0 mL DMF + 0.4 M $NaClO_4$ were added to the resin and shaken over-night. Free α-amino groups that have not reacted during the coupling reaction were then capped by treatment of the resin with 2.0 mL of a mixture of 10% (v/v) acetic anhydride and 10% (v/v) DIPEA in DMF three times for 10 min. After this, the resin was washed three times with each DMF and DCM.

Coupling of PEG(4)

PEGylation of peptides was usually performed on a 0.005 mmol scale. Coupling occurred with a 1.5-fold excess of FmocNH-PEG(4)-COOH and HCTU, as well as a three-fold excess of DIPEA in 0.5 mL of a 1:1 mixture of DMF:DCM for 2×12 h. Afterwards, the resin was washed with DMF and DCM (both 3×5.0 mL). To block free α-amino groups that have not reacted during the coupling reaction, the resin was treated with 1.0 mL of 10% (v/v) acetic anhydride and 10% (v/v) DIPEA in DMF three times for 10 min. After this, the resin was washed three times with each 2.0 mL of DMF and DCM.

Coupling of N-terminal Abz label

N-terminal labeling with *o*-aminobenzoic acid (Abz) was carried out manually using Boc-Abz-OH. Therefore, 5 eq. Boc-Abz-OH, 5eq. HOBt and 5 eq. DIC were dissolved in 2.0 mL DMF supplemented with 0.4 M $NaClO_4$, and after 7 min preactivation the mixture was added to the resin. The reaction was shaken for 1 h and repeated a second time under the same conditions. HOBt can also be replaced with HOAt. Afterwards, the resin was washed with DMF, DCM, and MeOH (3×5.0 mL each).

Capping

N-terminal capping was carried out by treatment of the resin with 2.0 mL of a mixture of 10% (v/v) acetic anhydride and 10% (v/v) DIPEA in DMF three times for 10 min. After this, the resin was washed three times with 5.0 mL of each DMF, DCM and MeOH.

The peptide sequences summarized in Table 7.11 were synthesized within the course of the present thesis. A detailed synthetic protocol for the peptides is given in the following sections.

Table 7.11: Names and sequences of peptides generated within the course of this study.

name	sequence
VPE	Abz-EVSALEKEVASLEKEVSALEKKVASLKKEVSALE-OH
VPK	Abz-KVSALKEKVASLKEKVSALKEEVASLEEKVSALK-OH
VPK-$5^3,5'^3$-F$_6$Leu$_{19}$	Abz-KVSALKEKVASLKEKVSA-$5^3,5'^3$-F$_6$Leu-KEEVASLEEKVSALK-OH
VPK-(3R)-4^3-F$_3$Val$_{16}$	Abz-KVSALKEKVASLKEK-(3R)-4^3-F$_3$Val-SALKEEVASLEEKVSALK-OH
VPK-(3S)-4^3-F$_3$Val$_{16}$	Abz-KVSALKEKVASLKEK-(3S)-4^3-F$_3$Val-SALKEEVASLEEKVSALK-OH
FA	Abz-KAAFAAAAK-OH
P2-IleFA	Abz-KAIleFAAAAK-OH
P2-5^3-F$_3$IleFA	Abz-KA-5^3-F$_3$Ile-FAAAAK-OH
P1'-IleFA	Abz-KAAFIleAAAK
P1'-5^3-F$_3$IleFA	Abz-KAAF-5^3-F$_3$Ile-AAAK
P2'-IleFA	Abz-KAAFAIleAAK
P2'-5^3-F$_3$IleFA	Abz-KAAFA-5^3-F$_3$Ile -AAK
C31	Ac-EQIWNNMTWMEWDREINNYTSLIHSLIEESQ-NH$_2$
C31-DfeGly	Ac-EQIWNNMTWMEWDRE-DfeGly-NNYTSLIHSLIEESQ-NH$_2$
C31-5^3-F$_3$Ile	Ac-EQIWNNMTWMEWDRE-5^3-F$_3$Ile-NNYTSLIHSLIEESQ-NH$_2$
C31-$5^3,5'^3$-F$_6$Leu	Ac-EQIWNNMTWMEWDRE-$5^3,5'^3$-F$_6$Leu-NNYTSLIHSLIEESQ-NH$_2$
C34	Ac-WMEWDREINNYTSLIHSLIEESQNQQEKNEQELL-NH$_2$
T21	Ac-NNLLRAIEAQQHLLQLTVWGIKQLQARILAVERYLKDQ-NH$_2$
N36	Ac-SGIVQQQNNLLRAIEAQQHLLQLTVWGIKQLQARIL-NH$_2$
N36-NH$_2$*	NH$_2$-SGIVQQQNNLLRAIEAQQHLLQLTVWGIKQLQARIL-NH$_2$
N36-PEG(4)*	NH$_2$-PEG(4)-SGIVQQQNNLLRAIEAQQHLLQLTVWGIKQLQARIL-NH$_2$
N36$_{TGT}$†	NH$_2$-SGIVQQQNNLLRAIEAQQHLLQLTVWGIKQLQARIL-NH$_2$
N36-PEG(4)$_{TGT}$†	NH$_2$-PEG(4)-SGIVQQQNNLLRAIEAQQHLLQLTVWGIKQLQARIL-NH$_2$
T21-PEG(4)*	NH$_2$-PEG(4)-NNLLRAIEAQQHLLQLTVWGIKQLQARILAVERYLKDQ-NH$_2$
T21-Cys	NH$_2$-CNNLLRAIEAQQHLLQLTVWGIKQLQARILAVERYLKDQ-NH$_2$
T21-PEG(4)-Cys	NH$_2$-C-PEG(4)-NNLLRAIEAQQHLLQLTVWGIKQLQARILAVERYLKDQ-NH$_2$

Abz: *o*-aminobenzoic acid

*These peptides were kept on resin for further reactions and thus used without purification.
†Synthesis on a NovaSyn®TGT resin gave fully protected peptides that were used without purification.

7.4.4 Synthesis of VPE/VPK

VPE, and VPK peptides were synthesized on Fmoc-L-Glu-(O^{t}Bu)- and Fmoc-L-Lys-(Boc)-NovaSyn®TGA resins (0.2 mmol/g or 0.23 mmol/g), respectively, using the Syro XP peptide synthesizer according to Table 7.7. Couplings occurred with a four-fold excess of amino acids and coupling reagents (TBTU/HOBt) as well as an eight-fold excess of DIPEA relative to the resin loading (2×30 min). Fluorinated amino acids as well as the first subsequent amino acid were coupled as described in Section 7.4.3. Fmoc deprotection was achieved by treatment with a mixture of piperidine (2% (v/v)) and DBU (2% (v/v)) in DMF. VPE and all VPK peptides were *N*-terminally labeled with *o*-aminobenzoic acid (Abz) to enable photometric concentration determination. Abz was coupled manually according to Section 7.4.3.

7.4.5 Synthesis of FA peptides

FA peptides were synthesized manually on a preloaded Fmoc-L-Lys(Boc)Wang resin (0.57 mmol/g loading). Couplings of non-fluorinated amino acids were performed as described in Section 7.4.3 using HOBt and DIC as activating agents. The fluorinated amino acid 5^3-F$_3$Ile was coupled according to the procedure described in Section 7.4.3. All peptides were *N*-terminally labeled with *o*-aminobenzoic acid (Abz) to enable photometric detection (see Section 7.4.3).

7.4.6 Synthesis of gp41-peptides

C31

The synthesis of the C31-peptides was carried on a NovaSyn®TGR-resin that was loaded with Fmoc-L-Glu(O^{t}Bu)-OH beforehand (loading 0.23 mmol/g, see Section 7.4.1).

The first part of the sequence (amino acid residues 21-31) was synthesized on the Syro XP instrument according to the standard protocol for the automated peptide synthesis in Table 7.7. 5eq. amino acid, HOBt/TBTU and 10 eq. DIPEA were used, and the coupling lasted 2×60min. This part of the sequence could also be synthesized on the Activo-P11 peptide synthesizer using either HOAt/DIC activation (8 eq., 2×90 min, Table 7.8) or HATU/DIPEA activation (Table 7.9). As Fmoc deprotection solution 20% (v/v) piperidine in DMF was used (4×5 min).

Residues 19-20 were coupled manually as pseudoproline dipeptide building block Fmoc-L-Tyr(^{t}Bu)-L-Thr[PSI(Me,Me)Pro]-OH following the procedure described in Section 7.4.3. The rest of the sequence for native C31 (residues 1-18) was afterwards synthesized in the Activo-P11 peptide synthesizer using the protocol given in Table 7.8. 10-fold excess of amino acids and coupling reagents (HOAt/DIC) were used for 2 2h. Fmoc-deprotection of these residues occurred with 20% (v/v) piperidine + 0.1 M HOBt in DMF for 4×5 min.

For the fluorinated C31 derivatives, Asn17 and Asn18 were coupled manually according to the procedure described in Section 7.4.3 (Table 7.10). The fluorinated amino acids in position 16

and the subsequent amino acid Glu15 were coupled manually as described in Section 7.4.3. The rest of the sequence (residues 1-14) was again synthesized automatically with the Activo-P11 synthesizer according to the protocol described in Table 7.8 using an 8-fold excess of amino acids, and activation agents (HOAt/DIC) for 2×2 h. As Fmoc-deprotection solution 20% (v/v) piperidine + 0.1 M HOBt in DMF was used. The deprotection step occurred four times for 5 min.

The *N*-terminal amino group of the C31-peptides was acetylated using acetic anhydride as described in Section 7.4.3 (see capping).

C34

Synthesis of C34 was conducted on a NovaSyn®TGR-resin that was loaded with Fmoc-L-Leu-OH beforehand (loading 0.25 mmol/g, Section 7.4.1). Amino acids residues 29-34 were coupled on the Syro XP peptide synthesizer according to Table 7.7 using 5 eq. of amino acid for 2×1 h. For Fmoc deprotection 20% (v/v) piperidine in DMF was used. Residues 13-28 were coupled with the Activo-P11 synthesizer, using 8 eq. amino acid/HOAt/DIC (2×1 h) and 20% (v/v) piperidine in DMF for Fmoc removal (2×5 min + 2×10 min). Amino acids 11+12 were coupled as the Fmoc-L-Tyr(^{t}Bu)-L-Thr[PSI(Me,Me)Pro]-OH pseudoproline building block as described in Section 7.4.3. Amino acid residue 10 was coupled manually following the protocol in Table 7.10. The final residues 1-9 were coupled again on Activo-P11 synthesizer using 8 eq. of amino acid with 8 eq HOAt and 8 eq DIC. Fmoc deprotection was conducted with a solution of 20% (v/v) piperidine + 0.1 M HOBt in DMF (2×5 min + 2×10 min) to avoid aspartimide formation at the Asp-residue. The coupling time was prolonged to 2×90 min. *N*-terminal capping was performed as described in Section 7.4.3.

T21

T21 was synthesized on a NovaSyn®TGR resin preloaded with Fmoc-L-Glu(O^{t}Bu)-OH (loading 0.23 mmol/g, see Section 7.4.1). The first five amino acid residues (33-38) were coupled on the Syro XP automated peptide synthesizer using five-fold excess of Fmoc-L-amino acid, HOBt, and TBTU, as well as a 10-fold excess of DIPEA according to the procedure described in Section 7.4.2 (see Table 7.7) for 2×60 min. Amino acid residues 23-32 were also coupled automatically, but this time using the Activo-P11 synthesizer. Couplings were conducted with eight equivalents of amino acid and coupling reagents (DIC/HOAt) for 2×60 min according to Section 7.4.2 (Table 7.8). Arg residues were coupled 2×90 min, and Fmoc-deprotection was conducted for 2×5 min and 2×10 min. Amino acid residues 18-22 were coupled in the same way on Activo-P11, but the reaction time was prolonged to 2×90 min. Coupling of the next two amino acids (16+17) occurred manually by incorporation of the pseudoproline building block Fmoc-L-Leu-L-Thr[PSI(Me,Me)Pro]-OH using HCTU/DIPEA activation following the method described in Section 7.4.3. The subsequent amino acid Gln15 was coupled manually as described in Table 7.10. The rest of the sequence was synthesized on the Activo-P11 automatic peptide

synthesizer using the general procedure given in Section 7.4.2 (Table 7.8). An eight-fold excess of amino acids and coupling reagents (HOAt/DIC) relative to the resin loading was used. Coupling reaction lasted 2×90 min for aa5-14 and 2×120 min for aa1-4, and Fmoc deprotection was performed 2×5 min and 2×10 min. For all deprotection steps during the synthesis of T21 a solution of 20% (v/v) piperidine containing 0.1 M HOBt in DMF was used to avoid aspartimide formation. For *N*-terminal acetylation see Section 7.4.3.

N36

Synthesis of N36 occurred on a NovaSyn®TGR-resin that was preloaded with Fmoc-L-Leu-OH (loading 0.25 mmol/g, Section 7.4.1). The synthesis of the complete sequence occurred at the Activo-P11 automated peptide synthesizer applying the procedure described in Section 7.4.2 (Table 7.8). Fmoc deprotection was performed with a solution of 2% (v/v) piperidine + 2% DBU (v/v) in DMF (2×5 min + 2×10 min). The first 15 amino acid residues (21-35) were coupled using an 8-fold excess of amino acid and coupling reagents (HOAt/DIC) for 2×1 h. For the second part of the peptide (residues 1-20) the excess of amino acid and coupling reagents was raised to 10-fold, and the coupling time was prolonged to 2×2 h. *N*-terminal capping was performed as described in Section 7.4.3.

7.4.6.1 N36 and T21 derivatives

N36 and T21 peptides were modified to test different approaches for coupling of a hetero-tetrameric linker (see Section 5.5).

Therefore, another 0.05 mmol of T21 without performing the *N*-terminal acetylation step[†] was synthesized as described before. A new batch of N36 was synthesized under slightly different conditions as described in the next paragraphs.

N36 with a free N-terminus[*]

Synthesis of an unacetylated N36 peptide that is used for SPR linker coupling tests occurred under optimized conditions. The synthesis was also performed on a NovaSyn®TGR-resin preloaded with Fmoc-L-Leu-OH (loading 0.25 mmol/g, Section 7.4.1) *via* the Activo-P11 automated peptide synthesizer using the procedure described in Section 7.4.2 (Table 7.8). Here, Fmoc deprotection was conducted with a solution of 20% (v/v) piperidine in DMF (2×5 min + 2×10 min). Residues 26-36 were coupled with an 8-fold excess of amino acid and coupling reagents (HOAt/DIC) for 2×90 min. For coupling of residues 1-25 a 10-fold excess of amino acid and coupling reagents was used.

[†]Synthesis on a NovaSyn®TGT resin gave fully protected peptides that were used without purification for further reactions.

[*]This peptide was kept on resin for further reactions and thus used without purification.

N36 on TGT resin[†]

For cleavage as fully protected peptide fragment, N36 was furthermore synthesized on a NovaSyn®TGT-resin preloaded with Fmoc-L-Leu-OH (loading 0.22 mmol/g). Synthesis was performed on the Actico-P11 synthesizer according to Section 7.4.2 (Table 7.8). Fmoc deprotection occurred with a solution of 20% (v/v) piperidine in DMF (2×5 min + 2×10 min). Residues 6-35 were coupled for 2×90 min, using an 8-fold excess of amino acid and coupling reagents (HOAt/DIC) for amino acids 16-35, and a 10-fold excess for residues 6-15. For coupling of residues 1-5 also a 10-fold excess of amino acid and coupling reagents was used, and the time for coupling reaction was prolonged to 2×2 h.

N36-PEG(4) and N36-PEG(4)$_{TGT}$*[†]

0.005 mmol of each N36 synthesized on either the TGT or TGR resin were PEGylated with FmocNH-PEG(4)-COOH according to the procedure given in Section 7.4.3. Final Fmoc cleavage was done manually by treatment of the resin with a solution of 20% (v/v) piperidine in DMF for 3×10 min (1.0 mL each). Afterwards, the resin was washed with DMF (3×2.0 mL) and DCM (3×2.0 mL).

*T21-PEG(4)**

0.005 mmol T21 were PEGylated as described in Section 7.4.3. Final Fmoc-deprotection occurred manually by treatment of the resin with 1.0 mL of a solution of 20% (v/v) piperidine + 0.1 M HOBt in DMF for 3×7 min. Afterwards, the resin was washed with DMF and DCM (each 3×2.0 mL).

T21-Cys and T21-PEG(4)-Cys

For an NCL approach, 0.005 mmol of T21 peptide was modified *N*-terminally with a Cys residue. Another 0.005 mmol were first modified with PEG(4) as spacer before coupling of the Cys residue. PEGylation occurred as described before for T21-PEG(4). The Cys residue was coupled manually for 2×1 h using 8-fold excess of Fmoc-L-Cys(Trt)-OH, and activation agents (HOAt/DIC) in 1.0 mL DMF (7 min preactivation). Final Fmoc cleavage was performed three times for 10 min using each 1.0 mL 20% (v/v) piperidine + 0.1 M HOBt in DMF. Afterwards, the resin was washed three times with DMF, and three times with DCM (2.0 mL each).

[†]Synthesis on a NovaSyn®TGT resin gave fully protected peptides that were used without purification for further reactions.

*These peptides were kept on resin for further reactions and thus used without purification.

7.5 Microwave assisted solid phase peptide synthesis

C31 peptide synthesis was tested with the help of MW irradiation as well. Synthesis occurred either manually or automated on a NovaSyn®TGR-resin preloaded with Fmoc-L-Glu(O^{t}Bu)-OH beforehand (loading 0.23 mmol/g, see Section 7.4.1) in 0.05 mmol scale.

Manual peptide synthesis under MW conditions was conducted using the Biotage® Initiator+ Microwave System. Temperature was set to 60°C (max. 75 W power) for both Fmoc-deprotection and amino acid coupling, and the stirring rate was 660. Fmoc deprotection occurred for 1×15 min with 3.0 mL 20% (v/v) Pip in DMF, and coupling reaction were performed for 2×30 min using 10-fold excess of amino acid and activating agents (HOAt/DIC) relative to the resin loading in 3.0 mL DMF. Washing after Fmoc-deprotection and the second coupling step was done 6×1 min with each 5.0 mL DMF without MW irradiation.

Automated peptide synthesis under MW conditions was performed with the CEM Liberty Blue™ Automated Microwave Peptide Synthesizer. Coupling occurred 2×5 min (3×5 min for Asn residues) using 5 eq. of amino acid and Oxyma/DIC as activating agents in 4.0 mL DMF. Fmoc deprotection was conducted 1×2 min (2×2 min for Asn17) in 4.0 mL 20% (v/v) Pip in DMF supplemented with 0.1 M HOBt to avoid aspartimide formation. Both coupling and deprotection steps were performed at 75°C. For the Arg residue a special protocol was used with a single coupling of 25 min without the use of MW, followed by 2 min at 75°C under MW irradiation to prevent γ-lactam formation. Furthermore, His was coupled at only 50°C for 2×10 min. The power of the MW was adjusted as such that the desired temperature was reached within the first 15 sec of the reaction step, and then set to a lower value so that the temperature is kept constant for the remaining reaction time. Washing steps occurred without the use of MW. The resin was washed with 3×5.0 mL DMF after the deprotection and coupling step. The synthesis started with 5 min resin swelling without MW.

N-terminal capping was done manually in both cases according to the procedure described in Section 7.4.3.

7.6 Cleavage from the resin, and purification

7.6.1 Test cleavage for validation of synthetic progress

To monitor the progress of the synthesis, test cleavages with a small amount of resin (spatula tip, ~ 0.5 - 1 mg) in 100 µL of cleavage cocktail were conducted. Therefore, the resin was placed in an Eppendorf tube, the cleavage cocktail was added, and it was shaken for 2 - 2.5 h. For peptide fragments containing Met-, Cys-, Trp- and/or Arg-residues a mixture of 85% (v/v) TFA, 5% (v/v) H$_2$O, 5% (v/v) TA, 2.5% (v/v) EDT and 2.5% (w/v) Phenol was used to avoid side-reactions. All

other peptide fragments were treated with a mixture of 10% (v/v) TIS, 1% (v/v) H_2O and 89% (v/v) TFA.

The peptide was then precipitated with 1.0 mL of ice-cold diethyl ether. After centrifugation, the ether was decanted and the peptide residue was dissolved in 1:1 ACN:H_2O + 0.1% TFA (~ 150 μL). The resin beads were separated *via* centrifugation, and the supernatant containing the peptide was injected into analytical HPLC to verify the success of the reaction step.

7.6.2 Full cleavage

After the synthesis, the resin was dried *in vacuo* and cleavage from the resin and side-chain deprotection of the peptides occurred by treatment with the cleavage cocktail solution given in Table 7.12 (2.0 mL per 150 mg of resin). The reaction mixture was shaken for 2-3 h at room temperature. Cleavage of the C31-peptides was performed under argon atmosphere. Afterwards, the reaction solution was filtered into a 100 mL flask and the resin was washed with TFA (2×2.0 mL) and DCM (4×2.0 mL). The washing solutions were combined with the cleavage solution and excess solvent was removed by evaporation. The crude peptide was precipitated by addition of ~ 80 mL ice-cold diethyl ether (Et$_2$O), and separated by centrifugation (4°C, 4.4 rpm, 4 min). The residue was washed with ice-cold Et$_2$O (2×10 mL) and dried *in vacuo* prior to purification.

Table 7.12: Used cleavage cocktails.

peptide	cleavage cocktail	duration
VPE **VPK-peptides**	2.5% (v/v) TIS 2.5% (v/v) H_2O 95% (v/v) TFA	2 h
FA peptides **N36**	10% (v/v) TIS 1% (v/v) H_2O 89% (v/v) TFA	3 h (FA-peptides) 2.5 h (N36)
C31-peptides **C34** **T21**	85% (v/v) TFA 5% (v/v) TA 5% (v/v) H_2O 2.5% (v/v) EDT 2.5% (w/v) Phenol	2.5 h

Cleavage of T21-Cys and T21-PEG(4)-Cys occurred with only 1 mL of 85% (v/v) TFA, 5% (v/v) TA, 5% (v/v) H_2O, 2.5% (v/v) EDT and 2.5% (w/v) Phenol. After shaking for 2.5 h, the resin was filtered off and washed with TFA (2×1.0 mL) and DCM (2×1.0 mL). The solvent was evaporated, and the crude peptide was precipitated with 15 mL ice-cold Et$_2$O. The peptide residue was separated by centrifugation (4°C, 4.4 rpm, 2 min) and dried *in vacuo*.

7.6.3 Cleavage of side-chain protected peptide fragments

Side-chain protected peptides were obtained by cleaving from NovaSyn®TGT resin under mild conditions with TFE. 0.005 mmol of resin were treated with 1.0 mL TFE/DCM (2:8) for 4×1h. After the appropriate time, the resin was removed by filtration und washed 3 times with the cleavage mixture (1.0 mL each). The solvent was evaporated, and the protected peptide was precipitated with ice-cold Et$_2$O (10 mL). The residue was separated by centrifugation (4°C, 4.4 rpm, 4 min) and dried *via* lyophilization. The protected peptide was used as such in further experiments.

7.6.4 Purification and Characterization

The crude peptides were dissolved in ACN/H$_2$O + 0.1% TFA (2.0 mL- 4.0 mL per 30-40 mg). For increasing the solubility of the C31-DfeGly peptide, a few drops of 0.1 M NaOH were added to the solution to yield a pH of ~ 8. C31-5^3,5'^{3}-F$_6$Leu was dissolved in MeOH. Purification occurred by reversed-phase preparative HPLC using linear ACN/H$_2$O gradients containing 0.1% TFA (Section 7.1.3). Used methods and columns are given in Table 7.13. Prior to injection, the peptide solution was filtered over 0.45 µm Acrodisc® syringe filters with GHP membrane (Pall Corporation, Port Washington, NY, USA). Up to a maximum of 40 mg crude peptide in maximal 4.0 mL were injected per run.

Table 7.13: Used methods and columns for purification of peptides. For detailed method parameters see Table 7.1.

peptide	used method	column	detection wavelength
VPE/VPK	P4	Luna® C8(2)	320nm
FA peptides	P5	Kinetex® C18	220 nm
C31 C31-5^3-F$_3$Ile- C31-5^3,5'^{3}-F$_6$Leu	1st purification: P6	Kinetex® C18	220 nm
	2nd purification: P7	Kinetex® C18	220 nm
C31-DfeGly	P8	Kinetex® C18	220 nm
C34	1st purification: P9	Kinetex® C18	280 nm
	2nd purification: P10	Kinetex® C18	220 nm
T21	P9	Kinetex® C18	220 nm
N36	1st purification: P4	Kinetex® C18	220 nm
	2nd purification: P11	Luna® C8(2)	220 nm
T21-Cys T21-PEG(4)-Cys	P12	Kinetex® C18	220 nm

Collected fractions were analyzed *via* analytical HPLC on the semi-micro Chromaster system (see Chapter 7.1.4) and the molecular masses were identified by ESI-ToF MS (Section 7.1.6). For VPE, and VPK-peptides, as well as all FA-peptides method **A3** (Table 7.2) was used. For all gp41 derived peptides method A**4** was applied.

Fractions containing the desired and pure peptide were combined, ACN was reduced *in vacuo*, and the remaining aqueous solution was dried by lyophilization to yield the pure peptides as white powder. The purity of the resulting products was confirmed by analytical HPLC (Section 7.1.4), and all peptides were identified by high resolution ESI-ToF-MS (Section 7.1.6). For fractions with insufficient purity, a second purification step was performed using optimized methods (see Table 7.13).

The detailed characterization data of the synthesized peptides are given in the next section.

7.7   Synthesized peptides

The peptide sequences synthesized within the scope of the present thesis were identified by ESI-ToF mass spectrometry (Section 7.1.6, Table 7.6). The results are shown in Table 7.14 - 7.17. HPLC chromatograms of pure peptides are depicted in Figure 7.1 - 7.8. Used HPLC settings (see Section 7.1.4) are given in the figure caption. HPLC-purity of all synthesized peptides is > 95%.

Table 7.14: Identification of synthesized VPE/VPK peptides by ESI-ToF MS using setting **B** (Table 7.6).

peptide	charge	m/z observed	m/z calculated
VPE	$[M+4H]^{4+}$	948.2762	948.2743
	$[M+5H]^{5+}$	758.8222	758.8210
VPK	$[M+4H]^{4+}$	947.8034	947.8005
	$[M+5H]^{5+}$	758.4444	758.4420
VPK-$5^3,5'^3$-F$_6$Leu$_{19}$	$[M+4H]^{4+}$	974.7974	974.7864
	$[M+5H]^{5+}$	780.0405	780.0306
VPK-(3*R*)-4^3-F$_3$Val$_{16}$	$[M+4H]^{4+}$	961.3033	961.2934
	$[M+5H]^{5+}$	769.2460	769.2363
VPK-(3*S*)-4^3-F$_3$Val$_{16}$	$[M+4H]^{4+}$	961.3044	961.2934
	$[M+5H]^{5+}$	769.2469	769.2363
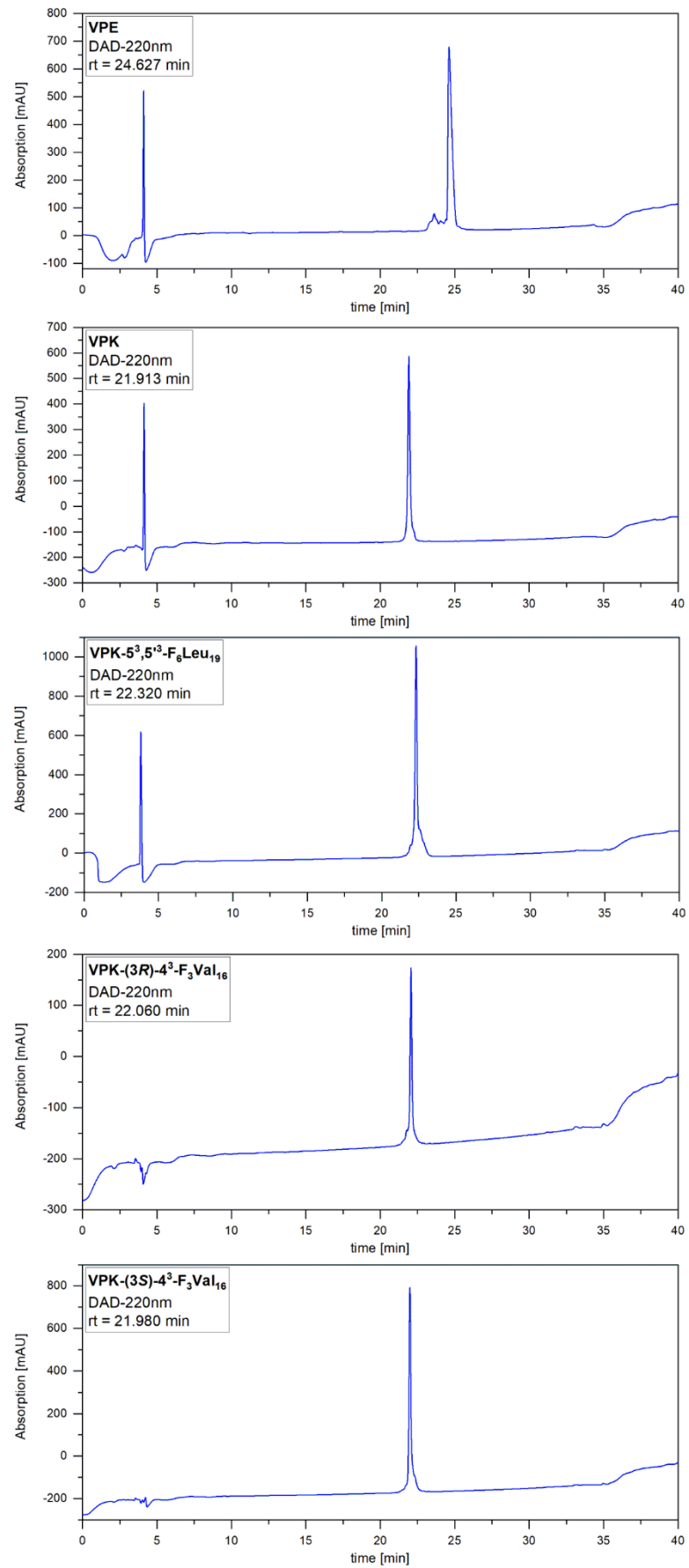
Figure 7.1: HPLC chromatograms of purified VPE/VPK-peptides. HPLC system: LaChrom ELITE®; column: Luna® C8(2); eluent: A = 0.1% TFA in water, B = 0.1% TFA in ACN; gradient: 5% → 70% B in 30min (method **A12**, Table 7.4).

Table 7.15: Identification of synthesized FA peptides by ESI-ToF mass spectrometry. Setting **A** was used (Table 7.6).

peptide	charge	m/z observed	m/z calculated
FA	$[M+H]^+$	967.5396	967.5364
	$[M+2H]^{2+}$	484.2736	484.2721
P2-IleFA	$[M+H]^+$	1009.5849	1009.5834
	$[M+2H]^{2+}$	505.2971	505.2956
P2-5³-F₃IleFA	$[M+H]^+$	1063.5576	1063.5551
	$[M+2H]^{2+}$	532.2845	532.2814
P1'-IleFA	$[M+H]^+$	1009.5858	1009.5834
	$[M+2H]^{2+}$	505.2975	505.2956
P1'-5³-F₃IleFA	$[M+H]^+$	1063.5556	1063.5551
	$[M+2H]^{2+}$	532.2816	532.2814
P2'-IleFA	$[M+H]^+$	1009.5864	1009.5834
	$[M+2H]^{2+}$	505.2980	505.2956
P2'-5³-F₃IleFA	$[M+H]^+$	1063.5576	1063.5551
	$[M+2H]^{2+}$	532.2835	532.2814
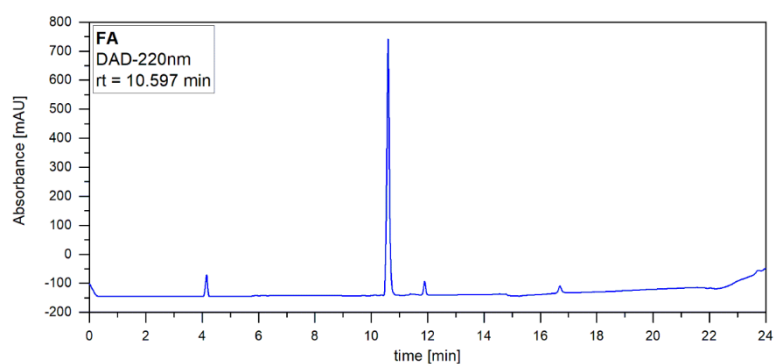
Figure 7.2: Analytical HPLC chromatogram of purified FA on a Chromaster 600 bar DAD HPLC system. Column: Luna® C8(2); eluent: A = H₂O + 0.1% (v/v) TFA, B = ACN + 0.1% (v/v) TFA; gradient: 5% → 70% B over 18 min (method **A7**, Table 7.3).
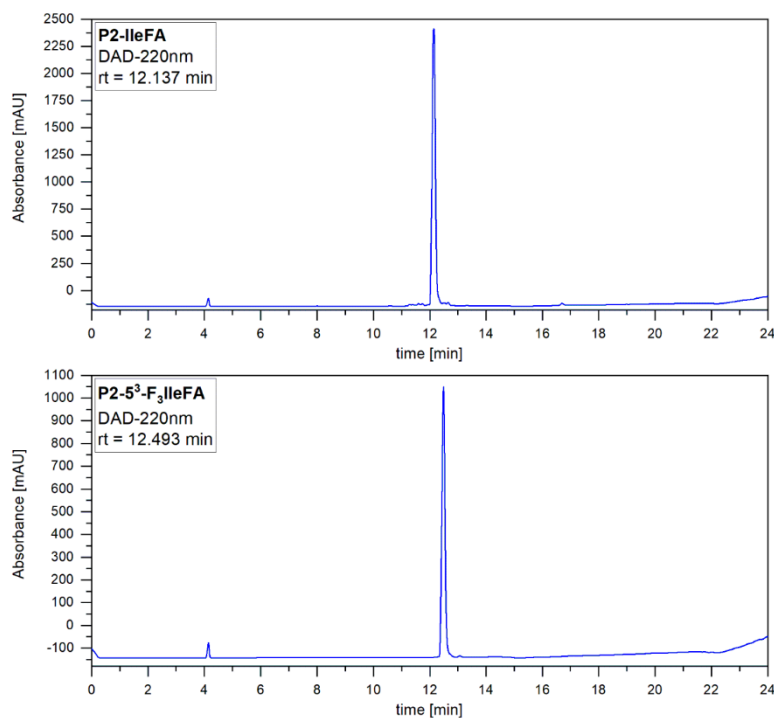
Figure 7.3: HPLC chromatograms of pure P2-IleFA, and P2-5³-F₃IleFA. HPLC system: Chromaster 600 bar DAD; column: Luna® C8(2); eluent: A = 0.1% TFA in water, B = 0.1% TFA in ACN; gradient: 5% → 70% B over 18 min (method **A7**, Table 7.3).
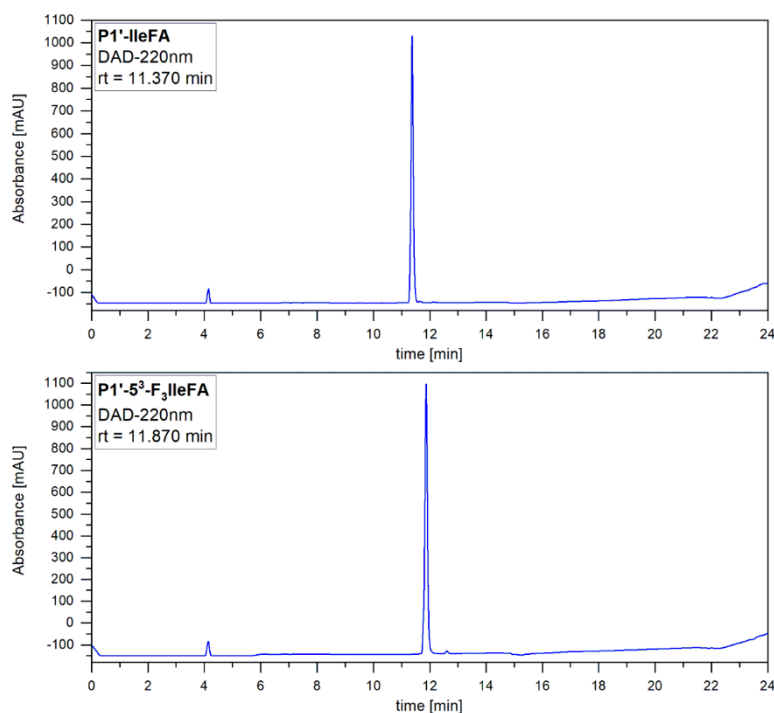
Figure 7.4: Analytical HPLC chromatograms of P1'-IleFA, and P1'-5³-F₃IleFA on a Chromaster 600 bar DAD HPLC system. Column: Luna® C8(2); eluent: A = H₂O + 0.1% (v/v) TFA, B = ACN + 0.1% (v/v) TFA; gradient: 5% → 70% B over 18 min (method **A7**, Table 7.3).
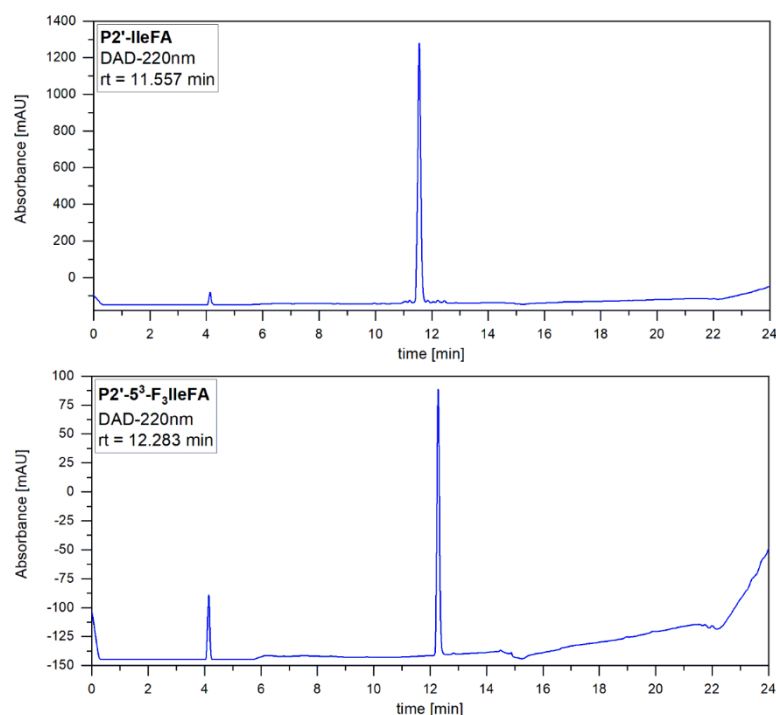
Figure 7.5: HPLC chromatograms of pure P2'-IleFA, and P2'-5³-F₃IleFA. Used HPLC system: Chromaster 600 bar DAD; column: Luna® C8(2); eluent: A = H₂O + 0.1% (v/v) TFA, B = ACN + 0.1% (v/v) TFA; gradient: 5% → 70% B over 18 min (method **A7**, Table 7.3).

Table 7.16: Identification of synthesized gp41-derived peptides by ESI-ToF mass spectrometry. Setting **C** was used (Table 7.6).

peptide	charge	m/z observed	m/z calculated
C31	$[M+2H]^{2+}$	1975.9083	1975.9097
	$[M+3H]^{3+}$	1317.6106	1317.6091
	$[M+4H]^{4+}$	988.4616	988.4588
C31-DfeGly	$[M+2H]^{2+}$	1979.8828	1979.8847
	$[M+3H]^{3+}$	1320.2624	1320.2590
	$[M+4H]^{4+}$	990.4486	990.4462
C31-5³-F₃Ile	$[M+2H]^{2+}$	2002.8959	2002.8956
	$[M+3H]^{3+}$	1335.6049	1335.5997
	$[M+4H]^{4+}$	1001.9576	1001.9517
C31-5³,5'³-F₆Leu	$[M+2H]^{2+}$	2029.8840	2029.8815
	$[M+3H]^{3+}$	1353.5940	1353.5902
	$[M+4H]^{4+}$	1015.4488	1015.4446
C34	$[M+3H]^{3+}$	1430.0119	1430.0137
	$[M+4H]^{4+}$	1072.7610	1072.7622
T21	$[M+3H]^{3+}$	1508.8586	1508.8612
	$[M+4H]^{4+}$	1131.8974	1131.8979
	$[M+5H]^{5+}$	905.7196	905.7199
	$[M+6H]^{6+}$	754.9346	754.9345
N36	$[M+3H]^{3+}$	1388.1278	1388.1295
	$[M+4H]^{4+}$	1041.3482	1041.3490
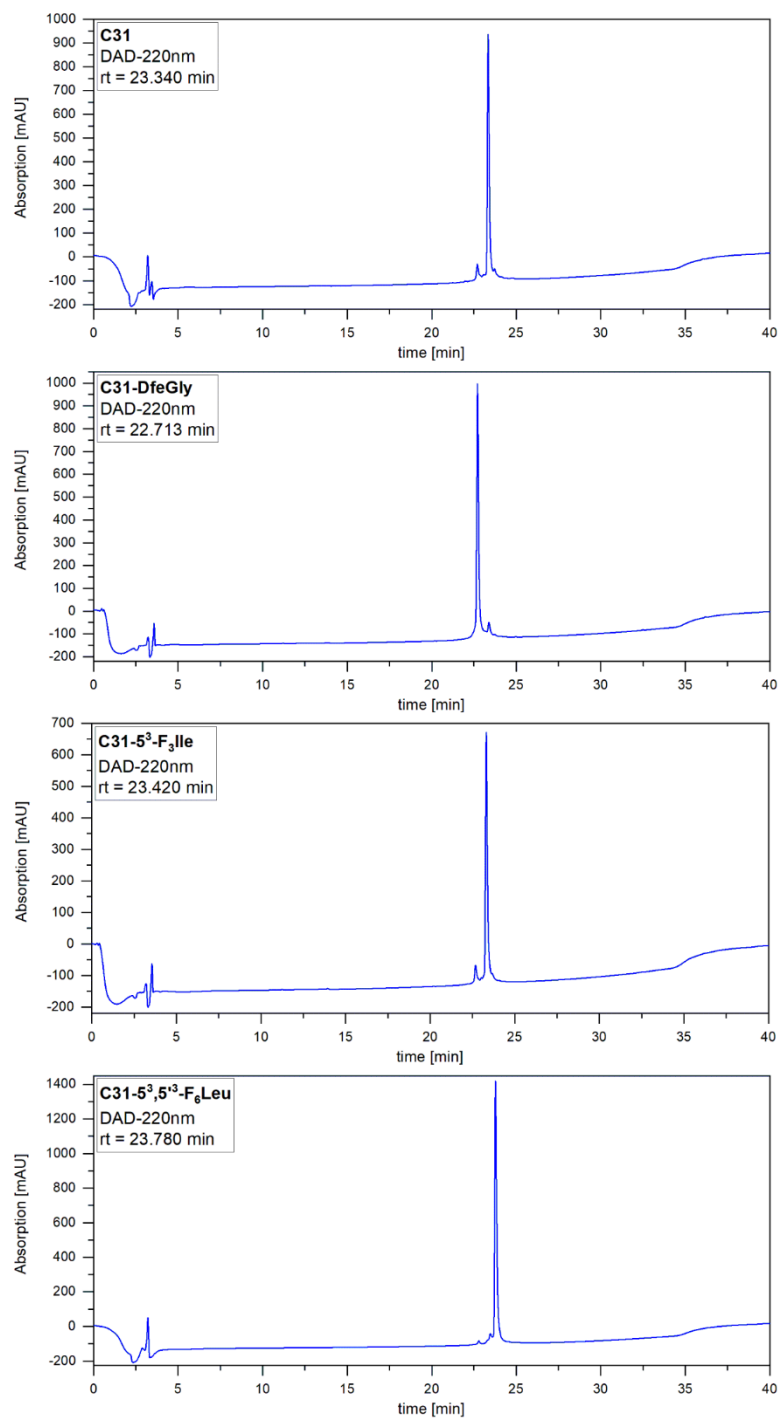
Figure 7.6: HPLC chromatograms of pure C31-peptides. Used HPLC system: LaChrom ELITE®; column: Kinetex® C18; eluent: A = H$_2$O + 0.1% (v/v) TFA, B = ACN + 0.1% (v/v) TFA; gradient: 10% → 80% B over 30 min (method **A13**, Table 7.4).
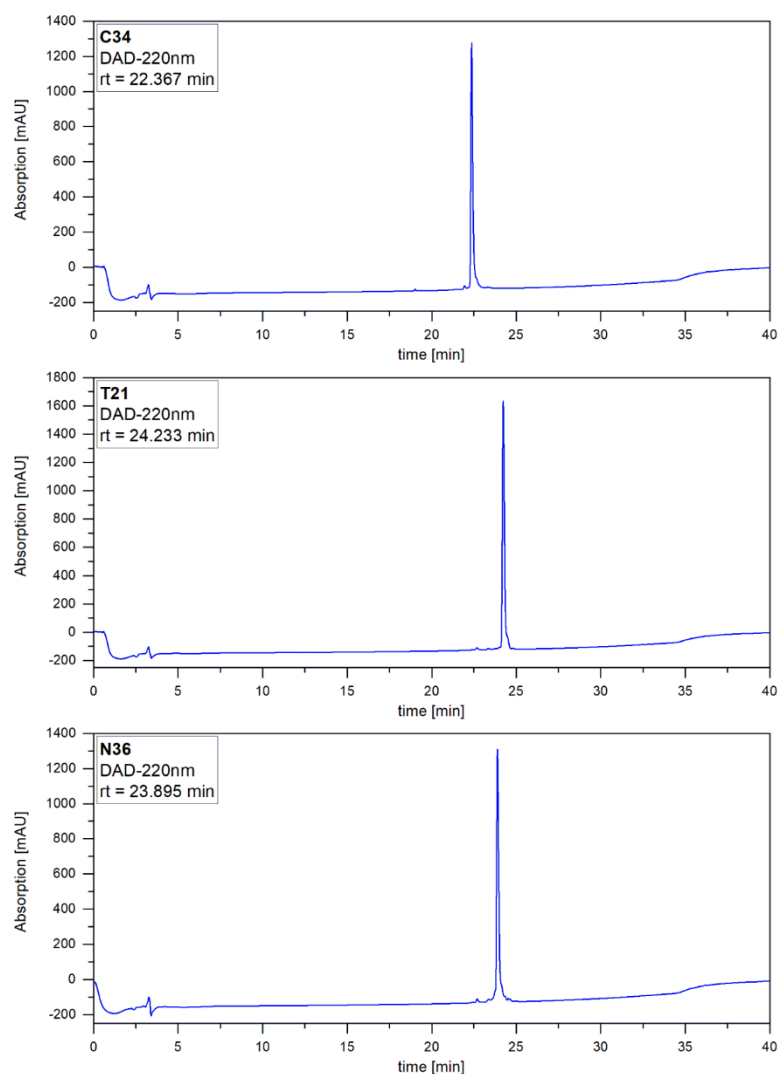
Figure 7.7: HPLC chromatograms of purified C34, T21 and N36. Used HPLC system: LaChrom ELITE®; column: Kinetex® C18; eluent: A = H$_2$O, B = ACN, both containing 0.1% (v/v) TFA; gradient: 10% → 80% B over 30 min (method **A13**, Table 7.4).

Table 7.17: Identification of T21-Cys and T21-PEG(4)-Cys peptides by ESI-ToF mass spectrometry. Setting **B** was used (Table 7.6).

peptide	charge	m/z observed	m/z calculated
T21-Cys	[M+4H]$^{4+}$	1147.1505	1147.1475
	[M+5H]$^{5+}$	917.9207	917.9196
T21-PEG(4)-Cys	[M+4H]$^{4+}$	1208.9383	1208.9330
	[M+5H]$^{5+}$	967.3525	967.3480
	[M+6H]$^{6+}$	806.2952	806.2913
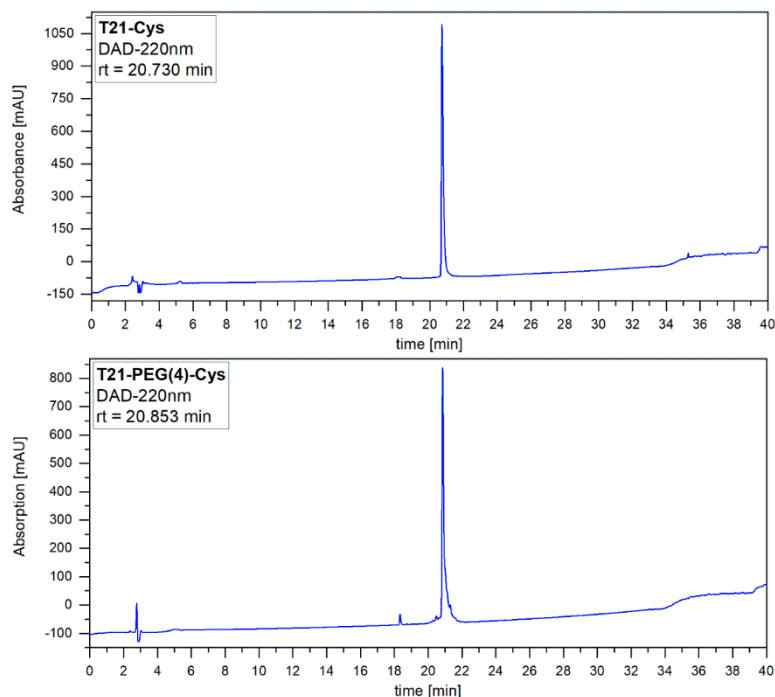
Figure 7.8: HPLC chromatograms of pure T21-Cys, and T21-PEG(4)-Cys. HPLC system: Chromaster 600 bar DAD; column: Kinetex® C18; eluent: A = 0.1% TFA in water, B = 0.1% TFA in ACN; gradient: 10% → 80% B over 30 min (method **A8**, Table 7.3).

7.8 Determination of peptide concentration

The concentration of peptide stock solutions was determined by UV detection (Section 7.1.8) using quartz cuvettes. The spectra were baseline corrected by the spectra of a sample containing solely buffer. The measurement was carried out in triplicate and the concentration was calculated according to the Lambert-Beer law (equation 7.3).

$$E_\lambda = \varepsilon_\lambda \cdot c \cdot d \tag{7.3}$$

Here, E_λ is the measured absorption at the wavelength λ, ε_λ is the extinction coefficient of the peptide at the wavelength λ in $M^{-1}m^{-1}$, c the peptide concentration in mol/L and the path length of the cell in m.

VPE/VPK peptides

Peptide concentrations were determined by measuring the absorbance of *o*-aminobenzoic acid (λ_{max} = 320 nm at pH 7.4), which is attached at the *N*-terminus of each peptide, as described before.[79, 251, 365] Therefore, a calibration curve was recorded using different concentrations of H$_2$N-Abz-Gly-COOH × HCl (Bachem AG, Bubendorf, Switzerland) in the buffer used for CD spectroscopy containing 6 M guanidine hydrochloride (Figure 7.9).
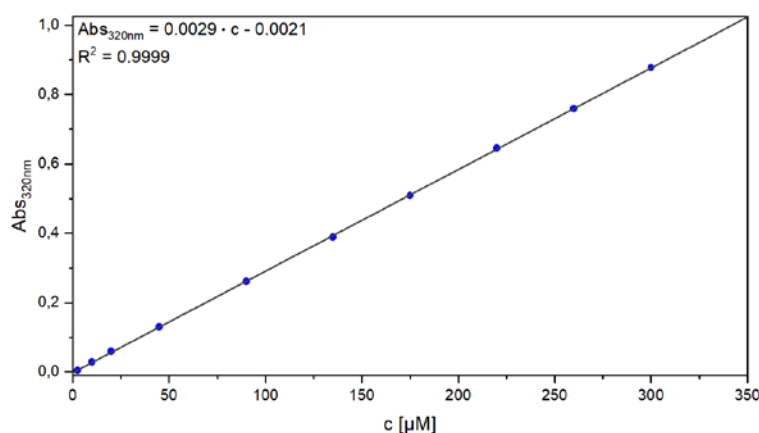
Figure 7.9: Calibration curve for the determination of peptide concentrations recorded at 20°C in 100 mM phosphate buffer containing 6 M GdnHCl (pH 7.4).

Gp41-derived peptides

Peptide stock solutions were prepared by dissolving the lyophilized peptide in HFIP. An aliquot of the stock solution (10 µL) was taken, and HFIP was removed carefully under a gentle stream of argon. The resulting film was dissolved in 1.0 mL 50 mM sodium phosphate and 150 mM NaCl buffer containing 6 M guanidinium chloride (pH 7.4), and the absorbance at 280 nm was measured. The extinction coefficient of the peptides was determined using equation 7.4 according to Pace *et al.*[366] and the concentration of the stock solution was then calculated *via* the Lambert-Beer law (equation 7.3).

$$\varepsilon_{280nm} \left(M^{-1} \cdot cm^{-1} \right) = \#Trp \cdot 5500 + \#Tyr \cdot 1490 + \#Cys \cdot 125 \tag{7.4}$$

$\#Trp$, $\#Tyr$ and $\#Cys$ are the numbers of tryptophan, tyrosine and cysteine residues in the peptide sequence.

Table 7.18: Calculated extinction coefficients.

peptide	$\varepsilon_{280nm}[M^{-1}\ cm^{-1}]$
C31	17990
C34	12490
T21	6990
N36	5500

Prior to the experiments, the desired amount of the peptide stock solution was aliquoted, HFIP was removed and the peptide was dissolved in freshly prepared 50 mM sodium phosphate and 150 mM NaCl buffer (pH 7.4). If necessary, the pH of this solution was adjusted to 7.4 by addition of NaOH and HCl. Stock solutions of 500 µM were prepared and stored at -20°C until use.

7.9 Structural analysis

7.9.1 CD spectroscopy

VPE/VPK peptides

CD spectra were recorded using Quartz Suprasil® cuvettes of 1.0 mm path length (Hellma Analytics, Müllheim, Germany) equipped with a stopper. Measurements were performed with an overall peptide concentration of 20 µM (for equimolar mixtures: 10 µM VPE and 10 µM VPK) in 100 mM phosphate buffer (pH 7.4) at 20°C. Each reported CD value represents the mean of at least 3 independent measurements. The spectra were recorded with the parameters listed in Table 7.19, and background-corrected by subtraction of the corresponding buffer spectra.

Table 7.19: Parameters of CD spectroscopy for VPE/VPK peptides.

parameter	value
sensitivity	Standard (100 mdeg)
wavelength start	240 nm
wavelength end	190 nm
data pitch	0.2 nm
scanning mode	continuous
scanning speed	100 nm/min
response	2 s
bandwith	2 nm
accumulation	3
N_2 flow	3 L/min

The measured CD data in mdeg were converted into molar ellipticity per residue $[\theta]$ [mdeg·cm^2·dmol^{-1}·residue^{-1}] according to equation 7.5.

$$[\theta] = \frac{\theta_{obs}}{10000 \cdot l \cdot c \cdot n} \tag{7.5}$$

Here, θ_{obs} is the measured ellipticity in deg, c the peptide concentration in mol/l, l the path length of the cell in cm and n the number of amino acid residues (here 35).

For thermal denaturation curves, the CD signal at 222 nm was recorded using the following parameters.

Table 7.20: Parameters for thermal denaturation studies of VPE/VPK peptides.

parameter	value
sensitivity	Standard (100 mdeg)
wavelength	222 nm
starting temperature	20°C
ending temperature	100°C
data pitch	0.1°C
delay time	0 s
temperature slope	3°C/min
response	1 s
bandwith	1 nm
N_2 flow	3.0 L/min

The melting curves were first normalized according to equation 7.5, and then fitted assuming two-state unfolding to determine the melting temperature and free energy of unfolding ($\Delta G^\emptyset$) as described before.[79] Each reported value represents the mean of at least 3 independent measurements.

The fractional helical content of peptide (f_H) was calculated from the mean residue molar ellipticity at 222 nm and the number of backbone amides (n = 35) using equation 7.6.

$$f_H = \frac{[\theta]_{222nm}}{-40000 \cdot \left(1 - \frac{4.6}{n}\right)}$$

(7.6)

Gp41-derived peptides

For this study 20 μM solutions of the peptides were prepared in 50 mM sodium phosphate and 150 mM NaCl buffer (pH 7.4). CD spectra of the CHR/NHR peptide mixtures were also measured at an overall peptide concentration of 20 μM (10 μM in each monomer). The samples were incubated at 37°C for 30 min using a thermoshaker (300 rpm) before measuring. CD spectra were recorded at 25°C and 37°C using 1.0 mm Quartz Suprasil® cuvettes (Hellma Analytics, Müllheim, Germany) equipped with a stopper applying the parameters shown in the following table.

Table 7.21: Parameters for CD spectroscopy of gp41 derived peptides.

parameter	value
sensitivity	Standard (100 mdeg)
wavelength start	240 nm
wavelength end	195 nm
data pitch	0.2 nm
scanning mode	continuous
scanning speed	100 nm/min
response	2 s
bandwith	2 nm
accumulation	3
N_2 flow	3.0 L/min

The measurements were carried out in triplicate. Spectra were background corrected by subtraction of the corresponding buffer spectra and normalized according to equation 7.5.

To ensure that an interaction between the CHR- and NHR-peptide has taken place, the measured CD data of the individual peptides were summed up and the result was then divided in half. The so obtained CD spectrums are different from the ones of the individual peptides and the 1:1 mixtures (data not shown). Thus, an interaction can be assumed.

Thermal denaturation curves were recorded under the following conditions:

Table 7.22: Parameters for thermal denaturation measurements of gp41 derived peptides.

parameter	value
sensitivity	Standard (100 mdeg)
wavelength	222 nm
starting temperature	25°C
ending temperature	100°C
data pitch	0.1°C
delay time	0 s
temperature slope	3°C/min
response	1 s
bandwith	1 nm
N_2 flow	3.0 L/min

Measurements occurred at a peptide concentration of 20 µM in 50 mM sodium phosphate with 150 mM NaCl buffer (pH 7.4) as well, and were repeated three times, in order to assure reproducibility and give standard deviations. The data were first normalized according to equation 7.5 and then fitted with the following formula to determine the melting points as described before.[79, 251, 365]

$$f_n(T) = \frac{\theta_{obs} - (m_f \cdot T + \theta_f)}{(m_{unf} \cdot T + \theta_{unf}) - (m_f \cdot T + \theta_f)} \tag{7.7}$$

Here, m_f is slope of the folded state, θ_f the CD signal of the folded state, m_{unf} the slope of the unfolded state θ_{unf} the CD signal of the unfolded state and T the temperature in K. The values can be obtained by fitting straight lines to the complete folded and unfolded state of the normalized melting curve (see Figure 7.10). The fits were performed in Microsoft® Excel Version 16.13 (Microsoft, Redmond, WA).
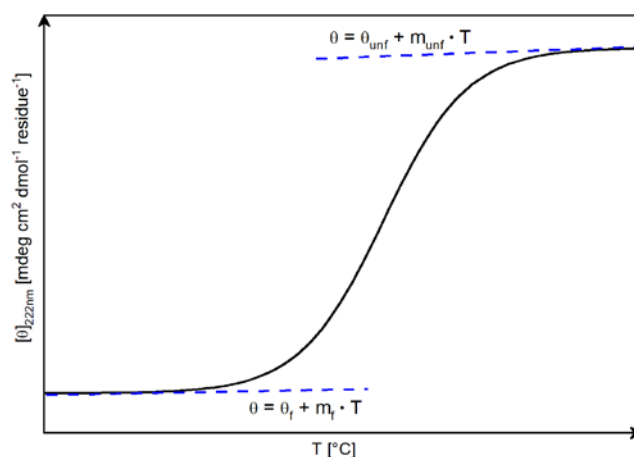
Figure 7.10: Representation of a peptides melting curve with the interpolated straight lines for the complete folded and unfolded state.[365]

The turning point of the melting curve represents the melting point of the investigated peptide or peptide assembly. For the fitted curve the melting point is marked by the temperature value for $f_n = 0.5$.[367]

7.9.2 Size exclusion/static light scattering

VPE/VPK peptides

The oligomerization state of the peptide assemblies was determined by applying size exclusion chromatography (SEC) in combination with static light scattering (SLS). SLC data were collected on a Dawn 8+ multi-angle static light scattering (MALS) detector and an Optilab T-rEX differential Refractive index (dRI) detector (both Wyatt Technology Europe GmbH, Dernbach, Germany) coupled with an analytical SEC system. The latter consists of a VWR-Hitachi LaChrom ELITE HPLC workstation containing an organizer, a pump L-2130, and an UV-detector L-2400 (all VWR International GmbH, Darmstadt, Germany). A WTC-015S5 column (5 μm, 150 Å, 7.8×300 mm, Wyatt Technology Europe GmbH, Dernbach, Germany) was used and UV detection of the peptides occurred at $\lambda = 220$ nm. All measurements were performed at room temperature with 10 mM PBS, pH 7.4 as eluent and a flow rate of 0.3 mL/min. The overall peptide concentration was 35 μM from a 1:1 mixture of the different VPK/VPE variants, and the injection volume was 100 μL in each case. All experiments were performed in triplicate to confirm reproducibility and give standard deviations. Data were analyzed using the ASTRA software version 5.3.4.20 (Wyatt Technology), and the program OriginPro 2018b version 9.55 (OriginLab Corporation, Northampton, MA, USA).

7.9.3 Isothermal Titration Calorimetry (ITC)

ITC assay was performed using a MicroCal iTC200 isothermal titration calorimeter (Malvern Panalytical Ltd, Malvern, United Kingdom). The CHR-peptide (100 µM) was injected into the cell containing the NHR-peptide (10 µM), both in 50 mM sodium phosphate with 150 mM NaCl buffer (pH 7.4). Measurements occurred at 25°C with the settings shown in Table 7.23 and 7.24. The reference cell contained Milli-Q-H_2O.

Table 7.23: Experimental parameters for ITC assay.

parameter	value
total # injections	20
cell temperature [°C]	25
reference power [µcal/sec]	5
initial delay [sec]	180
stirring speed [rpm]	750

Table 7.24: Injection parameters for the ITC assay.

injection #	volume [µL]	duration [sec]	spacing [sec]	filter period [sec]
1	0.5	1.0	180	5
2-20	2.0	4.0	180	5

Before the measurement, the peptide samples were dialyzed against the buffer for 3 h using the Pur-A-Lyzer™ Midi Dialysis Kit (MWCO 1 kDa, Sigma-Aldrich®/Merck KGaA, Darmstadt, Germany). Data analysis occurred using the MicroCal LLC ITC200 AddOn for the Origin software (version 7.0, SP4, OriginLab, Northampton, MA, USA).

7.10 Enzymatic digestion studies

All FA peptides were used as the TFA salts obtained after lyophilization. Stock solutions of α-chymotrypsin (from bovine pancreas, EC 3.4.21.1, ≥40.0 units/mg of protein, Sigma Aldrich, St. Louis, MO, USA), and pepsin (from porcine stomach mucosa, EC 3.4.23.1, ≥250 units/mg of protein, Sigma Aldrich, St. Louis, MO, USA) were prepared in phosphate buffer (10 mM, pH 7.4), or in acetate buffer (10 mM, pH 4.0), respectively. Proteinase K (from Tritirachium album, EC 3.4.21.64, ≥30 units/mg of protein, Sigma Aldrich, St. Louis, MO, USA) and elastase (from porcine pancreas, EC 3.4.21.36, 6.2 units/mg of protein, Sigma Aldrich, St. Louis, MO, USA) were dissolved in Tris/HCl (50 mM) + $CaCl_2$ (10 mM) buffer (pH 7.5), or in Tris/HCl buffer (100 mM, pH 8.4), respectively. All enzyme stocks were prepared at concentrations of 1 mg/mL.

Stock solutions of the peptides (2.00 µmol each) were prepared in DMSO (100 µL). Incubation with the respective enzymes occurred at 30°C (for α-chymotrypsin and pepsin) or

37°C (for proteinase K and elastase) with shaking at 300 rpm in a thermomixer over a period of 24 h. The reaction mixture consisted of DMSO (15 μL), corresponding buffer (25 μL), peptide solution (5 μL) and the corresponding enzyme solution (5 μL). The concentration of enzyme in the reaction mixture was optimized such that the hydrolysis of the control peptide FA was about 40% after 120 min incubation. Aliquots of 5 μL were taken at fixed time points (0, 15, 30, 60, 90, 120 min as well as 3 h and 24 h) and either quenched with ACN containing 0.1% (v/v) TFA (95 μL), in the case of α-chymotrypsin, proteinase K and elastase, or 2% aqueous ammonia (95 μL), in the case of pepsin.

For characterization of the enzymatic digestion reactions all samples were subjected to analytical HPLC on a LaChrom-ELITE system with fluorescence detection (see Section 7.1.4). Linear gradients of eluents were applied according to the methods described in Table 7.5. For the non-fluorinated peptides method **FL1** was used, and for the fluorinated peptides method **FL2** was applied to follow the digestion process. For chromatograms where an insufficient baseline separation was observed, measurements were repeated using methods **FL3** [FA (pepsin), P2-IleFA (pepsin), P2-IleFA (proteinase K), P1'-IleFA (proteinase K)] or **FL4** [P2-5^3-F$_3$IleFA (pepsin), P2-5^3-F$_3$IleFA (proteinase K), P1'-5^3-F$_3$IleFA (elastase), P2'-5^3-F$_3$IleFA (proteinase K)]. In all cases, the peaks corresponding to the starting materials (full-length peptides) or the *N*-terminal fragments (digestion products) were integrated and used to determine the amount of substrate still present (in %), and the velocity of the reaction. The FA peptide was used as a reference. Identification of each fragment cleaved from the full-length peptide (Table 8.1 - 8.4, Supplementary data) occurred according to the mass-to-charge ratios determined on an Agilent 6220 ESI-ToF-MS instrument using setting **A** (see Section 7.1.6, Table 7.6). For this, the quenched peptide-enzyme-solutions after 120 min and 24 h incubation were analyzed. Not all corresponding fragments could be detected. All experiments were performed in triplicate.

8. Supplementary Data

Crystal structure depiction

Graphics of the peptides crystal structures were created using the UCSF Chimera package. Chimera is developed by the Resource for Biocomputing, Visualization, and Informatics at the University of California, San Francisco (supported by NIGMS P41-GM103311).[368] The structural data were taken from the PDB (https://www.rcsb.org).

SEC/SLS to determine the oligomerization state of VPE/VPK bundles

The dimeric oligomerization states of the parent VPE/VPK assembly as well as the fluorinated variants have been determined by SEC/SLS. Single peaks were found for all VPE/VPK variants with SEC corresponding species of molecular weights comparable to the theoretical dimer mass (Table 5.2, Figure 8.1).
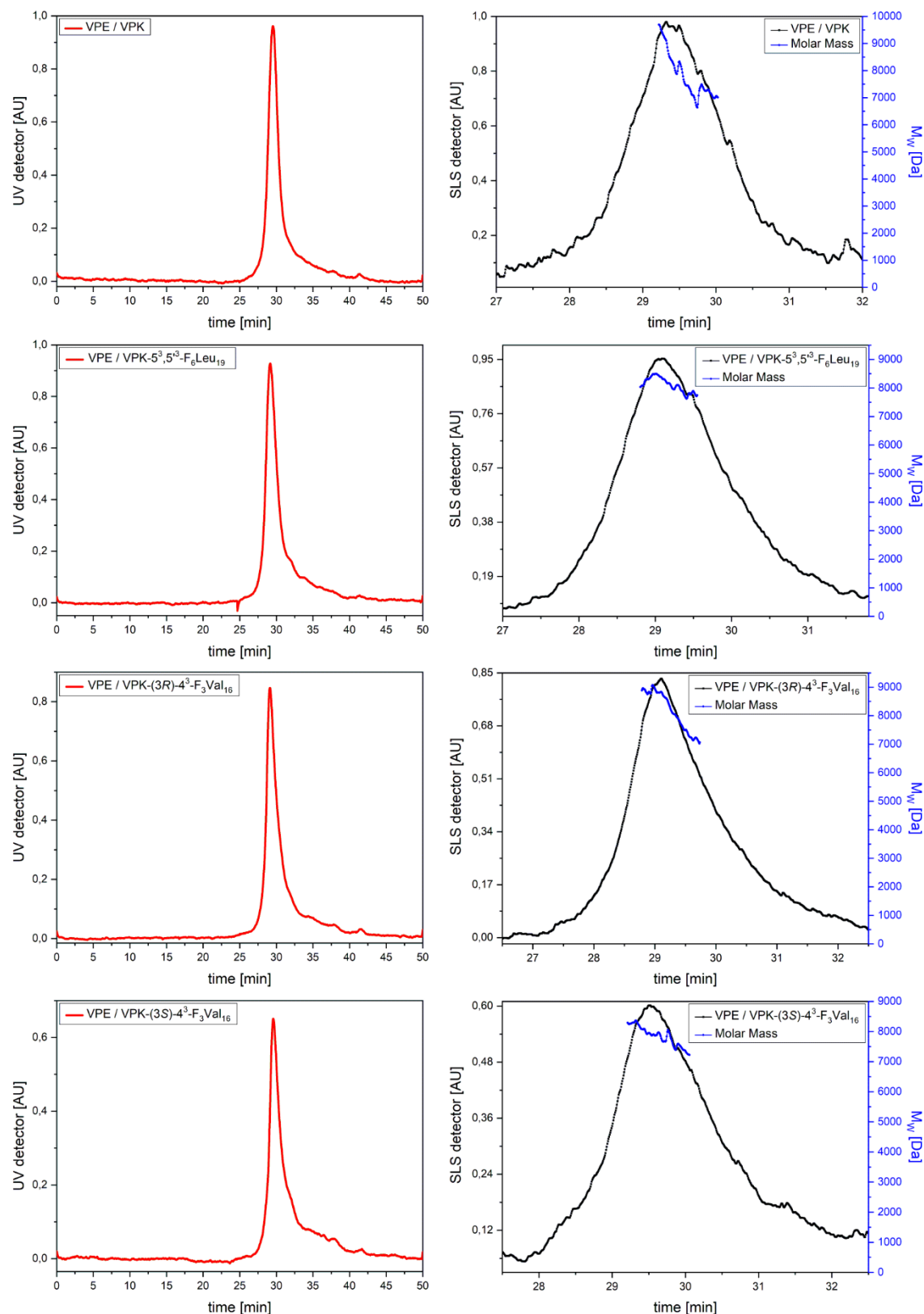
Figure 8.1: SEC/SLS chromatograms of VPE/VPK bundles. Peptide concentration: 35 µM; eluent: 10 mM PBS, pH 7.4; flow rate: 0.3 mL/min. Measurements were taken from equimolar mixtures of the different VPK/VPE variants and repeated two times to confirm reproducibility and give standard deviations. Single peaks were detected with UV at 220 nm (red). Corresponding Rayleigh ratio (black) and the molar mass distribution (blue) indicate dimeric species for all peptide variants.

Identification of the proteolytic cleavage products of the enzymatic digestion assay of FA peptides by ESI-ToF MS

Table 8.1: Identification of the cleavage products of the different peptides by ESI-ToF mass spectrometry after digestion with α-chymotrypsin.

peptide	fragment	$[M + H]^{1+}$ calculated	$[M + H]^{1+}$ observed
FA	Abz-KAAFAAAAK	967.5364	967.5376
	Abz-KAAF	555.2559	555.2938
	AAAAK	431.2617	431.2627
P2-IleFA	Abz-KAIleFAAAAK	1009.5463	1009.5851
	Abz-KAIleF	597.3029	597.3435
	AAAAK	431.2617	431.2647
P2-5^3-F$_3$IleFA	Abz-KA-5^3-F$_3$Ile-FAAAAK	1063.4622	1063.5577
P1'-IleFA	Abz-KAAFIleAAAK	1009.5463	1009.5825
	Abz-KAAF	555.2559	555.2951
	IleAAAK	473.3087	473.3104
P1'-5^3-F$_3$IleFA	Abz-KAAF-5^3-F$_3$Ile-AAAK	1063.4622	1063.5604
	Abz-KAAF	555.2559	555.2954
	5^3-F$_3$Ile-AAAK	527.2246	527.2827
P2'-IleFA	Abz-KAAFAIleAAK	1009.5463	1009.5875
	Abz-KAAF	555.2559	555.2943
	AIleAAK	473.3087	473.3112
P2'-5^3-F$_3$IleFA	Abz-KAAFA-5^3-F$_3$Ile-AAK	1063.4622	1063.5575
	Abz-KAAF	555.2559	555.2945
	A-5^3-F$_3$Ile-AAK	527.2246	527.2822

Table 8.2: Identification of the cleavage products of the different peptides by ESI-ToF mass spectrometry after digestion with pepsin.

peptide	fragment	$[M + H]^{1+}$ calculated	$[M + H]^{1+}$ observed
FA	Abz-KAAFAAAAK	96.5364	967.5434
	Abz-KAAF	555.2559	555.2967
	AAAAK	431.2617	431.2617
P2-IleFA	Abz-KAIleFAAAAK	1009.5463	1009.5916
	Abz-KAIleF	597.3029	597.3442
	AAAAK	431.2617	431.2647
P2-5^3-F$_3$IleFA	Abz-KA-5^3-F$_3$Ile-FAAAAK	1063.4622	1063.5639
P1'-IleFA	Abz-KAAFIleAAAK	1009.5463	1009.5908
	Abz-KAAF	555.2559	555.2969
	IleAAAK	473.3087	437.3087
P1'-5^3-F$_3$IleFA	Abz-KAAF-5^3-F$_3$Ile-AAAK	1063.4622	1063.5634
	Abz-KAAF	555.2559	555.2969
	5^3-F$_3$Ile-AAAK	527.2246	527.2843
P2'-IleFA	Abz-KAAFAIleAAK	1009.5463	1009.5889
	Abz-KAAF	555.2559	555.2970
	AIleAAK	473.3087	473.3121
P2'-5^3-F$_3$IleFA	Abz-KAAFA-5^3-F$_3$Ile-AAK	1063.4622	1063.5627
	FA-5^3-F$_3$Ile-AAK	674.2930	674.3530
	Abz-KAAFA	626.2930	626.3333
	Abz-KAAF	555.2559	555.2969
	A-5^3-F$_3$Ile-AAK	527.2246	527.2845
	5^3-F$_3$Ile-AAK	456.1875	456.2462

Table 8.3: Identification of the cleavage products of the different peptides by ESI-ToF mass spectrometry after digestion with elastase.

peptide	fragment	$[M + H]^{1+}$ calculated	$[M + H]^{1+}$ observed
FA	Abz-KAAFAAAAK	967.5364	967.5352
	Abz-KAAFAAA	768.3672	768.4080
	Abz-KAAFAA	697.3301	697.3690
	AFAAAAK	649.3673	648.2935
	Abz-KAAFA	626.2930	626.3308
	AAAK	360.2246	360.2238
	AAK	289.1875	289.1872
P2-IleFA	Abz-KAIleFAAAAK	1009.5463	1009.5884
	Abz-KAIleFAAAA	881.4513	881.4960
	Abz-KAIleFAAA	810.4142	810.4960
	Abz-KAIleFAA	739.3771	739.4176
	Abz-KAIleFA	668.3400	668.3787
	FAAAAK	578.3301	578.3322
	AAAK	360.2246	360.2256
	AAK	289.1875	289.1880
	AK	218.1504	218.1505
P2-5³-F₃IleFA	Abz-KA-5³-F₃Ile-FAAAAK	1063.4622	1063.5576
	Abz-KA-5³-F₃Ile-FAAA	864.3301	864.4210
	Abz-KA-5³-F₃Ile-FAA	793.2930	793.3844
	Abz-KA-5³-F₃Ile-FA	722.2559	722.3470
	FAAAAK	578.3301	578.3271
	AAAK	360.2246	360.224
P1'-IleFA	Abz-KAAFIleAAAK	1009.5463	1009.5853
	Abz-KAAFIleAA	810.4142	810.4500
	Abz-KAAFIleA	739.3771	739.4144
	FIleAAAK	620.3771	620.3747
P1'-5³-F₃IleFA	Abz-KAAF-5³-F₃Ile-AAAK	1063.4622	1063.5578
	Abz-KAAF-5³-F₃Ile-AA	864.3301	864.4205
	Abz-KAAF-5³-F₃Ile-A	793.2930	793.3844
	AF-5³-F₃Ile-AAAK	745.3301	745.3814
	AAK	289.1875	289.1857
	AK	218.1504	218.1483
P2'-IleFA	Abz-KAAFAIleAAK	1009.5463	1009.5866
	Abz-KAAFAIleAA	881.4513	881.4910
	Abz-KAAFAIleA	810.4142	810.4539
	Abz-KAAFAIle	739.3771	739.4171
	FAIleAAK	620.3771	620.3687
	Abz-KAA	408.1875	408.2252
P2'-5³-F₃IleFA	Abz-KAAFA-5³-F₃Ile-AAK	1063.4622	1063.5530
	Abz-KAAFA-5³-F₃Ile	793.2930	793.3851
	FA-5³-F₃Ile-AAK	674.2930	674.3441
	Abz-KAA	408.1875	408.2233
	AAK	289.1875	289.1855

Table 8.4: Identification of the cleavage products of the different peptides by ESI-ToF mass spectrometry after digestion with proteinase K.

peptide	fragment	$[M + H]^{1+}$ calculated	$[M + H]^{1+}$ observed
FA	Abz-KAAFAAAAK	967.5364	967.5376
	AFAAAAK	649.3673	649.2762
P2-IleFA	Abz-KAIleFAAAAK	1009.5463	1009.5872
	Abz-KAIleFAAA	810.4142	810.4551
	Abz-KAIleFAA	739.3771	739.4192
	Abz-KAIleFA	668.3400	889.3806
	Abz-KAIleF	597.3029	597.3422
	AAK	289.1875	289.1891
P2-5^3-F$_3$IleFA	Abz-KA-5^3-F$_3$Ile-FAAAAK	1063.4622	1063.5604
	Abz-KA-5^3-F$_3$Ile-FAAA	864.3301	864.4204
	Abz-KA-5^3-F$_3$Ile-FAA	793.2930	793.3895
	Abz-KA-5^3-F$_3$Ile-FA	722.2559	722.3512
	Abz-KA-5^3-F$_3$Ile-F	651.2188	651.3140
	AAAAK	431.2617	430.0513
	AAK	289.1875	289.1888
P1'-IleFA	Abz-KAAFIleAAAK	1009.5463	1009.5878
	Abz-KAAFIleAA	810.4142	810.4545
	Abz-KAAFIleA	739.3771	739.4169
	FIleAAAK	620.3771	620.3795
	Abz-KAA	408.1875	408.2265
	AAK	289.1504	289.1891
P1'-5^3-F$_3$IleFA	Abz-KAAF-5^3-F$_3$Ile-AAAK	1063.4622	1063.5580
	Abz-KAAF-5^3-F$_3$Ile-AA	864.3301	864.4253
	Abz-KAAF-5^3-F$_3$Ile-A	793.2930	793.3853
	F-5^3-F$_3$Ile-AAAK	647.2930	674.3504
	Abz-KAA	408.1875	408.2260
	AAK	289.1875	289.1880
	AK	218.1504	218.1508
P2'-IleFA	Abz-KAAFAIleAAK	1009.5463	1009.5854
	Abz-KAAFA	626.2930	626.338
	FAIleAAK	620.3771	620.3791
	Abz-KAA	408.1875	408.2260
P2'-5^3-F$_3$IleFA	Abz-KAAFA-5^3-F$_3$Ile-AAK	1063.4622	1063.5563
	FA-5^3-F$_3$Ile-AAK	674.2930	674.3496
	Abz-KAA	408.1875	408.2239

9. Bibliography

[1]   D. Voet, J. G. Voet, C. W. Pratt, *Lehrbuch der Biochemie, Vol. 2. aktualis. u. erw. Auflage*, Wiley-VCH, Weinheim, **2010**.

[2]   C. Branden, J. Tooze, *Introduction to Protein Structure, Vol. 2*, Garland Publishing, New York, **1998**.

[3]   D. J. Barlow, J. M. Thornton, Helix geometry in proteins. *J. Mol. Biol.* **1988**, *201*, 601-619.

[4]   A. Lupas, Coiled coils: new structures and new functions. *Trends Biochem. Sci* **1996**, *21*, 375-382.

[5]   P. Burkhard, J. Stetefeld, S. V. Strelkov, Coiled coils: a highly versatile protein folding motif. *Trends Cell Biol.* **2001**, *11*, 82-88.

[6]   http://www.unaids.org/en/resources/documents/2017/2017_data_book, *(accessed June 5th, 2018)*.

[7]   http://www.who.int/hiv/pub/arv/global-aids-update-2016-pub/en/, Global AIDS Update *(accessed June 27th, 2018)*.

[8]   http://www.who.int/hiv/data/en/, *(accessed June 27th, 2018)*.

[9]   E. Mutschler, G. Geisslinger, H. K. Kroemer, P. Ruth, M. Schäfer-Korting, *Mutschler Arzneimittelwirkungen - Lehrbuch der Pharmakologie und Toxikologie, Vol. 9*, Wissenschaftliche Verlagsgesellschaft mbH, Stuttgart, **2008**.

[10]   S. Lien, H. B. Lowman, Therapeutic peptides. *Trends Biotechnol.* **2003**, *21*, 556-562.

[11]   A. K. Sato, M. Viswanathan, R. B. Kent, C. R. Wood, Therapeutic peptides: technological advances driving peptides into development. *Curr. Opin. Biotechnol.* **2006**, *17*, 638-642.

[12]   P. Vlieghe, V. Lisowski, J. Martinez, M. Khrestchatisky, Synthetic therapeutic peptides: science and market. *Drug Discovery Today* **2010**, *15*, 40-56.

[13]   G. H. Bird, N. Madani, A. F. Perry, A. M. Princiotto, J. G. Supko, X. He, E. Gavathiotis, J. G. Sodroski, L. D. Walensky, Hydrocarbon double-stapling remedies the proteolytic instability of a lengthy peptide therapeutic. *Proc. Natl. Acad. Sci.* **2010**, *107*, 14093-14098.

[14]   C. Jäckel, B. Koksch, Fluorine in peptide design and protein engineering. *Eur. J. Org. Chem.* **2005**, *2005*, 4483-4503.

[15]   L. Di, Strategic Approaches to Optimizing Peptide ADME Properties. *AAPS J.* **2015**, *17*, 134-143.

[16]   A. Henninot, J. C. Collins, J. M. Nuss, The Current State of Peptide Drug Discovery: Back to the Future? *J. Med. Chem.* **2018**, *61*, 1382-1414.

[17]   K. Fosgerau, T. Hoffmann, Peptide therapeutics: current status and future directions. *Drug Discovery Today* **2015**, *20*, 122-128.

[18]   W.-G. Forssmann, Y.-H. The, M. Stoll, K. Adermann, U. Albrecht, H.-C. Tillmann, K. Barlos, A. Busmann, A. Canales-Mayordomo, G. Giménez-Gallego, J. Hirsch, J. Jiménez-Barbero, D. Meyer-Olson, J. Münch, J. Pérez-Castells, L. Ständker, F. Kirchhoff, R. E. Schmidt, Short-Term Monotherapy in HIV-Infected Patients with a Virus Entry Inhibitor Against the gp41 Fusion Peptide. *Sci. Transl. Med.* **2010**, *2*, 63re63.

[19]   B. E. Smart, Fluorine substituent effects (on bioactivity). *J. Fluorine Chem.* **2001**, *109*, 3-11.

[20]   H.-J. Böhm, D. Banner, S. Bendels, M. Kansy, B. Kuhn, K. Müller, U. Obst-Sander, M. Stahl, Fluorine in Medicinal Chemistry. *ChemBioChem* **2004**, *5*, 637-643.

[21]   M. Salwiczek, E. K. Nyakatura, U. I. M. Gerling, S. Ye, B. Koksch, Fluorinated amino acids: compatibility with native protein structures and effects on protein-protein interactions. *Chem. Soc. Rev.* **2012**, *41*, 2135-2171.

[22]   H. S. Duewel, E. Daub, V. Robinson, J. F. Honek, Elucidation of Solvent Exposure, Side-Chain Reactivity, and Steric Demands of the Trifluoromethionine Residue in a Recombinant Protein. *Biochemistry* **2001**, *40*, 13167-13176.

[23]   B. C. Buer, J. L. Meagher, J. A. Stuckey, E. N. G. Marsh, Comparison of the structures and stabilities of coiled-coil proteins containing hexafluoroleucine and t-butylalanine provides insight into the stabilizing effects of highly fluorinated amino acid side-chains. *Protein Sci.* **2012**, *21*, 1705-1715.

[24]   B. C. Buer, J. L. Meagher, J. A. Stuckey, E. N. G. Marsh, Structural basis for the enhanced stability of highly fluorinated proteins. *Proc. Natl. Acad. Sci.* **2012**, *109*, 4810-4815.

[25]   S. Purser, P. R. Moore, S. Swallow, V. Gouverneur, Fluorine in medicinal chemistry. *Chem. Soc. Rev.* **2008**, *37*, 320-330.

[26]   D. O'Hagan, Understanding organofluorine chemistry. An introduction to the C-F bond. *Chem. Soc. Rev.* **2008**, *37*, 308-319.

[27]   S. Swallow, Fluorine in Medicinal Chemistry. In *Progress in Medicinal Chemistry, Vol. 54* (Eds.: G. Lawton, D. R. Witty), Elsevier, **2015**, pp. 65-133.

[28]   J. Wang, M. Sánchez-Roselló, J. L. Aceña, C. del Pozo, A. E. Sorochinsky, S. Fustero, V. A. Soloshonok, H. Liu, Fluorine in Pharmaceutical Industry: Fluorine-Containing Drugs Introduced to the Market in the Last Decade (2001–2011). *Chem. Rev.* **2014**, *114*, 2432-2506.

[29]   Y. Zhou, J. Wang, Z. Gu, S. Wang, W. Zhu, J. L. Aceña, V. A. Soloshonok, K. Izawa, H. Liu, Next Generation of Fluorine-Containing Pharmaceuticals, Compounds Currently in Phase II–III Clinical Trials of Major Pharmaceutical Companies: New Structural Trends and Therapeutic Areas. *Chem. Rev.* **2016**, *116*, 422-518.

[30]   D. O'Hagan, Fluorine in health care: Organofluorine containing blockbuster drugs. *J. Fluorine Chem.* **2010**, *131*, 1071-1081.

[31]   A. A. Berger, J.-S. Völler, N. Budisa, B. Koksch, Deciphering the Fluorine Code—The Many Hats Fluorine Wears in a Protein Environment. *Acc. Chem. Res.* **2017**, *50*, 2093-2103.

[32]   E. N. G. Marsh, Fluorinated Proteins: From Design and Synthesis to Structure and Stability. *Acc. Chem. Res.* **2014**, *47*, 2878-2886.

[33]   G. Akcay, K. Kumar, A New Paradigm for Protein Design and Biological Self-Assembly. *J. Fluorine Chem.* **2009**, *130*, 1178-1182.

[34]   A. Bondi, van der Waals Volumes and Radii. *J. Phys. Chem.* **1964**, *68*, 441-451.

[35]   B. C. Buer, B. J. Levin, E. N. G. Marsh, Influence of Fluorination on the Thermodynamics of Protein Folding. *J. Am. Chem. Soc.* **2012**, *134*, 13027-13034.

[36]   Y. Tang, G. Ghirlanda, W. A. Petka, T. Nakajima, W. F. DeGrado, D. A. Tirrell, Fluorinated Coiled-Coil Proteins Prepared In Vivo Display Enhanced Thermal and Chemical Stability. *Angew. Chem. Int. Ed.* **2001**, *40*, 1494-1496.

[37]   T. Nagai, G. Nishioka, M. Koyama, A. Ando, T. Miki, I. Kumadaki, Reactions of trifluoromethyl ketones. IX. Investigation of the steric effect of a trifluoromethyl group based on the stereochemistry on the dehydration of trifluoromethyl homoallyl alcohols. *J. Fluorine Chem.* **1992**, *57*, 229-237.

[38]   M. Molteni, C. Pesenti, M. Sani, A. Volonterio, M. Zanda, Fluorinated peptidomimetics: synthesis, conformational and biological features. *J. Fluorine Chem.* **2004**, *125*, 1735-1743.

[39]   K. Müller, C. Faeh, F. Diederich, Fluorine in Pharmaceuticals: Looking Beyond Intuition. *Science* **2007**, *317*, 1881.

[40]   J. D. Dunitz, Organic Fluorine: Odd Man Out. *ChemBioChem* **2004**, *5*, 614-621.

[41]   B. K. Park, N. R. Kitteringham, P. M. O'Neill, Metabolism of fluorine-containing drugs. *Annu. Rev. Pharmacool. Toxicol.* **2001**, *41*, 443-470.

[42]   J. C. Biffinger, H. W. Kim, S. G. DiMagno, The Polar Hydrophobicity of Fluorinated Compounds. *ChemBioChem* **2004**, *5*, 622-627.

[43]   M. Schlosser, Parametrization of Substituents: Effects of Fluorine and Other Heteroatoms on OH, NH, and CH Acidities. *Angew. Chem. Int. Ed.* **1998**, *37*, 1496-1513.

[44]   M. Rowley, D. J. Hallett, S. Goodacre, C. Moyes, J. Crawforth, T. J. Sparey, S. Patel, R. Marwood, S. Patel, S. Thomas, L. Hitzel, D. O'Connor, N. Szeto, J. L. Castro, P. H. Hutson, A. M. MacLeod, 3-(4-Fluoropiperidin-3-yl)-2-phenylindoles as High Affinity, Selective, and Orally Bioavailable h5-HT2A Receptor Antagonists. *J. Med. Chem.* **2001**, *44*, 1603-1614.

[45]   G. R. Desiraju, Hydrogen Bridges in Crystal Engineering: Interactions without Borders. *Acc. Chem. Res.* **2002**, *35*, 565-573.

[46]   J. D. Dunitz, R. Taylor, Organic Fluorine Hardly Ever Accepts Hydrogen Bonds. *Chem. Eur. J.* **1997**, *3*, 89-98.

[47]   J. A. K. Howard, V. J. Hoy, D. O'Hagan, G. T. Smith, How good is fluorine as a hydrogen bond acceptor? *Tetrahedron* **1996**, *52*, 12613-12622.

[48]   J. A. Olsen, D. W. Banner, P. Seiler, U. Obst Sander, A. D'Arcy, M. Stihle, K. Müller, F. Diederich, A Fluorine Scan of Thrombin Inhibitors to Map the Fluorophilicity/Fluorophobicity of

an Enzyme Active Site: Evidence for C-F···C=O Interactions. *Angew. Chem. Int. Ed.* **2003**, *42*, 2507-2511.

[49] G. Gerebtzoff, X. Li-Blatter, H. Fischer, A. Frentzel, A. Seelig, Halogenation of Drugs Enhances Membrane Binding and Permeation. *ChemBioChem* **2004**, *5*, 676-684.

[50] S. A. Samsonov, M. Salwiczek, G. Anders, B. Koksch, M. T. Pisabarro, Fluorine in Protein Environments: A QM and MD Study. *J. Phys. Chem. B* **2009**, *113*, 16400-16408.

[51] E. Neil, G. Marsh, Towards the nonstick egg: designing fluorous proteins. *Chem. Biol.* **2000**, *7*, R153-R157.

[52] T. Greenway, J. S. Ross, US drug marketing: how does promotion correspond with health value? *BMJ* **2017**, *357*.

[53] https://www.igeahub.com/2017/08/08/top-20-drugs-in-the-world-2017/, *(accesssed June 19th, 2018)*.

[54] K. Sanford, M. Kumar, New proteins in a materials world. *Curr. Opin. Biotechnol.* **2005**, *16*, 416-421.

[55] C. Branden, J. Tooze, Alpha-Domain Structures. In *Introduction to Protein Structure, Vol. 2*, Garland Publishing, New York, **1998**, pp. 35-46.

[56] F. H. C. Crick, Is α-Keratin a Coiled Coil? *Nature* **1952**, *170*, 882.

[57] L. Pauling, R. B. Corey, Compound Helical Configurations of Polypeptide Chains: Structure of Proteins of the α-Keratin Type. *Nature* **1953**, *171*, 59-61.

[58] F. Crick, The Fourier transform of a coiled-coil. *Acta Crystallogr.* **1953**, *6*, 685-689.

[59] F. Crick, The packing of α-helices: simple coiled-coils. *Acta Crystallogr.* **1953**, *6*, 689-697.

[60] E. Wolf, P. S. Kim, B. Berger, MultiCoil: A program for predicting two-and three-stranded coiled coils. *Protein Sci.* **1997**, *6*, 1179-1189.

[61] J. M. Mason, K. M. Arndt, Coiled coil domains: stability, specificity, and biological implications. *ChemBioChem* **2004**, *5*, 170-176.

[62] J. Liu, Q. Zheng, Y. Deng, C.-S. Cheng, N. R. Kallenbach, M. Lu, A seven-helix coiled coil. *Proc. Natl. Acad. Sci.* **2006**, *103*, 15457.

[63] R. S. Hodges, De novo design of α-helical proteins: basic research to medical applications. *Biochem. Cell Biol.* **1996**, *74*, 133-154.

[64] Y. B. Yu, Coiled-coils: stability, specificity, and drug delivery potential. *Adv. Drug Delivery Rev.* **2002**, *54*, 1113-1129.

[65] A. D. McLachlan, M. Stewart, Tropomyosin coiled-coil interactions: Evidence for an unstaggered structure. *J. Mol. Biol.* **1975**, *98*, 293-304.

[66] P. Burkhard, M. Meier, A. Lustig, Design of a minimal protein oligomerization domain by a structural approach. *Protein Sci.* **2000**, *9*, 2294-2301.

[67] W. D. Kohn, C. T. Mant, R. S. Hodges, α-Helical protein assembly motifs. *J. Biol. Chem.* **1997**, *272*, 2583-2586.

[68] O. D. Testa, E. Moutevelis, D. N. Woolfson, CC+: a relational database of coiled-coil structures. *Nucleic Acids Res.* **2009**, *37*, D315-D322.

[69] J. F. Conway, D. A. D. Parry, Three-stranded α-fibrous proteins: the heptad repeat and its implications for structure. *Int. J. Biol. Macromol.* **1991**, *13*, 14-16.

[70] E. K. O'Shea, R. Rutkowski, P. S. Kim, Mechanism of specificity in the Fos-Jun oncoprotein heterodimer. *Cell* **1992**, *68*, 699-708.

[71] E. K. O'Shea, K. J. Lumb, P. S. Kim, Peptide Velcro : Design of a heterodimeric coiled coil. *Curr. Biol.* **1993**, *3*, 658-667.

[72] T. J. Graddis, D. G. Myszka, I. M. Chaiken, Controlled formation of model homo- and heterodimer coiled coil polypeptides. *Biochemistry* **1993**, *32*, 12664-12671.

[73] W. D. Kohn, C. M. Kay, R. S. Hodges, Protein destabilization by electrostatic repulsions in the two-stranded α-helical coiled-coil/leucine zipper. *Protein Sci.* **1995**, *4*, 237-250.

[74] Y. Yu, O. D. Monera, R. S. Hodges, P. L. Privalov, Ion Pairs Significantly Stabilize Coiled-coils in the Absence of Electrolyte. *J. Mol. Biol.* **1996**, *255*, 367-372.

[75] Y. B. Yu, P. Lavigne, P. L. Privalov, R. S. Hodges, The Measure of Interior Disorder in a Folded Protein and Its Contribution to Stability. *J. Am. Chem. Soc.* **1999**, *121*, 8443-8449.

[76]   D. L. McClain, H. L. Woods, M. G. Oakley, Design and characterization of a heterodimeric coiled coil that forms exclusively with an antiparallel relative helix orientation. *J. Am. Chem. Soc.* **2001**, *123*, 3151-3152.

[77]   P. Burkhard, S. Ivaninskii, A. Lustig, Improving coiled-coil stability by optimizing ionic interactions. *J. Mol. Biol.* **2002**, *318*, 901-910.

[78]   D. N. Woolfson, The Design of Coiled-Coil Structures and Assemblies. In *Adv. Protein Chem., Vol. 70* (Eds.: D. A. D. Parry, J. M. Squire), Academic Press, Cambridge, **2005**, pp. 79-112.

[79]   M. Salwiczek, S. Samsonov, T. Vagt, E. Nyakatura, E. Fleige, J. Numata, H. Cölfen, M. T. Pisabarro, B. Koksch, Position-Dependent Effects of Fluorinated Amino Acids on the Hydrophobic Core Formation of a Heterodimeric Coiled Coil. *Chem. Eur. J.* **2009**, *15*, 7628-7636.

[80]   J. F. Conway, D. A. D. Parry, Structural features in the heptad substructure and longer range repeats of two-stranded α-fibrous proteins. *Int. J. Biol. Macromol.* **1990**, *12*, 328-334.

[81]   N. E. Zhou, C. M. Kay, R. S. Hodges, Synthetic model proteins: the relative contribution of leucine residues at the nonequivalent positions of the 3-4 hydrophobic repeat to the stability of the two-stranded α-helical coiled-coil. *Biochemistry* **1992**, *31*, 5739-5746.

[82]   N. E. Zhou, C. M. Kay, R. S. Hodges, Synthetic model proteins. Positional effects of interchain hydrophobic interactions on stability of two-stranded α-helical coiled-coils. *J. Biol. Chem.* **1992**, *267*, 2664-2670.

[83]   K. Wagschal, B. Tripet, C. Mant, R. S. Hodges, P. Lavigne, The role of position a in determining the stability and oligomerization state of α-helical coiled coils: 20 amino acid stability coefficients in the hydrophobic core of proteins. *Protein Sci.* **1999**, *8*, 2312-2329.

[84]   B. Tripet, K. Wagschal, P. Lavigne, C. T. Mant, R. S. Hodges, Effects of side-chain characteristics on stability and oligomerization state of a *de Novo*-designed model coiled-coil: 20 amino acid substitutions in position "d". *J. Mol. Biol.* **2000**, *300*, 377-402.

[85]   P. B. Harbury, P. S. Kim, T. Alber, Crystal structure of an isoleucine-zipper trimer. *Nature* **1994**, *371*, 80-83.

[86]   P. B. Harbury, T. Zhang, P. S. Kim, T. Alber, A switch between two-, three-, and four-stranded coiled coils in GCN4 leucine zipper mutants. *Science* **1993**, *262*, 1401-1407.

[87]   Y. Tang, G. Ghirlanda, N. Vaidehi, J. Kua, D. T. Mainz, W. A. Goddard, W. F. DeGrado, D. A. Tirrell, Stabilization of Coiled-Coil Peptide Domains by Introduction of Trifluoroleucine. *Biochemistry* **2001**, *40*, 2790-2796.

[88]   Y. Tang, D. A. Tirrell, Biosynthesis of a Highly Stable Coiled-Coil Protein Containing Hexafluoroleucine in an Engineered Bacterial Host. *J. Am. Chem. Soc.* **2001**, *123*, 11089-11090.

[89]   O. D. Monera, F. D. Sönnichsen, L. Hicks, C. M. Kay, R. S. Hodges, The relative positions of alanine residues in the hydrophobic core control the formation of two-stranded or four-stranded α-helical coiled-coils. *Protein Eng.* **1996**, *9*, 353-363.

[90]   M. G. Oakley, P. S. Kim, A buried polar interaction can direct the relative orientation of helices in a coiled coil. *Biochemistry* **1998**, *37*, 12603-12610.

[91]   J. P. Schneider, J. D. Lear, W. F. DeGrado, A designed buried salt bridge in a heterodimeric coiled coil. *J. Am. Chem. Soc.* **1997**, *119*, 5742-5743.

[92]   A. N. Lupas, J. Bassler, Coiled Coils – A Model System for the 21st Century. *Trends Biochem. Sci* **2017**, *42*, 130-140.

[93]   E. K. O'Shea, J. D. Klemm, P. S. Kim, T. Alber, X-ray structure of the GCN4 leucine zipper, a two-stranded, parallel coiled coil. *Science* **1991**, *254*, 539-544.

[94]   D. C. Chan, D. Fass, J. M. Berger, P. S. Kim, Core Structure of gp41 from the HIV Envelope Glycoprotein. *Cell* **1997**, *89*, 263-273.

[95]   W. D. Kohn, R. S. Hodges, De novo design of α-helical coiled coils and bundles: models for the development of protein-design principles. *Trends Biotechnol.* **1998**, *16*, 379-389.

[96]   H. Chao, D. L. Bautista, J. Litowski, R. T. Irvin, R. S. Hodges, Use of a heterodimeric coiled-coil system for biosensor application and affinity purification. *J. Chromatogr. B: Biomed. Sci. Appl.* **1998**, *715*, 307-329.

[97]   A. A. McFarlane, G. L. Orriss, J. Stetefeld, The use of coiled-coil proteins in drug delivery systems. *Eur. J. Pharmacol.* **2009**, *625*, 101-107.

[98]   B. Bilgiçer, A. Fichera, K. Kumar, A Coiled Coil with a Fluorous Core. *J. Am. Chem. Soc.* **2001**, *123*, 4393-4399.

[99]   L. Gonzalez Jr, J. J. Plecs, T. Alber, An engineered allosteric switch in leucine-zipper oligomerization. *Nat. Struct. Biol.* **1996**, *3*, 510-515.

[100]   L. Gonzalez Jr, D. N. Woolfson, T. Alber, Buried polar residues and structural specificity in the GCN4 leucine zipper. *Nat. Struct. Biol.* **1996**, *3*, 1011–1018.

[101]   J. K. Montclare, S. Son, G. A. Clark, K. Kumar, D. A. Tirrell, Biosynthesis and Stability of Coiled-Coil Peptides Containing (2*S*,4*R*)-5,5,5-Trifluoroleucine and (2*S*,4*S*)-5,5,5-Trifluoroleucine. *ChemBioChem* **2009**, *10*, 84-86.

[102]   S. Son, I. C. Tanrikulu, D. A. Tirrell, Stabilization of bzip Peptides through Incorporation of Fluorinated Aliphatic Residues. *ChemBioChem* **2006**, *7*, 1251-1257.

[103]   B. Bilgiçer, X. Xing, K. Kumar, Programmed Self-Sorting of Coiled Coils with Leucine and Hexafluoroleucine Cores. *J. Am. Chem. Soc.* **2001**, *123*, 11815-11816.

[104]   B. Bilgiçer, K. Kumar, Synthesis and thermodynamic characterization of self-sorting coiled coils. *Tetrahedron* **2002**, *58*, 4105-4112.

[105]   N. C. Yoder, K. Kumar, Fluorinated amino acids in protein design and engineering. *Chem. Soc. Rev.* **2002**, *31*, 335-341.

[106]   H.-Y. Lee, K.-H. Lee, H. M. Al-Hashimi, E. N. G. Marsh, Modulating Protein Structure with Fluorous Amino Acids: Increased Stability and Native-like Structure Conferred on a 4-Helix Bundle Protein by Hexafluoroleucine. *J. Am. Chem. Soc.* **2006**, *128*, 337-343.

[107]   K.-H. Lee, H.-Y. Lee, M. M. Slutsky, J. T. Anderson, E. N. G. Marsh, Fluorous Effect in Proteins: De Novo Design and Characterization of a Four-α-Helix Bundle Protein Containing Hexafluoroleucine. *Biochemistry* **2004**, *43*, 16277-16284.

[108]   B. C. Buer, R. de la Salud-Bea, H. M. Al Hashimi, E. N. G. Marsh, Engineering Protein Stability and Specificity Using Fluorous Amino Acids: The Importance of Packing Effects. *Biochemistry* **2009**, *48*, 10810-10817.

[109]   S. S. Pendley, Y. B. Yu, T. E. Cheatham, Molecular dynamics guided study of salt bridge length dependence in both fluorinated and non-fluorinated parallel dimeric coiled-coils. *Proteins: Struct., Funct., Bioinf.* **2009**, *74*, 612-629.

[110]   T. Panchenko, W. W. Zhu, J. K. Montclare, Influence of global fluorination on chloramphenicol acetyltransferase activity and stability. *Biotechnol. Bioeng.* **2006**, *94*, 921-930.

[111]   J. K. Montclare, D. A. Tirrell, Evolving Proteins of Novel Composition. *Angew. Chem. Int. Ed.* **2006**, *45*, 4518-4521.

[112]   M. G. Woll, E. B. Hadley, S. Mecozzi, S. H. Gellman, Stabilizing and Destabilizing Effects of Phenylalanine → F5-Phenylalanine Mutations on the Folding of a Small Protein. *J. Am. Chem. Soc.* **2006**, *128*, 15932-15933.

[113]   H. Zheng, K. Comeforo, J. Gao, Expanding the Fluorous Arsenal: Tetrafluorinated Phenylalanines for Protein Design. *J. Am. Chem. Soc.* **2008**, *131*, 18-19.

[114]   C. Jäckel, W. Seufert, S. Thust, B. Koksch, Evaluation of the Molecular Interactions of Fluorinated Amino Acids with Native Polypeptides. *ChemBioChem* **2004**, *5*, 717-720.

[115]   C. Jäckel, M. Salwiczek, B. Koksch, Fluorine in a Native Protein Environment—How the Spatial Demand and Polarity of Fluoroalkyl Groups Affect Protein Folding. *Angew. Chem. Int. Ed.* **2006**, *45*, 4198-4203.

[116]   K. Pagel, K. Seeger, B. Seiwert, A. Villa, A. E. Mark, S. Berger, B. Koksch, Advanced approaches for the characterization of a de novo designed antiparallel coiled coil peptide. *Org. Biomol. Chem.* **2005**, *3*, 1189-1194.

[117]   M. Salwiczek, Biophysical Aspects of Single Fluoroalkylamino Acid Substitutions within a Natural Polypeptide Environment. Dissertation, Freie Universität Berlin, Department of Biology, Chemistry and Pharmacy, **2010**.

[118]   T. Vagt, E. Nyakatura, M. Salwiczek, C. Jackel, B. Koksch, Towards identifying preferred interaction partners of fluorinated amino acids within the hydrophobic environment of a dimeric coiled coil peptide. *Org. Biomol. Chem.* **2010**, *8*, 1382-1386.

[119]   E. K. Nyakatura, O. Reimann, T. Vagt, M. Salwiczek, B. Koksch, Accommodating fluorinated amino acids in a helical peptide environment. *RSC Adv.* **2013**, *3*, 6319-6322.

[120] C. J. Pace, D. Kim, J. Gao, Experimental Evaluation of CH–π Interactions in a Protein Core. *Chem. Eur. J.* **2012**, *18*, 5832-5836.

[121] M. Brandl, M. S. Weiss, A. Jabs, J. Sühnel, R. Hilgenfeld, C-h···π-interactions in proteins. *J. Mol. Biol.* **2001**, *307*, 357-377.

[122] M. Nishio, Y. Umezawa, J. Fantini, M. S. Weiss, P. Chakrabarti, CH-π hydrogen bonds in biological macromolecules. *Phys. Chem. Chem. Phys.* **2014**, *16*, 12648-12683.

[123] A. Anbarasu, S. Anand, M. M. Babu, R. Sethumadhavan, Investigations on C–H···π interactions in RNA binding proteins. *Int. J. Biol. Macromol.* **2007**, *41*, 251-259.

[124] L. M. Salonen, M. Ellermann, F. Diederich, Aromatic Rings in Chemical and Biological Recognition: Energetics and Structures. *Angew. Chem. Int. Ed.* **2011**, *50*, 4808-4842.

[125] M. Kumar, P. V. Balaji, C-H…pi interactions in proteins: prevalence, pattern of occurrence, residue propensities, location, and contribution to protein stability. *J. Mol. Model.* **2014**, *20*, 2136.

[126] T. Steiner, The Hydrogen Bond in the Solid State. *Angew. Chem. Int. Ed.* **2002**, *41*, 48-76.

[127] M. Nishio, The CH/π hydrogen bond in chemistry. Conformation, supramolecules, optical resolution and interactions involving carbohydrates. *Phys. Chem. Chem. Phys.* **2011**, *13*, 13873-13900.

[128] O. Takahashi, Y. Kohno, M. Nishio, Relevance of Weak Hydrogen Bonds in the Conformation of Organic Compounds and Bioconjugates: Evidence from Recent Experimental Data and High-Level ab Initio MO Calculations. *Chem. Rev.* **2010**, *110*, 6049-6076.

[129] V. Shanthi, K. Ramanathan, R. Sethumadhavan, Exploring the Role of C–H….π Interactions on the Structural Stability of Single Chain "All-Alpha" Proteins. *Appl. Biochem. Biotechnol.* **2010**, *160*, 1473-1483.

[130] H. Zheng, J. Gao, Highly Specific Heterodimerization Mediated by Quadrupole Interactions. *Angew. Chem. Int. Ed.* **2010**, *49*, 8635-8639.

[131] R. B. Hill, W. F. DeGrado, Solution Structure of α2D, a Nativelike de Novo Designed Protein. *J. Am. Chem. Soc.* **1998**, *120*, 1138-1145.

[132] C. J. Pace, H. Zheng, R. Mylvaganam, D. Kim, J. Gao, Stacked Fluoroaromatics as Supramolecular Synthons for Programming Protein Dimerization Specificity. *Angew. Chem. Int. Ed.* **2012**, *51*, 103-107.

[133] C. J. Pace, J. Gao, Exploring and Exploiting Polar−π Interactions with Fluorinated Aromatic Amino Acids. *Acc. Chem. Res.* **2012**, *46*, 907-915.

[134] U. I. M. Gerling, M. Salwiczek, C. D. Cadicamo, H. Erdbrink, C. Czekelius, S. L. Grage, P. Wadhwani, A. S. Ulrich, M. Behrends, G. Haufe, B. Koksch, Fluorinated amino acids in amyloid formation: a symphony of size, hydrophobicity and α-helix propensity. *Chem. Sci.* **2014**, *5*, 819-830.

[135] H. Erdbrink, E. K. Nyakatura, S. Huhmann, U. I. M. Gerling, D. Lentz, B. Koksch, C. Czekelius, Synthesis of enantiomerically pure (2*S*,3*S*)-5,5,5-trifluoroisoleucine and (2*R*,3*S*)-5,5,5-trifluoro-allo-isoleucine. *Beilstein J. Org. Chem.* **2013**, *9*, 2009-2014.

[136] J. R. Robalo, S. Huhmann, B. Koksch, A. Vila Verde, The Multiple Origins of the Hydrophobicity of Fluorinated Apolar Amino Acids. *Chem* **2017**, *3*, 881-897.

[137] M. S. Weiss, J. Metzner Hubert, R. Hilgenfeld, Two non-proline cis peptide bonds may be important for factor XIII function. *FEBS Lett.* **1998**, *423*, 291-296.

[138] M. J. Plevin, D. L. Bryce, J. Boisbouvier, Direct detection of CH/π interactions in proteins. *Nat. Chem.* **2010**, *2*, 466-471.

[139] Y. Umezawa, M. Nishio, CH/π Interactions as demonstrated in the crystal structure of guanine-nucleotide binding proteins, Src homology-2 domains and human growth hormone in complex with their specific ligands. *Biorg. Med. Chem.* **1998**, *6*, 493-504.

[140] G. B. Santos, A. Ganesan, F. S. Emery, Oral Administration of Peptide-Based Drugs: Beyond Lipinski's Rule. *ChemMedChem* **2016**, *11*, 2245-2251.

[141] B. Koksch, N. Sewald, H.-J. Hofmann, K. Burger, H.-D. Jakubke, Proteolytically stable peptides by incorporation of α-Tfm amino acids. *J. Pept. Sci.* **1997**, *3*, 157-167.

[142] B. Koksch, N. Sewald, K. Burger, H. D. Jakubke, Peptide modification by incorporation of α-trifluoromethyl substituted amino acids. *Amino Acids* **1996**, *11*, 425-434.

[143] R. Smits, B. Koksch, How C$^\alpha$-Fluoroalkyl Amino Acids and Peptides Interact with Enzymes:Studies Concerning the Influence on Proteolytic Stability, Enzymatic Resolution and Peptide Coupling. *Curr. Top. Med. Chem.* **2006**, *6*, 1483-1498.

[144] H. Meng, K. Kumar, Antimicrobial Activity and Protease Stability of Peptides Containing Fluorinated Amino Acids. *J. Am. Chem. Soc.* **2007**, *129*, 15615-15622.

[145] H. Meng, S. T. Krishnaji, M. Beinborn, K. Kumar, Influence of Selective Fluorination on the Biological Activity and Proteolytic Stability of Glucagon-like Peptide-1. *J. Med. Chem.* **2008**, *51*, 7303-7307.

[146] L. M. Gottler, H. Y. Lee, C. E. Shelburne, A. Ramamoorthy, E. N. Marsh, Using fluorous amino acids to modulate the biological activity of an antimicrobial peptide. *ChemBioChem* **2008**, *9*, 370-373.

[147] C. B. Park, K.-S. Yi, K. Matsuzaki, M. S. Kim, S. C. Kim, Structure–activity analysis of buforin II, a histone H2A-derived antimicrobial peptide: The proline hinge is responsible for the cell-penetrating ability of buforin II. *Proc. Natl. Acad. Sci.* **2000**, *97*, 8245.

[148] H.-C. Chen, J. H. Brown, J. L. Morell, C. M. Huang, Synthetic magainin analogues with improved antimicrobial activity. *FEBS Lett.* **1988**, *236*, 462-466.

[149] F. Porcelli, B. A. Buck-Koehntop, S. Thennarasu, A. Ramamoorthy, G. Veglia, Structures of the Dimeric and Monomeric Variants of Magainin Antimicrobial Peptides (MSI-78 and MSI-594) in Micelles and Bilayers, Determined by NMR Spectroscopy. *Biochemistry* **2006**, *45*, 5793-5799.

[150] C. F. Deacon, M. A. Nauck, M. Toft-Nielsen, L. Pridal, B. Willms, J. J. Holst, Both Subcutaneously and Intravenously Administered Glucagon-Like Peptide I Are Rapidly Degraded From the NH2-Terminus in Type II Diabetic Patients and in Healthy Subjects. *Diabetes* **1995**, *44*, 1126.

[151] J. J. Holst, C. F. Deacon, Glucagon-like peptide 1 and inhibitors of dipeptidyl peptidase IV in the treatment of type 2 diabetes mellitus. *Curr. Opin. Pharmacol.* **2004**, *4*, 589-596.

[152] D. J. Drucker, Development of Glucagon-Like Peptide-1-Based Pharmaceuticals as Therapeutic Agents for the Treatment of Diabetes. *Curr. Pharm. Des.* **2001**, *7*, 1399-1412.

[153] W. H. Vine, K.-H. Hsieh, G. R. Marshall, Synthesis of fluorine-containing peptides. Analogs of angiotensin II containing hexafluorovaline. *J. Med. Chem.* **1981**, *24*, 1043-1047.

[154] K. H. Hsieh, P. Needleman, G. R. Marshall, Long-acting angiotensin II inhibitors containing hexafluorovaline in position 8. *J. Med. Chem.* **1987**, *30*, 1097-1100.

[155] A. Khanna, S. W. English, X. S. Wang, K. Ham, J. Tumlin, H. Szerlip, L. W. Busse, L. Altaweel, T. E. Albertson, C. Mackey, M. T. McCurdy, D. W. Boldt, S. Chock, P. J. Young, K. Krell, R. G. Wunderink, M. Ostermann, R. Murugan, M. N. Gong, R. Panwar, J. Hästbacka, R. Favory, B. Venkatesh, B. T. Thompson, R. Bellomo, J. Jensen, S. Kroll, L. S. Chawla, G. F. Tidmarsh, A. M. Deane, Angiotensin II for the Treatment of Vasodilatory Shock. *N. Engl. J. Med.* **2017**, *377*, 419-430.

[156] M. B. Kaufman, Pharmaceutical Approval Update. *Pharm. Ther.* **2018**, *43*, 141-170.

[157] L. M. Gottler, R. de la Salud-Bea, E. N. G. Marsh, The Fluorous Effect in Proteins: Properties of α4F6, a 4-α-Helix Bundle Protein with a Fluorocarbon Core. *Biochemistry* **2008**, *47*, 4484-4490.

[158] I. Schechter, A. Berger, On the size of the active site in proteases. I. Papain. *Biochem. Biophys. Res. Commun.* **1967**, *27*, 157-162.

[159] V. Asante, J. Mortier, H. Schlüter, B. Koksch, Impact of fluorination on proteolytic stability of peptides in human blood plasma. *Biorg. Med. Chem.* **2013**, *21*, 3542-3546.

[160] V. Asante, J. Mortier, G. Wolber, B. Koksch, Impact of fluorination on proteolytic stability of peptides: a case study with α-chymotrypsin and pepsin. *Amino Acids* **2014**, *46*, 2733-2744.

[161] L. Hedstrom, Serine Protease Mechanism and Specificity. *Chem. Rev.* **2002**, *102*, 4501-4524.

[162] J. Antal, G. Pál, B. Asbóth, Z. Buzás, A. Patthy, L. Gráf, Specificity Assay of Serine Proteinases by Reverse-Phase High-Performance Liquid Chromatography Analysis of Competing Oligopeptide Substrate Library. *Anal. Biochem.* **2001**, *288*, 156-167.

[163] N. Voloshchuk, A. Y. Zhu, D. Snydacker, J. K. Montclare, Positional effects of monofluorinated phenylalanines on histone acetyltransferase stability and activity. *Biorg. Med. Chem. Lett.* **2009**, *19*, 5449-5451.

[164] N. Budisa, W. Wenger, B. Wiltschi, Residue-specific global fluorination of Candida antarctica lipase B in Pichia pastoris. *Mol. BioSyst.* **2010**, *6*, 1630-1639.

[165] S. J. Middendorp, J. Wilbs, C. Quarroz, S. Calzavarini, A. Angelillo-Scherrer, C. Heinis, Peptide Macrocycle Inhibitor of Coagulation Factor XII with Subnanomolar Affinity and High Target Selectivity. *J. Med. Chem.* **2017**, *60*, 1151-1158.

[166] J. Piekielna, R. Perlikowska, J. C. do-Rego, J.-L. do-Rego, M. C. Cerlesi, G. Calo, A. Kluczyk, K. Łapiński, C. Tömböly, A. Janecka, Synthesis of Mixed Opioid Affinity Cyclic Endomorphin-2 Analogues with Fluorinated Phenylalanines. *ACS Med. Chem. Lett.* **2015**, *6*, 579-583.

[167] A. Łęgowska, D. Dębowski, A. Lesner, M. Wysocka, K. Rolka, Introduction of non-natural amino acid residues into the substrate-specific P1 position of trypsin inhibitor SFTI-1 yields potent chymotrypsin and cathepsin G inhibitors. *Biorg. Med. Chem.* **2009**, *17*, 3302-3307.

[168] C. Hashimoto, T. Tanaka, T. Narumi, W. Nomura, H. Tamamura, The successes and failures of HIV drug discovery. *Expert Opin. Drug Discov.* **2011**, *6*, 1067-1090.

[169] M. J. Gomara, I. Haro, Updating the Use of Synthetic Peptides as Inhibitors of HIV-1 Entry. *Curr. Med. Chem.* **2014**, *21*, 1188-1200.

[170] L. R. Cirrincione, K. K. Scarsi, Drug Interactions in HIV: Nucleoside, Nucleotide, and Nonnucleoside Reverse Transcriptase Inhibitors and Entry Inhibitors. In *Drug Interactions in Infectious Diseases: Antimicrobial Drug Interactions* (Eds.: M. P. Pai, J. J. Kiser, P. O. Gubbins, K. A. Rodvold), Springer International Publishing AG, Cham, **2018**, pp. 297-356.

[171] P. Patel, S. Louie, Drug Interactions in HIV: Protease and Integrase Inhibitors. In *Drug Interactions in Infectious Diseases: Antimicrobial Drug Interactions* (Eds.: M. P. Pai, J. J. Kiser, P. O. Gubbins, K. A. Rodvold), Springer International Publishing AG, Cham, **2018**, pp. 255-295.

[172] Y.-S. Han, T. Mesplède, M. A. Wainberg, HIV-1 Resistance to Integrase Inhibitors. In *Antimicrobial Drug Resistance: Mechanisms of Drug Resistance, Vol. 1* (Eds.: D. L. Mayers, J. D. Sobel, M. Ouellette, K. S. Kaye, D. Marchaim), Springer International Publishing AG, Cham, **2017**, pp. 559-564.

[173] N. Sluis-Cremer, HIV-1 Resistance to the Nonnucleoside Reverse Transcriptase Inhibitors. In *Antimicrobial Drug Resistance: Mechanisms of Drug Resistance, Vol. 1* (Eds.: D. L. Mayers, J. D. Sobel, M. Ouellette, K. S. Kaye, D. Marchaim), Springer International Publishing AG, Cham, **2017**, pp. 521-533.

[174] N. K. Yilmaz, C. A. Schiffer, Drug Resistance to HIV-1 Protease Inhibitors: Molecular Mechanisms and Substrate Coevolution. In *Antimicrobial Drug Resistance: Mechanisms of Drug Resistance, Vol. 1* (Eds.: D. L. Mayers, J. D. Sobel, M. Ouellette, K. S. Kaye, D. Marchaim), Springer International Publishing AG, Cham, **2017**, pp. 535-544.

[175] B. D. Herman, R. A. Domaoal, M. Ehteshami, R. F. Schinazi, Resistance Mechanisms to HIV-1 Nucleoside Reverse Transcriptase Inhibitors. In *Antimicrobial Drug Resistance: Mechanisms of Drug Resistance, Vol. 1* (Eds.: D. L. Mayers, J. D. Sobel, M. Ouellette, K. S. Kaye, D. Marchaim), Springer International Publishing AG, Cham, **2017**, pp. 503-519.

[176] C. M. Venner, A. N. Ratcliff, M. Coutu, A. Finzi, E. J. Arts, HIV-1 Entry and Fusion Inhibitors: Mechanisms and Resistance. In *Antimicrobial Drug Resistance: Mechanisms of Drug Resistance, Vol. 1* (Eds.: D. L. Mayers, J. D. Sobel, M. Ouellette, K. S. Kaye, D. Marchaim), Springer International Publishing AG, Cham, **2017**, pp. 545-557.

[177] K. Qian, L. Morris-Natschke Susan, K.-H. Lee, HIV entry inhibitors and their potential in HIV therapy. *Med. Res. Rev.* **2008**, *29*, 369-393.

[178] S. Liu, S. Wu, S. Jiang, HIV Entry Inhibitors Targeting gp41: From Polypeptides to Small-Molecule Compounds. *Curr. Pharm. Des.* **2007**, *13*, 143-162.

[179] D. M. Eckert, P. S. Kim, Mechanisms of viral membrane fusion and its inhibition. *Annu. Rev. Biochem.* **2001**, *70*, 777-810.

[180] D. Eggink, B. Berkhout, R. W. Sanders, Inhibition of HIV-1 by Fusion Inhibitors. *Curr. Pharm. Des.* **2010**, *16*, 3716-3728.

[181] I. Steffen, S. Pöhlmann, Peptide-Based Inhibitors of the HIV Envelope Protein and Other Class I Viral Fusion Proteins. *Curr. Pharm. Des.* **2010**, *16*, 1143-1158.

[182] F. Naider, J. Anglister, Peptides in the treatment of AIDS. *Curr. Opin. Struct. Biol.* **2009**, *19*, 473-482.

[183]   D. C. Chan, P. S. Kim, HIV Entry and Its Inhibition. *Cell* **1998**, *93*, 681-684.

[184]   G. Löffler, Viren. In *Basiswissen Biochemie: mit Pathobiochemie, Vol. 7* (Ed.: G. Löffler), Springer Berlin Heidelberg, Berlin, Heidelberg, **2008**, pp. 287-294.

[185]   W. Weissenhorn, A. Dessen, S. C. Harrison, J. J. Skehel, D. C. Wiley, Atomic structure of the ectodomain from HIV-1 gp41. *Nature* **1997**, *387*, 426-430.

[186]   J. C. Tilton, R. W. Doms, Entry inhibitors in the treatment of HIV-1 infection. *Antiviral Res.* **2010**, *85*, 91-100.

[187]   J. A. Esté, A. Telenti, HIV entry inhibitors. *Lancet* **2007**, *370*, 81-88.

[188]   V. Buzon, G. Natrajan, D. Schibli, F. Campelo, M. M. Kozlov, W. Weissenhorn, Crystal structure of HIV-1 gp41 including both fusion peptide and membrane proximal external regions. *PLoS Pathog.* **2010**, *6*, e1000880.

[189]   G. B. Melikyan, R. M. Markosyan, H. Hemmati, M. K. Delmedico, D. M. Lambert, F. S. Cohen, Evidence that the transition of HIV-1 gp41 into a six-helix bundle, not the bundle configuration, induces membrane fusion. *J. Cell Biol.* **2000**, *151*, 413-423.

[190]   C. Magnus, P. Rusert, S. Bonhoeffer, A. Trkola, R. R. Regoes, Estimating the Stoichiometry of Human Immunodeficiency Virus Entry. *J. Virol.* **2009**, *83*, 1523-1531.

[191]   R. M. Markosyan, F. S. Cohen, G. B. Melikyan, G. Guidotti, HIV-1 Envelope Proteins Complete Their Folding into Six-helix Bundles Immediately after Fusion Pore Formation. *Mol. Biol. Cell* **2002**, *14*, 926-938.

[192]   R. M. Markosyan, M. Y. Leung, F. S. Cohen, The Six-Helix Bundle of Human Immunodeficiency Virus Env Controls Pore Formation and Enlargement and Is Initiated at Residues Proximal to the Hairpin Turn. *J. Virol.* **2009**, *83*, 10048-10057.

[193]   D. C. Chan, C. T. Chutkowski, P. S. Kim, Evidence that a prominent cavity in the coiled coil of HIV type 1 gp41 is an attractive drug target. *Proc. Natl. Acad. Sci.* **1998**, *95*, 15613-15617.

[194]   Y. He, J. Cheng, J. Li, Z. Qi, H. Lu, M. Dong, S. Jiang, Q. Dai, Identification of a critical motif for the human immunodeficiency virus type 1 (HIV-1) gp41 core structure: implications for designing novel anti-HIV fusion inhibitors. *J. Virol.* **2008**, *82*, 6349-6358.

[195]   K. Tan, J.-h. Liu, J.-h. Wang, S. Shen, M. Lu, Atomic structure of a thermostable subdomain of HIV-1 gp41. *Proc. Natl. Acad. Sci.* **1997**, *94*, 12303-12308.

[196]   Y. He, S. Liu, W. Jing, H. Lu, D. Cai, D. J. Chin, A. K. Debnath, F. Kirchhoff, S. Jiang, Conserved Residue Lys574 in the Cavity of HIV-1 Gp41 Coiled-coil Domain Is Critical for Six-helix Bundle Stability and Virus Entry. *J. Biol. Chem.* **2007**, *282*, 25631-25639.

[197]   D. M. Eckert, V. N. Malashkevich, L. H. Hong, P. A. Carr, P. S. Kim, Inhibiting HIV-1 entry: discovery of D-peptide inhibitors that target the gp41 coiled-coil pocket. *Cell* **1999**, *99*, 103-115.

[198]   M. Lu, P. S. Kim, A Trimeric Structural Subdomain of the HIV-1 Transmembrane Glycoprotein. *J. Biomol. Struct. Dyn.* **1997**, *15*, 465-471.

[199]   Y. He, J. Cheng, H. Lu, J. Li, J. Hu, Z. Qi, Z. Liu, S. Jiang, Q. Dai, Potent HIV fusion inhibitors against Enfuvirtide-resistant HIV-1 strains. *Proc. Natl. Acad. Sci.* **2008**, *105*, 16332-16337.

[200]   C. T. Wild, D. C. Shugars, T. K. Greenwell, C. B. McDanal, T. J. Matthews, Peptides corresponding to a predictive α-helical domain of human immunodeficiency virus type 1 gp41 are potent inhibitors of virus infection. *Proc. Natl. Acad. Sci.* **1994**, *91*, 9770-9774.

[201]   J. M. Kilby, S. Hopkins, T. M. Venetta, B. DiMassimo, G. A. Cloud, J. Y. Lee, L. Alldredge, E. Hunter, D. Lambert, D. Bolognesi, T. Matthews, M. R. Johnson, M. A. Nowak, G. M. Shaw, M. S. Saag, Potent suppression of HIV-1 replication in humans by T-20, a peptide inhibitor of gp41-mediated virus entry. *Nat. Med.* **1998**, *4*, 1302-1307.

[202]   H. Chong, X. Yao, Z. Qiu, B. Qin, R. Han, S. Waltersperger, M. Wang, S. Cui, Y. He, Discovery of critical residues for viral entry and inhibition through structural Insight of HIV-1 fusion inhibitor CP621–652. *J. Biol. Chem.* **2012**, *287*, 20281-20289.

[203]   Y. Kliger, S. A. Gallo, S. G. Peisajovich, I. Muñoz-Barroso, S. Avkin, R. Blumenthal, Y. Shai, Mode of action of an antiviral peptide from HIV-1 inhibition at a post-lipid mixing stage. *J. Biol. Chem.* **2001**, *276*, 1391-1397.

[204]   S. Veiga, S. Henriques, N. C. Santos, M. Castanho, Putative role of membranes in the HIV fusion inhibitor enfuvirtide mode of action at the molecular level. *Biochem. J.* **2004**, *377*, 107-110.

[205] J. P. Lalezari, K. Henry, M. O'Hearn, J. S. G. Montaner, P. J. Piliero, B. Trottier, S. Walmsley, C. Cohen, D. R. Kuritzkes, J. J. Eron, J. Chung, R. DeMasi, L. Donatacci, C. Drobnes, J. Delehanty, M. Salgo, Enfuvirtide, an HIV-1 Fusion Inhibitor, for Drug-Resistant HIV Infection in North and South America. *N. Engl. J. Med.* **2003**, *348*, 2175-2185.

[206] A. Lazzarin, B. Clotet, D. Cooper, J. Reynes, K. Arastéh, M. Nelson, C. Katlama, H.-J. Stellbrink, J.-F. Delfraissy, J. Lange, L. Huson, R. DeMasi, C. Wat, J. Delehanty, C. Drobnes, M. Salgo, Efficacy of Enfuvirtide in Patients Infected with Drug-Resistant HIV-1 in Europe and Australia. *N. Engl. J. Med.* **2003**, *348*, 2186-2195.

[207] M. L. Duffalo, C. W. James, Enfuvirtide: A Novel Agent for the Treatment of HIV-1 Infection. *Ann. Pharmacother.* **2003**, *37*, 1448-1456.

[208] V. D. Trivedi, S. F. Cheng, C. W. Wu, R. Karthikeyan, C. J. Chen, D. K. Chang, The LLSGIV stretch of the *N*-terminal region of HIV-1 gp41 is critical for binding to a model peptide, T20. *Protein Eng.* **2003**, *16*, 311-317.

[209] L. T. Rimsky, D. C. Shugars, T. J. Matthews, Determinants of Human Immunodeficiency Virus Type 1 Resistance to gp41-Derived Inhibitory Peptides. *J. Virol.* **1998**, *72*, 986-993.

[210] M. L. Greenberg, N. Cammack, Resistance to enfuvirtide, the first HIV fusion inhibitor. *J. Antimicrob. Chemother.* **2004**, *54*, 333-340.

[211] C. A. Derdeyn, J. M. Decker, J. N. Sfakianos, Z. Zhang, W. A. O'Brien, L. Ratner, G. M. Shaw, E. Hunter, Sensitivity of Human Immunodeficiency Virus Type 1 to Fusion Inhibitors Targeted to the gp41 First Heptad Repeat Involves Distinct Regions of gp41 and Is Consistently Modulated by gp120 Interactions with the Coreceptor. *J. Virol.* **2001**, *75*, 8605-8614.

[212] M. Kinomoto, M. Yokoyama, H. Sato, A. Kojima, T. Kurata, K. Ikuta, T. Sata, K. Tokunaga, Amino Acid 36 in the Human Immunodeficiency Virus Type 1 gp41 Ectodomain Controls Fusogenic Activity: Implications for the Molecular Mechanism of Viral Escape from a Fusion Inhibitor. *J. Virol.* **2005**, *79*, 5996-6004.

[213] C. V. Fletcher, Enfuvirtide, a new drug for HIV infection. *Lancet* **2003**, *361*, 1577-1578.

[214] S. E. Schneider, B. L. Bray, C. J. Mader, P. E. Friedrich, M. W. Anderson, T. S. Taylor, N. Boshernitzan, T. E. Niemi, B. C. Fulcher, S. R. Whight, J. M. White, R. J. Greene, L. E. Stoltenberg, M. Lichty, Development of HIV fusion inhibitors. *J. Pept. Sci.* **2005**, *11*, 744-753.

[215] A. Lazzarin, Enfuvirtide: the first HIV fusion inhibitor. *Expert. Opin. Pharmacother.* **2005**, *6*, 453-464.

[216] A. Otaka, M. Nakamura, D. Nameki, E. Kodama, S. Uchiyama, S. Nakamura, H. Nakano, H. Tamamura, Y. Kobayashi, M. Matsuoka, N. Fujii, Remodeling of gp41-C34 Peptide Leads to Highly Effective Inhibitors of the Fusion of HIV-1 with Target Cells. *Angew. Chem. Int. Ed.* **2002**, *41*, 2937-2940.

[217] S. Wang, J. York, W. Shu, M. O. Stoller, J. H. Nunberg, M. Lu, Interhelical Interactions in the gp41 Core: Implications for Activation of HIV-1 Membrane Fusion. *Biochemistry* **2002**, *41*, 7283-7292.

[218] H. Mo, A. K. Konstantinidis, K. D. Stewart, T. Dekhtyar, T. Ng, K. Swift, E. D. Matayoshi, W. Kati, W. Kohlbrenner, A. Molla, Conserved residues in the coiled-coil pocket of human immunodeficiency virus type 1 gp41 are essential for viral replication and interhelical interaction. *Virology* **2004**, *329*, 319-327.

[219] S. Jiang, A. K. Debnath, A Salt Bridge between an *N*-terminal Coiled Coil of gp41 and an Antiviral Agent Targeted to the gp41 Core Is Important for Anti-HIV-1 Activity. *Biochem. Biophys. Res. Commun.* **2000**, *270*, 153-157.

[220] Y. He, S. Liu, J. Li, H. Lu, Z. Qi, Z. Liu, A. K. Debnath, S. Jiang, Conserved Salt Bridge between the *N*- and *C*-Terminal Heptad Repeat Regions of the Human Immunodeficiency Virus Type 1 gp41 Core Structure Is Critical for Virus Entry and Inhibition. *J. Virol.* **2008**, *82*, 11129-11139.

[221] M. Gochin, L. Cai, The Role of Amphiphilicity and Negative Charge in Glycoprotein 41 Interactions in the Hydrophobic Pocket. *J. Med. Chem.* **2009**, *52*, 4338-4344.

[222] H. Chong, X. Yao, J. Sun, Z. Qiu, M. Zhang, S. Waltersperger, M. Wang, S. Cui, Y. He, The MT hook structure is critical for design of HIV-1 fusion inhibitors. *J. Biol. Chem.* **2012**, *287*, 34558-34568.

[223] F. Gaston, C. Granados Giovana , S. Madurga, F. Rabanal, F. Lakhdar-Ghazal, E. Giralt, E. Bahraoui, Development and Characterization of Peptidic Fusion Inhibitors Derived from HIV-1 gp41 with Partial D-Amino Acid Substitutions. *ChemMedChem* **2009**, *4*, 570-581.

[224] Y. He, Y. Xiao, H. Song, Q. Liang, D. Ju, X. Chen, H. Lu, W. Jing, S. Jiang, L. Zhang, Design and Evaluation of Sifuvirtide, a Novel HIV-1 Fusion Inhibitor. *J. Biol. Chem.* **2008**, *283*, 11126-11134.

[225] S. Jiang, K. Lin, N. Strick, A. R. Neurath, HIV-1 inhibition by a peptide. *Nature* **1993**, *365*, 113.

[226] S. Jiang, K. Lin, Effect of amino acid replacements, additions and deletions on the antiviral activity of a peptide derived from the HIV-1 GP41 sequence. *Pept. Res.* **1995**, *8*, 345-348.

[227] E. Noah, Z. Biron, F. Naider, B. Arshava, J. Anglister, The Membrane Proximal External Region of the HIV-1 Envelope Glycoprotein gp41 Contributes to the Stabilization of the Six-Helix Bundle Formed with a Matching N′ Peptide. *Biochemistry* **2008**, *47*, 6782-6792.

[228] H. Nishikawa, S. Nakamura, E. Kodama, S. Ito, K. Kajiwara, K. Izumi, Y. Sakagami, S. Oishi, T. Ohkubo, Y. Kobayashi, A. Otaka, N. Fujii, M. Matsuoka, Electrostatically constrained α-helical peptide inhibits replication of HIV-1 resistant to enfuvirtide. *Int. J. Biochem. Cell Biol.* **2009**, *41*, 891-899.

[229] T. Naito, K. Izumi, E. Kodama, Y. Sakagami, K. Kajiwara, H. Nishikawa, K. Watanabe, S. G. Sarafianos, S. Oishi, N. Fujii, SC29EK, a peptide fusion inhibitor with enhanced α-helicity, inhibits replication of human immunodeficiency virus type 1 mutants resistant to enfuvirtide. *Antimicrob. Agents Chemother.* **2009**, *53*, 1013-1018.

[230] Y. Su, H. Chong, S. Xiong, Y. Qiao, Z. Qiu, Y. He, Genetic Pathway of HIV-1 Resistance to Novel Fusion Inhibitors Targeting the Gp41 Pocket. *J. Virol.* **2015**, *89*, 12467-12479.

[231] Y. Su, H. Chong, Z. Qiu, S. Xiong, Y. He, Mechanism of HIV-1 Resistance to Short-Peptide Fusion Inhibitors Targeting the Gp41 Pocket. *J. Virol.* **2015**, *89*, 5801-5811.

[232] H. Chong, X. Yao, Z. Qiu, J. Sun, M. Zhang, S. Waltersperger, M. Wang, S.-L. Liu, S. Cui, Y. He, Short-peptide fusion inhibitors with high potency against wild-type and enfuvirtide-resistant HIV-1. *FASEB J.* **2012**, *27*, 1203-1213.

[233] S. K. Sia, P. A. Carr, A. G. Cochran, V. N. Malashkevich, P. S. Kim, Short constrained peptides that inhibit HIV-1 entry. *Proc. Natl. Acad. Sci.* **2002**, *99*, 14664–14669.

[234] J. J. Dwyer, K. L. Wilson, D. K. Davison, S. A. Freel, J. E. Seedorff, S. A. Wring, N. A. Tvermoes, T. J. Matthews, M. L. Greenberg, M. K. Delmedico, Design of helical, oligomeric HIV-1 fusion inhibitor peptides with potent activity against enfuvirtide-resistant virus. *Proc. Natl. Acad. Sci.* **2007**, *104*, 12772-12777.

[235] D. Eggink, C. E. Baldwin, Y. Deng, J. P. M. Langedijk, M. Lu, R. W. Sanders, B. Berkhout, Selection of T1249-Resistant Human Immunodeficiency Virus Type 1 Variants. *J. Virol.* **2008**, *82*, 6678-6688.

[236] D.-K. Chang, C.-S. Hsu, Biophysical evidence of two docking sites of the carboxyl heptad repeat region within the amino heptad repeat region of gp41 of human immunodeficiency virus type 1. *Antiviral Res.* **2007**, *74*, 51-58.

[237] M. L. Heil, J. M. Decker, J. N. Sfakianos, G. M. Shaw, E. Hunter, C. A. Derdeyn, Determinants of Human Immunodeficiency Virus Type 1 Baseline Susceptibility to the Fusion Inhibitors Enfuvirtide and T-649 Reside outside the Peptide Interaction Site. *J. Virol.* **2004**, *78*, 7582-7589.

[238] C. C. LaBranche, G. Galasso, J. P. Moore, D. P. Bolognesi, M. S. Hirsch, S. M. Hammer, HIV fusion and its inhibition. *Antiviral Res.* **2001**, *50*, 95-115.

[239] J. P. Lalezari, N. C. Bellos, K. Sathasivam, G. J. Richmond, C. J. Cohen, J. R. A. Myers, D. H. Henry, C. Raskino, T. Melby, H. Murchison, Y. Zhang, R. Spence, M. L. Greenberg, R. A. DeMasi, G. D. Miralles, T-1249 Retains Potent Antiretroviral Activity in Patients Who Had Experienced Virological Failure while on an Enfuvirtide-Containing Treatment Regimen. *J. Infect. Dis.* **2005**, *191*, 1155-1163.

[240] J. J. Eron, R. M. Gulick, J. A. Bartlett, T. Merigan, R. Arduino, J. M. Kilby, B. Yangco, A. Diers, C. Drobnes, R. DeMasi, M. Greenberg, T. Melby, C. Raskino, P. Rusnak, Y. Zhang, R. Spence, G. D. Miralles, Short-Term Safety and Antiretroviral Activity of T-1249, a Second-Generation Fusion Inhibitor of HIV. *J. Infect. Dis.* **2004**, *189*, 1075-1083.

[241] M. Lu, S. C. Blacklow, P. S. Kim, A trimeric structural domain of the HIV-1 transmembrane glycoprotein. *Nat. Struct. Biol.* **1995**, *2*, 1075-1082.

[242] H. Chong, Z. Qiu, J. Sun, Y. Qiao, X. Li, Y. He, Two M-T hook residues greatly improve the antiviral activity and resistance profile of the HIV-1 fusion inhibitor SC29EK. *Retrovirology* **2014**, *11*, 40.

[243] H. Chong, X. Yao, Z. Qiu, J. Sun, Y. Qiao, M. Zhang, M. Wang, S. Cui, Y. He, The M-T hook structure increases the potency of HIV-1 fusion inhibitor sifuvirtide and overcomes drug resistance. *J. Antimicrob. Chemother.* **2014**, *69*, 2759-2769.

[244] S. Xiong, P. Borrego, X. Ding, Y. Zhu, A. Martins, H. Chong, N. Taveira, Y. He, A Helical Short-Peptide Fusion Inhibitor with Highly Potent Activity against Human Immunodeficiency Virus Type 1 (HIV-1), HIV-2, and Simian Immunodeficiency Virus. *J. Virol.* **2017**, *91*, e01839 - 01816.

[245] J. Tan, H. Yuan, C. Li, X. Zhang, C. Wang, Insights into the Functions of M-T Hook Structure in HIV Fusion Inhibitor Using Molecular Modeling. *Comput. Biol. Chem.* **2016**, *61*, 202-209.

[246] L. M. Johnson, W. S. Horne, S. H. Gellman, Broad Distribution of Energetically Important Contacts across an Extended Protein Interface. *J. Am. Chem. Soc.* **2011**, *133*, 10038-10041.

[247] L. D. Walensky, A. L. Kung, I. Escher, T. J. Malia, S. Barbuto, R. D. Wright, G. Wagner, G. L. Verdine, S. J. Korsmeyer, Activation of Apoptosis in Vivo by a Hydrocarbon-Stapled BH3 Helix. *Science* **2004**, *305*, 1466.

[248] B. D. Welch, A. P. VanDemark, A. Heroux, C. P. Hill, M. S. Kay, Potent D-peptide inhibitors of HIV-1 entry. *Proc. Natl. Acad. Sci.* **2007**, *104*, 16828-16833.

[249] M. L. Bellows, M. S. Taylor, P. A. Cole, L. Shen, R. F. Siliciano, H. K. Fung, C. A. Floudas, Discovery of Entry Inhibitors for HIV-1 via a New De Novo Protein Design Framework. *Biophys. J.* **2010**, *99*, 3445-3453.

[250] D. Wang, M. Lu, S. Arora Paramjit Inhibition of HIV-1 Fusion by Hydrogen-Bond-Surrogate-Based α-Helices. *Angew. Chem. Int. Ed.* **2008**, *47*, 1879-1882.

[251] E. K. Nyakatura, Studying the Interaction Profiles of Nonnatural Amino Acids – Towards Predicting their Specific Applications at α-Helical Interfaces. Dissertation, Freie Universität Berlin, Department of Biology, Chemistry and Pharmacy, **2013**.

[252] J. Münch, L. Ständker, K. Adermann, A. Schulz, M. Schindler, R. Chinnadurai, S. Pöhlmann, C. Chaipan, T. Biet, T. Peters, B. Meyer, D. Wilhelm, H. Lu, W. Jing, S. Jiang, W.-G. Forssmann, F. Kirchhoff, Discovery and Optimization of a Natural HIV-1 Entry Inhibitor Targeting the gp41 Fusion Peptide. *Cell* **2007**, *129*, 263-275.

[253] C. Fasting, A. Schalley Christoph, M. Weber, O. Seitz, S. Hecht, B. Koksch, J. Dernedde, C. Graf, E.-W. Knapp, R. Haag, Multivalency as a Chemical Organization and Action Principle. *Angew. Chem. Int. Ed.* **2012**, *51*, 10472-10498.

[254] B. D. Welch, J. N. Francis, J. S. Redman, S. Paul, M. T. Weinstock, J. D. Reeves, Y. S. Lie, F. G. Whitby, D. M. Eckert, C. P. Hill, M. J. Root, M. S. Kay, Design of a Potent D-Peptide HIV-1 Entry Inhibitor with a Strong Barrier to Resistance. *J. Virol.* **2010**, *84*, 11235-11244.

[255] J. N. Francis, J. S. Redman, D. M. Eckert, M. S. Kay, Design of a Modular Tetrameric Scaffold for the Synthesis of Membrane-Localized d-Peptide Inhibitors of HIV-1 Entry. *Bioconjugate Chem.* **2012**, *23*, 1252-1258.

[256] A. Pessi, A. Langella, E. Capitò, S. Ghezzi, E. Vicenzi, G. Poli, T. Ketas, C. Mathieu, R. Cortese, B. Horvat, A. Moscona, M. Porotto, A General Strategy to Endow Natural Fusion-protein-Derived Peptides with Potent Antiviral Activity. *PLoS One* **2012**, *7*, e36833.

[257] T. Nakahara, W. Nomura, K. Ohba, A. Ohya, T. Tanaka, C. Hashimoto, T. Narumi, T. Murakami, N. Yamamoto, H. Tamamura, Remodeling of Dynamic Structures of HIV-1 Envelope Proteins Leads to Synthetic Antigen Molecules Inducing Neutralizing Antibodies. *Bioconjugate Chem.* **2010**, *21*, 709-714.

[258] W. Nomura, C. Hashimoto, A. Ohya, K. Miyauchi, E. Urano, T. Tanaka, T. Narumi, T. Nakahara, A. Komano Jun, N. Yamamoto, H. Tamamura, A Synthetic C34 Trimer of HIV-1 gp41 Shows Significant Increase in Inhibition Potency. *ChemMedChem* **2012**, *7*, 205-208.

[259] W. Nomura, C. Hashimoto, T. Suzuki, N. Ohashi, M. Fujino, T. Murakami, N. Yamamoto, H. Tamamura, Multimerized CHR-derived peptides as HIV-1 fusion inhibitors. *Biorg. Med. Chem.* **2013**, *21*, 4452-4458.

[260]   Y. Ling, H. Xue, X. Jiang, L. Cai, K. Liu, Increase of anti-HIV activity of C-peptide fusion inhibitors using a bivalent drug design approach. *Biorg. Med. Chem. Lett.* **2013**, *23*, 4770-4773.

[261]   J. P. Tam, Q. Yu, A Facile Ligation Approach to Prepare Three-Helix Bundles of HIV Fusion-State Protein Mimetics. *Org. Lett.* **2002**, *4*, 4167-4170.

[262]   M. J. Root, M. S. Kay, P. S. Kim, Protein Design of an HIV-1 Entry Inhibitor. *Science* **2001**, *291*, 884-888.

[263]   J. M. Louis, C. A. Bewley, G. M. Clore, Design and Properties of NCCG-gp41, a Chimeric gp41 Molecule with Nanomolar HIV Fusion Inhibitory Activity. *J. Biol. Chem.* **2001**, *276*, 29485-29489.

[264]   L. Ni, J. Zhu, J. Zhang, M. Yan, G. F. Gao, P. Tien, Design of recombinant protein-based SARS-CoV entry inhibitors targeting the heptad-repeat regions of the spike protein S2 domain. *Biochem. Biophys. Res. Commun.* **2005**, *330*, 39-45.

[265]   M. Lu, H. Ji, S. Shen, Subdomain Folding and Biological Activity of the Core Structure from Human Immunodeficiency Virus Type 1 gp41: Implications for Viral Membrane Fusion. *J. Virol.* **1999**, *73*, 4433-4438.

[266]   L. Ni, G. F. Gao, P. Tien, Rational design of highly potent HIV-1 fusion inhibitory proteins: Implication for developing antiviral therapeutics. *Biochem. Biophys. Res. Commun.* **2005**, *332*, 831-836.

[267]   C. Hashimoto, W. Nomura, A. Ohya, E. Urano, K. Miyauchi, T. Narumi, H. Aikawa, J. A. Komano, N. Yamamoto, H. Tamamura, Evaluation of a synthetic C34 trimer of HIV-1 gp41 as AIDS vaccines. *Biorg. Med. Chem.* **2012**, *20*, 3287-3291.

[268]   W. Nomura, T. Mizuguchi, H. Tamamura, Multimerized HIV-gp41-derived peptides as fusion inhibitors and vaccines. *Pept. Sci.* **2015**, *106*, 622-628.

[269]   V. Sofiyev, H. Kaur, B. A. Snyder, P. A. Hogan, R. G. Ptak, P. Hwang, M. Gochin, Enhanced potency of bivalent small molecule gp41 inhibitors. *Biorg. Med. Chem.* **2017**, *25*, 408-420.

[270]   H. Erdbrink, I. Peuser, U. I. M. Gerling, D. Lentz, B. Koksch, C. Czekelius, Conjugate hydrotrifluoromethylation of α,β-unsaturated acyl-oxazolidinones: synthesis of chiral fluorinated amino acids. *Org. Biomol. Chem.* **2012**, *10*, 8583-8586.

[271]   J. M. Kovacs, C. T. Mant, R. S. Hodges, Determination of intrinsic hydrophilicity/hydrophobicity of amino acid side chains in peptides in the absence of nearest-neighbor or conformational effects. *Pept. Sci.* **2006**, *84*, 283-297.

[272]   Y. H. Zhao, M. H. Abraham, A. M. Zissimos, Fast Calculation of van der Waals Volume as a Sum of Atomic and Bond Contributions and Its Application to Drug Compounds. *J. Org. Chem.* **2003**, *68*, 7368-7373.

[273]   H.-P. Chiu, Y. Suzuki, D. Gullickson, R. Ahmad, B. Kokona, R. Fairman, R. P. Cheng, Helix Propensity of Highly Fluorinated Amino Acids. *J. Am. Chem. Soc.* **2006**, *128*, 15556-15557.

[274]   H.-P. Chiu, R. P. Cheng, Chemoenzymatic Synthesis of (*S*)-Hexafluoroleucine and (*S*)-Tetrafluoroleucine. *Org. Lett.* **2007**, *9*, 5517-5520.

[275]   A. Chakrabartty, T. Kortemme, R. L. Baldwin, Helix propensities of the amino acids measured in alanine-based peptides without helix-stabilizing side-chain interactions. *Protein Sci.* **1994**, *3*, 843-852.

[276]   A. J. Doig, A. Chakrabartty, T. M. Klingler, R. L. Baldwin, Determination of Free Energies of *N*-Capping in α-Helixes by Modification of the Lifson-Roig Helix-Coil Theory To Include *N*- and *C*-Capping. *Biochemistry* **1994**, *33*, 3396-3403.

[277]   N. H. Andersen, H. Tong, Empirical parameterization of a model for predicting peptide helix/coil equilibrium populations. *Protein Sci.* **1997**, *6*, 1920-1936.

[278]   D. L. Minor, P. S. Kim, Measurement of the β-sheet-forming propensities of amino acids. *Nature* **1994**, *367*, 660-663.

[279]   M. Salwiczek, B. Koksch, Effects of Fluorination on the Folding Kinetics of a Heterodimeric Coiled Coil. *ChemBioChem* **2009**, *10*, 2867-2870.

[280]   M. Salwiczek, P. Mikhailiuk, S. Afonin, I. Komarov, A. Ulrich, B. Koksch, Compatibility of the conformationally rigid CF3-Bpg side chain with the hydrophobic coiled-coil interface. *Amino Acids* **2010**, *39*, 1589-1593.

[281] K. Folmert, Four Models for Peptide Engineering. Dissertation, Freie Universität Berlin, Department of Biology, Chemistry and Pharmacy, **2017**.

[282] D. M. Shotton, Elastase. In *Methods Enzymol., Vol. 19*, Academic Press, **1970**, pp. 113-140.

[283] M. A. Naughton, F. Sanger, Purification and specificity of pancreatic elastase. *Biochem. J.* **1961**, *78*, 156-163.

[284] P. J. Sweeney, J. M. Walker, Proteinase K (EC 3.4.21.14). In *Enzymes of Molecular Biology* (Ed.: M. M. Burrell), Humana Press, Totowa, NJ, **1993**, pp. 305-311.

[285] Y. Umezawa, S. Tsuboyama, H. Takahashi, J. Uzawa, M. Nishio, CH/π interaction in the conformation of peptides. A database study. *Biorg. Med. Chem.* **1999**, *7*, 2021-2026.

[286] O. Takahashi, Y. Kohno, S. Iwasaki, K. Saito, M. Iwaoka, S. Tomoda, Y. Umezawa, S. Tsuboyama, M. Nishio, Hydrogen-Bond-Like Nature of the CH/π Interaction as Evidenced by Crystallographic Database Analyses and Ab Initio Molecular Orbital Calculations. *Bull. Chem. Soc. Jpn.* **2001**, *74*, 2421-2430.

[287] M. Nishio, The CH/π hydrogen bond: Implication in chemistry. *J. Mol. Struct.* **2012**, *1018*, 2-7.

[288] S. Huhmann, Towards fluorinated HIV entry inhibitors. Master thesis, Freie Universität Berlin, Department of Biology, Chemistry and Pharmacy, **2013**.

[289] M. Quibell, T. Johnson, Difficult peptides. In *Fmoc Soild Phase Peptide Synthesis - A Practical Approach* (Eds.: W. C. Chan, P. D. White), Oxford University Press, Oxford, **2000**, pp. 115-136.

[290] P. D. White, W. C. Chan, Basic principles. In *Fmoc Soild Phase Peptide Synthesis - A Practical Approach* (Eds.: W. C. Chan, P. D. White), Oxford University Press, Oxford, **2000**, pp. 9-40.

[291] S. A. Palasek, Z. J. Cox, J. M. Collins, Limiting racemization and aspartimide formation in microwave-enhanced Fmoc solid phase peptide synthesis. *J. Pept. Sci.* **2007**, *13*, 143-148.

[292] S. L. Pedersen, A. P. Tofteng, L. Malik, K. J. Jensen, Microwave heating in solid-phase peptide synthesis. *Chem. Soc. Rev.* **2012**, *41*, 1826-1844.

[293] J. M. Collins, K. A. Porter, S. K. Singh, G. S. Vanier, High-Efficiency Solid Phase Peptide Synthesis (HE-SPPS). *Org. Lett.* **2014**, *16*, 940-943.

[294] H. Rodríguez, M. Suarez, F. Albericio, A convenient microwave-enhanced solid-phase synthesis of short chain N-methyl-rich peptides. *J. Pept. Sci.* **2010**, *16*, 136-140.

[295] R. Sampson Wayne, H. Patsiouras, J. Ede Nicholas, The synthesis of 'difficult' peptides using 2-hydroxy-4-methoxybenzyl or pseudoproline amino acid building blocks: a comparative study. *J. Pept. Sci.* **1999**, *5*, 403-409.

[296] M. Keller, A. D. Miller, Access to the inaccessible sequence of Cpn 60.1 (195–217) by temporary oxazolidine protection of selected amide bonds. *Biorg. Med. Chem. Lett.* **2001**, *11*, 857-859.

[297] P. White, W. Keyte John, K. Bailey, G. Bloomberg, Expediting the Fmoc solid phase synthesis of long peptides through the application of dimethyloxazolidine dipeptides. *J. Pept. Sci.* **2003**, *10*, 18-26.

[298] A. Abedini, D. P. Raleigh, Incorporation of Pseudoproline Derivatives Allows the Facile Synthesis of Human IAPP, a Highly Amyloidogenic and Aggregation-Prone Polypeptide. *Org. Lett.* **2005**, *7*, 693-696.

[299] F. García-Martín, P. White, R. Steinauer, S. Côté, J. Tulla-Puche, F. Albericio, The synergy of ChemMatrix resin® and pseudoproline building blocks renders Rantes, a complex aggregated chemokine. *Pept. Sci.* **2006**, *84*, 566-575.

[300] K. Page, A. Hood Christina, H. Patel, G. Fuentes, M. Menakuru, H. Park Jae, Fast Fmoc synthesis of hAmylin1–37 with pseudoproline assisted on-resin disulfide formation. *J. Pept. Sci.* **2007**, *13*, 833-838.

[301] Y. M. Coïc, L. Lan Charlotte, J. M. Neumann, N. Jamin, F. Baleux, Slightly modifying pseudoproline dipeptides incorporation strategy enables solid phase synthesis of a 54 AA fragment of caveolin-1 encompassing the intramembrane domain. *J. Pept. Sci.* **2009**, *16*, 98-104.

[302] T. Haack, M. Mutter, Serine derived oxazolidines as secondary structure disrupting, solubilizing building blocks in peptide synthesis. *Tetrahedron Lett.* **1992**, *33*, 1589-1592.

[303] M. Mutter, A. Nefzi, T. Sato, F. Wahl, T. Wöhr, Pseudo-prolines (psi Pro) for accessing "inaccessible" peptides. *Pept. Res.* **1995**, *8*, 145-153.

[304] T. Wöhr, F. Wahl, A. Nefzi, B. Rohwedder, T. Sato, X. Sun, M. Mutter, Pseudo-Prolines as a Solubilizing, Structure-Disrupting Protection Technique in Peptide Synthesis. *J. Am. Chem. Soc.* **1996**, *118*, 9218-9227.

[305] T. M. Postma, F. Albericio, Cysteine Pseudoprolines for Thiol Protection and Peptide Macrocyclization Enhancement in Fmoc-Based Solid-Phase Peptide Synthesis. *Org. Lett.* **2014**, *16*, 1772-1775.

[306] P. Dumy, M. Keller, D. E. Ryan, B. Rohwedder, T. Wöhr, M. Mutter, Pseudo-Prolines as a Molecular Hinge: Reversible Induction of cis Amide Bonds into Peptide Backbones. *J. Am. Chem. Soc.* **1997**, *119*, 918-925.

[307] G. A. Cremer, H. Tariq, F. Delmas Agnes, Combining a polar resin and a pseudo-proline to optimize the solid-phase synthesis of a 'difficult sequence'. *J. Pept. Sci.* **2006**, *12*, 437-442.

[308] S. E. Northfield, K. D. Roberts, S. J. Mountford, R. A. Hughes, D. Kaiserman, M. Mangan, R. N. Pike, P. I. Bird, P. E. Thompson, Synthesis of "Difficult" Fluorescence Quenched Substrates of Granzyme C. *Int. J. Pept. Res. Ther.* **2010**, *16*, 159-165.

[309] Y. Wexler-Cohen, B. T. Johnson, A. Puri, R. Blumenthal, Y. Shai, Structurally Altered Peptides Reveal an Important Role for N-terminal Heptad Repeat Binding and Stability in the Inhibitory Action of HIV-1 Peptide DP178. *J. Biol. Chem.* **2006**, *281*, 9005-9010.

[310] S. Huhmann, E. K. Nyakatura, H. Erdbrink, U. I. M. Gerling, C. Czekelius, B. Koksch, Effects of single substitutions with hexafluoroleucine and trifluorovaline on the hydrophobic core formation of a heterodimeric coiled coil. *J. Fluorine Chem.* **2015**, *175*, 32-35.

[311] M. M. Pierce, C. S. Raman, B. T. Nall, Isothermal Titration Calorimetry of Protein–Protein Interactions. *Methods* **1999**, *19*, 213-221.

[312] S. Leavitt, E. Freire, Direct measurement of protein binding energetics by isothermal titration calorimetry. *Curr. Opin. Struct. Biol.* **2001**, *11*, 560-566.

[313] A. Velazquez-Campoy, E. Freire, Isothermal titration calorimetry to determine association constants for high-affinity ligands. *Nat. Protoc.* **2006**, *1*, 186.

[314] M. W. Freyer, E. A. Lewis, Isothermal Titration Calorimetry: Experimental Design, Data Analysis, and Probing Macromolecule/Ligand Binding and Kinetic Interactions. In *Methods in Cell Biology, Vol. 84*, Academic Press, **2008**, pp. 79-113.

[315] J. L. Cole, V. M. Garsky, Thermodynamics of Peptide Inhibitor Binding to HIV-1 gp41. *Biochemistry* **2001**, *40*, 5633-5641.

[316] P. Murphy Kenneth, D. Xie, S. Thompson Kelly, L. M. Amzel, E. Freire, Entropy in biological binding processes: Estimation of translational entropy loss. *Proteins: Struct., Funct., Bioinf.* **1994**, *18*, 63-67.

[317] David J. Huggins, Quantifying the Entropy of Binding for Water Molecules in Protein Cavities by Computing Correlations. *Biophys. J.* **2015**, *108*, 928-936.

[318] J. D. Dunitz, Win some, lose some: enthalpy-entropy compensation in weak intermolecular interactions. *Chem. Biol.* **1995**, *2*, 709-712.

[319] J. Cavanagh, M. Akke, May the driving force be with you — whatever it is. *Nat. Struct. Biol.* **2000**, *7*, 11-13.

[320] N. London, D. Movshovitz-Attias, O. Schueler-Furman, The Structural Basis of Peptide-Protein Binding Strategies. *Structure* **2010**, *18*, 188-199.

[321] K. Sharp, Entropy—enthalpy compensation: Fact or artifact? *Protein Sci.* **2008**, *10*, 661-667.

[322] A. Cooper, C. M. Johnson, J. H. Lakey, M. Nöllmann, Heat does not come in different colours: entropy–enthalpy compensation, free energy windows, quantum confinement, pressure perturbation calorimetry, solvation and the multiple causes of heat capacity effects in biomolecular interactions. *Biophys. Chem.* **2001**, *93*, 215-230.

[323] P. Pattnaik, Surface plasmon resonance. *Appl. Biochem. Biotechnol.* **2005**, *126*, 79-92.

[324] M. Beseničar, P. Maček, J. H. Lakey, G. Anderluh, Surface plasmon resonance in protein–membrane interactions. *Chem. Phys. Lipids* **2006**, *141*, 169-178.

[325] J. Homola, Surface Plasmon Resonance Sensors for Detection of Chemical and Biological Species. *Chem. Rev.* **2008**, *108*, 462-493.

[326] P. Cao, G. Dou, Y. Cheng, J. Che, The improved efficacy of Sifuvirtide compared with enfuvirtide might be related to its selectivity for the rigid biomembrane, as determined through surface plasmon resonance. *PLoS One* **2017**, *12*, e0171567.

[327] D. G. Myszka, R. W. Sweet, P. Hensley, M. Brigham-Burke, P. D. Kwong, W. A. Hendrickson, R. Wyatt, J. Sodroski, M. L. Doyle, Energetics of the HIV gp120-CD4 binding reaction. *Proc. Natl. Acad. Sci.* **2000**, *97*, 9026–9031.

[328] S. M. Alam, C. Paleos, H.-X. Liao, R. Scearce, J. Robinson, B. F Haynes, An inducible HIV type 1 gp41 HR-2 peptide-binding site on HIV type 1 envelope gp120. *AIDS Res. Hum. Retroviruses* **2004**, *20*, 836-845.

[329] A. E. Hamburger, S. Kim, B. D. Welch, M. S. Kay, Steric Accessibility of the HIV-1 gp41 *N*-trimer Region. *J. Biol. Chem.* **2005**, *280*, 12567-12572.

[330] S. A. Gallo, W. Wang, S. S. Rawat, G. Jung, A. J. Waring, A. M. Cole, H. Lu, X. Yan, N. L. Daly, D. J. Craik, S. Jiang, R. I. Lehrer, R. Blumenthal, θ-Defensins Prevent HIV-1 Env-mediated Fusion by Binding gp41 and Blocking 6-Helix Bundle Formation. *J. Biol. Chem.* **2006**, *281*, 18787-18792.

[331] H. Wang, Z. Qi, A. Guo, Q. Mao, H. Lu, X. An, C. Xia, X. Li, A. K. Debnath, S. Wu, S. Liu, S. Jiang, ADS-J1 Inhibits Human Immunodeficiency Virus Type 1 Entry by Interacting with the gp41 Pocket Region and Blocking Fusion-Active gp41 Core Formation. *Antimicrob. Agents Chemother.* **2009**, *53*, 4987-4998.

[332] C. Li, M. Pazgier, J. Li, C. Li, M. Liu, G. Zou, Z. Li, J. Chen, S. G. Tarasov, W.-Y. Lu, W. Lu, Limitations of Peptide Retro-inverso Isomerization in Molecular Mimicry. *J. Biol. Chem.* **2010**, *285*, 19572-19581.

[333] S. M. Alam, N. R. J. Gascoigne, Binding Kinetics of Superantigen with TCR and MHC Class II. In *Superantigen Protocols* (Ed.: T. Krakauer), Humana Press, Totowa, NJ, **2003**, pp. 65-85.

[334] F. Vögtle, S. Gestermann, R. Hesse, H. Schwierz, B. Windisch, Functional dendrimers. *Prog. Polym. Sci.* **2000**, *25*, 987-1041.

[335] C. M. Cardona, R. E. Gawley, An Improved Synthesis of a Trifurcated Newkome-Type Monomer and Orthogonally Protected Two-Generation Dendrons. *J. Org. Chem.* **2002**, *67*, 1411-1413.

[336] M. Calderón, M. Martinelli, P. Froimowicz, A. Leiva, L. Gargallo, D. Radic´, C. Strumia Miriam, Synthesis and Characterization of Dendronized Polymers. *Macromol. Symp.* **2007**, *258*, 53-62.

[337] S.-K. Wang, P.-H. Liang, R. D. Astronomo, T.-L. Hsu, S.-L. Hsieh, D. R. Burton, C.-H. Wong, Targeting the carbohydrates on HIV-1: Interaction of oligomannose dendrons with human monoclonal antibody 2G12 and DC-SIGN. *Proc. Natl. Acad. Sci.* **2008**, *105*, 3690-3695.

[338] Y. J. Jung, Y. S. Park, K.-J. Yoon, Y.-Y. Kong, J. W. Park, H. G. Nam, Molecule-level imaging of Pax6 mRNA distribution in mouse embryonic neocortex by molecular interaction force microscopy. *Nucleic Acids Res.* **2009**, *37*, e10.

[339] M. A. Kostiainen, J. Kotimaa, M.-L. Laukkanen, G. M. Pavan, Optically Degradable Dendrons for Temporary Adhesion of Proteins to DNA. *Chem. Eur. J.* **2010**, *16*, 6912-6918.

[340] S. Munneke, K. Kodar, G. F. Painter, B. Stocker, M. S. M. Timmer, The modular synthesis of multivalent functionalised glycodendrons for the detection of lectins including DC-SIGN. *RSC Adv.* **2017**, *7*, 45260-45268.

[341] V. Asante, Impact of amino acid side chain fluorination on proteolytic stability of peptides. Dissertation, Freie Universität Berlin, Department of Biology, Chemistry and Pharmacy, **2015**.

[342] O. Seitz, H. Kunz, HYCRON, an Allylic Anchor for High-Efficiency Solid Phase Synthesis of Protected Peptides and Glycopeptides. *J. Org. Chem.* **1997**, *62*, 813-826.

[343] M. L. Miller, E. E. Roller, R. Y. Zhao, B. A. Leece, O. Ab, E. Baloglu, V. S. Goldmacher, R. V. J. Chari, Synthesis of Taxoids with Improved Cytotoxicity and Solubility for Use in Tumor-Specific Delivery. *J. Med. Chem.* **2004**, *47*, 4802-4805.

[344] M. Shan, Design, Synthesis, and Evaluation of Bivalent Estrogen Ligands. Dissertation, Freie Universität Berlin, Department of Biology, Chemistry and Pharmacy, **2011**.

[345] P. Basu, V. N. Nemykin, R. S. Sengar, Syntheses, Spectroscopy, and Redox Chemistry of Encapsulated Oxo−Mo(V) Centers: Implications for Pyranopterin-Containing Molybdoenzymes. *Inorg. Chem.* **2003**, *42*, 7489-7501.

[346] J. Jose, A. Loudet, Y. Ueno, R. Barhoumi, R. C. Burghardt, K. Burgess, Intracellular imaging of organelles with new water-soluble benzophenoxazine dyes. *Org. Biomol. Chem.* **2010**, *8*, 2052-2059.

[347] A. M. Sanders, T. S. Kale, H. E. Katz, J. D. Tovar, Solid-Phase Synthesis of Self-Assembling Multivalent π-Conjugated Peptides. *ACS Omega* **2017**, *2*, 409-419.

[348] P. E. Dawson, T. W. Muir, I. Clark-Lewis, S. B. Kent, Synthesis of proteins by native chemical ligation. *Science* **1994**, *266*, 776-779.

[349] P. E. Dawson, M. J. Churchill, M. R. Ghadiri, S. B. H. Kent, Modulation of Reactivity in Native Chemical Ligation through the Use of Thiol Additives. *J. Am. Chem. Soc.* **1997**, *119*, 4325-4329.

[350] T. Kimmerlin, D. Seebach, '100 years of peptide synthesis': ligation methods for peptide and protein synthesis with applications to β-peptide assemblies. *J. Pept. Res.* **2008**, *65*, 229-260.

[351] P. R. Hackenberger Christian , D. Schwarzer, Chemoselective Ligation and Modification Strategies for Peptides and Proteins. *Angew. Chem. Int. Ed.* **2008**, *47*, 10030-10074.

[352] A. Cooper, Microcalorimetry of Protein-Protein Interactions. In *Protein Targeting Protocols* (Ed.: R. A. Clegg), Humana Press, Totowa, NJ, **1998**, pp. 11-22.

[353] http://www.chem.gla.ac.uk/staff/alanc/itcnotes.pdf, *(accessed June 9th, 2018)*.

[354] C. E. Schafmeister, J. Po, G. L. Verdine, An All-Hydrocarbon Cross-Linking System for Enhancing the Helicity and Metabolic Stability of Peptides. *J. Am. Chem. Soc.* **2000**, *122*, 5891-5892.

[355] Y.-W. Kim, P. S. Kutchukian, G. L. Verdine, Introduction of All-Hydrocarbon i,i+3 Staples into α-Helices via Ring-Closing Olefin Metathesis. *Org. Lett.* **2010**, *12*, 3046-3049.

[356] W. C. Still, M. Kahn, A. Mitra, Rapid chromatographic technique for preparative separations with moderate resolution. *J. Org. Chem.* **1978**, *43*, 2923-2925.

[357] H. E. Gottlieb, V. Kotlyar, A. Nudelman, NMR Chemical Shifts of Common Laboratory Solvents as Trace Impurities. *J. Org. Chem.* **1997**, *62*, 7512-7515.

[358] D. Winkler, K. Burger, Synthesis of Enantiomerically Pure D- and L-Armentomycin and Its Difluoro Analogues from Aspartic Acid. *Synthesis* **1996**, *1996*, 1419-1421.

[359] C. Zhang, C. Ludin, M. K. Eberle, H. Stoeckli-Evans, R. Keese, Asymmetric Synthesis of (*S*)-5,5,5,5′,5′,5′,5′-Hexafluoroleucine. *Helv. Chim. Acta* **1998**, *81*, 174-181.

[360] S. Huhmann, A.-K. Stegemann, K. Folmert, D. Klemczak, J. Moschner, M. Kube, B. Koksch, Position-dependent impact of hexafluoroleucine and trifluoroisoleucine on protease digestion. *Beilstein J. Org. Chem.* **2017**, *13*, 2869-2882.

[361] H. Herzner, H. Kunz, Spacer-separated sialyl LewisX cyclopeptide conjugates as potential E-selectin ligands. *Carbohydr. Res.* **2007**, *342*, 541-557.

[362] H. Frisch, Y. Nie, S. Raunser, P. Besenius, pH-Regulated Selectivity in Supramolecular Polymerizations: Switching between Co- and Homopolymers. *Chem. Eur. J.* **2015**, *21*, 3304-3309.

[363] G. B. Fields, R. L. Noble, Solid phase peptide synthesis utilizing 9-fluorenylmethoxycarbonyl amino acids. *Int. J. Pept. Protein Res.* **1990**, *35*, 161-214.

[364] M. Gude, J. Ryf, P. White, An accurate method for the quantitation of Fmoc-derivatized solid phase supports. *Lett. Pept. Sci.* **2002**, *9*, 203-206.

[365] T. Vagt, Entwicklung eines coiled coil-basierten Screeningsystems zur Bestimmung spezifischer Wechselwirkungspartner fluoralkylsubstituierter Aminosäuren. Dissertation, Freie Universität Berlin, Department of Biology, Chemistry and Pharmacy, **2009**.

[366] C. N. Pace, F. Vajdos, L. Fee, G. Grimsley, T. Gray, How to measure and predict the molar absorption coefficient of a protein. *Protein Sci.* **1995**, *4*, 2411-2423.

[367] D. L. Allen, G. J. Pielak, Baseline length and automated fitting of denaturation data. *Protein Sci.* **1998**, *7*, 1262-1263.

[368] E. F. Pettersen, T. D. Goddard, C. C. Huang, G. S. Couch, D. M. Greenblatt, E. C. Meng, T. E. Ferrin, UCSF Chimera—A visualization system for exploratory research and analysis. *J. Comput. Chem.* **2004**, *25*, 1605-1612.